

CONTROLLING THE CASIMIR FORCE

KHOO YEE YANG

FACULTY OF SCIENCE
UNIVERSITY OF MALAYA
KUALA LUMPUR

2013

CONTROLLING THE CASIMIR FORCE

KHOO YEE YANG

DISSERTATION SUBMITTED IN FULFILMENT
OF THE REQUIREMENTS
FOR THE DEGREE OF MASTER OF SCIENCE

FACULTY OF SCIENCE
UNIVERSITY OF MALAYA
KUALA LUMPUR

2013

UNIVERSITI MALAYA

ORIGINAL LITERARY WORK DECLARATION

Name of Candidate: Khoo Yee Yang (I.C./Passport No.: 881219-56-6205)

Registration/Matrix No.: SGR120039

Name of Degree: Master of Science

Title of Project Paper/Research Report/Dissertation/Thesis ("this Work"):

Controlling the Casimir Force

Field of Study: Theoretical Physics

I do solemnly and sincerely declare that:

- (1) I am the sole author/writer of this Work;
- (2) This work is original;
- (3) Any use of any work in which copyright exists was done by way of fair dealing and for permitted purposes and any excerpt or extract from, or reference to or reproduction of any copyright work has been disclosed expressly and sufficiently and the title of the Work and its authorship have been acknowledged in this Work;
- (4) I do not have any actual knowledge nor do I ought reasonably to know that the making of this work constitutes an infringement of any copyright work;
- (5) I hereby assign all and every rights in the copyright to this Work to the University of Malaya ("UM"), who henceforth shall be owner of the copyright in this Work and that any reproduction or use in any form or by any means whatsoever is prohibited without the written consent of UM having been first had and obtained;
- (6) I am fully aware that if in the course of making this Work I have infringed any copyright whether intentionally or otherwise, I may be subject to legal action or any other action as may be determined by UM.

Candidate's Signature

Date

Subscribed and solemnly declared before,

Witness's Signature

Date

Name:

Designation:

ABSTRACT

This research is devoted to a detailed study of the Casimir effect, and means to control it. The study is subdivided into two objectives. First, the origin of Casimir force and its physical significance is explored. Several different approaches and interpretations of the Casimir force is detailed and discussed. In particular, the Casimir force was derived from the vacuum field approach, the vacuum radiation approach and the source theory approach. It is concluded that the Casimir force may be equally interpreted as the manifestation of vacuum field, or the source field. Second, the possible means of controlling the Casimir force is detailed. By analysing the Lifshitz formula, we have discussed the material dependence of Casimir force. Metamaterial, with its unique ability to behave electrically and magnetically at different frequency range is shown to exhibit stable and unstable equilibrium in its Casimir force. The idea of controlling the Casimir force via optical means is then introduced theoretically. A system consisting of a metamaterial placed parallel to a Kerr material is shown to exhibit tunable Casimir force by varying the impinging laser intensity. As a result, it is shown that the Casimir force may be controlled both optically and by varying the materials involved. This finding is important, as it provides new possibilities of integrating optical devices into nanoelectromechanical systems.

ABSTRAK

Kajian ini ditumpukan kepada kesan Casimir antara dua plat selari. Objektif kajian ini terbahagi kepada dua. Pertama, asal daya Casimir serta kepentingan fizikalnya diterokai. Dalam kajian ini, beberapa pendekatan serta tafsiran yang berbeza terhadap kesan Casimir telah dibincangkan. Khususnya, daya Casimir telah diterbitkan dengan menggunakan pendekatan medan vakuum, medan sumber serta tekanan radiasi vakuum. Sebagai kesimpulan, daya Casimir boleh ditafsirkan sebagai manifestasi medan vakuum atau medan sumber. Objektif kedua pula merupakan kajian atas kemungkinan untuk mengawal daya Casimir. Dengan menganalisa formula Lifshitz, kami mendapati bahawa daya Casimir bergantung kepada jenis bahan yang dipertimbangkan. Metamaterial, dengan sifat uniknya untuk berkelakuan sebagai bahan elektrik, atau bahan magnet pada julat frekuensi yang berbeza membolehkan bahan tersebut mencapai keseimbangan stabil serta keseimbangan tidak stabil dalam daya Casimir. Seterusnya, idea mengawal daya Casimir melalui optik pula diperkenalkan secara teori. Sistem yang terdiri daripada satu plat metamaterial yang diletakkan secara selari dengan satu plat yang bersifat Kerr membolehkan daya Casimir di antara plat-plat tersebut diubah apabila keamatan laser diubah. Hasilnya, kami berjaya menunjukkan bahawa daya Casimir boleh dikawal secara optik atau dengan mengubah sifat bahan-bahan dalam sistem. Penemuan ini amat penting kerana ia menunjukkan kemungkinan baru untuk mengintegrasikan peranti optik ke dalam sistem nanoelektromekanikal.

ACKNOWLEDGEMENTS

Many individuals have been instrumental in aiding me in this educational process. Pivotal in this role was my research supervisor, Assoc. Prof. Dr. Raymond Ooi, who guides me through the entire endeavour, and gave me the opportunity to develop the fundamental knowledge of scientific research. It was indeed a great experience and I would like to express my deepest gratitude again, to Dr. Raymond Ooi.

Here, I would also like to express my deepest gratitude to University Malaya's High Impact Research grant and the Institute of Graduate Study's Scholarship, which funded the endeavour.

Also, I am glad to have the pleasure to share my masters' experience with interesting, helpful peers all along. Finally, to my parents, Khoo and Liew, and my family: thanks for supporting me all along.

TABLE OF CONTENTS

ORIGINAL LITERARY WORK DECLARATION	ii
ABSTRACT	iii
ABSTRAK	iv
ACKNOWLEDGEMENTS	v
TABLE OF CONTENTS	vi
LIST OF FIGURES	viii
LIST OF TABLES	x
LIST OF APPENDICES	xi
CHAPTER 1: INTRODUCTION	1
1.1 Casimir Force - A manifestation of zero-point energy	1
1.2 Casimir Force as a macroscopic manifestation of Van der Waals forces	2
1.3 Theories of Casimir Force	3
1.4 Experimental Verification and Applications	4
1.5 Motivations & Objectives	5
1.6 Thesis Organization	5
CHAPTER 2: THE CASIMIR EFFECT IN ITS ORIGINAL FORMULATION	7
2.1 Euler-Maclaurin Formula Approach	7
2.2 Vacuum Radiation Pressure	11
2.3 Regularization Process	13
2.3.1 Frequency Cut-off Regularization	13
2.3.2 Zeta Function Regularization	14
CHAPTER 3: LIFSHITZ THEORY	15
3.1 Derivation of Lifshitz Theory	15
3.2 Lifshitz theory & Barash-Ginzburg Theory	27
3.3 Factors affecting the Casimir Force at absolute zero	27
CHAPTER 4: SOURCE THEORY	30
4.1 Field Quantization and Operator Ordering	31
4.2 Casimir Force in Source Theory	33
4.3 Source Field and Vacuum Field	46
4.4 The Energy Variation Approach	50
4.5 Discussions	57

CHAPTER 5: MATERIAL DEPENDENT CASIMIR FORCE	58
5.1 Changes in Material Constant	58
5.2 Casimir Force in Equilibrium: Piecewise Model	61
5.3 Metamaterials	65
5.3.1 Metamaterials - An Introduction	65
5.3.2 Casimir force on Metamaterials	68
5.4 Optimizing the Casimir Force	70
5.4.1 Changes of Casimir force for different ϵ & μ	70
5.4.2 Optimizing the Metamaterial Model	74
5.5 Discussions	76
CHAPTER 6: INTENSITY DEPENDENT CASIMIR FORCE	79
6.1 AC Kerr Effect	79
6.1.1 Classical Anharmonic Oscillator Model	82
6.1.2 Quantum Theory Model	83
6.2 Intensity Dependence - An Overview	85
6.3 Optical control on Piecewise Model	87
6.4 Chalcogenide Glass	90
6.4.1 Wemple Model for n_0	91
6.4.2 Two-Band Model for n_2	93
6.5 Metamaterial & Chalcogenide Glass	96
6.5.1 Constant $n_0(\omega)$ and $n_2(\omega)$ model	96
6.5.2 Complex Linear and Nonlinear Coefficients	97
6.6 Discussions	100
CHAPTER 7: CONCLUSION	104
APPENDICES	106
REFERENCES	134

LIST OF FIGURES

Figure 1.1	An illustration of the Casimir force, F on two parallel, perfectly conducting plate in vacuum spaced by distance l apart.	2
Figure 1.2	A spider mite's leg resting on a microelectromechanical mirror assembly. It is interesting to note the relative small size of the gears and assembly compared to the size of a mite's leg. As NEMS technology advances, we expect even smaller systems in the near future. Image courtesy of Sandia National Laboratories, SUMMiTTM Technologies.	5
Figure 5.1	The variation of (normalized) Casimir force between a perfectly conducting plate with a plate with varied material constant, at arbitrary distance. (a) 3D plot and (b) The increase of Casimir attraction as the ratio of ϵ/μ increases.	60
Figure 5.2	The variation of Casimir force between a perfectly conducting plate and (a) a perfectly conducting plate and (b) a perfect magnetic plate, at different distances.	63
Figure 5.3	The variation of Casimir force between a perfectly conducting plate and a material with material constant given by (a) Eq. (5.6) and (b) Eq. (5.7), at different distances.	64
Figure 5.4	Variation of $\frac{dF_c}{d\xi}$ vs frequencies ξ , for different inter-plate distance l . It is interesting to note that there is a discontinuity at $\xi \approx 10^{15} s^{-1}$, for both cases.	66
Figure 5.5	The structure of a left hand metamaterial is shown above. (a) A schematic drawing of a two dimensional split-ring resonator on the front, and wires on the back of the printed circuit board. (b) A three layer 2D slab shaped left-hand metamaterial. (c) A prism-shaped left-hand metamaterial. Image courtesy of Ozbay and Aydin (2008).	67
Figure 5.6	(a) The dielectric function and magnetic permeability of metamaterial modelled with Eq. (5.8) as a function of frequency. (b) Variation of Casimir force for a system of two parallel plates consists of a metamaterial plate and a perfectly conducting plate against distances.	69
Figure 5.7	Variation of Casimir force for a system of two parallel plates consists of a metamaterial plate and a perfectly conducting plate against distances. (a) Changes in dielectric function's plasma frequency ω_{p_e} and (b) changes in magnetic permeability's plasma frequency ω_{p_m} , in units of ω_0 . Blue line indicates the original configuration that was considered.	71
Figure 5.8	Variation of Casimir force for a system of two parallel plates consists of a metamaterial plate and a perfectly conducting plate against distances. (a) Changes in resonant frequency ω_{T_e} and (b) ω_{T_m} , in units of ω_0 . Blue line indicates the original configuration that was considered.	72
Figure 5.9	Variation in normalized Casimir force as ϵ and μ changes.	73

Figure 5.10	Changes in Casimir force between a perfectly conducting metal and a plate made of material: (a) ϵ complex, $\mu = 1$. (b) $\epsilon = 1$, μ complex.	75
Figure 5.11	Change in normalized Casimir force for a parallel plate configuration consists of a perfectly conducting plate and (a) a metamaterial with $\mu = 1$, ϵ given by Eq. (5.8); (b) a metamaterial with $\epsilon = 1$, μ given by Eq. (5.8).	77
Figure 6.1	Casimir force between a perfectly conducting plate and a plate with (a) $\epsilon = 10$, $\mu = 1$ and b) $\epsilon = 1$, $\mu = 10$, as a function of intensity of impinging laser $n_2 I$. Inter-plate separation is taken as $l = 0.1\lambda_0$. A stationary point (maxima or minima) was observed at $n_2 I \approx 2$. This is an effect whereby for $\epsilon > \mu$ ($\epsilon < \mu$), r_{TE} (r_{TM}) decreases quicker compared to r_{TM} (r_{TE}), giving a small increase in magnitude on the original attractive (repulsive) Casimir force at very low intensities.	88
Figure 6.2	Casimir force, F_c between a perfectly conducting plate and a piecewise-dispersive material with material constants given by Eq. (6.23), as a function of inter-plate separation and laser intensity. (a) 3D plot and (b) curves for several interesting inter-plate distances.	89
Figure 6.3	The Casimir force between a metamaterial and a chalcogenide glass, As_2Se_3 is plotted as a function of inter-plate distances and impinging laser intensity. The refractive indices for As_2Se_3 is assumed constant over the whole range of frequencies. (a) 3D plot and (b) curve for several specific inter-plate spacing.	98
Figure 6.4	(a) n_0 of As_2Se_3 as modelled using the Wemple equation. (b) n_2 of As_2Se_3 as modeled by Eq. (6.31)	99
Figure 6.5	The variation of Casimir force between a metamaterial, and a chalcogenide glass, As_2Se_3 for different inter-plate distances and impinging laser intensity. (a) 3D plot and (b) curve for several specific inter-plate spacing.	101
Figure 6.6	The derivative of Casimir force, $dF_c/d\xi$ at different frequencies ξ . The inter-plate distance is (a) $l = 0.2\lambda_0$ and (b) $l = \lambda_0$. It is noted that the derivative of Casimir force increase with frequency for sufficiently large laser intensity.	102
Figure B.1	An illustration of the change in normalized Casimir force for two different integration methods, as the grid size increases	116
Figure B.2	An illustration of the integral of Lifshitz formula, against the wavevector k and frequency ξ , for (a) two perfect conductor separated at distance $l = 10^{-7}m$, and (b) a perfect conducting plate and a magnetic plate with $\mu = 10$, at distance $l = 10^{-8}m$.	118
Figure B.3	An illustration of the change in the computed Casimir force against the number of grid points, S .	120

LIST OF TABLES

Table 6.1	The dispersion of the nonlinear refraction, $G(x)$. $\Theta(x)$ is the Heaviside step function. (Sheik-Bahae, Hutchings, Hagan, & Van Stryland, 1991)	94
Table B.1	Comparison of the theoretical value of Casimir force and the computed value of Casimir force for (a) a system of two perfectly conducting plate, and (b) a system consists of a perfectly conducting plate and a perfectly magnetic plate.	119

LIST OF APPENDICES

Appendix A	Two-Band Model: Derivation of $G(x)$	107
Appendix B	Numerical Methods & Program Verification	115
Appendix C	Source Code	122

CHAPTER 1

INTRODUCTION

1.1 Casimir Force - A manifestation of zero-point energy

Electricity and magnetism in classical physics are modelled by the Maxwell's equations. It describes the relationship of electric fields and magnetic fields, with or without the presence of charges. Maxwell's equations also give rise, in empty space, oscillating propagations of electric and magnetic fields known as the plane waves (Wangsness, 1986). It turns out that a monochromatic, plane electromagnetic field is mathematically equivalent to a simple harmonic oscillator of the same frequency (P. Milonni & Eberlein, 1994).

In classical mechanics, simple harmonic oscillator may have any arbitrary value of energy. However, in quantum mechanics, it was well known that simple harmonic oscillator can only have specific energies (Griffiths, 2005), as given by Eq. (1.1).

$$E(n) = \left(\frac{1}{2} + n\right) \hbar\omega \quad (1.1)$$

In the equation, $\hbar = 1.0546 \times 10^{-34} Js$ is the Planck's constant, and ω is the frequency of the oscillator. By substituting $n = 0$ into the equation, we notice that the quantum harmonic oscillator, unlike the classical oscillator, can never possess zero energy. This implies that some energy remains even when an electromagnetic system have no photons. It is known as the zero-point energy, and Mulliken (1924) reported the first experimental evidence of it. Vacuum is then regarded as an infinite collection of harmonic oscillators with non-zero ground state energy, representing the fluctuations of electric and magnetic field at each point in space (Bordag, Klimchitskaya, Mohideen, & Mostepanenko, 2009).

By introducing boundaries into an electromagnetic field, we can change the allowed frequencies for the oscillatory system. This may result in a lower energy density in a part of space. The difference between the energy densities of different parts in space may then give rise to a small but experimentally observable force on the boundaries, known as the Casimir force. The Casimir effect, postulated by Casimir (1948) is one of the most direct

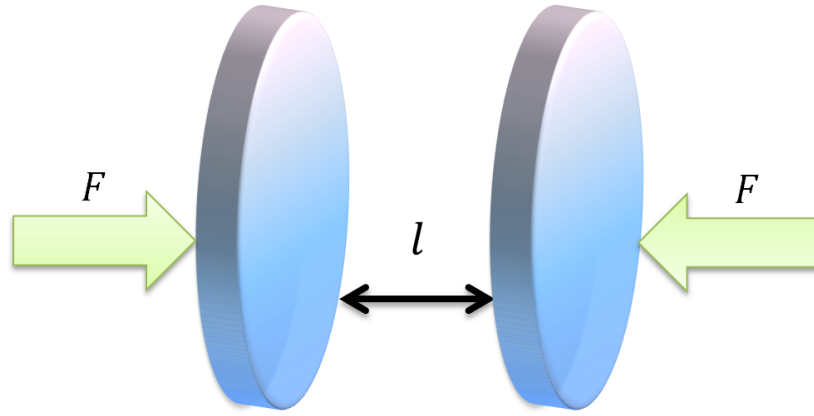


Figure 1.1: An illustration of the Casimir force, F on two parallel, perfectly conducting plate in vacuum spaced by distance l apart.

manifestations of the existence of zero-point vacuum oscillation. In the simplest form, the Casimir effect is the attraction between two electrically neutral, infinitely large, parallel, perfectly conducting plates in a vacuum, as depicted in Fig. (1.1). According to classical electrodynamics' prediction, there would be no net force on two neutral plates. However, when a quantized electromagnetic field is considered, it was noted that the ground state of quantum electrodynamics is not zero. This would then manifest as an attractive force between both plates. According to Casimir's prediction, the Casimir pressure between two infinitely large, neutral parallel plates made of perfectly conducting metal at zero temperature is (Casimir, 1948):

$$F(l) = -\frac{\pi^2 \hbar c}{240 l^4} \quad (1.2)$$

In Eq. (1.2), l is the inter-plate separation while c is the speed of light in vacuum. This is a profound and striking result, as it directly shows the quantum mechanical effect of second quantization, and indicates the existence of zero-point oscillation.

1.2 Casimir Force as a macroscopic manifestation of Van der Waals forces

The Van der Waals forces was originally proposed in order to explain the deviation of molecules from the ideal gas law. It was later derived from first principles by London (1930). By using the fourth order perturbation theory, London found that the attractive interaction between molecules is inversely proportional to the sixth power of intermolecular distance. In 1948, Casimir and Polder rederived the Van der Waals interaction based on the zero-point field energy - and shockingly, the result agrees quite well with London's

theory. In addition, the potential energy was found to have $U(r) \propto r^{-7}$ and was later attributed to the finite speed of light, and the phenomenon is then called the "retarded Van der Waals force". This modifies London's theory to account for the attraction force at larger interatomic separation.

Qualitatively, we may think of the existence of Casimir force as the result of interactions between induced dipole moments, much like Van der Waals. The induced dipole moments may be thought as quantum fluctuations in matter. These fluctuations then leads to imbalance in energy, ΔE due to virtual charge separation, for a time interval of Δt . Here, the Heisenberg uncertainty principle, $\Delta E \Delta t \leq \hbar/2$ holds true. The fluctuations in these induced dipoles are then responsible for the fluctuating zero-point field in the space around the conductors. The fluctuation in zero-point field in space, in this case is basically the Casimir effect. This is a striking feature, where we can think of the Casimir effect both as a macroscopic manifestation of Van der Waals forces, or as the change in the zero-point energy due to presence of boundaries (P. Milonni & Shih, 1992). With this, we notice the calculation of the Casimir attraction between bulk media is greatly simplified by employing the idea of zero-point energy.

1.3 Theories of Casimir Force

With two alternative views accepted, we can move forward to calculate the Casimir force between two media. In essence, the vacuum energy is obtained by simply calculating the allowed modes of electromagnetic waves in space, as determined by the Maxwell equations with appropriate boundary conditions. The Casimir force is then obtained by taking the negative derivative of the energy over the entire space considered. This approach is justified as long as the most significant (virtual) wavelengths are much larger compared to the spacing between both media (P. Milonni & Eberlein, 1994).

Since inception, various models had been proposed to compute the Casimir force for different configurations. Casimir (1948) used the classical Euler-Maclaurin approach to normalize the Casimir force between two parallel, perfectly conducting slab. Later, Lifshitz (1956) developed the Lifshitz formula, which gives the Casimir force between two parallel plate with arbitrary material constants, at absolute zero temperature. This model was developed as to include the non-additive effect of the Van der Waals forces.

The model was expanded to include nonzero temperature, and high temperature limits (Brown & Maclay, 1969; Mehra, 1967). Later, the dynamical Casimir effect, which arise from the movement of planes was proposed and theorized by Bordag, Petrov, and Robashik (1984) using the Green's function approach. Furthermore, with the advancement of computational techniques, Casimir force between any arbitrary three-dimensional objects was successfully modelled (Reid, Rodriguez, White, & Johnson, 2009).

1.4 Experimental Verification and Applications

Several attempts had been done to confirm the existence of Casimir force. Sparnaay (1958) pioneered this effort, but was not able to unambiguously confirm the existence of Casimir force due to difficulty in keeping the plates parallel. The final decisive verification did not come by until 1997, when Lamoreaux used a torsional pendulum and sphere-plate configuration to perform the first high precision measure of the Casimir force. This discovery was then followed by several experimental studies, which produced further confirmation (Ederth, 2000; Harris, Chen, & Mohideen, 2000; Roy, Lin, & Mohideen, 1999).

The Casimir force can be repulsive for several cases. For example, in 1968, Boyer's calculation showed that in the case of a perfectly conducting spherical shell, the Casimir forces are repulsive. Also in 2009, the team of Capasso replaced the vacuum between both plates in Casimir's original thought with liquid bromobenzene, and various other materials (such as gold and silica) in place of metal plates. Liquid bromobenzene, having higher dielectric permittivity than silica but lower than gold, causes a repulsive force between gold and silica. The cantilever was used to measure the force at all length of separations and was proved to be highest at 20nm separation (Munday, Capasso, & Parsegian, 2009).

With microelectromechanical systems (MEMS) and nanoelectromechanical systems (NEMS) becoming increasingly complex, scaling issues had become the center of attention. Scaling NEMS systems downwards will inevitably bring up the issue of Casimir interaction between metallic and dielectric surfaces in close proximity, such as stiction (Chan, Aksyuk, Kleiman, Bishop, & Capasso, 2001; De Los Santos, 2003; Serry, Walliser, & Maclay, 1998). This problem may be avoided if the Casimir force is repulsive (Capasso, Munday, Iannuzzi, & Chan, 2007; Yang, Zeng, Chen, Zhu, & Zubairy, 2010).

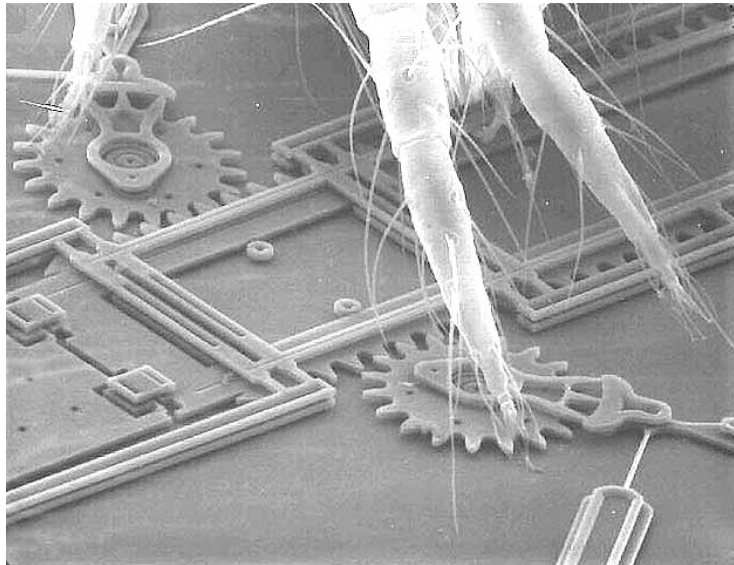


Figure 1.2: A spider mite's leg resting on a microelectromechanical mirror assembly. It is interesting to note the relative small size of the gears and assembly compared to the size of a mite's leg. As NEMS technology advances, we expect even smaller systems in the near future. Image courtesy of Sandia National Laboratories, SUMMiTTM Technologies.

Therefore, repulsive Casimir force had received renewed interest (Kenneth, Klich, Mann, & Revzen, 2002; Levin, McCauley, Rodriguez, Reid, & Johnson, 2010; Munday et al., 2009).

1.5 Motivations & Objectives

With quick advancement in the design and fabrication of NEMS composing of nanogaps or nanostructures, it is important and interesting at this point to have a deeper understanding on the Casimir force, with a focus towards repulsive Casimir force. Furthermore, it is interesting to consider the possibility of controlling it. With these motivations in mind, the objectives for this study are set as below:

- To explore the origin of Casimir force, and its physical significance.
- To explore the possibilities of controlling the Casimir force, particularly by optical means and by using different classes of optical materials.

1.6 Thesis Organization

This thesis is roughly arranged into two sections. The first section was devoted to explore the origin of Casimir effect. In Chapter 2, the Casimir force is derived by several conventional methods, which includes Euler-Maclaurin approach and Vacuum Pressure

approach. In Chapter 3, the Lifshitz formula was derived for arbitrary dielectric and magnetic materials at zero temperature. The derivation is then contrasted with the source theory approach, which made no explicit references to zero-point energy. The source theory is discussed in Chapter 4. All theories presented in this section are generally based on established theories, along with discussion on each theory's implication.

In the second section, the possibilities of controlling the Casimir force are explored. Firstly, the dependence of Casimir force on the materials are discussed in Chapter 5. A majority of work from this chapter is based on an article by Yang et al. (2010). We then introduce optical control over the Casimir force in Chapter 6.

This thesis was written with two main contributions in mind. Firstly, existing theories on the computation of Casimir force is presented and reviewed in a more pedagogical manner. Discussions were presented to give a better insight into each theory. Then, the possibilities of controlling the Casimir force are explored particularly by optical means and by using different classes of optical materials. In particular, the idea of controlling Casimir force by inducing optical Kerr effect is introduced to allow optical control on Casimir force.

This thesis is then concluded with a short recap, and several thoughts on the future of research on Casimir force in Chapter 7.

CHAPTER 2

THE CASIMIR EFFECT IN ITS ORIGINAL FORMULATION

Although the Casimir force can be regarded as a macroscopic manifestation of the retarded Van der Waals force, it is mostly derived by considering the zero-point energy instead of solving the many-body problem. To illustrate the simplification and elegance of considering the zero-point energy, the derivation of Casimir force between two perfectly conducting plate, by Casimir (1948) himself is presented here. Then, the notion of vacuum radiation pressure is introduced as yet another alternative way to interpret the Casimir force. Lastly, we discussed the regularization procedure and introduce several methods to extract finite quantities from divergent sums.

2.1 Euler-Maclaurin Formula Approach

For pedagogical reasons, the original derivation by Casimir (1948) is worked out in detail. In the derivation, an empty (vacuum) cavity made of perfectly conducting plate, and edges of L , L , and l along x , y , and z direction respectively is considered. In essence, the derivation will take place by considering two different inter-plate distance on the xy -plane, that is: $l \approx L$ and $l \ll L$. The continuity conditions for electromagnetic field at the vacuum-mirror interface require the electromagnetic field to vanish on the wall of the cavity.

$$\vec{E} = \vec{H} = 0 \quad (2.1)$$

The electromagnetic field inside the cavity is quantized, much like the formalism of a particle in a box. The possible electromagnetic vibration in the cavity in this case is, with $0 \leq x \leq L$, $0 \leq y \leq L$, $0 \leq z \leq l$ have wavevectors:

$$\begin{aligned} k_x &= \frac{\pi}{L} n_x \\ k_y &= \frac{\pi}{L} n_y \\ k_z &= \frac{\pi}{l} n_z \end{aligned} \quad (2.2)$$

where n_x, n_y, n_z are positive integers. The allowed field frequencies inside the cavity is given by the relation

$$\omega_{n_x, n_y, n_z} = c \sqrt{\left(\frac{\pi}{L} n_x\right)^2 + \left(\frac{\pi}{L} n_y\right)^2 + \left(\frac{\pi}{l} n_z\right)^2} \quad (2.3)$$

For a perfect reflector, the frequencies do not depend on the polarization state of the light. Hence, we have omitted the sum over both polarization states. Similar to a harmonic oscillator, the quantum energy of a mode is then given by

$$E_{n_x, n_y, n_z} = \hbar \omega_{n_x, n_y, n_z} \left(\frac{1}{2} + N_{n_x, n_y, n_z} \right) \quad (2.4)$$

where N_{n_x, n_y, n_z} represents the number of photons inside the cavity. Here, we introduce the zero-point energy by setting $N = 0$, i.e. there are no photons inside the cavity. This is a fundamental result of quantum theory, which is derived directly from Heisenberg uncertainty principle. It shows a fundamental, irreducible fluctuation of the electromagnetic field around a mean value of $\frac{1}{2} \hbar \omega$. Now, any arbitrary field may be written as a linear combination of all field modes. With that, the ground state radiation energy inside the cavity is given by

$$E_0(l) = \frac{1}{2} \sum_{n_x, n_y, n_z} \hbar \omega_{n_x, n_y, n_z} \quad (2.5)$$

By considering the situation of physical interest, we then let $l \ll L$, which then allows us to replace the sum over k_x and k_y with an integral (by approximating both space as a continuum). The energy then become

$$\begin{aligned} E_0(l) &= \frac{\hbar c L^2}{\pi^2} \int_0^\infty \int_0^\infty \left[\frac{1}{2} \sqrt{k_x^2 + k_y^2} + \sum_{n=1}^\infty \sqrt{\frac{n^2 \pi^2}{l^2} + k_x^2 + k_y^2} \right] dk_x dk_y \\ &= \frac{\hbar c L^2}{\pi^2} \int_0^\infty \int_0^{\pi/2} \frac{1}{2} r + \sum_{n=1}^\infty \sqrt{\left(\frac{n\pi}{l}\right)^2 + r^2} r dr d\theta \\ &= \frac{\hbar c L^2}{2\pi} \int_0^\infty \sum'_{n=0} \sqrt{\left(\frac{n\pi}{l}\right)^2 + r^2} r dr \end{aligned} \quad (2.6)$$

Here, the polar coordinate (r, θ) is used in place of the Cartesian coordinate (k_x, k_y) , and the prime notation is used to note that the term corresponding to $n = 0$ will be multiplied by $\frac{1}{2}$.

It is important to note at this point that the quantity E_0 is infinite, as there are infinite number of vacuum modes. To extract a physical quantity from this expression, Casimir

(1948) then proposed to take the difference between two infinite quantities, which is a procedure known as regularization.

$$E(l) = E_0(l) - E_0(l \rightarrow \infty) \quad (2.7)$$

Again, the sum may be approximated by an integral for the second case. With that we arrive at

$$E(l) = \frac{\hbar c L^2}{2\pi} \left[\int_0^\infty \sum_{n=0}^\infty 'r \sqrt{\left(\frac{n\pi}{l}\right)^2 + r^2} dr - \frac{1}{\pi} \int_0^\infty \int_0^\infty lr \sqrt{(k_z^2 + r^2)} dr dk_z \right] \quad (2.8)$$

The finite energy may be extracted by introducing a function $f(\omega/\omega_{max})$, which is unity for $\omega \ll \omega_{max}$, but tend to zero as $\omega/\omega_{max} \rightarrow \infty$. This procedure was justified by Casimir (1948) by assuming that photons of short wavelength (e.g. X-ray) is hardly obstructed by the cavity, and hence similarly, the zero-point energy of these waves is presumed to not influence the position of the plates.

With some algebra and a change of variable, Eq. (2.8) may be rewritten as

$$E(l) = \lim_{\omega_{max} \rightarrow \infty} \frac{\hbar c L^2 \pi^2}{4l^3} \left[\sum_{n=0}^\infty 'G(n) - \int_0^\infty G(n) dn \right] \quad (2.9)$$

where

$$G(n) = \int_0^\infty \sqrt{n^2 + v} \times f\left(\frac{\pi \sqrt{n^2 + v}}{l \omega_{max}}\right) dv, \quad v = \frac{l^2 r^2}{\pi^2} \quad (2.10)$$

We then apply the Euler-Maclaurin formula on Eq. (2.9) (Abramowitz & Stegun, 1965),

$$\sum_{n=0}^\infty G(n) - \int_0^\infty G(n) dn = - \sum_{m=2}^\infty \frac{B_m}{m!} G^{(m-1)}(0) \quad (2.11)$$

where B_m is known as the Bernoulli numbers given by the contour integral over a curve c , in counter clockwise direction as below.

$$B_m = \frac{m!}{2\pi i} \oint_c \frac{z}{e^z - 1} \frac{dz}{z^{m+1}} \quad (2.12)$$

The contour encloses the origin, and has a radius less than 2π to avoid poles at $\pm 2\pi i$ (Abramowitz & Stegun, 1965). Putting everything together, we notice that all terms vanish except for the case $m = 4$, which gives:

$$G^{(3)}(0) = -4 \quad (2.13)$$

The Casimir energy is then given by

$$E(l) = -\frac{\hbar c \pi^2}{720} \left(\frac{L^2}{l^3} \right) \quad (2.14)$$

This result is finite, and it is independent of the cut-off function introduced. Finally by taking the negative gradient of Eq. (2.14), we arrive at the Casimir pressure between two plates,

$$F(l) = -\frac{\pi^2 \hbar c}{240 l^4} \quad (2.15)$$

Notice that Eq. (2.15) only depends on the distance between plates, l . This indicates that the Casimir effect between two perfectly conducting plate is a pure geometrical effect, which is connected to the existence of boundaries in vacuum. This idea will be expanded further to include real materials in Chapter 3.

In the above derivation, a finite quantity was obtained from a difference of two infinite quantities. It is useful now to note the physical implication of these steps. Firstly, the Casimir energy was taken as the difference between the vacuum energy of a cavity and the free vacuum energy $E_0(l \rightarrow \infty)$. To understand this step, we have to first accept that the Casimir energy is a measure of the shift in zero-point energy of the field, due to a change in the boundary conditions. The shift of energy may be measured by taking the difference between the vacuum energy when both plate are in place, and the vacuum energy when both plate placed at infinity (i.e. when the space considered is pure vacuum). To strengthen this statement, we know that the vacuum energy density (without subjected to boundary) is given by:

$$\zeta = \int_{\mathbb{R}^3} \frac{d^3k}{(2\pi)^3} \frac{\hbar}{2} \omega \quad (2.16)$$

Hence, for a cavity of dimension $L \times L \times l$, the vacuum energy that will fill in the volume is given by

$$\begin{aligned} E_0(l \rightarrow \infty) &= (L^2 l) \zeta \\ &= \frac{\hbar c L^2}{2\pi^2} \int_0^\infty \int_0^\infty l r \sqrt{k_z^2 + r^2} dr dk_z \end{aligned} \quad (2.17)$$

which is equal to the second half of Eq. (2.8).

Secondly, it is noted that a cut-off function was multiplied to the integrand of Eq. (2.8). It allows the integrals to converge as we sum over all frequencies. This is crucial to ensure the integrals are finite, and Euler-Maclaurin formula is still applicable. Physically,

the function serves as a cut-off point, where the mirrors become transparent. This is true for real materials whereby $\varepsilon \rightarrow 1$ as $\omega \rightarrow \infty$.

As a final remark, we notice that Eq. (2.9) was simplified by using the Euler-Maclaurin formula. An alternative treatment may be done by using the Abel-Plana formula, as shown below (Erdélyi, Magnus, Oberhettinger, Tricomi, & Bateman, 1953).

$$\sum_{n=0}^{\infty} F(n) - \int_0^{\infty} F(t) dt = \frac{1}{2}F(0) + i \int_0^{\infty} \frac{dt}{e^{2\pi t} - 1} [F(it) - F(-it)] \quad (2.18)$$

2.2 Vacuum Radiation Pressure

In the previous section, the Casimir force was directly derived from the vacuum energy. However, it seems less intuitive, as it does not provide an explanation for the reason that the force is attractive. P. W. Milonni, Cook, and Goggin (1988) proposed an alternative view on the Casimir effect, which uses the concept of vacuum radiation pressure. The Casimir force, in this case is regarded as the consequences of radiation pressure associated with the zero-point energy, with $\hbar\omega/2$ per mode. The zero-point field, then, is thought to have momentum of $p_i = \hbar k_i/2$. In this section, the derivation of Casimir force from this approach is outlined.

Consider the radiation pressure exerted by a plane wave incident at an angle θ_{inc} on a plate. Given that the plate is perfectly reflecting, the radiation pressure exerted is twice the normal component of energy per unit volume, $E \cos \theta_{inc}$ of the incident field. With that, the radiation pressure is given by

$$P = \frac{F}{A} = 2E \cos^2 \theta_{inc} \quad (2.19)$$

The second factor, $\cos \theta_{inc}$ appeared because the effective irradiated area, A , increases by a factor of $(\cos \theta_{inc})^{-1}$ compared to the case where light is incident normally. Now each mode of frequency, ω , will contribute a pressure of

$$\begin{aligned} P &= 2E \cos^2 \theta_{inc} \\ &= (2) \left(\frac{1}{2}\right) \left(\frac{1}{2}\hbar\omega\right) \frac{1}{V} \cos^2 \theta_{inc} \\ &= \left(\frac{\hbar\omega}{2V}\right) \frac{k_z^2}{k^2} \end{aligned} \quad (2.20)$$

where $k = \omega/c$ is the wavevector, and V is the quantization volume. A factor of $1/2$ was inserted because each mode's energy is divided equally between waves propagating

towards, and away, from the plate. The derivation will be continued by considering the parallel plate arrangement. The calculation may be separated into two cases, i.e. (1) vacuum field between the plates, and (2) vacuum field outside the parallel plate structure.

For the vacuum field between the plates, we notice the vacuum radiation pressure act to push the plates apart. For an infinitely large plate, k_x and k_y may be regarded as continuous, while $k_z = n\pi/l$. As usual, n is taken as a positive integer. The outwards pressure on each plate due to all possible modes can then be written as

$$P_{out} = \frac{\Theta_k \hbar c}{2\pi^2 l} \sum_{n=1}^{\infty} \int_0^{\infty} \int_0^{\infty} \frac{(n\pi/l)^2}{\sqrt{k_x^2 + k_y^2 + (n\pi/l)^2}} dk_x dk_y \quad (2.21)$$

where Θ_k is the number of independent polarizations.

On the external side of each plate, the allowed field modes are continuous on all directions. These vacuum field modes will act to push the plates together. Hence, by replacing the summation in Eq. (2.21) with an integral, the total inwards pressure is given by

$$P_{in} = \frac{\Theta_k \hbar c}{2\pi^3 l} \int_0^{\infty} \int_0^{\infty} \int_0^{\infty} \frac{k_z^2}{\sqrt{k_x^2 + k_y^2 + k_z^2}} dk_x dk_y dk_z \quad (2.22)$$

Notice that both P_{in} and P_{out} are infinite. However, their difference is finite, and physically meaningful. With some algebraic manipulation, we have

$$P_{out} - P_{in} = \left(\frac{\pi^2 \hbar c}{4l^4} \right) \left(\sum_{n=1}^{\infty} G(n) - \int_0^{\infty} G(u) du \right) \quad (2.23)$$

where

$$G(y) = y^2 \int_0^{\infty} \frac{dx}{\sqrt{x+y^2}} \quad (2.24)$$

By employing regularization technique, such as the Euler-Maclaurin formula then yields, for two independent polarization ($\Theta_k = 2$),

$$P_{out} - P_{in} = -\frac{\pi^2 \hbar c}{240l^4} \quad (2.25)$$

which is same as Casimir's result. Here, the Casimir force between both plates is simply the consequence of the radiation pressure associated with the zero-point oscillation of vacuum field. One may intuitively argue that the Casimir force is attractive because there are "more" modes on the external part of the plates pushing on the plate (k_z is continuous), compared to the space between the plates (k_z is discrete). However, this intuition may be

regarded as superficial, as both inwards and outwards pressure on the plate is infinite. Nevertheless, this provides a new insight on the nature of the Casimir force. Furthermore, this simple interpretation of Casimir force by regarding it as radiation pressure suggests an approach based on the vacuum electromagnetic stress tensor. This approach was taken by Brown and Maclay (1969). The stress tensor in this case was calculated using the image method for both zero, and finite temperature.

2.3 Regularization Process

It is fairly clear now that the vacuum energy is a divergent quantity. To extract physical quantity from it, the regularization procedure must be introduced. A regularization parameter is introduced into a divergent quantity such that the original expression is restored at appropriate limit. Beyond mathematical definition, regularization scheme sometimes have a direct physical meaning. For example, in the cut-off function we have employed in Section 2.1 corresponds to a real material, which become transparent soon above the plasma frequency. Here, some regularization schemes are introduced.

2.3.1 Frequency Cut-off Regularization

In the frequency cut-off scheme, a cut-off function is introduced into the mode expansion, which makes the corresponding sum or integral converges. This scheme was employed in Section 2.1, alongside with the Euler-Maclaurin formula. Other forms of cut-off function exists, such as the exponential decay function (Ruggiero & Zimmerman, 1977). With the exponential decay function, the regularized vacuum energy will take the below form

$$E(\delta) = \frac{\hbar}{2} \sum_i \omega_i e^{-\delta \omega_i} \quad (2.26)$$

where δ defines the cut-off strength, and $\delta = 0$ removes the regularization scheme. Furthermore, it is possible to introduce a sharp frequency cut-off by using a step function.

$$\Theta(\delta) = \begin{cases} 1, & \omega_i \leq \delta \\ 0, & \omega_i > \delta \end{cases} \quad (2.27)$$

2.3.2 Zeta Function Regularization

The zeta function regularization involves a temporary change in the power of the frequency ω_i in the mode sum, with the mode sum take the below form.

$$E(s) = \frac{\hbar v^{2s}}{2} \sum_i \omega_i^{1-2s} \quad (2.28)$$

In the equation, the factor v^{2s} , with v takes the dimension of mass, is arbitrarily introduced in order to keep the dimension of E intact. As expected, the factor disappears upon removing of the regularization, when $s \rightarrow 0$. Eq. (2.28) will converge if $\text{Re } s > (l+1)/2$, where l is the dimensionality of the space. It is called the zeta function regularization because the vacuum energy is given by

$$E(s) = \frac{\hbar v^{2s}}{2} \zeta_p \left(s - \frac{1}{2} \right) \quad (2.29)$$

where ζ is the generalized Riemann-zeta function,

$$\zeta_p(s) = \sum_i \frac{1}{\omega_i^{2s}} \quad (2.30)$$

By exploiting the zeta function $\zeta_p(s)$, it is possible to regularize the infinite quantities found in some Casimir force problems. An example of such application is found in Elizalde and Romeo (1991).

CHAPTER 3

LIFSHITZ THEORY

Several methods of deriving the Casimir force between two perfectly conducting plates had been explored in previous section. In this chapter, we will expand the notion of Casimir force to real dielectric and magnetic materials, which have finite permeability ε and permittivity μ . With this we introduce the Lifshitz formula. The Lifshitz theory was first proposed in 1956 to calculate the Casimir force between two parallel, infinitely thick plates placed at a distance l in vacuum. Later, the Lifshitz formula was confirmed in a neatly design experiment by Sabisky and Anderson (1973), who measured Casimir force holding a film of superfluid liquid helium to a SrF_2 substrate, to high precision, over distance scales differing by a factor of 1000. In this chapter, a theoretical proof of the formula is outlined. A discussion on the Barash-Ginzburg theory entails to justify the feasibility of our derivation. Lastly, we explore the factors that affect the Casimir force, according to the Lifshitz's formula.

3.1 Derivation of Lifshitz Theory

In this part, an attempt is made to derive the Lifshitz formula, with boundary at $z = \pm l/2$, for two plates with dielectric function $\varepsilon_A(\omega)$, $\varepsilon_B(\omega)$, and permeability of $\mu_A(\omega)$, $\mu_B(\omega)$, at absolute zero. This derivation, which was a simplified version of Lifshitz's original derivation (Bordag et al., 2009), takes place by first considering the Maxwell equations on all spaces. The Maxwell equations are then solved with appropriate boundary condition to obtain the generating functions. Argument principle is then applied to obtain the photon eigenfrequencies from the generating functions, and lastly the result is regularized to obtain the Casimir pressure.

First, materials are considered with the absence of charge and current densities. With

these assumption, the Maxwell equations are given as in Eq. (3.1).

$$\begin{aligned}
\nabla \cdot \vec{D}(t, \vec{r}) &= 0 \\
\nabla \times \vec{H}(t, \vec{r}) &= \frac{\partial \vec{D}(t, \vec{r})}{\partial t} \\
\nabla \cdot \vec{B}(t, \vec{r}) &= 0 \\
\nabla \times \vec{E}(t, \vec{r}) &= -\frac{\partial \vec{B}(t, \vec{r})}{\partial t}
\end{aligned} \tag{3.1}$$

The standard continuity boundary conditions is applied to both plates at $z = \pm l/2$ (Jackson, 1998), as in Eq. (3.2).

$$\begin{aligned}
E_{1t} &= E_{2t} \\
D_{1n} &= D_{2n} \\
B_{1n} &= B_{2n} \\
H_{1t} &= H_{2t}
\end{aligned} \tag{3.2}$$

Here, the subscripts “ n ” and “ t ” refers to the normal and tangential components, respectively. The subscript 1 refers to the vacuum and the subscript 2 to the semispaces.

Spatial dispersion is ignored in the Lifshitz theory. With that, the connection between electric displacement, \vec{D} and electric field strength, \vec{E} is given by Eq. (3.3), where the kernel of integration is known as the dielectric permittivity, $\varepsilon(\tau, \vec{r})$, for $\tau = t - t'$. Similarly, the relationship between magnetic induction, \vec{B} and magnetic field intensity, \vec{H} were given by Eq. (3.4).

$$\vec{D}(t, \vec{r}) = \int_{-\infty}^t \varepsilon_0 \varepsilon(t - t', \vec{r}) \vec{E}(t', \vec{r}) dt' \tag{3.3}$$

$$\vec{B}(t, \vec{r}) = \int_{-\infty}^t \mu_0 \mu(t - t', \vec{r}) \vec{H}(t', \vec{r}) dt' \tag{3.4}$$

By representing all fields as Fourier transforms, Eq. (3.3) and Eq. (3.4) may be written as:

$$\vec{D}(\omega, \vec{r}) = \vec{E}(\omega, \vec{r}) \varepsilon_0 \varepsilon(\omega, \vec{r}) \tag{3.5}$$

$$\vec{B}(\omega, \vec{r}) = \vec{H}(\omega, \vec{r}) \mu_0 \mu(\omega, \vec{r})$$

where the frequency-dependent permittivity and permeability is given by Eq. (3.6), which is a concept central to the Lifshitz theory. Also, ε_0 and μ_0 are the permittivity and permeability in free space. For simplicity, all dielectric function ε and magnetic permeability μ

are given in terms of the relative permeability and permittivity.

$$\begin{aligned}\varepsilon(\omega, \vec{r}) &= \int_0^\infty \varepsilon(\tau, \vec{r}) e^{i\omega\tau} d\tau \\ \mu(\omega, \vec{r}) &= \int_0^\infty \mu(\tau, \vec{r}) e^{i\omega\tau} d\tau\end{aligned}\tag{3.6}$$

There are several different approaches to derive the Lifshitz formula. The original approach by Lifshitz (1956) was done under the assumption that dielectric materials in thermal equilibrium are characterized by randomly fluctuating sources of long-wavelength electromagnetic fields. The theory was later derived based on scattering theory (Genet, Lambrecht, & Reynaud, 2003). Here, we will derive the Lifshitz formula directly from the zero-point energy of electromagnetic field in the presence of dielectric semispaces (Van Kampen, Nijboer, & Schram, 1968).

Firstly, the electromagnetic field present in space is modelled with a monochromatic electromagnetic field, i.e. $\vec{E}(t, \vec{r}) = \vec{E}(\vec{r}) e^{-i\omega t}$, $\vec{H}(t, \vec{r}) = \vec{H}(\vec{r}) e^{-i\omega t}$. It is then assumed that both semispaces are isotropic, that is ε and μ does not depends on \vec{r} . By substituting all information into the Maxwell equations, Eq. (3.1), Eq. (3.7) is then obtained.

$$\begin{aligned}\nabla \cdot \vec{E}(\vec{r}) &= 0 \\ \nabla \times \vec{H}(\vec{r}) + i\omega\varepsilon_0\vec{E}(\vec{r})\varepsilon(\omega) &= 0 \\ \nabla \cdot \vec{H}(\vec{r}) &= 0 \\ \nabla \times \vec{E}(\vec{r}) - i\omega\mu_0\vec{H}(\vec{r})\mu(\omega) &= 0\end{aligned}\tag{3.7}$$

It is noteworthy that in this derivation, it is assumed that two semispace have different dielectric function, $\varepsilon_A(\omega)$, $\varepsilon_B(\omega)$ and magnetic permeability, $\mu_A(\omega)$, $\mu_B(\omega)$. Since the Maxwell equations are valid for all 3 regions, the dielectric function and permeability used in Eq. (3.7) may then be written as:

$$\varepsilon(\omega) = \begin{cases} \varepsilon_A(\omega), & z < -\frac{l}{2}; \\ 1, & |z| < \frac{l}{2}; \\ \varepsilon_B(\omega), & z > \frac{l}{2}; \end{cases}\tag{3.8}$$

$$\mu(\omega) = \begin{cases} \mu_A(\omega), & z < -\frac{l}{2}; \\ 1, & |z| < \frac{l}{2}; \\ \mu_B(\omega), & z > \frac{l}{2}; \end{cases}\tag{3.9}$$

Eq. (3.7) may be solved by equating them into two second order equations (Jackson, 1998).

$$\begin{aligned}
\nabla \times \vec{H}(\vec{r}) &= -i\omega\epsilon_0\vec{E}(\vec{r})\epsilon(\omega) \\
\nabla \times (\nabla \times \vec{H}(\vec{r})) &= -i\omega\epsilon_0\epsilon(\omega) (\nabla \times \vec{E}(\vec{r})) \\
\nabla (\nabla \cdot \vec{H}(\vec{r})) - \nabla^2 \vec{H}(\vec{r}) &= -i\omega\epsilon_0\epsilon(\omega) (i\omega\mu_0\vec{H}(\vec{r})\mu(\omega)) \\
\nabla^2 \vec{H}(\vec{r}) + \frac{\omega^2}{c^2} \vec{H}(\vec{r})\epsilon(\omega)\mu(\omega) &= 0
\end{aligned} \tag{3.10}$$

$$\begin{aligned}
\nabla \times \vec{E}(\vec{r}) &= i\omega\mu_0\vec{H}(\vec{r})\mu(\omega) \\
\nabla \times (\nabla \times \vec{E}(\vec{r})) &= i\omega\mu_0\mu(\omega) (\nabla \times \vec{H}(\vec{r})) \\
\nabla (\nabla \cdot \vec{E}(\vec{r})) - \nabla^2 \vec{E}(\vec{r}) &= i\omega\mu_0\mu(\omega) (-i\omega\epsilon_0\vec{E}(\vec{r})\epsilon(\omega)) \\
\nabla^2 \vec{E}(\vec{r}) + \frac{\omega^2}{c^2} \vec{E}(\vec{r})\epsilon(\omega)\mu(\omega) &= 0
\end{aligned} \tag{3.11}$$

Both equations may be solved by first assuming the orthonormal, complete solution be Eq. (3.12).

$$\begin{aligned}
\vec{E}_j(\vec{r}) &= \vec{e}_p(z, k_\perp) e^{i\vec{k}_\perp \cdot \vec{r}_\perp} \\
\vec{H}_j(\vec{r}) &= \vec{g}_p(z, k_\perp) e^{i\vec{k}_\perp \cdot \vec{r}_\perp}
\end{aligned} \tag{3.12}$$

where $\vec{r} = (x, y, z) = (\vec{r}_\perp, z)$, $\vec{k}_\perp = (k_x, k_y)$, and the index $j = \{p, \vec{k}_\perp, \omega\}$. Here $p = TE, TM$ are the index for two mutually independent polarization of electromagnetic waves, i.e. transverse electric and transverse magnetic, respectively.

Then, $k^2 = k_\perp^2 - \frac{\omega^2}{c^2}\epsilon(\omega)\mu(\omega)$ was defined to be the wavevector inside the plane, while $q^2 = k_\perp^2 - \frac{\omega^2}{c^2}$ is taken to be the wavevector in the interspace vacuum. Substituting the solutions Eq. (3.12) into the second order differential equation, Eq. (3.10), we then obtain:

$$\begin{aligned}
\nabla^2 \vec{e}_p(z, k_\perp) e^{i\vec{k}_\perp \cdot \vec{r}_\perp} + \frac{\omega^2}{c^2} \vec{e}_p(z, k_\perp) e^{i\vec{k}_\perp \cdot \vec{r}_\perp} \epsilon(\omega)\mu(\omega) &= 0 \\
-k_x^2 \vec{e}_p(z, k_\perp) e^{i\vec{k}_\perp \cdot \vec{r}_\perp} - k_y^2 \vec{e}_p(z, k_\perp) e^{i\vec{k}_\perp \cdot \vec{r}_\perp} \\
+ e^{i\vec{k}_\perp \cdot \vec{r}_\perp} \vec{e}_p''(z, k_\perp) + \frac{\omega^2}{c^2} \vec{e}_p(z, k_\perp) e^{i\vec{k}_\perp \cdot \vec{r}_\perp} \epsilon(\omega)\mu(\omega) &= 0 \\
-k_x^2 \vec{e}_p(z, k_\perp) - k_y^2 \vec{e}_p(z, k_\perp) + \vec{e}_p''(z, k_\perp) + \frac{\omega^2}{c^2} \vec{e}_p(z, k_\perp) \epsilon(\omega)\mu(\omega) &= 0 \\
\vec{e}_p''(z, k_\perp) - \vec{e}_p(z, k_\perp) k^2 &= 0
\end{aligned} \tag{3.13}$$

Similarly, the solutions Eq. (3.12) may be substituted into the magnetic part of second order differential equation, Eq. (3.11) to obtain Eq. (3.14):

$$\begin{aligned}
& \nabla^2 \vec{g}_p(z, k_\perp) e^{i\vec{k}_\perp \cdot \vec{r}_\perp} + \frac{\omega^2}{c^2} \vec{g}_p(z, k_\perp) e^{i\vec{k}_\perp \cdot \vec{r}_\perp} \varepsilon(\omega) \mu(\omega) = 0 \\
& -k_x^2 \vec{g}_p(z, k_\perp) e^{i\vec{k}_\perp \cdot \vec{r}_\perp} - k_y^2 \vec{g}_p(z, k_\perp) e^{i\vec{k}_\perp \cdot \vec{r}_\perp} \\
& + \vec{g}_p''(z, k_\perp) e^{i\vec{k}_\perp \cdot \vec{r}_\perp} + \frac{\omega^2}{c^2} \vec{g}_p(z, k_\perp) e^{i\vec{k}_\perp \cdot \vec{r}_\perp} \varepsilon(\omega) \mu(\omega) = 0 \\
& -k_x^2 \vec{g}_p(z, k_\perp) - k_y^2 \vec{g}_p(z, k_\perp) + \vec{g}_p''(z, k_\perp) + \frac{\omega^2}{c^2} \vec{g}_p(z, k_\perp) \varepsilon(\omega) \mu(\omega) = 0 \\
& \vec{g}_p''(z, k_\perp) - k^2 \vec{g}_p(z, k_\perp) = 0 \quad (3.14)
\end{aligned}$$

On the other hand, the orthonormal set of solutions Eq. (3.12) may also be substituted into the first and third Maxwell equations in Eq. (3.7), which then gives the equations for projections of \vec{e}_p and \vec{g}_p on x , y , and z axes.

$$\begin{aligned}
& \nabla \cdot \vec{E}(\vec{r}) = 0 \\
& \nabla \cdot \vec{e}_p(z, k_\perp) e^{i\vec{k}_\perp \cdot \vec{r}_\perp} = 0 \\
& \frac{\partial}{\partial x} e_{p,x}(z, k_\perp) e^{i\vec{k}_\perp \cdot \vec{r}_\perp} + \frac{\partial}{\partial y} e_{p,y}(z, k_\perp) e^{i\vec{k}_\perp \cdot \vec{r}_\perp} + \frac{\partial}{\partial z} e_{p,z}(z, k_\perp) e^{i\vec{k}_\perp \cdot \vec{r}_\perp} = 0 \\
& ik_x e_{p,x}(z, k_\perp) + ik_y e_{p,y}(z, k_\perp) + e'_{p,z}(z, k_\perp) = 0 \quad (3.15)
\end{aligned}$$

$$\begin{aligned}
& \nabla \cdot \vec{H}(\vec{r}) = 0 \\
& \nabla \cdot \vec{g}_p(z, k_\perp) e^{i\vec{k}_\perp \cdot \vec{r}_\perp} = 0 \\
& \frac{\partial}{\partial x} g_{p,x}(z, k_\perp) e^{i\vec{k}_\perp \cdot \vec{r}_\perp} + \frac{\partial}{\partial y} g_{p,y}(z, k_\perp) e^{i\vec{k}_\perp \cdot \vec{r}_\perp} + \frac{\partial}{\partial z} g_{p,z}(z, k_\perp) e^{i\vec{k}_\perp \cdot \vec{r}_\perp} = 0 \\
& ik_x g_{p,x}(z, k_\perp) + ik_y g_{p,y}(z, k_\perp) + g'_{p,z}(z, k_\perp) = 0 \quad (3.16)
\end{aligned}$$

With these equations in place, we may then attempt to satisfy the boundary conditions Eq. (3.2). We start by considering the electric field and electric displacement boundary conditions, which will then result in the magnetic mode-generating function. For the first boundary condition, we have:

$$\begin{aligned}
& E_{1t} = E_{2t} \\
& \vec{E}_{1t} \left(z = \pm \frac{l}{2} \right) = \vec{E}_{2t} \left(z = \pm \frac{l}{2} \right) \\
& \vec{e}_{p,1t} \left(\pm \frac{l}{2}, k_\perp \right) e^{i\vec{k}_\perp \cdot \vec{r}_\perp} = \vec{e}_{p,2t} \left(\pm \frac{l}{2}, k_\perp \right) e^{i\vec{k}_\perp \cdot \vec{r}_\perp} \\
& \vec{e}_{p,1t} \left(\pm \frac{l}{2}, k_\perp \right) = \vec{e}_{p,2t} \left(\pm \frac{l}{2}, k_\perp \right) \quad (3.17)
\end{aligned}$$

This condition is equivalent to both $e_{p,x}$, and $e_{p,y}$ being continuous when crossing the boundaries $z = \pm \frac{l}{2}$. From Eq. (3.15), it is noted that these conditions are satisfied with $e'_{p,z}$ being continuous at boundaries $z = \pm \frac{l}{2}$.

For the second boundary condition in Eq. (3.2),

$$\begin{aligned}
D_{1n} &= D_{2n} \\
\vec{E}_{1n} \left(z = \pm \frac{l}{2} \right) \varepsilon_0 \varepsilon_1(\omega) &= \vec{E}_{2n} \left(z = \pm \frac{l}{2} \right) \varepsilon_0 \varepsilon_2(\omega) \\
\vec{e}_{p,1n} \left(\pm \frac{l}{2}, k_{\perp} \right) e^{i\vec{k}_{\perp} \cdot \vec{r}_{\perp}} \varepsilon_1(\omega) &= \vec{e}_{p,2n} \left(\pm \frac{l}{2}, k_{\perp} \right) e^{i\vec{k}_{\perp} \cdot \vec{r}_{\perp}} \varepsilon_2(\omega) \\
\vec{e}_{p,1n} \left(\pm \frac{l}{2}, k_{\perp} \right) \varepsilon_1(\omega) &= \vec{e}_{p,2n} \left(\pm \frac{l}{2}, k_{\perp} \right) \varepsilon_2(\omega)
\end{aligned} \tag{3.18}$$

In Eq. (3.18), ε_1 and ε_2 are arbitrary dielectric functions for materials on each side of the boundary. The condition in Eq. (3.18) is equivalent to $\varepsilon(\omega)e_{p,z}$ being continuous while crossing the boundaries $z = \pm \frac{l}{2}$. It is noteworthy to mention that $e_{TE,z} = 0$ due to the definition of transverse electric component of electromagnetic field. With all these information, the solution for Eq. (3.13) for z direction may be written as exponentially decreasing solutions:

$$e_{TM,z}(z, k_{\perp}) = \begin{cases} C_1(k_{\perp}) e^{kz}, & z < -l/2 \\ C_2(k_{\perp}) e^{qz} + C_3(k_{\perp}) e^{-qz}, & |z| < l/2 \\ C_4(k_{\perp}) e^{-kz}, & z > l/2 \end{cases} \tag{3.19}$$

The continuity of $\varepsilon(\omega)e_{TM,z}$ and $e'_{TM,z}$ at $z = \pm l/2$ then implies the following system of equations:

$$\begin{aligned}
C_1 k e^{-kl/2} &= C_2 q e^{-ql/2} - C_3 q e^{ql/2} \\
-C_4 k e^{-kl/2} &= C_2 q e^{ql/2} - C_3 q e^{-ql/2} \\
C_1 \varepsilon_A(\omega) e^{-kl/2} &= C_2 e^{-ql/2} + C_3 e^{ql/2} \\
C_4 \varepsilon_B(\omega) e^{-kl/2} &= C_2 e^{ql/2} + C_3 e^{-ql/2}
\end{aligned} \tag{3.20}$$

By putting the system of equations in matrix form, we have:

$$\begin{pmatrix} -k e^{-kl/2} & q e^{-ql/2} & -q e^{ql/2} & 0 \\ 0 & q e^{ql/2} & -q e^{-ql/2} & k e^{-kl/2} \\ -\varepsilon_A(\omega) e^{-kl/2} & e^{-ql/2} & e^{ql/2} & 0 \\ 0 & e^{ql/2} & e^{-ql/2} & -\varepsilon_B(\omega) e^{-kl/2} \end{pmatrix} \begin{pmatrix} C_1 \\ C_2 \\ C_3 \\ C_4 \end{pmatrix} = \begin{pmatrix} 0 \\ 0 \\ 0 \\ 0 \end{pmatrix} \tag{3.21}$$

The system of equations (3.20) will have non-trivial solution if and only if the first matrix on the left hand side of Eq. (3.21) have determinant of zero. With that, we may simplify the determinant to obtain Eq. (3.22).

$$\Delta^{TM}(\omega, k_{\perp}) = e^{-kl} \left[(\epsilon_A q + k)(\epsilon_B q + k) e^{ql} - (\epsilon_A q - k)(\epsilon_B q - k) e^{-ql} \right] = 0 \quad (3.22)$$

Similar mathematical treatment may be done to satisfy the boundary conditions Eq. (3.2), for \vec{B} and \vec{H} fields, which ultimately results in the electric mode-generating function. For the third boundary condition,

$$\begin{aligned} B_{1n} &= B_{2n} \\ \mu_0 \mu_1(\omega) \vec{g}_{p,1n}(\pm \frac{l}{2}, k_{\perp}) e^{i\vec{k}_{\perp} \cdot \vec{r}_{\perp}} &= \mu_0 \mu_2(\omega) \vec{g}_{p,2n}(\pm \frac{l}{2}, k_{\perp}) e^{i\vec{k}_{\perp} \cdot \vec{r}_{\perp}} \\ \mu_1(\omega) \vec{g}_{p,1n}(\pm \frac{l}{2}, k_{\perp}) &= \mu_2(\omega) \vec{g}_{p,2n}(\pm \frac{l}{2}, k_{\perp}) \end{aligned} \quad (3.23)$$

In Eq. (3.23), μ_1 and μ_2 are arbitrary permeability for materials on each side of the boundary. Again, the condition in Eq. (3.23) is equivalent to $\mu(\omega) g_{p,z}$ being continuous while crossing the boundaries $z = \pm l/2$. Also, it is noteworthy to mention that $g_{TM,z} = 0$ due to the definition of transverse magnetic component of electromagnetic field.

For the last boundary condition in Eq. (3.2),

$$\begin{aligned} H_{1t} &= H_{2t} \\ \vec{g}_{p,1t}(\pm \frac{l}{2}, k_{\perp}) e^{i\vec{k}_{\perp} \cdot \vec{r}_{\perp}} &= \vec{g}_{p,2t}(\pm \frac{l}{2}, k_{\perp}) e^{i\vec{k}_{\perp} \cdot \vec{r}_{\perp}} \\ \vec{g}_{p,1t}(\pm \frac{l}{2}, k_{\perp}) &= \vec{g}_{p,2t}(\pm \frac{l}{2}, k_{\perp}) \end{aligned} \quad (3.24)$$

This condition is equivalent to both $g_{p,x}$ and $g_{p,y}$ being continuous when crossing the boundaries $z = \pm l/2$. By comparing with Eq. (3.16), it is noted that these conditions may be satisfied if $g'_{p,z}$ is continuous while crossing the boundaries $z = \pm l/2$. With all these information, the solution for Eq. (3.14) for z direction may be written as below.

$$g_{TE,z}(z, k_{\perp}) = \begin{cases} C_5(k_{\perp}) e^{kz}, & z < -l/2 \\ C_6(k_{\perp}) e^{qz} + C_7(k_{\perp}) e^{-qz}, & |z| < l/2 \\ C_8(k_{\perp}) e^{-kz}, & z > l/2 \end{cases} \quad (3.25)$$

The continuity of $g'_{p,z}$ and $\mu(\omega)g_{p,z}$ at $z = \pm l/2$ then implies the following system of equations:

$$\begin{aligned}
C_5 k e^{-kl/2} &= C_6 q e^{-ql/2} - C_7 q e^{ql/2} \\
-C_8 k e^{-kl/2} &= C_6 q e^{ql/2} - C_7 q e^{-ql/2} \\
C_5 \mu_A(\omega) e^{-kl/2} &= C_6 e^{-ql/2} + C_7 e^{ql/2} \\
C_8 \mu_B(\omega) e^{-kl/2} &= C_6 e^{ql/2} + C_7 e^{-ql/2}
\end{aligned} \tag{3.26}$$

Again, by putting the system of equations Eq. (3.26) in matrix form:

$$\begin{pmatrix} -k e^{-kl/2} & q e^{-ql/2} & -q e^{ql/2} & 0 \\ 0 & q e^{ql/2} & -q e^{-ql/2} & k e^{-kl/2} \\ -\mu_A(\omega) e^{-kl/2} & e^{-ql/2} & e^{ql/2} & 0 \\ 0 & e^{ql/2} & e^{-ql/2} & -\mu_B(\omega) e^{-kl/2} \end{pmatrix} \begin{pmatrix} C_5 \\ C_6 \\ C_7 \\ C_8 \end{pmatrix} = \begin{pmatrix} 0 \\ 0 \\ 0 \\ 0 \end{pmatrix} \tag{3.27}$$

The system of equations (3.26) will then have non-trivial solution if and only if the first matrix on the left hand side of Eq. (3.27) have determinant of zero. With that, we may simplify the determinant to obtain Eq. (3.28).

$$\Delta^{TE}(\omega, k_{\perp}) = e^{-kl} \left[(\mu_A q + k)(\mu_B q + k) e^{ql} - (\mu_A q - k)(\mu_B q - k) e^{-ql} \right] = 0 \tag{3.28}$$

The solution to both transcendental equations Eq. (3.22) and Eq. (3.28) are the photon eigenfrequencies, $\omega_{k_{\perp},n}^{TM}$ and $\omega_{k_{\perp},n}^{TE}$. Hence both Δ^{TE} and Δ^{TM} are known as the mode-generating function. It should be noted that the eigenfrequencies $\omega_{k_{\perp},n}^{TM}$ and $\omega_{k_{\perp},n}^{TE}$ are usually complex. However we may neglect the imaginary parts of the photon eigenfrequencies, as justified by Barash and Ginzburg (1975). In terms of unknown photon eigenfrequencies, the vacuum energy of electromagnetic field at zero temperature is then given by Eq. (3.29).

$$\frac{E_0(l)}{S} = \frac{\hbar}{4\pi} \int_0^{\infty} k_{\perp} dk_{\perp} \sum_n (\omega_{k_{\perp},n}^{TM} + \omega_{k_{\perp},n}^{TE}) \tag{3.29}$$

Here, S is the surface area on the plates. By using the argument principle in the form of Eq. (3.30) (Ahlfors, 1979), the mode generating functions are solved by integrating over a semicircle C_+ , of infinite radius, on the right half of complex plane ω . The right hand side summation of Eq. (3.29) may then be written as Eq. (3.31).

$$\sum_n g(a_n) - \sum_m g(b_m) = \frac{1}{2\pi i} \oint_{C_+} g(z) d \ln \Delta(z) \tag{3.30}$$

$$\sum_n \omega_{k_\perp, n}^{TM, TE} = \frac{1}{2\pi i} \left[\int_{i\infty}^{-i\infty} \omega d [\ln \Delta^{TM, TE}(\omega, k_\perp)] + \int_{C_+} \omega d [\ln \Delta^{TM, TE}(\omega, k_\perp)] \right] \quad (3.31)$$

The second integral in right hand side of Eq. (3.31) may be evaluated by using the natural assumption in Eq. (3.32). The assumption is based on the fact that all real materials are transparent for very high frequency electromagnetic radiations.

$$\begin{aligned} \lim_{\omega \rightarrow \infty} \varepsilon(\omega) &= 1 \\ \lim_{\omega \rightarrow \infty} \frac{d\varepsilon(\omega)}{\varepsilon(\omega)} &= 0 \end{aligned} \quad (3.32)$$

From the phase velocity relationship, it is noted that as $\omega \rightarrow \infty$, $k \rightarrow \infty$. Also, as $\omega \rightarrow \infty$, $q \rightarrow \infty$. It is evident that the mode-generating functions will go to infinity, but notice that it does not depend on l , as demonstrated below.

$$\begin{aligned} \lim_{\omega \rightarrow \infty} \Delta^{TM}(\omega, k_\perp) &= \lim_{\omega \rightarrow \infty} e^{-kl} \left[(\varepsilon q + k)^2 e^{ql} - (\varepsilon q - k)^2 e^{-ql} \right] \\ &= \infty \end{aligned} \quad (3.33)$$

By introducing the imaginary frequency, $\omega = i\xi$, and by setting the second integration in Eq. (3.31) to be $Q(\omega, k_\perp)$, Eq. (3.31) can then be written as Eq. (3.34).

$$\begin{aligned} \sum_n \omega_{k_\perp, n}^{TM, TE} &= \frac{1}{2\pi i} \left[\int_{i\infty}^{-i\infty} \omega d [\ln \Delta^{TM, TE}(\omega, k_\perp)] + \int_{C_+} \omega d [\ln \Delta^{TM, TE}(\omega, k_\perp)] \right] \\ &= \frac{1}{2\pi} \int_{\infty}^{-\infty} \xi d [\ln \Delta^{TM, TE}(i\xi, k_\perp)] + Q(\xi, k_\perp) \end{aligned} \quad (3.34)$$

It is noted that the energy given by Eq. (3.29) and Eq. (3.34) are infinite. The finite Casimir energy per unit area of the boundary plate $z = \pm l/2$ is obtained by subtracting the energy when both plate are infinitely separated, $\lim_{l \rightarrow \infty} E_0(l)$ from $E_0(l)$. The subtraction process is equivalent to the dropping of the integral $Q(\omega, k_\perp)$ and the replacement of $\Delta^{TM, TE}(i\xi, k_\perp)$ with $\Delta_l^{TM, TE} / \Delta_\infty^{TM, TE}$. This replacement step may be justified by using a simple expansion process involving differentials. Here, both TM and TE terms are

combined to simplify the derivation, as differentials are linear. We have

$$\begin{aligned}
& \int_{-\infty}^{\infty} \xi d \left[\ln \Delta_l^{TM,TE} \right] - \int_{-\infty}^{\infty} \xi d \left[\ln \Delta_{\infty}^{TM,TE} \right] \\
&= \int_{-\infty}^{\infty} \xi \left[\frac{1}{\Delta_l^{TM,TE}} \frac{d\Delta_l^{TM,TE}}{d(i\xi)} d(i\xi) + \frac{1}{\Delta_l^{TM,TE}} \frac{d\Delta_l^{TM,TE}}{dk_{\perp}} d(k_{\perp}) \right] \\
&\quad - \int_{-\infty}^{\infty} \xi \left[\frac{1}{\Delta_{\infty}^{TM,TE}} \frac{d\Delta_{\infty}^{TM,TE}}{d(i\xi)} d(i\xi) + \frac{1}{\Delta_{\infty}^{TM,TE}} \frac{d\Delta_{\infty}^{TM,TE}}{dk_{\perp}} d(k_{\perp}) \right] \\
&= \int_{-\infty}^{\infty} \xi d \left[\ln \frac{\Delta_l^{TM,TE}(i\xi, k_{\perp})}{\Delta_{\infty}^{TM,TE}(i\xi, k_{\perp})} \right] \tag{3.35}
\end{aligned}$$

With all these information in place, the difference in vacuum energy is then given by

$$\begin{aligned}
E(l) &= \frac{E_0(l)}{S} - \lim_{l \rightarrow \infty} \frac{E_0(l)}{S} \\
&= \frac{\hbar}{4\pi} \int_0^{\infty} k_{\perp} dk_{\perp} \left[\left(\frac{1}{2\pi} \int_{-\infty}^{\infty} \xi d \left[\ln \Delta_l^{TM}(i\xi, k_{\perp}) \right] + \xi d \left[\ln \Delta_l^{TE}(i\xi, k_{\perp}) \right] + 2Q(\xi, k_{\perp}) \right) \right. \\
&\quad \left. - \left(\frac{1}{2\pi} \int_{-\infty}^{\infty} \xi d \left[\ln \Delta_{\infty}^{TM}(i\xi, k_{\perp}) \right] + \xi d \left[\ln \Delta_{\infty}^{TE}(i\xi, k_{\perp}) \right] + 2Q(\xi, k_{\perp}) \right) \right] \\
&= \frac{\hbar}{8\pi^2} \int_0^{\infty} k_{\perp} dk_{\perp} \int_{-\infty}^{\infty} \xi d \left[\ln \frac{\Delta_l^{TM}(i\xi, k_{\perp})}{\Delta_{\infty}^{TM}(i\xi, k_{\perp})} + \ln \frac{\Delta_l^{TE}(i\xi, k_{\perp})}{\Delta_{\infty}^{TE}(i\xi, k_{\perp})} \right] \tag{3.36}
\end{aligned}$$

Here, $\Delta_{\infty}^{TM,TE}$ is the mode-generating function when both plates are separated at infinity. They may be computed by taking the limits $l \rightarrow \infty$ (Klimchitskaya, Mohideen, & Mostepanenko, 2000).

$$\begin{aligned}
\Delta_{\infty}^{TM}(\omega, k_{\perp}) &= \lim_{l \rightarrow \infty} e^{-kl} \left[(\epsilon_A q + k)(\epsilon_B q + k) e^{ql} - (\epsilon_A q - k)(\epsilon_B q - k) e^{-ql} \right] \\
&= \lim_{l \rightarrow \infty} \left[(\epsilon_A q + k)(\epsilon_B q + k) e^{(q-k)l} - (\epsilon_A q - k)(\epsilon_B q - k) e^{(-q-k)l} \right] \\
&= (\epsilon_A q + k)(\epsilon_B q + k) e^{(q-k)l} \tag{3.37}
\end{aligned}$$

$$\begin{aligned}
\Delta_{\infty}^{TE}(\omega, k_{\perp}) &= \lim_{l \rightarrow \infty} e^{-kl} \left[(\mu_A q + k)(\mu_B q + k) e^{ql} - (\mu_A q - k)(\mu_B q - k) e^{-ql} \right] \\
&= \lim_{l \rightarrow \infty} \left[(\mu_A q + k)(\mu_B q + k) - (\mu_A q - k)(\mu_B q - k) e^{(-q-k)l} \right] \\
&= (\mu_A q + k)(\mu_B q + k) e^{(q-k)l} \tag{3.38}
\end{aligned}$$

Eq. (3.36) is then solved by using integration by parts to obtain the change in vacuum energy upon introduction of two semispaces. To achieve that, we first expand Eq. (3.36)

by parts:

$$\begin{aligned}
E(l) &= \frac{\hbar}{8\pi^2} \int_0^\infty k_\perp dk_\perp \int_{-\infty}^\infty \xi d \left[\ln \frac{\Delta_l^{TM}(i\xi, k_\perp)}{\Delta_\infty^{TM}(i\xi, k_\perp)} + \ln \frac{\Delta_l^{TE}(i\xi, k_\perp)}{\Delta_\infty^{TE}(i\xi, k_\perp)} \right] \\
&= \frac{\hbar}{8\pi^2} \int_0^\infty k_\perp dk_\perp \left[\left(\ln \frac{\Delta_l^{TM}(i\xi, k_\perp)}{\Delta_\infty^{TM}(i\xi, k_\perp)} + \ln \frac{\Delta_l^{TE}(i\xi, k_\perp)}{\Delta_\infty^{TE}(i\xi, k_\perp)} \right) \frac{\xi^2}{2} \Big|_{\xi=-\infty}^{-\infty} \right. \\
&\quad \left. - \int_{-\infty}^\infty \ln \frac{\Delta_l^{TM}(i\xi, k_\perp)}{\Delta_\infty^{TM}(i\xi, k_\perp)} + \ln \frac{\Delta_l^{TE}(i\xi, k_\perp)}{\Delta_\infty^{TE}(i\xi, k_\perp)} d\xi \right] \tag{3.39}
\end{aligned}$$

Then, the first term on the right hand side of Eq. (3.39) may be evaluated as below.

$$\begin{aligned}
&\left(\ln \frac{\Delta_l^{TM}(i\xi, k_\perp)}{\Delta_\infty^{TM}(i\xi, k_\perp)} + \ln \frac{\Delta_l^{TE}(i\xi, k_\perp)}{\Delta_\infty^{TE}(i\xi, k_\perp)} \right) \frac{\xi^2}{2} \Big|_{\xi=-\infty}^{-\infty} \\
&= \ln \left(\frac{e^{-kl} [(\epsilon_{Aq} + k)(\epsilon_{Bq} + k)e^{ql} - (\epsilon_{Aq} - k)(\epsilon_{Bq} - k)e^{-ql}]}{(\epsilon_{Aq} + k)(\epsilon_{Bq} + k)e^{(q-k)l}} \right. \\
&\quad \left. \times \frac{e^{-kl} [(\mu_{Aq} + k)(\mu_{Bq} + k)e^{ql} - (\mu_{Aq} - k)(\mu_{Bq} - k)e^{-ql}]}{(\mu_{Aq} + k)(\mu_{Bq} + k)e^{(q-k)l}} \right) \frac{\xi^2}{2} \Big|_{\xi=-\infty}^{-\infty} \\
&= \ln \left[\left(1 - \frac{(\epsilon_{Aq} - k)(\epsilon_{Bq} - k)}{(\epsilon_{Aq} + k)(\epsilon_{Bq} + k)} e^{-2ql} \right) \left(1 - \frac{(\mu_{Aq} - k)(\mu_{Bq} - k)}{(\mu_{Aq} + k)(\mu_{Bq} + k)} e^{-2ql} \right) \right] \frac{\xi^2}{2} \Big|_{\xi=-\infty}^{-\infty} \\
&= f(\xi, k) \Big|_{\xi=-\infty}^{-\infty} \\
&= 0 \tag{3.40}
\end{aligned}$$

It was noticed that $k^2 = k_\perp^2 + \frac{\xi^2}{c^2} \epsilon(\omega)$, $q^2 = k_\perp^2 + \frac{\xi^2}{c^2}$ are both even with respect to ξ . Since the function $f(\xi, k)$ only contains terms of ξ^2 , we may conclude that $f(\xi, k)$ is even with respect to ξ , and $f(-\infty, k) - f(\infty, k) = 0$.

Continuing from Eq. (3.39), we have:

$$\begin{aligned}
E(l) &= \frac{\hbar}{8\pi^2} \int_0^\infty k_\perp dk_\perp \left[0 - \int_{-\infty}^\infty \ln \frac{\Delta_l^{TM}(i\xi, k_\perp)}{\Delta_\infty^{TM}(i\xi, k_\perp)} + \ln \frac{\Delta_l^{TE}(i\xi, k_\perp)}{\Delta_\infty^{TE}(i\xi, k_\perp)} d\xi \right] \\
&= \frac{\hbar}{8\pi^2} \int_0^\infty k_\perp dk_\perp \int_{-\infty}^\infty \ln \frac{e^{-kl} [(\epsilon_{Aq} + k)(\epsilon_{Bq} + k)e^{ql} - (\epsilon_{Aq} - k)(\epsilon_{Bq} - k)e^{-ql}]}{(\epsilon_{Aq} + k)(\epsilon_{Bq} + k)e^{(q-k)l}} \\
&\quad + \ln \frac{e^{-kl} [(\mu_{Aq} + k)(\mu_{Bq} + k)e^{ql} - (\mu_{Aq} - k)(\mu_{Bq} - k)e^{-ql}]}{(\mu_{Aq} + k)(\mu_{Bq} + k)e^{(q-k)l}} d\xi \\
&= \frac{\hbar}{4\pi^2} \int_0^\infty k_\perp dk_\perp \int_0^\infty \ln \left(1 - \frac{(\epsilon_{Aq} - k)(\epsilon_{Bq} - k)}{(\epsilon_{Aq} + k)(\epsilon_{Bq} + k)} e^{-2ql} \right) \\
&\quad + \ln \left(1 - \frac{(\mu_{Aq} - k)(\mu_{Bq} - k)}{(\mu_{Aq} + k)(\mu_{Bq} + k)} e^{-2ql} \right) d\xi \\
&= \frac{\hbar}{4\pi^2} \int_0^\infty k_\perp dk_\perp \int_0^\infty d\xi \left[\ln(1 - r_{TM}^A r_{TM}^B e^{-2ql}) + \ln(1 - r_{TE}^A r_{TE}^B e^{-2ql}) \right] \tag{3.41}
\end{aligned}$$

This is the change in vacuum energy upon introduction of two semispaces. Here reflection coefficients, r_{TM}^N and r_{TE}^N are defined as below. It is noted that the reflection coefficients

are same as the familiar Fresnel reflection coefficients.

$$\begin{aligned} r_{TM}^N(i\xi, k_\perp) &= \frac{\varepsilon_N(i\xi)q(i\xi, k_\perp) - k_N(i\xi, k_\perp)}{\varepsilon_N(i\xi)q(i\xi, k_\perp) + k_N(i\xi, k_\perp)} \\ r_{TE}^N(i\xi, k_\perp) &= \frac{\mu_N(i\xi)q(i\xi, k_\perp) - k_N(i\xi, k_\perp)}{\mu_N(i\xi)q(i\xi, k_\perp) + k_N(i\xi, k_\perp)} \end{aligned} \quad (3.42)$$

Finally, the Casimir Pressure is then obtained by differentiating Eq. (3.41) against l .

$$\begin{aligned} F(l) &= -\frac{\partial E(l)}{\partial l} \\ &= -\frac{\hbar}{4\pi^2} \int_0^\infty k_\perp dk_\perp \int_0^\infty d\xi \left(\frac{2r_{TM}^A r_{TM}^B q e^{-2ql}}{1 - r_{TM}^A r_{TM}^B e^{-2ql}} + \frac{2r_{TE}^A r_{TE}^B q e^{-2ql}}{1 - r_{TE}^A r_{TE}^B e^{-2ql}} \right) \\ &= -\frac{\hbar}{2\pi^2} \int_0^\infty k_\perp dk_\perp \int_0^\infty d\xi q \left(\left(\frac{e^{2ql}}{r_{TM}^A r_{TM}^B} - 1 \right)^{-1} + \left(\frac{e^{2ql}}{r_{TE}^A r_{TE}^B} - 1 \right)^{-1} \right) \end{aligned} \quad (3.43)$$

It is noteworthy to recall that $k^2 = k_\perp^2 + \frac{\xi^2}{c^2} \varepsilon(\omega) \mu(\omega)$, $q^2 = k_\perp^2 + \frac{\xi^2}{c^2}$. Furthermore, with some algebraic manipulations, we may arrive at the equations as used by Ooi and Khoo (2012), as below.

$$F(l) = -\frac{\hbar}{2\pi^2} \int_0^\infty k_\perp dk_\perp \int_0^\infty d\xi \sqrt{k_\perp^2 + \frac{\xi^2}{c^2}} \sum_{N=TE, TM} \left(\frac{r_N^A r_N^B e^{-2l\sqrt{k_\perp^2 + \xi^2/c^2}}}{1 - r_N^A r_N^B e^{-2l\sqrt{k_\perp^2 + \xi^2/c^2}}} \right) \quad (3.44)$$

$$\begin{aligned} r_{TM}^N(i\xi, k_\perp) &= \frac{\varepsilon_N \sqrt{k_\perp^2 + \frac{\xi^2}{c^2}} - n_N \sqrt{\frac{k_\perp^2}{n_N^2} + \frac{\xi^2}{c^2}}}{\varepsilon_N \sqrt{k_\perp^2 + \frac{\xi^2}{c^2}} + n_N \sqrt{\frac{k_\perp^2}{n_N^2} + \frac{\xi^2}{c^2}}} \\ r_{TE}^N(i\xi, k_\perp) &= \frac{\mu_N \sqrt{k_\perp^2 + \frac{\xi^2}{c^2}} - n_N \sqrt{\frac{k_\perp^2}{n_N^2} + \frac{\xi^2}{c^2}}}{\mu_N \sqrt{k_\perp^2 + \frac{\xi^2}{c^2}} + n_N \sqrt{\frac{k_\perp^2}{n_N^2} + \frac{\xi^2}{c^2}}} \end{aligned} \quad (3.45)$$

Intuitively, the derivation of Lifshitz theory we have proposed here is somewhat similar to the original derivation by Casimir (1948). The original idea of "difference in vacuum energy" remains intact. However, the validity of Lifshitz theory was sometimes being doubted, although it had been generally accepted now (P. Milonni & Eberlein, 1994). As a sidenote, the Lifshitz theory was reproduced by a variety of methods. In example, Schwinger, DeRaad, and Milton (1978) had obtained similar result as Lifshitz "by adopting far superior and more physically transparent methods for computing the force", by using the source theory, "where the vacuum is regarded as truly a state with all physical properties equal to zero". The derivation of Lifshitz formula from the source theory will be presented in Chapter 4.

3.2 Lifshitz theory & Barash-Ginzburg Theory

In Eq. (3.22) and Eq. (3.28), we have assumed that the solutions of the mode-generating functions are real. This is an oversimplified derivation, as $\epsilon(\omega)$ and $\mu(\omega)$ for real materials are always complex to take into account the absorption of material as required by the Kramers-Kronig relation. With complex dielectric function and permeability taken into account, the sum in Eq. (3.29) is no longer valid. It is noted, however, that the original derivation by Lifshitz takes proper account that the fact that $\epsilon(\omega)$ and $\mu(\omega)$ is generally complex. It is now important to justify the simplification we have taken.

In Lifshitz's original derivation, the use of a complex dielectric function and permeability in Lifshitz theory requires a random field, \vec{K} . This may be explained in terms of fluctuation-dissipation relation: dissipative influence of the medium must be balanced by a fluctuating source term, which correlate to the form of the dissipation and the imaginary part of $\epsilon(\omega)$ and $\mu(\omega)$. It is remarkable (P. Milonni & Eberlein, 1994) that our approach, by completely violating causality may reproduce Lifshitz's result. This raises doubt on this derivation, which was answered by Barash and Ginzburg (1975). It is noted that $\omega_{k\perp,n}^{TM}$ and $\omega_{k\perp,n}^{TE}$ are complex, and the respective eigenfunctions are not orthogonal. According to Barash and Ginzburg (1975), however, both solutions may be expanded in terms of the orthogonal eigenfunctions of some auxiliary electrodynamic system that have real eigenfrequencies. The validity of Eq. (3.29) no longer holds, but the final Eq. (3.43) for Casimir force remains true for complex eigenvalues. Qualitatively, we note that the energy Eq. (3.41) depends only on the dielectric permittivity along the imaginary frequency axis, which is always real. The exact formulation of the auxiliary electrodynamic problem may be found in the article by Barash and Ginzburg (1975), and is beyond the present scope of this thesis.

3.3 Factors affecting the Casimir Force at absolute zero

At this point, it is worthy to look into the Lifshitz Formula, Eq. (3.44) and Eq. (3.45). From Eq. (3.44), the Casimir force between two parallel plate clearly depends on a few factors, i.e.:

- Distance between the plates, l .

- Reflectivity of plate A, r_{TE}^A and r_{TM}^A .
- Reflectivity of plate B, r_{TE}^B and r_{TM}^B .

From Eq. (3.45), the reflectivity coefficient of each plate in turn depends on the material constants, i.e. the dielectric function ϵ , the magnetic permeability μ , and the reflective index n . This result can be compared to the original derivation of Casimir (1948). In Casimir's case, the force between two perfectly conducting plate depends only on geometrical factors. Upon the introduction of arbitrary dielectric function and magnetic permeability, however, shows that the Casimir force in turn depends on the material constants too. In fact, the Lifshitz theory may be reduced to Casimir's original result by taking both plates' permittivity to be infinitely large, i.e. $\epsilon \rightarrow \infty$, μ finite. Using Eq. (3.42), we have

$$\begin{aligned}
\lim_{\epsilon \rightarrow \infty} r_{TE}(i\xi, k_{\perp}) &= \lim_{\epsilon \rightarrow \infty} \frac{\mu q - k}{\mu q + k} \\
&= \lim_{\epsilon \rightarrow \infty} \frac{\mu \sqrt{k_{\perp}^2 + \frac{\xi^2}{c^2}} - \sqrt{k_{\perp}^2 + \frac{\xi^2}{c^2}} \epsilon \mu}{\mu \sqrt{k_{\perp}^2 + \frac{\xi^2}{c^2}} + \sqrt{k_{\perp}^2 + \frac{\xi^2}{c^2}} \epsilon \mu} \\
&= -1
\end{aligned} \tag{3.46}$$

$$\begin{aligned}
\lim_{\epsilon \rightarrow \infty} r_{TM}(i\xi, k_{\perp}) &= \lim_{\epsilon \rightarrow \infty} \frac{\epsilon q - k}{\epsilon q + k} \\
&= \lim_{\epsilon \rightarrow \infty} \frac{\epsilon \sqrt{k_{\perp}^2 + \frac{\xi^2}{c^2}} - \sqrt{k_{\perp}^2 + \frac{\xi^2}{c^2}} \epsilon \mu}{\epsilon \sqrt{k_{\perp}^2 + \frac{\xi^2}{c^2}} + \sqrt{k_{\perp}^2 + \frac{\xi^2}{c^2}} \epsilon \mu} \\
&= 1
\end{aligned} \tag{3.47}$$

Taking a simple limit shows that the reflectivity coefficients of a perfectly conducting plate takes value of $r_{TE} = -1$, and $r_{TM} = 1$. Inserting these values into Eq. (3.44) yields:

$$F(l) = -\frac{\hbar}{\pi^2} \int_0^{\infty} k_{\perp} dk_{\perp} \int_0^{\infty} d\xi \sqrt{k_{\perp}^2 + \frac{\xi^2}{c^2}} \left(\frac{e^{-2l\sqrt{k_{\perp}^2 + \xi^2/c^2}}}{1 - e^{-2l\sqrt{k_{\perp}^2 + \xi^2/c^2}}} \right) \tag{3.48}$$

A coordinate transform was then done from Cartesian coordinate $(k_{\perp}, \xi/c)$ to polar coordinate (r, θ) . We then obtain:

$$\begin{aligned}
 F(l) &= -\frac{\hbar c}{\pi^2} \int_0^{\infty} \left(\frac{r^3 e^{-2lr}}{1 - e^{-2lr}} \right) dr \int_0^{\frac{\pi}{2}} \cos(\theta) d\theta \\
 &= -\frac{\hbar c}{\pi^2} \int_0^{\infty} \left(\frac{r^3 e^{-2lr}}{1 - e^{-2lr}} \right) dr \\
 &= -\frac{\hbar c \pi^2}{240l^4}
 \end{aligned} \tag{3.49}$$

which is identical to Casimir's derivation, Eq. (2.15). The dependence of Casimir force (at absolute zero) on various factors were discussed in depth by researchers such as Kenneth and Klich (2006); Yang et al. (2010), and will be discussed in more details in Chapter 5.

CHAPTER 4

SOURCE THEORY

Julian Schwinger, a Nobel laureate in Physics (1965) began the construction of source theory as a substitute for quantum field theory (QFT) in 1966, in response to the apparent failure of QFT in describing several quantum phenomena, e.g. the strong interactions, and the physical interpretation of the renormalization process (Schwinger, 1968, 1970). Essentially, in the source theory, the free action for a photon is defined in terms of the propagation of virtual photons between photon sources. The free action is conserved in this case, in order to remove the scalar degree of freedom. However, a virtual photon may in turn act as a pair of electron-positron source, through "primitive interaction" between electrons and photons. This multi-particle exchange gives rise to several phenomenon mentioned without any reference to renormalization (Schwinger, 1967).

In 1975, Schwinger became interested in explaining the Casimir effect in source theory language, which unlike Casimir or Lifshitz, "makes no reference to quantum oscillators and their associated zero-point energy" (Schwinger, 1975). His work eventually led to a full rederivation of Lifshitz formula in an elegant manner, by using the Green's function approach (Schwinger et al., 1978). It was noted as the "most unconventional approach to the force between dielectric, and the Casimir force between perfect conductors" (P. Milonni & Eberlein, 1994).

In this chapter, a quick introduction to second quantization, as well as two different operators ordering is introduced. We then look into a full derivation of the Lifshitz formalism using the source theory, making no explicit reference to zero-point energy. Then, the connection between source theory and the vacuum field is made. Next, the energy variation approach to the source theory derivation is outlined, followed by a short discussion.

4.1 Field Quantization and Operator Ordering

In the field theory, it is well established that a field mode (with no external sources) of frequency ω is mathematically equivalent to a harmonic oscillator of the same frequency. Without derivation, we state the Hamiltonian for the field mode with no external source as (P. Milonni & Eberlein, 1994)

$$H_F = \hbar\omega \left(a^\dagger a + \frac{1}{2} \right) \quad (4.1)$$

where a and a^\dagger are the lowering and raising operators for the eigenvectors of the field mode $|n\rangle$, which satisfy the following equations.

$$\begin{aligned} a |n\rangle &= \sqrt{n} |n-1\rangle \\ a^\dagger |n\rangle &= \sqrt{n+1} |n+1\rangle \end{aligned} \quad (4.2)$$

The vector potential in the Maxwell equations is given by

$$\vec{A}(\vec{r}, t) = \sqrt{\frac{\hbar c^2 \mu_0}{2\omega}} \left[a(t) \vec{A}_0(r) + a^\dagger(t) \vec{A}_0^*(\vec{r}) \right] \quad (4.3)$$

where the vector potential \vec{A} is defined by $\vec{B} = \nabla \times \vec{A}$. Here \vec{A}_0 is the spatial variation of $\vec{A}(\vec{r}, t)$, where

$$\vec{A}(\vec{r}, t) = \alpha(0) e^{-i\omega t} \vec{A}_0(r) + \alpha^*(0) e^{i\omega t} \vec{A}_0^*(r) \quad (4.4)$$

Also $\vec{A}_0(r)$ satisfies the Helmholtz equation:

$$\nabla^2 \vec{A}_0(r) + \omega^2 \vec{A}_0(r) = 0 \quad (4.5)$$

From Eq. (4.3), the electric and magnetic field operators may be directly derived.

$$\vec{E}(\vec{r}, t) = i \sqrt{\frac{\hbar\omega}{2\epsilon_0}} \left[a(t) \vec{A}_0(r) - a^\dagger(t) \vec{A}_0^*(\vec{r}) \right] \quad (4.6)$$

$$\vec{B}(\vec{r}, t) = \sqrt{\frac{\hbar c^2 \mu_0}{2\omega}} \left[a(t) \nabla \times \vec{A}_0(r) + a^\dagger(t) \nabla \times \vec{A}_0^*(\vec{r}) \right] \quad (4.7)$$

Now, let's look into the vacuum state $|0\rangle$. The vacuum state has no photons, but it has nonzero energy.

$$\langle 0 | H_F | 0 \rangle = \frac{1}{2} \hbar\omega \quad (4.8)$$

The quantum theory of radiation then predicts the existence of a zero-point electromagnetic field. However, for all stationary states $|n\rangle$, the expectation values of electric and

magnetic field vanishes.

$$\begin{aligned}\langle \vec{E}(\vec{r}, t) \rangle &= i\sqrt{\frac{\hbar\omega}{2\epsilon_0}} \left[\langle n | a(t) \vec{A}_0(r) | n \rangle - \langle n | a^\dagger(t) \vec{A}_0^*(\vec{r}) | n \rangle \right] \\ &= 0\end{aligned}\quad (4.9)$$

$$\begin{aligned}\langle \vec{B}(\vec{r}, t) \rangle &= \sqrt{\frac{\hbar c^2 \mu_0}{2\omega}} \left[\langle n | a(t) \nabla \times \vec{A}_0(r) | n \rangle + \langle n | a^\dagger(t) \nabla \times \vec{A}_0^*(\vec{r}) | n \rangle \right] \\ &= 0\end{aligned}\quad (4.10)$$

This follows naturally since $\langle n | a | n \rangle = \langle n | a^\dagger | n \rangle = 0$. Physically, it means that the electric and magnetic flux fluctuate with a zero mean, although the field have a finite, non-fluctuating energy of $(n + \frac{1}{2}) \hbar\omega$ for each state $|n\rangle$.

The square of electric field, on the other hand have an expectation value of

$$\begin{aligned}\langle \vec{E}^2(\vec{r}, t) \rangle &= -\frac{\hbar\omega}{2\epsilon_0} \left[\langle a(t)^2 \rangle \vec{A}_0(r)^2 - \langle a^\dagger(t) a(t) + a(t) a^\dagger(t) \rangle \right. \\ &\quad \left. \times \left| \vec{A}_0(\vec{r}) \right|^2 + \langle a^\dagger(t)^2 \rangle \vec{A}_0^*(\vec{r})^2 \right]\end{aligned}\quad (4.11)$$

By noticing several relationships, i.e. $\langle a^2 \rangle = \langle a^{\dagger 2} \rangle = 0$, and

$$\begin{aligned}\langle a^\dagger a + a a^\dagger \rangle &= \langle 2a^\dagger a + 1 \rangle \\ &= 2\sqrt{n} \langle n | a^\dagger | n-1 \rangle + 1 \\ &= 2n + 1\end{aligned}\quad (4.12)$$

we can rewrite Eq. (4.11) as

$$\begin{aligned}\langle \vec{E}^2(\vec{r}, t) \rangle &= \frac{\hbar\omega}{2\epsilon_0} (2n + 1) \left| \vec{A}_0(\vec{r}) \right|^2 \\ &= \left(n + \frac{1}{2} \right) \frac{\hbar\omega}{\epsilon_0} \left| \vec{A}_0(\vec{r}) \right|^2 \\ &= \frac{\hbar\omega n}{\epsilon_0} \left| \vec{A}_0(\vec{r}) \right|^2 + \langle \vec{E}^2(\vec{r}) \rangle_0\end{aligned}\quad (4.13)$$

Notice in Eq. (4.13), if we take $n = 0$, $\langle \vec{E}^2(\vec{r}, t) \rangle = \frac{\hbar\omega}{2\epsilon_0} \left| \vec{A}_0(\vec{r}) \right|^2 = \langle \vec{E}^2(\vec{r}) \rangle_0$, which is a constant. This raises a question: what is the physical significance of these vacuum-state expectation values appearing in Eq. (4.1) and Eq. (4.13)? We may interpret this result as an indication that the vacuum-field is a stationary state, with statistical fluctuations of the electric and magnetic fields. However, one may also argue that the entire universe

is immersed in a zero-point field. Hence, taking a measurement will only reveal the difference from the vacuum state. That being said, it is impossible to observe the vacuum-field directly by measurement alone. A simple analogy to this case involves the classical potential field, where only the difference is between two points is meaningful. Hence, the Hamiltonian in Eq. (4.1) can be replaced by

$$\begin{aligned} H_F - \langle 0 | H_F | 0 \rangle &= \hbar\omega \left(aa^\dagger + \frac{1}{2} \right) - \frac{1}{2}\hbar\omega \\ &= \hbar\omega aa^\dagger \end{aligned} \quad (4.14)$$

without affecting the predicting power of the theory. This Hamiltonian is said to be in normal ordering. A product of quantum fields are said to be normally ordered (Wick ordered) when all creation operators, a^\dagger are to the left of all annihilation operators, a , in the product. The normally ordered Hamiltonian is usually denoted as $:H_F:$.

As we can see, the normal ordering process eliminates contributions from the zero-point field. This is a reasonable move, as the zero-point term merely adds a constant energy, which can be eliminated by simple redefinition of the energy of zero-point. This leads to the source theory interpretation of Casimir effect, which we will see in the next section. Another ordering procedure that we might be interested is the symmetric ordering. In this scheme, the creation and annihilation operators appear in the combination that defines the vector potential, and it will be discussed in details in Section 4.3.

4.2 Casimir Force in Source Theory

In Section 3.1, the Lifshitz equation was derived by field theory approach, with explicit reference to zero-point energy. In this section, we set forward to rederive the Casimir Effect between two parallel dielectric plate via the source theory approach (P. Milonni & Eberlein, 1994).

First, an induced dipole \vec{d} in an electric field \vec{E} has an energy of $-\frac{1}{2}\vec{d} \cdot \vec{E}$, and for N dipoles per unit volume, the polarization is given by $\vec{P} = N\vec{d}$. Hence, the expectation value of the electromagnetic energy is given as below.

$$\langle E \rangle = -\frac{1}{2} \int d^3r \langle \vec{P} \cdot \vec{E} \rangle \quad (4.15)$$

To emphasise the role of source field, a normal ordering of field operators was used. In essence, the conditions in Eq. (4.16) were used to rewrite Eq. (4.15) into Eq. (4.17).

Physically, we may recall from previous section that the normal ordering removes the contribution of zero-point energy from the Hamiltonian. This is the key in source theory's derivation of Casimir effect, as we may see later that a different ordering may result in an entirely different interpretation.

$$\begin{aligned}\vec{E} &= \vec{E}^{(+)} + \vec{E}^{(-)} + \langle \vec{E} \rangle \\ \vec{E}^{(-)} |\Psi\rangle &= 0 \\ \langle \Psi | \vec{E}^{(+)} &= 0\end{aligned}\tag{4.16}$$

$$\langle E \rangle = -\frac{1}{2} \int d^3r \langle \vec{E}^{(-)} \cdot \vec{P} + \vec{P} \cdot \vec{E}^{(+)} \rangle\tag{4.17}$$

Here, $\vec{E}^{(+)}$ is the "positive frequency" (photon annihilation) part of \vec{E} , while $\vec{E}^{(-)}$ is the "negative frequency" (photon creation) part. Also the electric field was separated into both the source free, and sourced part by Eq. (4.18).

$$\vec{E}^{(+)}(\vec{r}, t) = \vec{E}_o^{(+)}(\vec{r}, t) + \vec{E}_s^{(+)}(\vec{r}, t)\tag{4.18}$$

Here, $\vec{E}_o^{(+)}(\vec{r}, t)$ is source free (vacuum) part of $\vec{E}^{(+)}(\vec{r}, t)$, while $\vec{E}_s^{(+)}(\vec{r}, t)$ is the part due to any sources. Eq. (4.17) may then be rewritten as below.

$$\begin{aligned}\langle E \rangle &= -\frac{1}{2} \int \langle \vec{E}^{(-)} \cdot \vec{P} + \vec{P} \cdot \vec{E}^{(+)} \rangle d^3r \\ &= -\frac{1}{2} \int \langle \vec{E}^{(-)} \cdot \vec{P} + \vec{P} \cdot \vec{E}_o^{(+)} + \vec{P} \cdot \vec{E}_s^{(+)} + \vec{E}_s^{(-)} \cdot \vec{P} \rangle d^3r \\ &= -\frac{1}{2} \int \langle \vec{E}^{(-)} \cdot \vec{P} \rangle + \langle \vec{P} \cdot \vec{E}_o^{(+)} \rangle + \langle \vec{P} \cdot \vec{E}_s^{(+)} \rangle + \langle \vec{E}_s^{(-)} \cdot \vec{P} \rangle d^3r\end{aligned}\tag{4.19}$$

Since we have used the normal-ordering, the source-free vacuum expectation energy will be zero, i.e.:

$$\begin{aligned}\vec{E}_o^{(+)} |0\rangle &= 0 \\ \langle 0 | \vec{E}_o^{(-)} &= 0\end{aligned}\tag{4.20}$$

which simplifies the expectation value of energy to:

$$\langle E \rangle = -\frac{1}{2} \int \langle \vec{P} \cdot \vec{E}_s^{(+)} \rangle + \langle \vec{E}_s^{(-)} \cdot \vec{P} \rangle d^3r\tag{4.21}$$

To obtain an expression for $\vec{E}_s^{(+)}(\vec{r}, t)$, we first recall that the electric field operator may be written as an expansion in terms of mode functions, $\vec{A}_\alpha(\vec{r})$. Here the field modes, which are taken to form a complete set, are labelled with the subscript α .

$$\vec{E}(\vec{r}, t) = i \sum_{\alpha} \sqrt{\frac{\hbar \omega_{\alpha}}{2\epsilon_0}} \left[a_{\alpha}(t) \vec{A}_{\alpha}(\vec{r}) - a_{\alpha}^{\dagger}(t) \vec{A}_{\alpha}^*(\vec{r}) \right]\tag{4.22}$$

It is recalled that the electromagnetic interaction term is given by (P. Milonni & Eberlein, 1994):

$$H_{INT} = - \int d^3 r \vec{P}(\vec{r}, t) \cdot \vec{E}(\vec{r}, t) \quad (4.23)$$

In the above equation, the $\vec{j} \cdot \vec{A}$ term had been omitted (where \vec{j} is the current density inside the material, and \vec{A} is the magnetic vector potential). This is justified as we are considering dielectric materials with no free charge inside the material. Mathematically, we have $\vec{j} = 0$.

With this, the full Hamiltonian for the field may be written as a sum of the interaction term and the oscillator term.

$$\begin{aligned} H_T &= H_{OSC} + H_{INT} \\ &= \frac{1}{2} \hbar \omega \left(a a^\dagger + a^\dagger a \right) - \int d^3 r \vec{P}(\vec{r}, t) \cdot \vec{E}(\vec{r}, t) \end{aligned} \quad (4.24)$$

The Heisenberg equation of motion is then applied on $a_\alpha(t)$. Here, both commutation relations, i.e. $[a_\alpha(t), H_{OSC}]$ and $[a_\alpha(t), H_{INT}]$ must be first evaluated. We start off by first computing $[a_\alpha(t), H_{OSC}]$.

$$\begin{aligned} [a_\alpha(t), H_{OSC}] &= a_\alpha(t) H_{OSC} - H_{OSC} a_\alpha(t) \\ &= \frac{1}{2} \hbar \omega_\alpha a_\alpha(t) \left(a_\alpha(t) a_\alpha^\dagger(t) + a_\alpha^\dagger(t) a_\alpha(t) \right) \\ &\quad - \frac{1}{2} \hbar \omega_\alpha \left(a_\alpha(t) a_\alpha^\dagger(t) + a_\alpha^\dagger(t) a_\alpha(t) \right) a_\alpha(t) \\ &= \frac{1}{2} \hbar \omega_\alpha \left[a_\alpha(t) a_\alpha(t) a_\alpha^\dagger(t) - a_\alpha^\dagger(t) a_\alpha(t) a_\alpha(t) \right] \end{aligned} \quad (4.25)$$

The commutation relation between a_α and a_α^\dagger , i.e. $[a_\alpha, a_\alpha^\dagger] = 1$ is then used. With this, we have

$$\begin{aligned} [a_\alpha(t), H_{OSC}] &= \frac{1}{2} \hbar \omega_\alpha \left[a_\alpha(t) \left(1 + a_\alpha^\dagger(t) a_\alpha(t) \right) - a_\alpha^\dagger(t) a_\alpha(t) a_\alpha(t) \right] \\ &= \frac{1}{2} \hbar \omega_\alpha \left[a_\alpha(t) + a_\alpha(t) a_\alpha^\dagger(t) a_\alpha(t) - a_\alpha^\dagger(t) a_\alpha(t) a_\alpha(t) \right] \\ &= \frac{1}{2} \hbar \omega_\alpha \left[a_\alpha(t) + \left(1 + a_\alpha^\dagger(t) a_\alpha(t) \right) a_\alpha(t) - a_\alpha^\dagger(t) a_\alpha(t) a_\alpha(t) \right] \\ &= \hbar \omega_\alpha a_\alpha(t) \end{aligned} \quad (4.26)$$

It is noteworthy to know that the evaluation of commutation relation $[a_\alpha(t), H_{OSC}]$ is

usually shown in standard text. Next, we set off to evaluate $[a_\alpha(t), H_{INT}]$.

$$\begin{aligned}
[a_\alpha(t), H_{INT}] &= - \int d^3r \left(a_\alpha(t) \vec{P}(\vec{r}, t) \cdot \vec{E}(\vec{r}, t) - \vec{P}(\vec{r}, t) \cdot \vec{E}(\vec{r}, t) a_\alpha(t) \right) \\
&= - \int d^3r \left(a_\alpha(t) \vec{P}(\vec{r}, t) \cdot i \sum_\beta \sqrt{\frac{\hbar \omega_\beta}{2\epsilon_0}} \left[a_\beta(t) \vec{A}_\beta(\vec{r}) - a_\beta^\dagger(t) \vec{A}_\beta^*(\vec{r}) \right] \right. \\
&\quad \left. - \vec{P}(\vec{r}, t) \cdot i \sum_\beta \sqrt{\frac{\hbar \omega_\beta}{2\epsilon_0}} \left[a_\beta(t) \vec{A}_\beta(\vec{r}) - a_\beta^\dagger(t) \vec{A}_\beta^*(\vec{r}) \right] a_\alpha(t) \right) \\
&= -i \sum_\beta \sqrt{\frac{\hbar \omega_\beta}{2\epsilon_0}} \int d^3r \left[(a_\alpha(t) a_\beta(t) - a_\beta(t) a_\alpha(t)) \vec{P}(\vec{r}, t) \cdot \vec{A}_\beta(\vec{r}) \right. \\
&\quad \left. - (a_\alpha(t) a_\beta^\dagger(t) - a_\beta^\dagger(t) a_\alpha(t)) \vec{P}(\vec{r}, t) \cdot \vec{A}_\beta^*(\vec{r}) \right] \tag{4.27}
\end{aligned}$$

Here, the operator terms are basically:

$$\begin{aligned}
a_\alpha(t) a_\beta(t) - a_\beta(t) a_\alpha(t) &= \delta_{\alpha\beta} - \delta_{\beta\alpha} \\
&= 0 \tag{4.28}
\end{aligned}$$

$$\begin{aligned}
a_\alpha(t) a_\beta^\dagger(t) - a_\beta^\dagger(t) a_\alpha(t) &= [a_\alpha(t), a_\beta^\dagger(t)] \\
&= \delta_{\alpha\beta} \tag{4.29}
\end{aligned}$$

Substituting into Eq. (4.27),

$$\begin{aligned}
[a_\alpha(t), H_{INT}] &= i \sum_\beta \sqrt{\frac{\hbar \omega_\beta}{2\epsilon_0}} \int d^3r \delta_{\alpha\beta} \vec{P}(\vec{r}, t) \cdot \vec{A}_\beta^*(\vec{r}) \\
&= i \sqrt{\frac{\hbar \omega_\alpha}{2\epsilon_0}} \int d^3r \vec{P}(\vec{r}, t) \cdot \vec{A}_\alpha^*(\vec{r}) \tag{4.30}
\end{aligned}$$

With both commutation relation in place, the Heisenberg equation of motion for $a_\alpha(t)$ may then be written as:

$$\begin{aligned}
i\hbar \frac{da_\alpha(t)}{dt} &= [a_\alpha(t), H_T] \\
&= [a_\alpha(t), H_{OSC}] + [a_\alpha(t), H_{INT}] \\
&= \hbar \omega_\alpha a_\alpha(t) + i \sqrt{\frac{\hbar \omega_\alpha}{2\epsilon_0}} \int d^3r \vec{P}(\vec{r}, t) \cdot \vec{A}_\alpha^*(\vec{r}) \\
a'_\alpha(t) &= -i \omega_\alpha a_\alpha(t) + \sqrt{\frac{\omega_\alpha}{2\hbar \epsilon_0}} \int d^3r \vec{P}(\vec{r}, t) \cdot \vec{A}_\alpha^*(\vec{r}) \tag{4.31}
\end{aligned}$$

Eq. (4.31) is basically a non-homogenous first order differential equation, which takes the form of

$$a'_\alpha(t) + C_1 a(t) = C_2 f(\vec{r}, t) \tag{4.32}$$

where the dummy variables in this case, $C_1 = -i\omega_\alpha$ and $C_2 f(\vec{r}, t)$ is the last part of Eq. (4.31). The solution of Eq. (4.32) is simply as below, with C as the integration constant (Arfken, Weber, & Harris, 2005).

$$a(t) = e^{-C_1 t} \left[\int C_2 f(\vec{r}, t) e^{C_1 t} dt + C \right] \quad (4.33)$$

The solution Eq. (4.33) is applied to Eq. (4.31) to obtain Eq. (4.34) The subscript s is given to denote the source part of $a_\alpha(t)$.

$$a_{\alpha s}(t) = e^{-i\omega_\alpha t} \left[\int \sqrt{\frac{\omega_\alpha}{2\hbar\epsilon_0}} \int d^3 r \vec{A}_\alpha^*(\vec{r}) \cdot \vec{P}(\vec{r}, t) e^{i\omega_\alpha t} dt + C \right] \quad (4.34)$$

The initial condition $a_{\alpha s}(0) = 0$ is then applied to remove the constant of integration C .

$$\begin{aligned} a_{\alpha s}(0) &= \sqrt{\frac{\omega_\alpha}{2\hbar\epsilon_0}} \int \int d^3 r \vec{A}_\alpha^*(\vec{r}) \cdot \vec{P}(\vec{r}, t) e^{i\omega_\alpha t} dt + C = 0 \\ C &= - \sqrt{\frac{\omega_\alpha}{2\hbar\epsilon_0}} \int \int d^3 r \vec{A}_\alpha^*(\vec{r}) \cdot \vec{P}(\vec{r}, t) e^{i\omega_\alpha t} dt \Big|_{t=0} \end{aligned} \quad (4.35)$$

The final form of $a_{\alpha s}(t)$ then is given by:

$$\begin{aligned} a_\alpha(t) &= e^{-i\omega_\alpha t} \sqrt{\frac{\omega_\alpha}{2\hbar\epsilon_0}} \int \int d^3 r \vec{A}_\alpha^*(\vec{r}) \cdot \vec{P}(\vec{r}, t) e^{i\omega_\alpha t} dt \\ &\quad - \sqrt{\frac{\omega_\alpha}{2\hbar\epsilon_0}} \int \int d^3 r \vec{A}_\alpha^*(\vec{r}) \cdot \vec{P}(\vec{r}, t) e^{i\omega_\alpha t} dt \Big|_{t=0} e^{-i\omega_\alpha t} \\ &= e^{-i\omega_\alpha t} \sqrt{\frac{\omega_\alpha}{2\hbar\epsilon_0}} \int_0^t \int \vec{A}_\alpha^*(\vec{r}) \cdot \vec{P}(\vec{r}, t') e^{i\omega_\alpha t'} d^3 r dt' \\ &= \sqrt{\frac{\omega_\alpha}{2\hbar\epsilon_0}} \int_0^t dt' e^{i\omega_\alpha(t'-t)} \int d^3 r \vec{A}_\alpha^*(\vec{r}) \cdot \vec{P}(\vec{r}, t') \end{aligned} \quad (4.36)$$

Thus, the positive frequency (photon annihilation) part of $\vec{E}_s(\vec{r}, t)$ is given by Eq. (4.37).

$$\begin{aligned} \vec{E}_s^{(+)}(\vec{r}, t) &= i \sum_\alpha \sqrt{\frac{\hbar\omega_\alpha}{2\epsilon_0}} \left[a_{\alpha s}(t) \vec{A}_\alpha(\vec{r}) \right] \\ &= i \sum_\alpha \sqrt{\frac{\hbar\omega_\alpha}{2\epsilon_0}} \sqrt{\frac{\omega_\alpha}{2\hbar\epsilon_0}} \int_0^t dt' e^{i\omega_\alpha(t'-t)} \int d^3 r' \vec{A}_\alpha^*(\vec{r}') \cdot \vec{P}(\vec{r}', t') \vec{A}_\alpha(\vec{r}) \\ &= \frac{i}{2\epsilon_0} \int d^3 r' \int_0^t dt' \sum_\alpha \omega_\alpha \vec{A}_\alpha(\vec{r}) \vec{A}_\alpha^*(\vec{r}') e^{i\omega_\alpha(t'-t)} \cdot \vec{P}(\vec{r}', t') \\ &= \frac{2}{\epsilon_0} \int d^3 r' \int_0^t dt' \overleftrightarrow{\mathbf{G}}^{(+)}(\vec{r}, \vec{r}'; t, t') \cdot \vec{P}(\vec{r}', t') \end{aligned} \quad (4.37)$$

where $\overleftrightarrow{\mathbf{G}}^{(+)}(\vec{r}, \vec{r}'; t, t') = \frac{i}{4} \sum_\alpha \omega_\alpha \vec{A}_\alpha(\vec{r}) \vec{A}_\alpha^*(\vec{r}') e^{i\omega_\alpha(t'-t)}$ is a dyadic Green function. With

this crucial piece of information, Eq. (4.21) may be written as:

$$\begin{aligned}
\langle E \rangle &= -\frac{1}{2} \int d^3 r \langle \vec{P} \cdot \vec{E}_s^{(+)} \rangle + c.c. \\
&= -\frac{1}{2} \int d^3 r \left\langle \vec{P}(\vec{r}, t) \cdot \frac{2}{\epsilon_0} \int d^3 r' \int_0^t dt' \overleftrightarrow{G}^{(+)}(\vec{r}, \vec{r}'; t, t') \cdot \vec{P}(\vec{r}', t') \right\rangle + c.c. \\
&= -\frac{2}{\epsilon_0} \text{Re} \left[\int d^3 r \int d^3 r' \int_0^t dt' G_{ij}^{(+)}(\vec{r}, \vec{r}'; t, t') \langle P_i(\vec{r}, t) P_j(\vec{r}', t') \rangle \right] \quad (4.38)
\end{aligned}$$

where the Einstein notation had been used. The energy $\langle E \rangle$ here is the energy of the induced dipoles inside a medium, due to the source field produced by the dipoles.

It is important at this point to highlight that the Casimir force was calculated for dielectric configuration given by Eq. (4.39), with $\mu = 1$ throughout the region. This approach is consistent with Schwinger's original derivation (Schwinger et al., 1978). We may later substitute $\epsilon_C(\omega) = 1$ to obtain similar result as Lifshitz (1956).

$$\epsilon(\omega) = \begin{cases} \epsilon_A(\omega), & z < 0; \\ \epsilon_C(\omega), & 0 < z < l; \\ \epsilon_B(\omega), & z > l; \end{cases} \quad (4.39)$$

To proceed with the computation of Casimir force between the dielectrics, a small change in the dielectric constant was introduced by adding some polarizable particles to the dielectric media. With this, the polarization density will change from \vec{P} to $\vec{P} + \vec{P}'$. The change in energy due to the interactions of these added dipoles will then be:

$$\begin{aligned}
\langle \delta E \rangle &= E' - E \\
&= -\frac{2}{\epsilon_0} \text{Re} \int d^3 r \int d^3 r' \int_0^t dt' G_{ij}^{(+)}(\vec{r}, \vec{r}'; t, t') [\langle (P_i(\vec{r}, t) + P'_i(\vec{r}, t)) \\
&\quad (P_j(\vec{r}', t') + P'_j(\vec{r}', t')) \rangle - \langle P_i(\vec{r}, t) P_j(\vec{r}', t') \rangle] \\
&= -\frac{2}{\epsilon_0} \text{Re} \int d^3 r \int d^3 r' \int_0^t dt' G_{ij}^{(+)}(\vec{r}, \vec{r}'; t, t') \langle P'_i(\vec{r}, t) P'_j(\vec{r}', t') \rangle \quad (4.40)
\end{aligned}$$

In Eq. (4.40), the terms of type $\langle P_i(\vec{r}, t) P'_j(\vec{r}', t') \rangle$ are omitted, under the assumption that the new atoms that were introduced are independent and uncorrelated from the original atoms in the dielectric media.

Then, from Maxwell's equations for the Heisenberg-picture field operators, we have (Jackson, 1998)

$$-\nabla \times \nabla \times \vec{E} - \mu_0 \frac{\partial^2 \vec{D}}{\partial t^2} = \mu_0 \frac{\partial^2 \vec{P}'}{\partial t^2} \quad (4.41)$$

To proceed, it is noted that the dyadic Green function, \overleftrightarrow{G} may be transformed to frequency domain, as in Eq. (4.42). With that, the Maxwell equation Eq. (4.41) may have a Green function in terms of $\overleftrightarrow{\Gamma}$, in the frequency domain.

$$\overleftrightarrow{G}(\vec{r}, \vec{r}'; t, t') = \frac{1}{2\pi} \int_{-\infty}^{\infty} d\omega \overleftrightarrow{\Gamma}(\vec{r}, \vec{r}', \omega) e^{-i\omega(t-t')} \quad (4.42)$$

By substituting the Fourier transform for \vec{E} and \vec{P}' into Eq. (4.41), and by using the constitutive relation $\vec{D}(\vec{r}, \omega) = \epsilon_0 \epsilon(\vec{r}, \omega) \vec{E}(\vec{r}, \omega)$, we have

$$\begin{aligned} -\nabla \times \nabla \times \vec{E} - \mu_0 \frac{\partial^2 \vec{D}}{\partial t^2} &= \mu_0 \frac{\partial^2 \vec{P}'}{\partial t^2} \\ -\nabla \times \nabla \times \left(\vec{E}(\vec{r}, \omega) e^{-i\omega t} \right) - \epsilon_0 \mu_0 \epsilon \frac{\partial^2}{\partial t^2} \left(\vec{E}(\vec{r}, \omega) e^{-i\omega t} \right) &= \mu_0 \frac{\partial^2}{\partial t^2} \left(\vec{P}'(\vec{r}, \omega) e^{-i\omega t} \right) \\ \left((-\nabla \times \nabla \times) + \frac{\epsilon \omega^2}{c^2} \right) \vec{E}(\vec{r}, \omega) &= -\mu_0 \omega^2 \vec{P}'(\vec{r}, \omega) \end{aligned} \quad (4.43)$$

It is useful at this stage to rewrite Eq. (4.43) using the Green function. It may be shown that the dyadic $\overleftrightarrow{\Gamma}(\vec{r}, \vec{r}', \omega)$ defined in Eq. (4.42) is the Green function for the Maxwell equation in the frequency domain, Eq. (4.43). The mathematical details are elaborated as below. Firstly, we start by recalling the source electric field as

$$\begin{aligned} \vec{E}_s^{(+)}(\vec{r}, t) &= \frac{2}{\epsilon_0} \int d^3 r' \int_0^t dt' \overleftrightarrow{G}^{(+)}(\vec{r}, \vec{r}'; t, t') \cdot \vec{P}(\vec{r}', t') \\ \vec{E}_{s,(i)}^{(+)}(\vec{r}, t) &= \frac{2}{\epsilon_0} \int d^3 r' \int_0^t dt' G_{ij}^{(+)}(\vec{r}, \vec{r}'; t, t') P_j(\vec{r}', t') \\ &= \frac{2}{\epsilon_0} \int d^3 r' G_{ij}^{(+)}(\vec{r}, \vec{r}'; t, t') * P_j(\vec{r}', t) \end{aligned} \quad (4.44)$$

where the Einstein notation had been introduced. Then, the electric field \vec{E} in frequency domain is written in frequency domain. By using the convolution theorem, we have

$$\vec{E}_{s,(i)}^{(+)}(\vec{r}, \omega) = \frac{2}{\epsilon_0} \int d^3 r' F \left\{ G_{ij}^{(+)}(\vec{r}, \vec{r}'; t, t') \right\} F \left\{ P_j(\vec{r}', t) \right\} \quad (4.45)$$

Here we notice that $\overleftrightarrow{\Gamma}^{(+)}(\vec{r}, \vec{r}', \omega)$ may be taken as the Fourier transform for Green function $\overleftrightarrow{G}^{(+)}(\vec{r}, \vec{r}'; t, t')$, as shown in Eq. (4.42).

$$\vec{E}_{s,(i)}^{(+)}(\vec{r}, \omega) = \frac{2}{\epsilon_0} \int d^3 r' \Gamma_{ij}^{(+)}(\vec{r}, \vec{r}', \omega) P_j(\vec{r}', \omega) \quad (4.46)$$

We then arrive at

$$\vec{E}_s^{(+)}(\vec{r}, \omega) = \frac{2}{\epsilon_0} \int d^3 r' \overleftrightarrow{\Gamma}^{(+)}(\vec{r}, \vec{r}', \omega) \cdot \vec{P}(\vec{r}', \omega) \quad (4.47)$$

From Maxwell equation, Eq. (4.43), we define the linear differential function as $L = -\nabla \times \nabla \times + \frac{\epsilon\omega^2}{c^2}$, and the non-linear term as $f(\vec{r}, \omega) = -\mu_0\omega^2 [\vec{P}'(\vec{r}, \omega)]$.

$$\begin{aligned} \left((-\nabla \times \nabla \times) + \frac{\epsilon\omega^2}{c^2} \right) \vec{E}(\vec{r}, \omega) &= -\mu_0\omega^2 [\vec{P}'(\vec{r}, \omega)] \\ L\vec{E}(\vec{r}, \omega) &= f(\vec{r}, \omega) \end{aligned} \quad (4.48)$$

We then notice the Green function for Eq. (4.48), $Y(\vec{r}, \vec{r}', \omega)$ will satisfy the equation (Arfken et al., 2005):

$$LY(\vec{r}, \vec{r}', \omega) = \overleftrightarrow{\Gamma} \delta(\vec{r}, \vec{r}') \quad (4.49)$$

The solution to equation (4.48) will then be:

$$\begin{aligned} \vec{E}(\vec{r}, \omega) &= \int Y(\vec{r}, \vec{r}', \omega) \cdot f(\vec{r}', \omega) d^3r' \\ &= \frac{2}{\epsilon_0} \int Y(\vec{r}, \vec{r}', \omega) \cdot \left(\frac{-\mu_0\epsilon_0\omega^2}{2} \right) \vec{P}'(\vec{r}', \omega) d^3r' \end{aligned} \quad (4.50)$$

Now, we compare Eq. (4.47) and Eq. (4.50). We then have:

$$\begin{aligned} Y(\vec{r}, \vec{r}', \omega) \left(\frac{-\omega^2}{2c^2} \right) &= \overleftrightarrow{\Gamma}^{(+)}(\vec{r}, \vec{r}', \omega) \\ Y(\vec{r}, \vec{r}', \omega) &= -\frac{c^2}{\omega^2} \left(2\overleftrightarrow{\Gamma}^{(+)}(\vec{r}, \vec{r}', \omega) \right) \\ &= -\frac{c^2}{\omega^2} \overleftrightarrow{\Gamma}(\vec{r}, \vec{r}', \omega) \end{aligned} \quad (4.51)$$

And by substituting Eq. (4.51) into Eq. (4.48), we arrive at:

$$\begin{aligned} LY(\vec{r}, \vec{r}', \omega) &= \overleftrightarrow{\Gamma} \delta(\vec{r}, \vec{r}') \\ \left(-\nabla \times \nabla \times + \frac{\epsilon\omega^2}{c^2} \right) \left(-\frac{c^2}{\omega^2} \overleftrightarrow{\Gamma}(\vec{r}, \vec{r}', \omega) \right) &= \overleftrightarrow{\Gamma} \delta(\vec{r}, \vec{r}') \\ -\nabla \times \nabla \times \overleftrightarrow{\Gamma}(\vec{r}, \vec{r}', \omega) + \frac{\omega^2}{c^2} \epsilon(\omega) \overleftrightarrow{\Gamma}(\vec{r}, \vec{r}', \omega) &= -\frac{\omega^2}{c^2} \overleftrightarrow{\Gamma} \delta(\vec{r}, \vec{r}') \end{aligned} \quad (4.52)$$

With this in place, Eq. (4.43) can finally be rewritten in terms of its Green function:

$$\left(-\nabla \times \nabla \times + \frac{\epsilon\omega^2}{c^2} \right) \overleftrightarrow{\Gamma}(\vec{r}, \vec{r}', \omega) = -\frac{\omega^2}{c^2} \delta^3(\vec{r} - \vec{r}') \quad (4.53)$$

The positive-frequency Green function will take the positive end of frequencies, that is:

$$\overleftrightarrow{G}^{(+)}(\vec{r}, \vec{r}'; t, t') = \frac{1}{2\pi} \int_0^\infty d\omega \overleftrightarrow{\Gamma}(\vec{r}, \vec{r}', \omega) e^{-i\omega(t-t')} \quad (4.54)$$

From Eq. (4.40), the small change in energy due to adding more polarizable particle would then be:

$$\begin{aligned}
\langle \delta E \rangle &= -\frac{2}{\epsilon_0} \text{Re} \int d^3 r \int d^3 r' \int_0^t dt' G_{ij}^{(+)}(\vec{r}, \vec{r}'; t, t') \langle P'_i(\vec{r}, t) P'_j(\vec{r}', t') \rangle \\
&= -\frac{2}{\epsilon_0} \text{Re} \int d^3 r \int d^3 r' \int_0^t dt' \left(\frac{1}{2\pi} \int_0^\infty d\omega \overleftrightarrow{\Gamma}(\vec{r}, \vec{r}', \omega) e^{-i\omega(t-t')} \right) \langle P'_i(\vec{r}, t) P'_j(\vec{r}', t') \rangle \\
&= -\frac{1}{\epsilon_0 \pi} \text{Re} \int d^3 r \int d^3 r' \int_0^t dt' \int_0^\infty d\omega \Gamma_{ij}(\vec{r}, \vec{r}', \omega) \langle P'_i(\vec{r}, t) P'_j(\vec{r}', t') \rangle e^{-i\omega(t-t')}
\end{aligned} \tag{4.55}$$

Here, the connection between Eq. (4.55) and Eq. (4.38) must be emphasised. It is noticed that both equations are similar. In fact, Eq. (4.55) is the change in the energy of Eq. (4.38), due to the addition of the atoms associated with the polarization density \vec{P}' . The fields that are associated with these "added atoms" will propagate at a velocity as determined by the dielectric function ϵ produced by the original, unperturbed polarization density \vec{P} .

Next, we would like to express the expectation value in the integrand of Eq. (4.55) in terms of dielectric function associated with \vec{P}' . Firstly, we recall from the definition of polarizability,

$$\vec{P}'_i(\vec{r}, t) = \sum_{\beta} d_{\beta i}(t) \delta^3(\vec{r} - \vec{r}_{\beta}) \tag{4.56}$$

where $d_{\beta i}(t)$ is the i th-component of the dipole moment operator $d_{\beta}(t)$ for an atom at position r_{β} . Then, by multiplying Eq. (4.56) to itself and by changing indices, we have

$$\begin{aligned}
\vec{P}'_i(\vec{r}, t) \vec{P}'_j(\vec{r}', t') &= \sum_{\beta} d_{\beta i}(t) \delta^3(\vec{r} - \vec{r}_{\beta}) \sum_{\gamma} d_{\gamma j}(t') \delta^3(\vec{r}' - \vec{r}_{\gamma}) \\
&= \sum_{\beta} \sum_{\gamma} d_{\beta i}(t) d_{\gamma j}(t') \delta^3(\vec{r} - \vec{r}_{\beta}) \delta^3(\vec{r}' - \vec{r}_{\gamma}) \\
\langle P'_i(\vec{r}, t) P'_j(\vec{r}', t') \rangle &= \sum_{\beta} \sum_{\gamma} \langle d_{\beta i}(t) d_{\gamma j}(t') \rangle \delta^3(\vec{r} - \vec{r}_{\beta}) \delta^3(\vec{r}' - \vec{r}_{\gamma})
\end{aligned} \tag{4.57}$$

We will assume all atoms are in their ground states $|g\rangle$ at all times, and that the multiatomic wave function has the uncorrelated form $|g\rangle = |g\rangle_{\beta} |g\rangle_{\gamma} \dots$. The expectation operator on the right hand side of Eq. (4.57) is then:

$$\begin{aligned}
\langle d_{\beta i}(t) d_{\gamma j}(t') \rangle &= \langle g | d_{\beta i}(t) d_{\gamma j}(t') | g \rangle \\
&= \langle g_{\beta} g_{\gamma} \dots | d_{\beta i}(t) d_{\gamma j}(t') | g_{\beta} g_{\gamma} \dots \rangle \\
&= \delta_{\beta\gamma} \langle d_{\beta i}(t) d_{\beta j}(t') \rangle
\end{aligned} \tag{4.58}$$

This assumption is then substituted into Eq. (4.57).

$$\begin{aligned}
\langle P'_i(\vec{r}, t) P'_j(\vec{r}', t') \rangle &= \sum_{\beta} \sum_{\gamma} \langle d_{\beta i}(t) d_{\gamma j}(t') \rangle \delta^3(\vec{r} - \vec{r}_{\beta}) \delta^3(\vec{r}' - \vec{r}_{\gamma}) \\
&= \sum_{\beta} \sum_{\gamma} \delta_{\beta\gamma} \langle d_{\beta i}(t) d_{\gamma j}(t') \rangle \delta^3(\vec{r} - \vec{r}_{\beta}) \delta^3(\vec{r}' - \vec{r}_{\beta}) \\
&= \sum_{\beta} \langle d_{\beta i}(t) d_{\beta j}(t') \rangle \delta^3(\vec{r} - \vec{r}_{\beta}) \delta^3(\vec{r}' - \vec{r}_{\beta}) \quad (4.59)
\end{aligned}$$

Then, the continuum approximation was used, whereby we have assumed that there are $N(\vec{r})$ atoms per unit volume at the position \vec{r} . Also we have assumed that all atoms are identical, so that $\langle d_{\beta i}(t) d_{\beta j}(t') \rangle \rightarrow \langle d_i(t) d_j(t') \rangle$ for all β . Hence, Eq. (4.59) may be rewritten as:

$$\begin{aligned}
\langle P'_i(\vec{r}, t) P'_j(\vec{r}', t') \rangle &\rightarrow \int d^3 r'' \langle d_i(t) d_j(t') \rangle N(\vec{r}'') \delta^3(\vec{r} - \vec{r}'') \delta^3(\vec{r}' - \vec{r}'') \\
&= \langle d_i(t) d_j(t') \rangle \int d^3 r'' N(\vec{r}'') \delta^3(\vec{r} - \vec{r}'') \delta^3(\vec{r}' - \vec{r}'') \\
&= \langle d_i(t) d_j(t') \rangle N(\vec{r}) \delta^3(\vec{r} - \vec{r}') \quad (4.60)
\end{aligned}$$

This result is then inserted into Eq. (4.55) to yield:

$$\begin{aligned}
\langle \delta E \rangle &= -\frac{1}{\epsilon_0 \pi} \text{Re} \int d^3 r \int d^3 r' \int_0^t dt' \int_0^{\infty} d\omega \Gamma_{ij}(\vec{r}, \vec{r}', \omega) \langle d_i(t) d_j(t') \rangle N(\vec{r}) \delta^3(\vec{r} - \vec{r}') e^{-i\omega(t-t')} \\
&= -\frac{1}{\epsilon_0 \pi} \text{Re} \int d^3 r N(\vec{r}) \int_0^{\infty} d\omega \Gamma_{ij}(\vec{r}, \vec{r}, \omega) \int_0^t dt' \langle d_i(t) d_j(t') \rangle e^{-i\omega(t-t')} \quad (4.61)
\end{aligned}$$

The derivation is continued by further expressing the expectation value on the right hand side of Eq. (4.61) in terms of the dielectric function. Here, the Heisenberg-picture of quantum mechanics is used. The Heisenberg operator $d_i(t)$ is known to evolve in time according to $d_i(t) = U^\dagger(t) d_i U(t)$. In the equation, $d_i = d_i(0)$ is the Schrodinger-picture operator and $U(t)$ is known as the time-evolution operator, satisfying both $i\hbar U = HU$ and $U(0) = 1$. With this information, we have:

$$\begin{aligned}
\langle d_i(t) d_j(t') \rangle &= \langle g | U^\dagger(t) d_i U(t) U^\dagger(t') d_j U(t') | g \rangle \\
&= \sum_k \langle g | U^\dagger(t) d_i U(t) | k \rangle \langle k | U^\dagger(t') d_j U(t') | g \rangle \quad (4.62)
\end{aligned}$$

The unit operator, $\sum_k |k\rangle \langle k|$ was inserted here, where $\{|k\rangle\}$ is the complete set of eigenstates of the Hamiltonian, H_A for a single atom. If we approximate $U(t)$ by $e^{-iH_A t/\hbar}$,

Eq. (4.62) may then be written as:

$$\begin{aligned}
\langle d_i(t) d_j(t') \rangle &= \sum_k \langle g | U^\dagger(t) d_i U(t) | k \rangle \langle k | U^\dagger(t') d_j U(t') | g \rangle \\
&\approx \sum_k \langle g | e^{iH_A t/\hbar} d_i e^{-iH_A t/\hbar} | k \rangle \langle k | e^{iH_A t'/\hbar} d_j e^{-iH_A t'/\hbar} | g \rangle \\
&= \sum_k e^{i(E_g - E_k)t/\hbar} e^{i(E_k - E_g)t'/\hbar} \langle g | d_i | k \rangle \langle k | d_j | g \rangle \\
&= \sum_k e^{i\omega_{kg}(t'-t)} \langle g | d_i | k \rangle \langle k | d_j | g \rangle
\end{aligned} \tag{4.63}$$

and the change in energy, Eq. (4.61) is then given by:

$$\begin{aligned}
\langle \delta E \rangle &= -\frac{1}{\epsilon_0 \pi} \text{Re} \int d^3 r N(\vec{r}) \int_0^\infty d\omega \Gamma_{ij}(\vec{r}, \vec{r}, \omega) \int_0^t dt' \langle d_i(t) d_j(t') \rangle e^{-i\omega(t-t')} \\
&= -\frac{1}{\epsilon_0 \pi} \text{Re} \int d^3 r N(\vec{r}) \int_0^\infty d\omega \Gamma_{ij}(\vec{r}, \vec{r}, \omega) \sum_k \langle g | d_i | k \rangle \langle k | d_j | g \rangle \int_0^t dt' e^{i(\omega + \omega_{kg})(t'-t)} \\
&= -\frac{1}{\epsilon_0 \pi} \text{Re} \int d^3 r N(\vec{r}) \int_0^\infty d\omega \Gamma_{ij}(\vec{r}, \vec{r}, \omega) \\
&\quad \sum_k \langle g | d_i | k \rangle \langle k | d_j | g \rangle \left(\frac{i}{\omega + \omega_{kg}} \right) \left(e^{-i(\omega + \omega_{kg})t} - 1 \right)
\end{aligned} \tag{4.64}$$

In the above equation, the rapidly oscillating term $e^{-i(\omega + \omega_{kg})t}$, that was associated with an artificial turn-on of the atom-field interaction at $t = 0$ does not contribute to the Casimir force (Schwinger et al., 1978). With this we have:

$$\begin{aligned}
\langle \delta E \rangle &\rightarrow -\frac{1}{\epsilon_0 \pi} \text{Re} \int d^3 r N(\vec{r}) \int_0^\infty d\omega \Gamma_{ij}(\vec{r}, \vec{r}, \omega) \sum_k \langle g | d_i | k \rangle \langle k | d_j | g \rangle \left(\frac{i}{\omega + \omega_{kg}} \right) (-1) \\
&= \frac{1}{\epsilon_0 \pi} \text{Re} i \int d^3 r N(\vec{r}) \int_0^\infty d\omega \Gamma_{ij}(\vec{r}, \vec{r}, \omega) \sum_k \frac{\langle g | d_i | k \rangle \langle k | d_j | g \rangle}{\omega + \omega_{kg}}
\end{aligned} \tag{4.65}$$

The integration is then rewritten by substituting $\omega = i\xi$, where ξ , a real number, is the imaginary frequency term.

$$\begin{aligned}
\langle \delta E \rangle &= \frac{1}{\epsilon_0 \pi} \text{Re} i \int d^3 r N(\vec{r}) \int_0^\infty d\omega \Gamma_{ij}(\vec{r}, \vec{r}, \omega) \sum_k \frac{\langle g | d_i | k \rangle \langle k | d_j | g \rangle}{\omega + \omega_{kg}} \\
&= \frac{1}{\epsilon_0 \pi} \text{Re} i \int d^3 r N(\vec{r}) \int_0^{-i\infty} id\xi \Gamma_{ij}(\vec{r}, \vec{r}, i\xi) \sum_k \frac{\langle g | d_i | k \rangle \langle k | d_j | g \rangle}{i\xi + \omega_{kg}} \\
&= -\frac{1}{\epsilon_0 \pi} \text{Re} \int d^3 r N(\vec{r}) \int_0^{-i\infty} d\xi \Gamma_{ij}(\vec{r}, \vec{r}, i\xi) \sum_k \frac{\langle g | d_i | k \rangle \langle k | d_j | g \rangle}{i\xi + \omega_{kg}}
\end{aligned} \tag{4.66}$$

We then apply Cauchy integral formula to change the integral contour to obtain:

$$\langle \delta E \rangle = -\frac{1}{\epsilon_0 \pi} \int d^3 r N(\vec{r}) \int_0^\infty d\xi \Gamma_{ij}(\vec{r}, \vec{r}, i\xi) \sum_k \frac{\omega_{kg} \langle g | d_i | k \rangle \langle k | d_j | g \rangle}{\xi^2 + \omega_{kg}^2} \tag{4.67}$$

Now, the polarizability tensor for the ground state, $|g\rangle$ is known to be (Davydov, 1969):

$$\alpha_{ij}(\omega) = \frac{1}{\hbar} \sum_k \frac{2\omega_{kg} \langle g|d_i|k\rangle \langle k|d_j|g\rangle}{\omega_{kg}^2 - \omega^2} \quad (4.68)$$

Since we are considering an atom, which is a spherically symmetric system, we have $\alpha_{ij}(\omega) = \alpha(\omega) \delta_{ij}$, where $\alpha(\omega)$ is the usual polarizability of a medium. Hence,

$$\begin{aligned} \alpha_{ij}(i\xi) &= \frac{1}{\hbar} \sum_k \frac{2\omega_{kg} \langle g|d_i|k\rangle \langle k|d_j|g\rangle}{\omega_{kg}^2 + \xi^2} \\ &= \frac{1}{3\hbar} \delta_{ij} \sum_k \frac{2\omega_{kg} |\vec{d}_{kg}|^2}{\omega_{kg}^2 + \xi^2} \\ &= \delta_{ij} \alpha(i\xi) \end{aligned} \quad (4.69)$$

With this, we may insert the polarizability $\alpha(\omega)$ into Eq. (4.67).

$$\begin{aligned} \langle \delta E \rangle &= -\frac{1}{\epsilon_0 \pi} \int d^3 r N(\vec{r}) \int_0^\infty d\xi \Gamma_{ij}(\vec{r}, \vec{r}, i\xi) \sum_k \frac{\omega_{kg} \langle g|d_i|k\rangle \langle k|d_j|g\rangle}{\xi^2 + \omega_{kg}^2} \\ &= -\frac{\hbar}{2\epsilon_0 \pi} \int d^3 r N(\vec{r}) \int_0^\infty d\xi \Gamma_{ij}(\vec{r}, \vec{r}, i\xi) \left(\frac{1}{\hbar} \sum_k \frac{2\omega_{kg} \langle g|d_i|k\rangle \langle k|d_j|g\rangle}{\xi^2 + \omega_{kg}^2} \right) \\ &= -\frac{\hbar}{2\epsilon_0 \pi} \int d^3 r N(\vec{r}) \int_0^\infty d\xi \Gamma_{ij}(\vec{r}, \vec{r}, i\xi) \delta_{ij} \alpha(i\xi) \\ &= -\frac{\hbar}{2\epsilon_0 \pi} \int d^3 r N(\vec{r}) \int_0^\infty d\xi \Gamma_{jj}(\vec{r}, \vec{r}, i\xi) \alpha(i\xi) \end{aligned} \quad (4.70)$$

Furthermore, the relation $\epsilon_0(\epsilon(\vec{r}, \omega) - 1) = N\alpha$ between the dielectric constant and the polarizability is noted (Davydov, 1969). With these relationships, Eq. (4.70) may then be written as:

$$\begin{aligned} \langle \delta E \rangle &= -\frac{\hbar}{2\pi} \int d^3 r N(\vec{r}) \int_0^\infty d\xi \Gamma_{jj}(\vec{r}, \vec{r}, i\xi) \left[\frac{\epsilon(\vec{r}, i\xi) - 1}{N(\vec{r})} \right] \\ &= -\frac{\hbar}{2\pi} \int d^3 r \int_0^\infty d\xi (\epsilon(\vec{r}, i\xi) - 1) \Gamma_{jj}(\vec{r}, \vec{r}, i\xi) \end{aligned} \quad (4.71)$$

We then proceed to calculate the Casimir force between the plates A and B , for a configuration as depicted in Eq. (4.39). Here, we will consider the change in $\langle \delta E \rangle$ as a result of an infinitesimal change δl in l . This process may be imagined as the atoms that we have added (to causes the change in energy) constitutes a layer of width δl at $z = l$. This result in a change in dielectric constant, $\epsilon \rightarrow \epsilon + \delta\epsilon$, and the corresponding Casimir

force, f is given by:

$$\begin{aligned}
f &= -\frac{\langle \delta E \rangle}{\delta l} \\
&= \frac{\hbar}{2\pi} \int d^3 r \int_0^\infty d\xi \frac{\delta(\varepsilon(\vec{r}, i\xi) - 1)}{\delta l} \Gamma_{jj}(\vec{r}, \vec{r}, i\xi) \\
&= \frac{\hbar}{2\pi} \int d^3 r \int_0^\infty d\xi \frac{\delta \varepsilon}{\delta l} \Gamma_{jj}(\vec{r}, \vec{r}, i\xi)
\end{aligned} \tag{4.72}$$

Now using the Heaviside step function, $\Theta(x)$, we may write the dielectric function for the entire space as:

$$\begin{aligned}
\varepsilon(\vec{r}, \omega) &= \varepsilon_A(\vec{r}_\perp, z, \omega) \Theta(-z) + \varepsilon_C(\vec{r}_\perp, z, \omega) \Theta(z) \Theta(l-z) \\
&\quad + \varepsilon_B(\vec{r}_\perp, z, \omega) \Theta(z-l)
\end{aligned} \tag{4.73}$$

and since $d\Theta(x)/dx = \delta(x)$, we have:

$$\begin{aligned}
\frac{\delta \varepsilon}{\delta l} &= \frac{\delta}{\delta l} [\varepsilon_A(\vec{r}_\perp, z, \omega) \Theta(-z) + \varepsilon_C(\vec{r}_\perp, z, \omega) \Theta(z) \Theta(l-z) + \varepsilon_B(\vec{r}_\perp, z, \omega) \Theta(z-l)] \\
&= \varepsilon_C(\vec{r}_\perp, z, \omega) \Theta(z) \frac{\delta}{\delta l} \Theta(l-z) + \varepsilon_B(\vec{r}_\perp, z, \omega) \frac{\delta}{\delta l} \Theta(z-l) \\
&= (\varepsilon_C - \varepsilon_B) \delta(z-l)
\end{aligned} \tag{4.74}$$

where \vec{r}_\perp is the component of \vec{r} in the xy -plane, for $z > 0$. Since the dielectric function of the space considered only varies in the z direction, it is natural to write (using Fourier transform on xy -plane.)

$$\overleftrightarrow{\Gamma}(\vec{r}, \vec{r}', \omega) = \left(\frac{1}{2\pi}\right)^2 \int d^2 k_\perp \overleftrightarrow{\Gamma}(z, z', \vec{k}_\perp, \omega) e^{i\vec{k}_\perp \cdot (\vec{r} - \vec{r}')} \tag{4.75}$$

With this, Eq.(4.72) may be rewritten as

$$\begin{aligned}
f(l) &= \frac{\hbar}{2\pi} \int d^3 r \int_0^\infty d\xi \frac{\delta \varepsilon}{\delta l} \Gamma_{jj}(\vec{r}, \vec{r}, i\xi) \\
&= \frac{\hbar}{2\pi} \int d^3 r \int_0^\infty d\xi (\varepsilon_C - \varepsilon_B) \delta(z-l) \left[\left(\frac{1}{2\pi}\right)^2 \int d^2 k_\perp \Gamma_{jj}(z, z, \vec{k}_\perp, \omega) e^{i\vec{k}_\perp \cdot (\vec{r} - \vec{r})} \right] \\
&= -i\hbar \left(\frac{1}{2\pi}\right)^3 \int d^3 r \int_0^\infty d\omega (\varepsilon_C - \varepsilon_B) \delta(z-l) \int d^2 k_\perp \Gamma_{jj}(z, z, \vec{k}_\perp, \omega)
\end{aligned} \tag{4.76}$$

and the Casimir pressure (force per area) is given by

$$\begin{aligned}
F(l) &= \frac{f(l)}{A} \\
&= -\frac{i\hbar}{A} \left(\frac{1}{2\pi}\right)^3 \int \int \int dx dy dz \int_0^\infty d\omega (\varepsilon_C - \varepsilon_B) \delta(z-l) \int d^2 k_\perp \Gamma_{jj}(z, z, \vec{k}_\perp, \omega) \\
&= i\hbar \left(\frac{1}{2\pi}\right)^3 \int_0^\infty d\omega \int d^2 k_\perp (\varepsilon_B - \varepsilon_C) \Gamma_{jj}(l, l, \vec{k}_\perp, \omega)
\end{aligned} \tag{4.77}$$

The calculation of $\Gamma_{jj} = \Gamma_{xx} + \Gamma_{yy} + \Gamma_{zz}$ may be done using classical electromagnetic theory, where $\overleftrightarrow{\Gamma}$ satisfies Eq. (4.53), and boundary conditions at the dielectric interfaces at $z = 0$ and $z = l$. The result is (Schwinger et al., 1978),

$$(\varepsilon_B - \varepsilon_C) \Gamma_{jj}(l, l, \vec{k}_\perp, \omega) = 2(K_C - K_B) + 2K_C \left[\left(\frac{K_A + K_C}{K_A - K_C} \frac{K_B + K_C}{K_B - K_C} e^{2K_C l} - 1 \right)^{-1} + \left(\frac{\varepsilon_C K_A + \varepsilon_1 K_C}{\varepsilon_C K_A - \varepsilon_A K_C} \frac{\varepsilon_3 K_B + \varepsilon_B K_C}{\varepsilon_C K_B - \varepsilon_B K_C} e^{2K_C l} - 1 \right)^{-1} \right] \quad (4.78)$$

where $K_n^2 = k_\perp^2 - \omega^2 \varepsilon_n(\omega)/c^2$. The first term on the right hand side corresponds to a change in the volume energy of the system. It does not depend on l , and hence may be omitted. The remaining terms then provide the Casimir force between plate A and plate B. Finally, the Casimir pressure in Eq. (4.77) may be written as:

$$F(l) = \frac{i\hbar}{2\pi^2} \int_0^\infty d\omega \int_0^\infty k dk K_C \left[\left(\frac{K_A + K_C}{K_A - K_C} \frac{K_B + K_C}{K_B - K_C} e^{2K_C l} - 1 \right)^{-1} + \left(\frac{\varepsilon_C K_A + \varepsilon_A K_C}{\varepsilon_C K_A - \varepsilon_A K_C} \frac{\varepsilon_C K_B + \varepsilon_B K_C}{\varepsilon_C K_B - \varepsilon_B K_C} e^{2K_C l} - 1 \right)^{-1} \right] \quad (4.79)$$

This result is identical to the Lifshitz's formula. We may further simplify it by assuming $\varepsilon_C = 1$, that is we assume the inter-plate medium to be vacuum as in the derivation of Lifshitz formula in Chapter 3. Then, we take $K_C = \sqrt{k^2 + \xi^2/c^2}$ to obtain the Lifshitz formula used by Ooi and Khoo (2012). Here we take the usual Fresnel reflectivity as

$$r_{TM,n} = \frac{\varepsilon_n K_C - K_n}{\varepsilon_n K_C + K_n} \quad (4.80)$$

$$r_{TE,n} = \frac{K_C - K_n}{K_C + K_n}$$

and with some simple algebraic manipulation, we arrive at

$$F(l) = -\frac{\hbar}{2\pi^2} \int_0^\infty d\xi \int_0^\infty k dk \sqrt{k^2 + \frac{\xi^2}{c^2}} \sum_{N=TE, TM} \left(\frac{r_N^A r_N^B e^{-2d\sqrt{k^2 + \xi^2/c^2}}}{1 - r_N^A r_N^B e^{-2d\sqrt{k^2 + \xi^2/c^2}}} \right) \quad (4.81)$$

which is identical compared to Eq. (3.44).

4.3 Source Field and Vacuum Field

In the previous section, we have witnessed a remarkable perception regarding the Casimir effect, where the effect may be naturally attributed to the source field. This derivation looks much elegant as it does not attribute the force to the vacuum field, which

is not intuitive. However, in this section, we will show that the Casimir force can be derived equally from the vacuum field by using a different ordering.

Instead of using the Wick order (as in Eq. (4.17)), we consider a symmetrically ordered form of the expectation value of energy as below (P. Milonni & Eberlein, 1994).

$$\begin{aligned}
\langle E \rangle &= -\frac{1}{2} \int d^3 r \langle \vec{P} \cdot \vec{E} \rangle \\
&= -\frac{1}{2} \int d^3 r \left\langle \frac{1}{2} \vec{P} \cdot [\vec{E}^{(+)} + \vec{E}^{(-)}] + \frac{1}{2} [\vec{E}^{(+)} + \vec{E}^{(-)}] \cdot \vec{P} \right\rangle \\
&= \langle E \rangle_{VF} + \langle E \rangle_S
\end{aligned} \tag{4.82}$$

where for $\vec{E}^{(+)}(\vec{r}, t) = \vec{E}_o^{(+)}(\vec{r}, t) + \vec{E}_s^{(+)}(\vec{r}, t)$, we have

$$\langle E \rangle_{VF} = -\frac{1}{2} \int d^3 r \left\langle \frac{1}{2} \vec{P} \cdot [\vec{E}_o^{(+)} + \vec{E}_o^{(-)}] + \frac{1}{2} [\vec{E}_o^{(+)} + \vec{E}_o^{(-)}] \cdot \vec{P} \right\rangle \tag{4.83}$$

$$\langle E \rangle_S = -\frac{1}{2} \int d^3 r \left\langle \frac{1}{2} \vec{P} \cdot [\vec{E}_s^{(+)} + \vec{E}_s^{(-)}] + \frac{1}{2} [\vec{E}_s^{(+)} + \vec{E}_s^{(-)}] \cdot \vec{P} \right\rangle \tag{4.84}$$

Now, we will attempt to show that the source field in this case is zero. Recall that the source field operator $E_s = \vec{E}_s^{(+)} + \vec{E}_s^{(-)}$ can be written as their respective Green functions (as in Eq. (4.37) and Eq. (4.42)), i.e.

$$\begin{aligned}
\vec{E}_s(\vec{r}, t) &= \frac{2}{\epsilon_0} \int d^3 r' \int_0^t dt' \overleftrightarrow{G}(\vec{r}, \vec{r}'; t, t') \cdot \vec{P}(\vec{r}', t') \\
&= \frac{1}{\epsilon_0 \pi} \int d^3 r' \int_0^t dt' \int_{-\infty}^{\infty} d\omega \overleftrightarrow{\Gamma}(\vec{r}, \vec{r}', \omega) e^{-i\omega(t-t')} \cdot \vec{P}(\vec{r}', t')
\end{aligned} \tag{4.85}$$

With that, we substitute everything into Eq. (4.84),

$$\begin{aligned}
\langle E \rangle_S &= -\frac{1}{2} \int d^3 r \left\langle \frac{1}{2} \vec{P} \cdot \left[\frac{1}{\epsilon_0 \pi} \int d^3 r' \int_0^t dt' \int_{-\infty}^{\infty} d\omega \overleftrightarrow{\Gamma}(\vec{r}, \vec{r}', \omega) e^{-i\omega(t-t')} \cdot \vec{P}(\vec{r}', t') \right] \right. \\
&\quad \left. + \frac{1}{2} \left[\frac{1}{\epsilon_0 \pi} \int d^3 r' \int_0^t dt' \int_{-\infty}^{\infty} d\omega \overleftrightarrow{\Gamma}(\vec{r}, \vec{r}', \omega) e^{-i\omega(t-t')} \cdot \vec{P}(\vec{r}', t') \right] \cdot \vec{P} \right\rangle \\
&= -\frac{1}{4\pi\epsilon_0} \int d^3 r \int d^3 r' \int_{-\infty}^{\infty} d\omega \overleftrightarrow{\Gamma}(\vec{r}, \vec{r}', \omega) \\
&\quad \cdot \int_0^t dt' \left\langle \vec{P}(\vec{r}, t) \cdot \vec{P}(\vec{r}', t') + \vec{P}(\vec{r}', t') \cdot \vec{P}(\vec{r}, t) \right\rangle e^{-i\omega(t-t')} \\
&= -\frac{1}{4\pi\epsilon_0} \int d^3 r \int d^3 r' \int_{-\infty}^{\infty} d\omega \overleftrightarrow{\Gamma}_{ij}(\vec{r}, \vec{r}', \omega) \\
&\quad \times \int_0^t dt' \left[\left\langle \vec{P}_i(\vec{r}, t) \vec{P}_j(\vec{r}', t') \right\rangle + \left\langle \vec{P}_j(\vec{r}', t') \vec{P}_i(\vec{r}, t) \right\rangle \right] e^{-i\omega(t-t')}
\end{aligned} \tag{4.86}$$

where we have again introduced the Einstein notation to represent the dot products. By substituting previously known result from Eq. (4.60) and Eq. (4.63) into the equation, we

have

$$\begin{aligned}
\langle E \rangle_S &= -\frac{1}{4\pi\epsilon_0} \int d^3r \int d^3r' \int_{-\infty}^{\infty} d\omega \Gamma_{ij}(\vec{r}, \vec{r}', \omega) \\
&\quad \times \int_0^t dt' \left[\langle \vec{P}_i(\vec{r}, t) \vec{P}_j(\vec{r}', t') \rangle + \langle \vec{P}_j(\vec{r}', t') \vec{P}_i(\vec{r}, t) \rangle \right] e^{-i\omega(t-t')} \\
&= -\frac{1}{4\pi\epsilon_0} \int d^3r \int d^3r' \int_{-\infty}^{\infty} d\omega \Gamma_{ij}(\vec{r}, \vec{r}', \omega) \int_0^t dt' \left[\langle d_i(t) d_j(t') \rangle N(\vec{r}) \delta^3(\vec{r} - \vec{r}') \right. \\
&\quad \left. + \langle d_j(t') d_i(t) \rangle N(\vec{r}') \delta^3(\vec{r} - \vec{r}') \right] e^{-i\omega(t-t')} \\
&= -\frac{1}{12\pi\epsilon_0} \int d^3r \int_{-\infty}^{\infty} d\omega \Gamma_{jj}(\vec{r}, \vec{r}, \omega) \sum_k \left| \vec{d}_{kg} \right|^2 \\
&\quad \times \int_0^t dt' \left[e^{i(\omega_{kg} + \omega)(t'-t)} + e^{i(\omega - \omega_{kg})(t'-t)} \right] N(\vec{r})
\end{aligned} \tag{4.87}$$

We then employ a similar approximation as Eq. (4.65), i.e.: the rapidly oscillating term $e^{-i(\omega + \omega_{kg})t}$, that was associated with an artificial turn-on of the atom-field interaction at $t = 0$ was ignored. We then arrive at

$$\langle E \rangle_S \rightarrow \frac{i}{12\pi\epsilon_0} \int d^3r \int_{-\infty}^{\infty} d\omega \Gamma_{jj}(\vec{r}, \vec{r}, \omega) \sum_k \left| \vec{d}_{kg} \right|^2 \left[\frac{1}{\omega + \omega_{kg}} + \frac{1}{\omega - \omega_{kg}} \right] N(\vec{r}) \tag{4.88}$$

Since both $\Gamma_{jj}(\vec{r}, \vec{r}, \omega)$ and $(\omega + \omega_{kg})^{-1} + (\omega - \omega_{kg})^{-1}$ is an even function of ω , we then see that:

$$\langle E \rangle_S = 0 \tag{4.89}$$

This is an interesting result - when field operators are symmetrically ordered, the source field vanishes. This result is particularly important, as we now notice that a different ordering in field operators may result in different physical interpretation. We shall see later that the Casimir effect in this scheme is attributed to the vacuum field.

To prove that, we then proceed to calculate the vacuum field $\langle E \rangle_{VF}$. First, we define the Fourier transform of \vec{E}_o as:

$$\vec{E}_o^{(\pm)}(\vec{r}, t) = \int_0^{\infty} d\omega \vec{F}_o^{(\pm)}(\vec{r}, \omega) e^{\mp i\omega t} \tag{4.90}$$

Then, it is noted that \vec{E}_o does not depends on electron charge e (P. Milonni & Eberlein, 1994). Hence, in order to derive an energy to the order of e^2 , we consider:

$$\vec{P}(\vec{r}, t) = N(\vec{r}) \int_0^{\infty} d\omega \alpha(\omega) \left[\vec{F}_o^{(+)}(\vec{r}, \omega) e^{-i\omega t} + \vec{F}_o^{(-)}(\vec{r}, \omega) e^{i\omega t} \right] \tag{4.91}$$

where α is the polarizability. With this, we have

$$\begin{aligned}
\langle E \rangle_{VF} &= -\frac{1}{2} \int d^3r \left\langle \frac{1}{2} \vec{P} \cdot \left[\vec{E}_o^{(+)} + \vec{E}_o^{(-)} \right] + \frac{1}{2} \left[\vec{E}_o^{(+)} + \vec{E}_o^{(-)} \right] \cdot \vec{P} \right\rangle \\
&= -\frac{1}{2} \int d^3r N(\vec{r}) \int_0^{\infty} d\omega \alpha(\omega) \left\langle \vec{F}_o^{(+)}(\vec{r}, \omega) \cdot \vec{F}_o^{(-)}(\vec{r}, \omega) \right\rangle
\end{aligned} \tag{4.92}$$

Now, by considering Eq. (4.54), Eq. (4.42), Eq. (4.22), and Eq. (4.90), the dyadic Green function may be written as

$$\overleftrightarrow{\Gamma}(\vec{r}, \vec{r}', \omega) = \frac{i\pi\epsilon_0}{\hbar} \left\langle \vec{F}_o^{(+)}(\vec{r}, \omega) \vec{F}_o^{(-)}(\vec{r}', \omega) \right\rangle \quad (4.93)$$

which we can write in Einstein notation as

$$\Gamma_{jj}(\vec{r}, \vec{r}', \omega) = \frac{i\pi\epsilon_0}{\hbar} \left\langle \vec{F}_o^{(+)}(\vec{r}, \omega) \cdot \vec{F}_o^{(-)}(\vec{r}', \omega) \right\rangle \quad (4.94)$$

With that, Eq. (4.92) can be written as

$$\langle E \rangle_{VF} = \frac{\hbar i}{2\pi\epsilon_0} \int d^3r N(\vec{r}) \int_0^\infty d\omega \alpha(\omega) \Gamma_{jj}(\vec{r}, \vec{r}, \omega) \quad (4.95)$$

Again, by noting that $\epsilon_0(\epsilon(\vec{r}, \omega) - 1) = N\alpha$, the expected value of vacuum field energy reads

$$\begin{aligned} \langle E \rangle_{VF} &= \frac{\hbar i}{2\pi\epsilon_0} \int d^3r N(\vec{r}) \int_0^\infty d\omega \frac{\epsilon_0(\epsilon - 1)}{N(\vec{r})} \Gamma_{jj}(\vec{r}, \vec{r}, \omega) \\ &= \frac{\hbar i}{2\pi} \int d^3r \int_0^\infty d\omega (\epsilon - 1) \Gamma_{jj}(\vec{r}, \vec{r}, \omega) \end{aligned} \quad (4.96)$$

Lastly, by changing the frequency integration from real axis to imaginary axis using the Cauchy Integral formula, and by substituting $\xi = -i\omega$, we arrive at

$$\langle E \rangle_{VF} = -\frac{\hbar}{2\pi} \int d^3r \int_0^\infty d\xi (\epsilon - 1) \Gamma_{jj}(\vec{r}, \vec{r}, i\xi) \quad (4.97)$$

which is identical to Eq. (4.71). By following the same derivation presented in the previous section, we are able to obtain the same final result for the Casimir force, as in Eq. (4.77).

The results may be summarized as follows. We have presented the Casimir force from the source theory's point of view in Section 4.2. Essentially, we have considered the change in the dipole energy due to the field produced by the dipole itself. We have removed the contribution from vacuum field, i.e. $\langle E \rangle_{VF} = 0$ by using a normal ordering of operators. By switching the ordering of operators to a symmetric ordering, we manage to remove the contribution from the source field, i.e. $\langle E \rangle_S = 0$. This allows us to consider the interaction of the dipole with a source free, vacuum field in this section. Albeit different in terms of approach, both methods eventually lead to the derivation of Lifshitz formula.

4.4 The Energy Variation Approach

In the previous section, we have outlined the general derivation of Casimir force, from the source and vacuum field using the Quantum Electrodynamics approach. The use of QED's approach highlights the fact that operator ordering will result in different interpretations of the Casimir effect. While the derivation is complete, it is still interesting to follow Schwinger et al. (1978)'s original derivation. Apart from pedagogical reasons, this exercise provides a better insight towards the original idea of source theory, which neatly incorporates the idea of energy variation. Furthermore, the full calculation of dyadic Green's function Γ_{jj} , as in Eq. (4.78) is elaborated.

First, we start off by writing the action for a macroscopic electromagnetic fields that was produced by an external polarization source, \vec{P} . This idea is the core of source theory.

$$W = \int dx \vec{P} \cdot \left(-\frac{\partial \vec{A}}{\partial t} - \nabla \phi \right) + \epsilon_0 \epsilon(\vec{r}, \omega) \vec{E} \cdot \left(-\frac{\partial \vec{A}}{\partial t} - \nabla \phi \right) - \vec{H} \cdot (\nabla \times \vec{A}) + \frac{\mu_0}{2} H^2 - \frac{1}{2} \epsilon_0 \epsilon(\vec{r}, \omega) E^2 \quad (4.98)$$

In the above equation, $dx = d\vec{r}dt$. For nonlinear media, the linear relationship between the field and source allows us to write:

$$\vec{E}(x) = \frac{1}{\epsilon_0} \int dx' \overleftrightarrow{\Gamma}(x, x') \cdot \vec{P}(x') \quad (4.99)$$

The change in action is then being integrated to a source variation, i.e.

$$\delta_{\vec{P}} W = \int dx \delta \vec{P} \cdot \vec{E} \quad (4.100)$$

With that, the electromagnetic energy (or more strictly, the integral of response of the action), may be written as

$$\begin{aligned} W &= \frac{1}{2} \int \vec{P}(x) \cdot \vec{E}(x) dx \\ &= \frac{1}{2\epsilon_0} \int \int \vec{P}(x) \cdot \overleftrightarrow{\Gamma}(x, x') \cdot \vec{P}(x') dx dx' \end{aligned} \quad (4.101)$$

Then, we consider the variation in action under an infinitesimal deviation in the dielectric function, $\delta\epsilon$. Since the other actions in Eq. (4.98) is stationary under field variations, we have

$$\delta_{\epsilon} W = \frac{1}{2} \epsilon_0 \int dx \delta\epsilon E^2 \quad (4.102)$$

The product of polarization sources may be written as (Schwinger et al., 1978)

$$i\vec{P}(x)\vec{P}(x')\Big|_{eff} = \overleftrightarrow{\Gamma} \hbar\epsilon_0\delta\epsilon\delta(x-x') \quad (4.103)$$

By introducing Einstein notation to Eq. (4.101), and by substituting Eq. (4.103) into it, we then have

$$\begin{aligned} \delta W &= \frac{1}{2\epsilon_0} \int \int \vec{P}(x) \cdot \overleftrightarrow{\Gamma}(x,x') \cdot \vec{P}(x') dx dx' \\ &= \frac{1}{2\epsilon_0} \int \int \vec{P}_i(x) \Gamma_{ij}(x,x') \vec{P}_j(x') dx dx' \\ &= -\frac{i\hbar}{2} \int \delta\epsilon(x) \Gamma_{jj}(x,x) dx \end{aligned} \quad (4.104)$$

At this point, it is important to include dispersion. The dispersion (at zero temperature) may be introduced by adding a Fourier transform in time.

$$\overleftrightarrow{\Gamma}(x,x') = \int_{-\infty}^{\infty} \frac{d\omega}{2\pi} e^{-i\omega(t-t')} \overleftrightarrow{\Gamma}(\vec{r},\vec{r}',\omega) \quad (4.105)$$

Hence the change in energy,

$$\begin{aligned} \delta E &= -\delta W \\ &= \frac{i\hbar}{4\pi} \int_{-\infty}^{\infty} \int \delta\epsilon(\vec{r},\omega) \Gamma_{jj}(\vec{r},\vec{r},\omega) d\vec{r} d\omega \end{aligned} \quad (4.106)$$

The problem now will be focused in finding the Green function $\overleftrightarrow{\Gamma}$ in Eq. (4.106). From the electromagnetic wave equation in a medium, we have

$$-\nabla \times (\nabla \times \vec{E}) - \mu_0 \frac{\partial^2 \vec{D}}{\partial t^2} = \mu_0 \frac{\partial^2 \vec{P}}{\partial t^2} \quad (4.107)$$

Using the Fourier transform, and the constitutive relation $\vec{D}(\vec{r},\omega) = \epsilon_0\epsilon(\vec{r},\omega)\vec{E}(\vec{r},\omega)$.

$$\begin{aligned} -\nabla \times \nabla \times (\vec{E}(\vec{r},\omega) e^{-i\omega t}) - \mu_0 \frac{\partial^2}{\partial t^2} (\vec{D}(\vec{r},\omega) e^{-i\omega t}) &= \mu_0 \frac{\partial^2}{\partial t^2} (\vec{P}(\vec{r},\omega) e^{-i\omega t}) \\ -\nabla \times \nabla \times \vec{E}(\vec{r},\omega) + \mu_0 \omega^2 \vec{D}(\vec{r},\omega) &= -\omega^2 \mu_0 \vec{P}(\vec{r},\omega) \\ -\nabla \times \nabla \times \vec{E}(\vec{r},\omega) + \frac{\epsilon\omega^2}{c^2} \vec{E}(\vec{r},\omega) &= -\omega^2 \mu_0 \vec{P}(\vec{r},\omega) \end{aligned} \quad (4.108)$$

By putting Eq. (4.105) into the electromagnetic wave equation, we then see that $\overleftrightarrow{\Gamma}$ is the Green function of the Eq. (4.108).

$$\begin{aligned} \left((-\nabla \times \nabla \times) + \frac{\epsilon\omega^2}{c^2} \right) \left(\frac{1}{\epsilon_0} \int d\vec{r}' \overleftrightarrow{\Gamma}(\vec{r},\vec{r}',\omega) \cdot \vec{P}(\vec{r}',\omega) \right) &= -\omega^2 \mu_0 \vec{P}(\vec{r},\omega) \\ \left(-\nabla \times \nabla \times + \frac{\epsilon\omega^2}{c^2} \right) \overleftrightarrow{\Gamma}(\vec{r},\vec{r}',\omega) &= -\frac{\omega^2}{c^2} \overleftrightarrow{\Gamma} \delta(\vec{r}-\vec{r}') \\ -\nabla \times (\nabla \times \overleftrightarrow{\Gamma}(\vec{r},\vec{r}',\omega)) + \frac{\epsilon\omega^2}{c^2} \overleftrightarrow{\Gamma}(\vec{r},\vec{r}',\omega) &= -\frac{\omega^2}{c^2} \overleftrightarrow{\Gamma} \delta(\vec{r}-\vec{r}') \end{aligned} \quad (4.109)$$

For now, it is convenient to obtain a first-order differential equation instead, by defining

$$\nabla \times \overleftrightarrow{\Gamma} = \frac{i\omega}{c} \overleftrightarrow{\Phi} \quad (4.110)$$

With this, Eq. (4.109) then become

$$\begin{aligned} -\nabla \times \left(\frac{i\omega}{c} \overleftrightarrow{\Phi} \right) + \frac{\varepsilon\omega^2}{c^2} \overleftrightarrow{\Gamma}(\vec{r}, \vec{r}', \omega) &= -\frac{\omega^2}{c^2} \overleftrightarrow{\Gamma} \delta(\vec{r} - \vec{r}') \\ -\nabla \times \overleftrightarrow{\Phi} - \frac{i\varepsilon\omega}{c} \overleftrightarrow{\Gamma}(\vec{r}, \vec{r}', \omega) &= \frac{i\omega}{c} \overleftrightarrow{\Gamma} \delta(\vec{r} - \vec{r}') \end{aligned} \quad (4.111)$$

Up to this point, it is worthy to recall the geometry of the system that we are deriving. As usual, we imagine two semi-infinite plate with dielectric function ε_A and ε_B , separated apart by a finite space with dielectric function ε_C , along the xy -plane. Mathematically, the dielectric function is given by:

$$\varepsilon(\omega) = \begin{cases} \varepsilon_A(\omega), & z < 0; \\ \varepsilon_C(\omega), & 0 < z < l; \\ \varepsilon_B(\omega), & z > l; \end{cases} \quad (4.112)$$

Again, since the dielectric function considered in this case varies only in the z -axis, we may write, for $\vec{k} = (k_x, k_y, k_z) = (\vec{k}_\perp, k_z)$, where $\vec{k}_\perp = (k_x, k_y)$. Furthermore, we choose a particular coordinate system where \vec{k}_\perp points along the $+x$ axis. With this, the spatial Fourier transform may be written as

$$\overleftrightarrow{\Gamma}(\vec{r}, \vec{r}', \omega) = \frac{1}{(2\pi)^2} \int d\vec{k}_\perp e^{i\vec{k}_\perp \cdot (\vec{r} - \vec{r}')_\perp} \overleftrightarrow{\Gamma}(z, z', \vec{k}_\perp, \omega) \quad (4.113)$$

Eq. (4.109) and Eq. (4.110) can then be separated into its respective components. By doing so, we recall that the general formula for curl is:

$$\nabla \times \overleftrightarrow{S} = e_{ijk} S_{mj,i} \vec{e}_k \otimes \vec{e}_m \quad (4.114)$$

With that, we can write Eq. (4.110) in its respective component.

$$\begin{aligned} \frac{i\omega}{c} \overleftrightarrow{\Phi}_x &= \frac{\partial \overleftrightarrow{\Gamma}_z}{\partial y} - \frac{\partial \overleftrightarrow{\Gamma}_y}{\partial z} \\ \frac{i\omega}{c} \overleftrightarrow{\Phi}_y &= \frac{\partial \overleftrightarrow{\Gamma}_x}{\partial z} - \frac{\partial \overleftrightarrow{\Gamma}_z}{\partial x} \\ \frac{i\omega}{c} \overleftrightarrow{\Phi}_z &= \frac{\partial \overleftrightarrow{\Gamma}_y}{\partial x} - \frac{\partial \overleftrightarrow{\Gamma}_x}{\partial y} \end{aligned} \quad (4.115)$$

Also with that, we can write Eq. (4.109) as

$$\begin{aligned}
-\frac{\partial \vec{\Phi}_z}{\partial y} + \frac{\partial \vec{\Phi}_y}{\partial z} - \frac{i\omega}{c} \epsilon \vec{\Gamma}_x &= \frac{i\omega}{c} \delta(\vec{r}, \vec{r}') \hat{x} \\
-\frac{\partial \vec{\Phi}_x}{\partial z} + \frac{\partial \vec{\Phi}_z}{\partial x} - \frac{i\omega}{c} \epsilon \vec{\Gamma}_y &= \frac{i\omega}{c} \delta(\vec{r}, \vec{r}') \hat{y} \\
-\frac{\partial \vec{\Phi}_y}{\partial x} + \frac{\partial \vec{\Phi}_x}{\partial y} - \frac{i\omega}{c} \epsilon \vec{\Gamma}_z &= \frac{i\omega}{c} \delta(\vec{r}, \vec{r}') \hat{z}
\end{aligned} \tag{4.116}$$

Since the coordinate system we have chosen imply that \vec{k}_\perp points along the $+x$ axis, the equations may be simplified by noticing $\frac{\partial \vec{\Gamma}_j}{\partial y} = 0$, and $\frac{\partial \vec{\Gamma}_j}{\partial x} = ik \vec{\Gamma}_j$. In this case, $j = x, y, z$ is the second tensor's index, and $k = |\vec{k}_\perp|$. With this in place, we have

$$\begin{aligned}
\vec{\Phi}_x &= \frac{ic}{\omega} \frac{\partial \vec{\Gamma}_y}{\partial z} \\
\vec{\Phi}_z &= \frac{kc}{\omega} \vec{\Gamma}_y \\
\vec{\Gamma}_x &= -\frac{1}{\epsilon} \delta(z-z') \hat{x} - \frac{ic}{\omega \epsilon} \frac{\partial \vec{\Phi}_y}{\partial z} \\
\vec{\Gamma}_z &= -\frac{1}{\epsilon} \delta(z-z') \hat{z} - \frac{kc}{\omega \epsilon} \vec{\Phi}_y
\end{aligned} \tag{4.117}$$

These equations are then substituted into the y-components of Eq. (4.109) and Eq. (4.110).

We start by considering the y-components of Eq. (4.110),

$$\begin{aligned}
\frac{i\omega}{c} \vec{\Phi}_y &= \left(\frac{\partial \vec{\Gamma}_x}{\partial z} - \frac{\partial \vec{\Gamma}_z}{\partial x} \right) \\
\frac{i\omega}{c} \vec{\Phi}_y &= \frac{\partial}{\partial z} \left(-\frac{1}{\epsilon} \delta(z-z') \hat{x} - \frac{ic}{\omega \epsilon} \frac{\partial \vec{\Phi}_y}{\partial z} \right) \\
&\quad - ik \left(-\frac{1}{\epsilon} \delta(z-z') \hat{z} - \frac{kc}{\omega \epsilon} \vec{\Phi}_y \right) \\
\left[-\frac{\partial}{\partial z} \left(\frac{1}{\epsilon} \frac{\partial}{\partial z} \right) - \frac{\omega^2}{c^2} + \frac{k^2}{\epsilon} \right] \vec{\Phi}_y &= -\frac{i\omega}{c} \hat{x} \frac{\partial}{\partial z} \left(\frac{\delta(z-z')}{\epsilon} \right) - \frac{\omega k}{\epsilon c} \delta(z-z') \hat{z}
\end{aligned} \tag{4.118}$$

The y-component of Eq. (4.109) is then

$$\begin{aligned}
-\frac{\partial \vec{\Phi}_x}{\partial z} + \frac{\partial \vec{\Phi}_z}{\partial x} - \frac{i\omega}{c} \epsilon \vec{\Gamma}_y &= \frac{i\omega}{c} \delta(z-z') \hat{y} \\
-\frac{\partial}{\partial z} \left(\frac{i}{\omega} \frac{\partial \vec{\Gamma}_y}{\partial z} \right) + ik \vec{\Phi}_z - \frac{i\omega}{c} \epsilon \vec{\Gamma}_y &= \frac{i\omega}{c} \delta(z-z') \hat{y} \\
\left(-\frac{\partial^2}{\partial z^2} + k^2 - \frac{\omega^2 \epsilon}{c^2} \right) \vec{\Gamma}_y &= \frac{\omega^2}{c^2} \delta(z-z') \hat{y}
\end{aligned} \tag{4.119}$$

By rearranging the y-component of Eq. (4.109) and Eq. (4.110), we see that the results, Eq. (4.118) and Eq. (4.119) resembles the Green function's definition. The transverse electric (TE) and transverse magnetic (TM) Green function, $g^E(z, z')$ and $g^H(z, z')$

is then defined to be

$$\begin{aligned}\vec{\Gamma}_y &= \frac{\omega^2}{c^2} \hat{y} g^E(z, z') \\ \vec{\Phi}_y &= \frac{i\omega \hat{x}}{\epsilon' c} \frac{\partial}{\partial z'} (g^H(z, z')) - \frac{\omega k}{\epsilon' c} \hat{z} g^H(z, z')\end{aligned}\quad (4.120)$$

The Green functions $g^E(z, z')$ and $g^H(z, z')$ then satisfies

$$\begin{aligned}\left[-\frac{\partial}{\partial z} \left(\frac{1}{\epsilon} \frac{\partial}{\partial z} \right) - \frac{\omega^2}{c^2} + \frac{k^2}{\epsilon} \right] g^H(z, z') &= \delta(z - z') \\ \left(-\frac{\partial^2}{\partial z^2} + k^2 - \frac{\omega^2 \epsilon}{c^2} \right) g^E(z, z') &= \delta(z - z')\end{aligned}\quad (4.121)$$

Now, all components of $\vec{\Gamma}$ may be calculated from Eq. (4.117). First, by substituting the $\vec{\Phi}_y$ into $\vec{\Gamma}_x$ and $\vec{\Gamma}_z$, we have

$$\begin{aligned}\vec{\Gamma}_x &= -\frac{1}{\epsilon} \delta(z - z') \hat{x} - \frac{i}{\omega \epsilon} \frac{\partial}{\partial z} \left(\frac{i\omega \hat{x}}{\epsilon'} \frac{\partial}{\partial z'} (g^H(z, z')) - \frac{\omega k}{\epsilon'} \hat{z} g^H(z, z') \right) \\ \vec{\Gamma}_z &= -\frac{1}{\epsilon} \delta(z - z') \hat{z} - \frac{k}{\omega \epsilon} \left(\frac{i\omega \hat{x}}{\epsilon'} \frac{\partial}{\partial z'} (g^H(z, z')) - \frac{\omega k}{\epsilon'} \hat{z} g^H(z, z') \right)\end{aligned}\quad (4.122)$$

With that, all 9 elements of the dyadic $\overleftrightarrow{\Gamma}$ are listed as below.

$$\begin{aligned}\Gamma_{xx} &= -\frac{1}{\epsilon} \delta(z - z') + \frac{1}{\epsilon} \frac{\partial}{\partial z} \left(\frac{1}{\epsilon'} \frac{\partial}{\partial z'} (g^H(z, z')) \right) \\ \Gamma_{xy} &= 0 \\ \Gamma_{xz} &= \frac{ik}{\epsilon \epsilon'} \frac{\partial}{\partial z} (g^H(z, z')) \\ \Gamma_{yx} &= 0 \\ \Gamma_{yy} &= \frac{\omega^2}{c^2} g^E(z, z') \\ \Gamma_{yz} &= 0 \\ \Gamma_{zx} &= -\frac{ik}{\epsilon \epsilon'} \frac{\partial}{\partial z'} (g^H(z, z')) \\ \Gamma_{zy} &= 0 \\ \Gamma_{zz} &= -\frac{1}{\epsilon} \delta(z - z') + \frac{k^2}{\epsilon \epsilon'} (g^H(z, z'))\end{aligned}\quad (4.123)$$

With this, the attention is refocused toward the change in energy, Eq. (4.106). By inserting Eq. (4.113), we see that the change in energy per area is given by

$$\frac{\delta E}{A} = \frac{i\hbar}{4\pi(2\pi)^2} \int_{-\infty}^{\infty} \int \int \delta \epsilon(z) \Gamma_{jj} \left(z, z', \vec{k}_{\perp}, \omega \right) dz d\vec{k}_{\perp} d\omega \quad (4.124)$$

It is noticed that the integral of the exponential term in Eq. (4.113) gives the area, A . The equation involving change in the energy requires the evaluation of the trace of the dyadic

Green's function $\overleftrightarrow{\Gamma}$. By taking the limit $z' \rightarrow z$, we may omit the δ -functions appearing in Eq. (4.123), which then yields

$$\Gamma_{jj} = \left(\frac{1}{\varepsilon} \frac{\partial}{\partial z} \left(\frac{1}{\varepsilon'} \frac{\partial}{\partial z'} g^H \right) + \frac{\omega^2}{c^2} g^E + \frac{k^2}{\varepsilon \varepsilon'} g^H \right) \Big|_{z=z'} \quad (4.125)$$

The variation of dielectric constant between interface may be computed by recalling Eq. (4.73) from the previous source theory derivation. By varying the distance l , we have

$$\delta \varepsilon(z) = \delta l (\varepsilon_3 - \varepsilon_2) \delta(z-l) \quad (4.126)$$

The limit in Eq. (4.125) can now be evaluated. First we recall the definition of force per area as the distance variation of energy,

$$\begin{aligned} F &= -\frac{1}{A} \frac{\partial E}{\partial l} \\ &= -\frac{\partial}{\partial l} \left(\frac{i\hbar}{4\pi(2\pi)^2} \int_{-\infty}^{\infty} \int \int \delta \varepsilon(z) \Gamma_{jj}(z, z', \vec{k}_{\perp}, \omega) dz d\vec{k}_{\perp} d\omega \right) \\ &= \left(\frac{i\hbar}{4\pi(2\pi)^2} \int_{-\infty}^{\infty} \int (\varepsilon_2 - \varepsilon_3) \left(\frac{1}{\varepsilon} \frac{\partial}{\partial z} \left(\frac{1}{\varepsilon'} \frac{\partial}{\partial z'} g^H \right) + \frac{\omega^2}{c^2} g^E + \frac{k^2}{\varepsilon_2 \varepsilon_3} g^H \right) d\vec{k}_{\perp} d\omega \right) \Big|_{z=z'=l} \end{aligned} \quad (4.127)$$

where we have evaluated the integral at the interface between media 3 and 2, at $z = l$. The continuity of E_x , E_y , and εE_z at the interface implies that g^E , g^H , and

$$\frac{1}{\varepsilon} \frac{\partial}{\partial z} \left(\frac{1}{\varepsilon'} \frac{\partial}{\partial z'} g^H \right) \quad (4.128)$$

must be continuous too. With this, the Green functions g^E , g^H may be solved.

To solve the Green functions, the quantity

$$K^2 = k^2 - \frac{\omega^2 \varepsilon}{c^2} \quad (4.129)$$

is introduced. Here we notice K is positive because ω^2 is negative if we consider a complex rotation. Hence, the electric Green function in region 2 takes a simple form:

$$g^E(z, z') = \frac{e^{-K_2|z-z'|} + r e^{-K_2(z+z'-2l)}}{2K_2} \quad (4.130)$$

Now, the reflection coefficient is given by

$$1 + r = \frac{2K_2}{K_2 + K_3} + \frac{4K_2K_3}{K_3^2 - K_2^2} \left[\frac{K_3 + K_1}{K_3 - K_1} \frac{K_3 + K_2}{K_3 - K_2} e^{2K_3l} - 1 \right]^{-1} \quad (4.131)$$

The magnetic Green function will then take the same form, with a minor replacement of

$$K \rightarrow \frac{K}{\varepsilon} = K' \quad (4.132)$$

in all K , except the ones in the exponential. With this, we have

$$g^H(z, z') = \frac{e^{-K_2|z-z'|} + r'e^{-K_2(z+z'-2l)}}{2K_2'} \quad (4.133)$$

$$1 + r' = \frac{2K_2'}{K_2' + K_3'} + \frac{4K_2'K_3'}{K_3'^2 - K_2'^2} \left[\frac{K_3' + K_1' K_3' + K_2'}{K_3' - K_1' K_3' - K_2'} e^{2K_3'l} - 1 \right]^{-1} \quad (4.134)$$

Now with all these information, the force per unit area in Eq. (4.127) can be evaluated as below.

$$\begin{aligned} F &= \left(\frac{i\hbar}{4\pi(2\pi)^2} \int_{-\infty}^{\infty} \int (\varepsilon_2 - \varepsilon_3) \left(\frac{1}{\varepsilon} \frac{\partial}{\partial z} \left(\frac{1}{\varepsilon'} \frac{\partial}{\partial z'} g^H \right) + \frac{\omega^2}{c^2} g^E + \frac{k^2}{\varepsilon_2 \varepsilon_3} g^H \right) d\vec{k}_{\perp} d\omega \right) \Big|_{z=z'=l} \\ &= \left(\frac{i\hbar}{4\pi(2\pi)^2} \int_{-\infty}^{\infty} \int (\varepsilon_2 - \varepsilon_3) \left(\frac{1}{\varepsilon_2} \frac{\partial}{\partial z} \left(\frac{1}{\varepsilon_3} \frac{\partial}{\partial z'} \left(\frac{e^{-K_2|z-z'|} + r'e^{-K_2(z+z'-2l)}}{2K_2'} \right) \right) \right) \right. \\ &\quad \left. + \frac{\omega^2}{c^2} \left(\frac{1 + re^{-2K_2(z-l)}}{2K_2} \right) + \frac{k^2}{\varepsilon_2 \varepsilon_3} \left(\frac{1 + r'e^{-2K_2(z-l)}}{2K_2'} \right) \right) d\vec{k}_{\perp} d\omega \Big|_{z=z'=l} \\ &= \frac{i\hbar}{4\pi(2\pi)^2} \int_{-\infty}^{\infty} \int \left(\frac{\omega^2}{2K_2 c^2} (\varepsilon_2 - \varepsilon_3) (1 + r) + \left(\frac{K_2 K_3 + k^2}{2K_2' \varepsilon_2 \varepsilon_3} \right) (\varepsilon_2 - \varepsilon_3) (1 + r') \right) d\vec{k}_{\perp} d\omega \\ &= \frac{i\hbar}{4\pi(2\pi)^2} \int_{-\infty}^{\infty} \int (A + B) d\vec{k}_{\perp} d\omega \quad (4.135) \end{aligned}$$

The integrand A and B in Eq. (4.135) can be evaluated now. For A , we have

$$\begin{aligned} A &= \frac{\omega^2}{2K_2 c^2} (\varepsilon_2 - \varepsilon_3) (1 + r) \\ &= \frac{1}{2K_2} \left(-k^2 + \frac{\omega^2 \varepsilon_2}{c^2} + k^2 - \frac{\omega^2 \varepsilon_3}{c^2} \right) \left(\frac{2K_2}{K_2 + K_3} + \frac{4K_2 K_3}{K_3^2 - K_2^2} \left[\frac{K_3 + K_1 K_3 + K_2}{K_3 - K_1 K_3 - K_2} e^{2K_3'l} - 1 \right]^{-1} \right) \\ &= (K_3 - K_2) + 2K_3 \left[\frac{K_3 + K_1 K_3 + K_2}{K_3 - K_1 K_3 - K_2} e^{2K_3'l} - 1 \right]^{-1} \quad (4.136) \end{aligned}$$

By similar mathematical manipulation for integrand B in Eq. (4.135), we have

$$B = (K_3 - K_2) + 2K_3 \left[\frac{K_3 + K_1 K_3 + K_2}{K_3 - K_1 K_3 - K_2} e^{2K_3'l} - 1 \right]^{-1} \quad (4.137)$$

We then substitute everything into Eq. (4.135) to arrive at

$$\begin{aligned} F &= \frac{i\hbar}{4\pi(2\pi)^2} \int_{-\infty}^{\infty} \int 2(K_3 - K_2) + 2K_3 \left(\left[\frac{K_3' + K_1' K_3' + K_2'}{K_3' - K_1' K_3' - K_2'} e^{2K_3'l} - 1 \right]^{-1} \right. \\ &\quad \left. + \left[\frac{K_3 + K_1 K_3 + K_2}{K_3 - K_1 K_3 - K_2} e^{2K_3'l} - 1 \right]^{-1} \right) d\vec{k}_{\perp} d\omega \quad (4.138) \end{aligned}$$

We see that the first term on the right is again, corresponding to a change in the volume energy of the system, and it does not depend on l . This term is then omitted. The remaining term, then, provides the Casimir force, and may be written in terms of imaginary frequency, $\xi = -i\omega$.

$$F = -\frac{\hbar}{2\pi^2} \int_0^\infty \int_0^\infty kdkK_3 \left(\left[\frac{K_3' + K_1'}{K_3' - K_1'} \frac{K_3' + K_2'}{K_3' - K_2'} e^{2K_3'l} - 1 \right]^{-1} + \left[\frac{K_3 + K_1}{K_3 - K_1} \frac{K_3 + K_2}{K_3 - K_2} e^{2K_3l} - 1 \right]^{-1} \right) d\xi \quad (4.139)$$

This result is again identical to the Lifshitz's formula. With some algebraic manipulation, and taking the usual Fresnel reflectivity in Eq. (4.80), we arrive at the final Eq. (3.44).

4.5 Discussions

In this chapter, we have revised the second quantization of quantum mechanics. Focus was made on the operator ordering. We then show, by using quantum electrodynamics, that the Casimir effect may be derived directly by considering the source field. When we first consider Casimir effect in this alternative explanation, it seems rather implausible. Such an effect was typically explained in terms of the changes in the vacuum field due to presence of boundary. However upon using the normal ordering, it is noted that the Casimir force can be equally explained by the source theory. It might be compelling now to agree that the source field is a much elegant explanation of the origin of Casimir effect, as it made no explicit reference to the vacuum field, which is counter-intuitive. However, from another point of view, both theories are equally intriguing, and we may calculate whatever we need from either theory. Since it's impossible to experimentally distinguish between the "vacuum" effect, and the "source" effect, it is safe to say that both theories should be equally appreciated.

Also, the original derivation of Casimir effect from source theory, using the energy variation approach was revisited. The derivation is rather elegant, where we have considered the response of the action to a source variation, due to the polarization of the particle itself. While the derivation may be far-fetched, it is appreciated for both its historical value and elegance.

CHAPTER 5

MATERIAL DEPENDENT CASIMIR FORCE

In the previous chapters, several alternative theories and interpretations of the Casimir force have been presented. With these theories in mind, we raised a concern: How can the Casimir force affect the direction of our technology advancement? Is it possible to utilize the Casimir force to our advantage in designing the next generation technology? Indeed, it turns out that as NEMS technology advances, we are effectively scaling down the size of those mechanical systems. This will then inevitably forces surfaces to be on close proximity with each other. The Casimir force that acts on these surfaces will then causes problem such as stiction. Furthermore, since NEMS components are small, a relatively small force (such as Casimir force) is sufficient to interfere with the normal operation of the system. A repulsive Casimir force may prevent such problems. In this chapter, we attempt to address such concerns by examining the change in Casimir force with material constants for two parallel plate configurations. We will arbitrary take each of the plate as plate *A* and plate *B*.

In the first section, we will build up an intuition on the change in Casimir force due to the change in the dielectric permittivity ϵ and magnetic permeability μ of a material. We then look into the possibility of finding a "stable equilibrium", i.e. an inter-plate distance $l = x$ where the force is repulsive when $l = x - \delta x$ and attractive when $l = x + \delta x$. Later, we attempt to find local maxima and minima in the range of material in an attempt to maximize the Casimir force.

5.1 Changes in Material Constant

Generally, the Casimir force between two parallel plates is attractive if both plates are identical, i.e. $r_N^A(\xi, k) = r_N^B(\xi, k)$ (Kenneth & Klich, 2006). A notable configuration for this case is that when both plates are perfectly conducting. Mathematically, we can take $\epsilon \rightarrow \infty$ and μ as finite in the Lifshitz formula to obtain the original result derived by Casimir, as shown in Section 3.3.

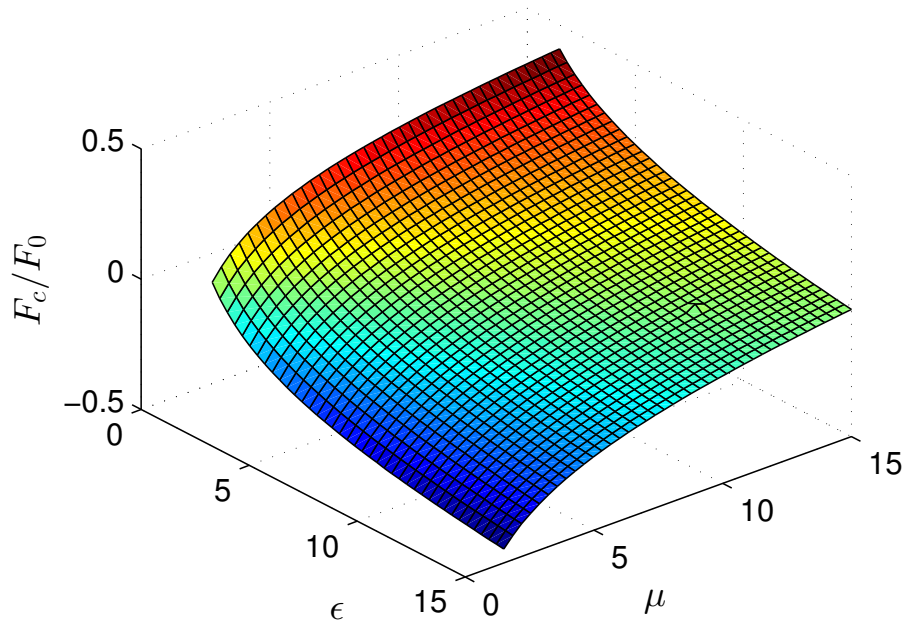
However, the Casimir force may be repulsive if both plates' behaviour is not identical over a range of frequency. In fact, by looking at the Lifshitz formula, Eq. (3.44), we may deduce that the integrand of Casimir force can be negative when the reflection coefficient of both plates, $r_N^A(\xi, k)$ and $r_N^B(\xi, k)$, are different in sign. From the reflectivity coefficient, Eq. (3.45), both plates will have different sign on the reflectivity coefficient if they have different electromagnetic properties over some range of frequency, i.e.:

$$\begin{aligned} \frac{\text{Re}[\varepsilon_A(\omega)]}{\text{Re}[\mu_A(\omega)]} &\gg 1 \\ \frac{\text{Re}[\mu_B(\omega)]}{\text{Re}[\varepsilon_B(\omega)]} &\gg 1 \end{aligned} \quad (5.1)$$

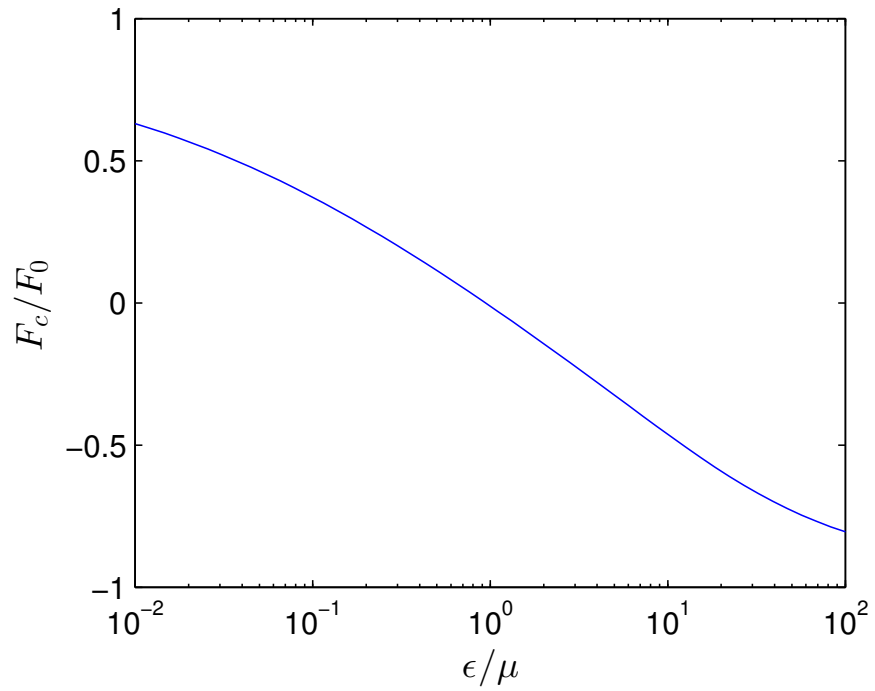
To visualize the variation of force between two plates, the Casimir force between a perfectly conducting plate (i.e. $r_{TE} = -1$, $r_{TM} = 1$), and a plate of real, arbitrary material constant is plotted in Fig. (5.1). The inter-plate distance l is arbitrary in this case. As a side note, the positive (negative) sign of F_c corresponds to repulsive (attractive) Casimir force. Both plots are normalized to the maximum Casimir attraction F_0 between two plates, i.e. the Casimir force between two perfectly conducting plate. As expected, we notice a general increase in the Casimir attraction as the plate become non-magnetic (i.e. $\varepsilon/\mu \gg 1$), while Casimir repulsion occur as the plate become magnetic (i.e. $\varepsilon/\mu \ll 1$).

It is also interesting to find the maximum repulsive force possible between two plates. It may be achieved when both plates are not-identical over the whole range of frequency. Here, we take plate A as an infinitely permeable plate, $r_{TE} = -1$, $r_{TM} = 1$, and plate B as a pure magnetic material, that is $\mu \rightarrow \infty$, ε finite. From Eq. (3.42) we have:

$$\begin{aligned} \lim_{\mu \rightarrow \infty} r_{TE}(i\xi, k_{\perp}) &= \lim_{\mu \rightarrow \infty} \frac{\mu q - k}{\mu q + k} \\ &= \lim_{\mu \rightarrow \infty} \frac{\mu \sqrt{k_{\perp}^2 + \frac{\xi^2}{c^2}} - \sqrt{k_{\perp}^2 + \frac{\xi^2}{c^2} \varepsilon \mu}}{\mu \sqrt{k_{\perp}^2 + \frac{\xi^2}{c^2}} + \sqrt{k_{\perp}^2 + \frac{\xi^2}{c^2} \varepsilon \mu}} \\ &= 1 \end{aligned} \quad (5.2)$$



a)



b)

Figure 5.1: The variation of (normalized) Casimir force between a perfectly conducting plate with a plate with varied material constant, at arbitrary distance. (a) 3D plot and (b) The increase of Casimir attraction as the ratio of ϵ/μ increases.

$$\begin{aligned}
\lim_{\mu \rightarrow \infty} r_{TM}(i\xi, k_{\perp}) &= \lim_{\mu \rightarrow \infty} \frac{\varepsilon q - k}{\varepsilon q + k} \\
&= \lim_{\mu \rightarrow \infty} \frac{\varepsilon \sqrt{k_{\perp}^2 + \frac{\xi^2}{c^2}} - \sqrt{k_{\perp}^2 + \frac{\xi^2}{c^2}} \varepsilon \mu}{\varepsilon \sqrt{k_{\perp}^2 + \frac{\xi^2}{c^2}} + \sqrt{k_{\perp}^2 + \frac{\xi^2}{c^2}} \varepsilon \mu} \\
&= -1
\end{aligned} \tag{5.3}$$

Again, by simple limit computation, we notice that the reflectivity coefficients of a perfect magnetic material is $r_{TE} = 1$, $r_{TM} = -1$, which is exactly opposite of a perfect conductor. Inserting these values into Eq. (3.44) yields:

$$F(l) = \frac{\hbar}{\pi^2} \int_0^{\infty} k_{\perp} dk_{\perp} \int_0^{\infty} d\xi \sqrt{k_{\perp}^2 + \frac{\xi^2}{c^2}} \left(\frac{e^{-2l\sqrt{k_{\perp}^2 + \xi^2/c^2}}}{1 + e^{-2l\sqrt{k_{\perp}^2 + \xi^2/c^2}}} \right) \tag{5.4}$$

We then take the coordinate transform from Cartesian coordinate $(k_{\perp}, \xi/c)$ to polar coordinate (r, θ) . The equation then reads

$$\begin{aligned}
F(l) &= \frac{\hbar c}{\pi^2} \int_0^{\infty} \int_0^{\pi/2} (r \cos \theta) r^2 dr d\theta \left(\frac{e^{-2lr}}{1 + e^{-2lr}} \right) \\
&= \frac{\hbar c}{\pi^2} \int_0^{\infty} r^3 dr \left(\frac{e^{-2lr}}{1 + e^{-2lr}} \right) \\
&= \frac{\hbar c}{\pi^2} \left(\frac{7\pi^4}{1290l^4} \right) \\
&= \left(\frac{7}{8} \right) \frac{\hbar c \pi^2}{240l^4} \\
&= -\frac{7}{8} F_0(l)
\end{aligned} \tag{5.5}$$

where $F_0(l)$ is the Casimir attraction between two perfectly conducting plate. This result is pretty noteworthy, as the ideal case for repulsion force is always smaller than the attractive force by a factor of $7/8$.

5.2 Casimir Force in Equilibrium: Piecewise Model

We have noticed a general trend in the Casimir force as the material constants change, in particular the ratio of ε/μ . In this section, we will explore the change in Casimir force as the distance between plates, l increases.

To simplify the discussion, we have adopted a similar normalization scheme as Yang et al. (2010), which have done an interesting discussion on this topic. In this scheme,

the frequencies are expressed in units of ω_0 , wavelengths in vacuum are in units of $\lambda_0 = 2\pi c/\omega_0$, and Casimir forces are expressed in terms of $K = hc/(64\pi^3\lambda_0^4)$. The values of λ_0 is arbitrary, but for an experimental reasonable force we may take it as $\lambda_0 = 10^{-7}m^{-1}$.

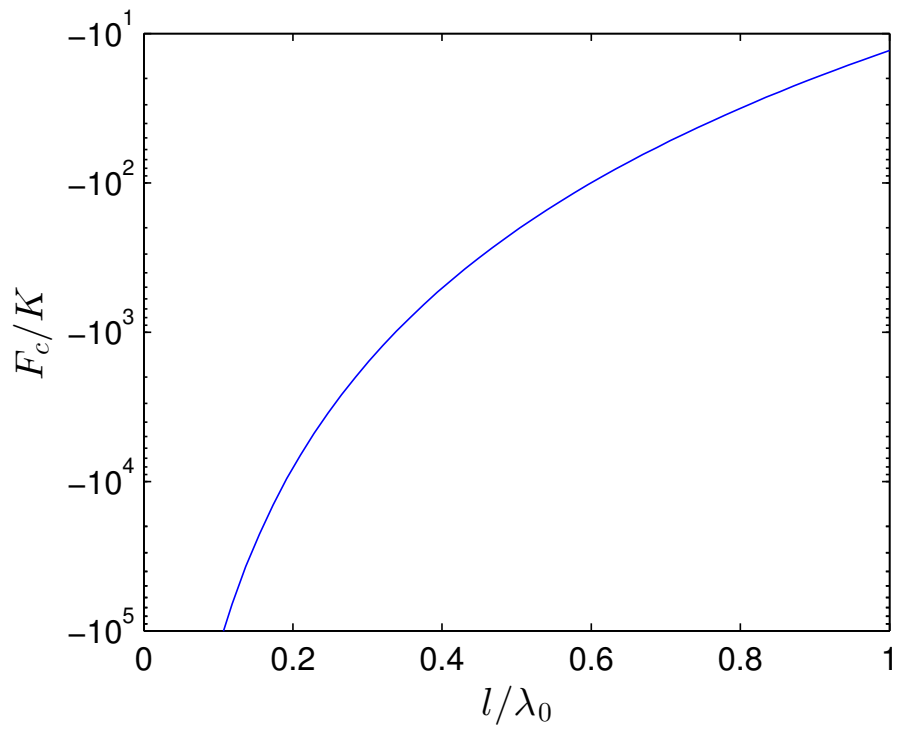
First, we have plotted the change of Casimir force between two perfect conductor in Fig. (5.2 a), as a function of distance. Also the Casimir force between a perfect conducting plate and a perfect magnetic plate is plotted in Fig. (5.2 b). In these figures, it is noticed that the magnitude of Casimir force generally decreases as distances increases, which is expected. However, there are no changes in the sign of Casimir force at different distances. A change in sign for the force (with respect to distance) is an interesting feature, as we may discover equilibrium points where the effective Casimir force is zero.

To demonstrate the possibility of equilibrium points, an ideal material with piecewise material constants shown in Eq. (5.6) is considered (Yang et al., 2010). Upon first glance, we noticed that this material behaves magnetically at low frequencies, and at higher frequencies, it behaves as a dielectric material. The Casimir force between this plate placed parallel to a perfectly conducting plate is plotted in Fig. (5.3 a). The Casimir force is noted to be attractive at short distances. However, as distances between plate increases to about $l \approx 0.2\lambda_0$, the Casimir force switched to repulsive force. An unstable equilibrium exist here, as the force varies from attractive at short distances, to zero, then to repulsive at longer distance.

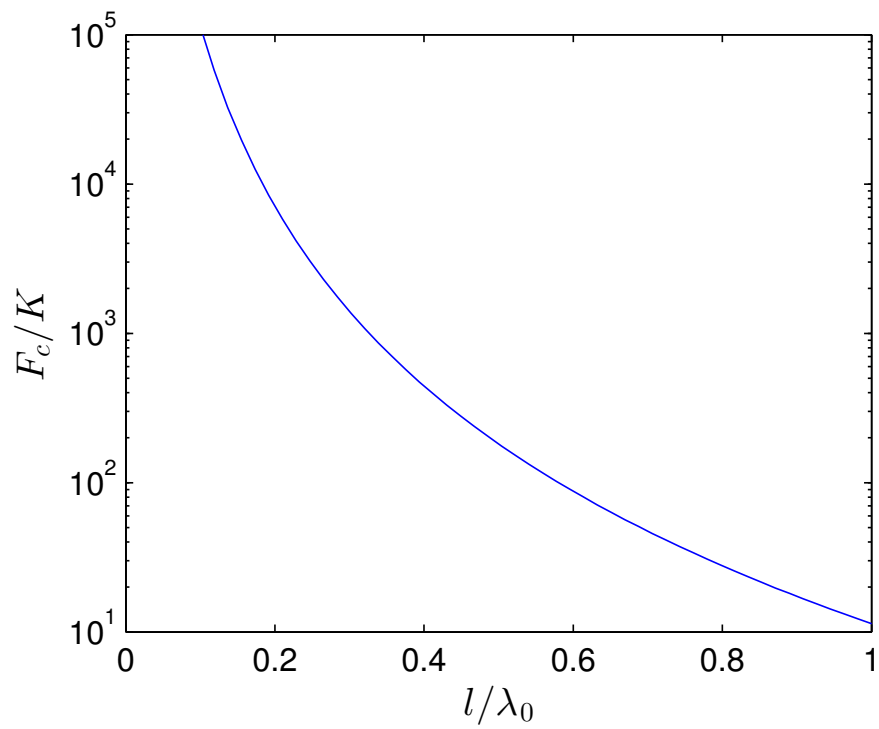
$$\varepsilon = \begin{cases} 1, & \omega < 0.75\omega_0, \\ 15, & \omega \geq 0.75\omega_0, \end{cases} \quad \mu = \begin{cases} 50, & \omega < 0.75\omega_0, \\ 0.5, & \omega \geq 0.75\omega_0, \end{cases} \quad (5.6)$$

Let's consider a material in Eq. (5.7) that behaves as a dielectric material at low frequencies, and magnetically at higher frequencies. Similarly, the Casimir force between this plate placed parallel to a perfectly conducting plate is plotted in Fig. (5.3 b). In this case, the Casimir force varies from repulsive at short distances, to zero and lastly attractive. This is a typical characteristic of a stable equilibrium, where a small change in distance from the equilibrium will be counteracted by a force in the opposite direction.

$$\varepsilon = \begin{cases} 5, & \omega < 0.8\omega_0, \\ 1, & \omega \geq 0.8\omega_0, \end{cases} \quad \mu = \begin{cases} 0.5, & \omega < 0.8\omega_0, \\ 50, & \omega \geq 0.8\omega_0, \end{cases} \quad (5.7)$$

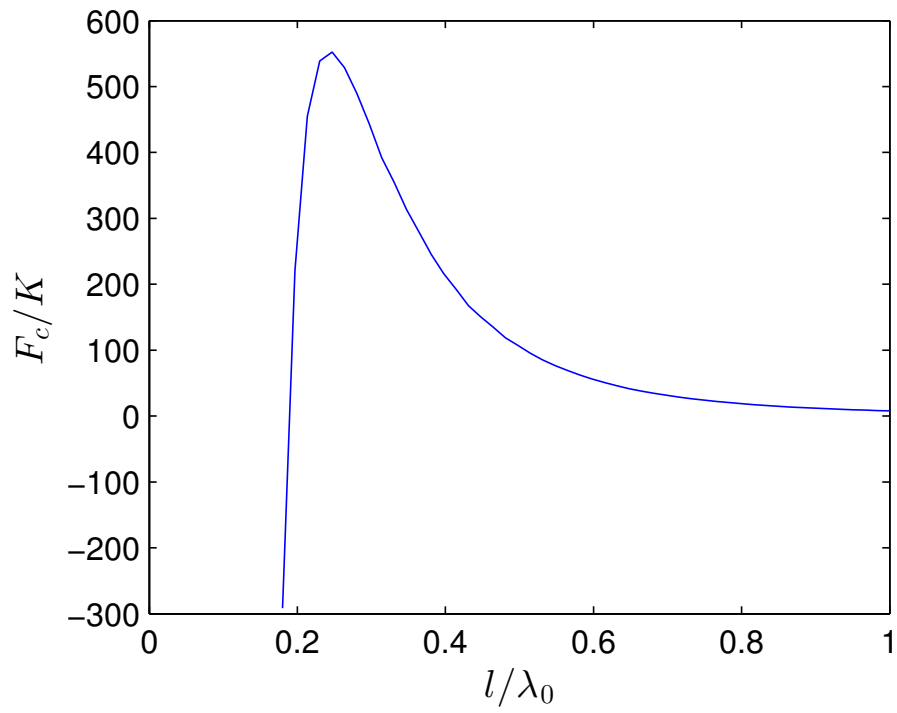


a)

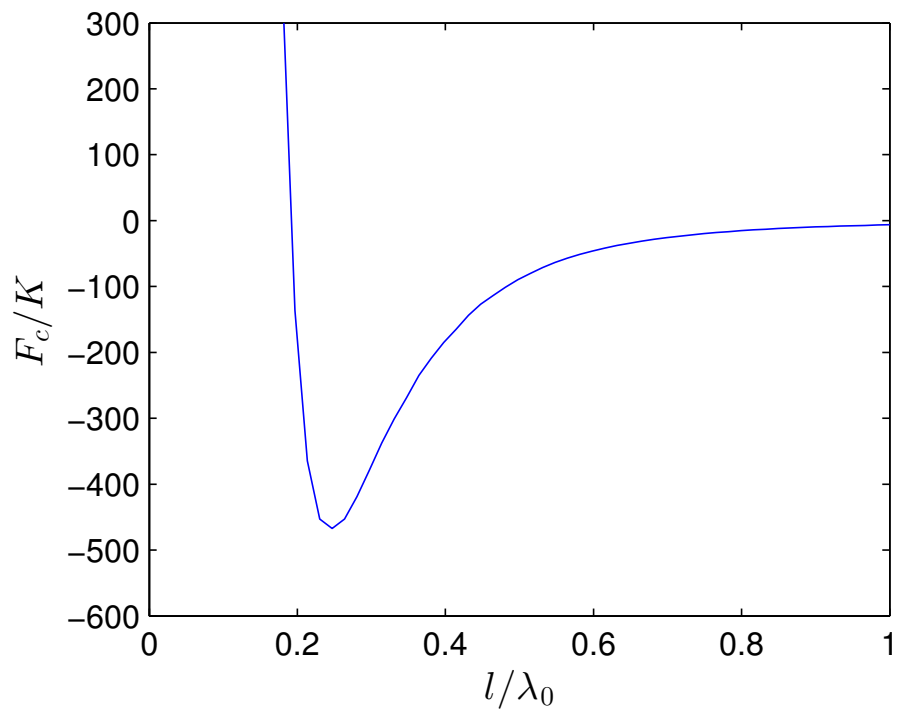


b)

Figure 5.2: The variation of Casimir force between a perfectly conducting plate and (a) a perfectly conducting plate and (b) a perfect magnetic plate, at different distances.



a)



b)

Figure 5.3: The variation of Casimir force between a perfectly conducting plate and a material with material constant given by (a) Eq. (5.6) and (b) Eq. (5.7), at different distances.

There is another interesting result here. From the second case with Eq. (5.7), we have noticed that the Casimir force at short distance is repulsive. This corresponds to the material's behaviour at high frequency, which is magnetic (different from the second plate we are considering). As the distance increases, the force becomes attractive. This corresponds to the material's behaviour at low frequency, where both plates behaves as dielectric material. This suggest that as inter-plate distance decreases (increases), the Casimir force depends more on the behaviour of the system at higher (lower) frequency. To confirm the suspicion we have, the differential of Casimir force, $\frac{dF_c}{d\xi}$ for the material in Eq. (5.7) is plotted in Fig. (5.4), for distance $l = 0.25\lambda_0$ and $l = \lambda_0$. The figure shows a discontinuity at $\xi \approx 10^{15}$ for both curve, corresponding to $\omega = 0.75\omega_0$. Apart from the decrease in the overall magnitude of $\frac{1}{K} \frac{dF_c}{d\xi}$ when the inter-plate distance increases, the overall features have also been shifted to lower frequency. For example, the peak in attraction force had been shifted by almost one order of magnitude towards the left. Furthermore, the repulsion force, provided by frequencies $\omega > 0.75\omega_0$ is very much lower in magnitude for the case of $l = \lambda_0$. This effectively confirms our suspicion: When inter-plate distance increases (decreases), the Casimir force depends on the behaviour of system at lower (higher) frequency. This interesting phenomenon was highlighted by Yang et al. (2010).

5.3 Metamaterials

In the previous section, an ideal material with piecewise material constant was shown to exhibits stable equilibrium. This is rather interesting, as a stable equilibrium in a NEMS system implies no stiction. Furthermore, the system will be subjected to a restoring force as soon as it is out of equilibrium. In this section, the concept will be realized by considering practical materials (Yang et al., 2010). In particular, metamaterials are considered due to its exotic magnetic property.

5.3.1 Metamaterials - An Introduction

Metamaterials are artificially engineered composites which offer control on electromagnetic wave propagation through structuring on a fine scale (compared to the wavelength of light). When the dimension of the constituent structure, and it's separation

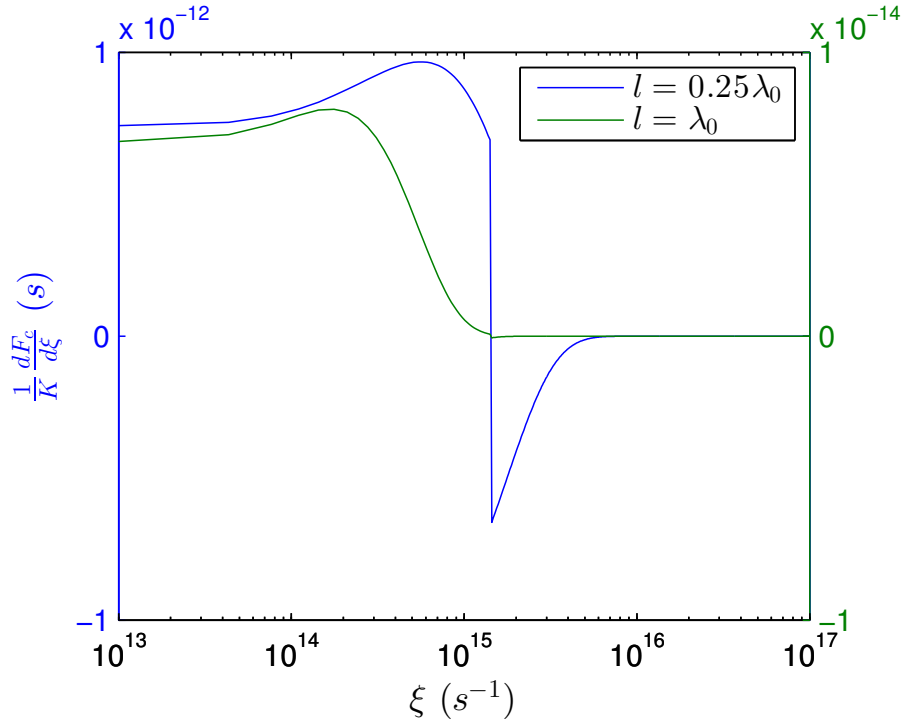


Figure 5.4: Variation of $\frac{dF_c}{d\xi}$ vs frequencies ξ , for different inter-plate distance l . It is interesting to note that there is a discontinuity at $\xi \approx 10^{15} s^{-1}$, for both cases.

between neighbouring structure are much smaller compared to wavelength of the electromagnetic wave, the entire ensemble will then behave as a continuum for the electromagnetic waves. Unlike conventional materials, metamaterials did not gain their properties from the composition, but rather from the uniquely designed structures.

The use of metallic structures as artificial media has been studied at frequencies below microwave frequencies since 1940s (Collin, 1991). However, initial efforts only allow control on the permittivity of the metamaterial. In 1999, Pendry et al. proposed methods for fabricating artificial magnetic metamaterial. The microstructure, known as a split-ring resonator (SRR) was engineered with nonmagnetic conductors. By tuning the dimension and design of the structural unit, SRR was shown to have tunable magnetic permeability over the microwave regime. Furthermore, the relative permeability can even be negative over a range of frequency as a result of resonance, due to internal capacitance and inductance. This removes the previously known limitation whereby most natural occurring materials are non-magnetic in high frequency regions.

With the development of metamaterial, exotic phenomena were discovered. For example, in 2000, a media with negative refractive index (NIMs, also known as left-handed

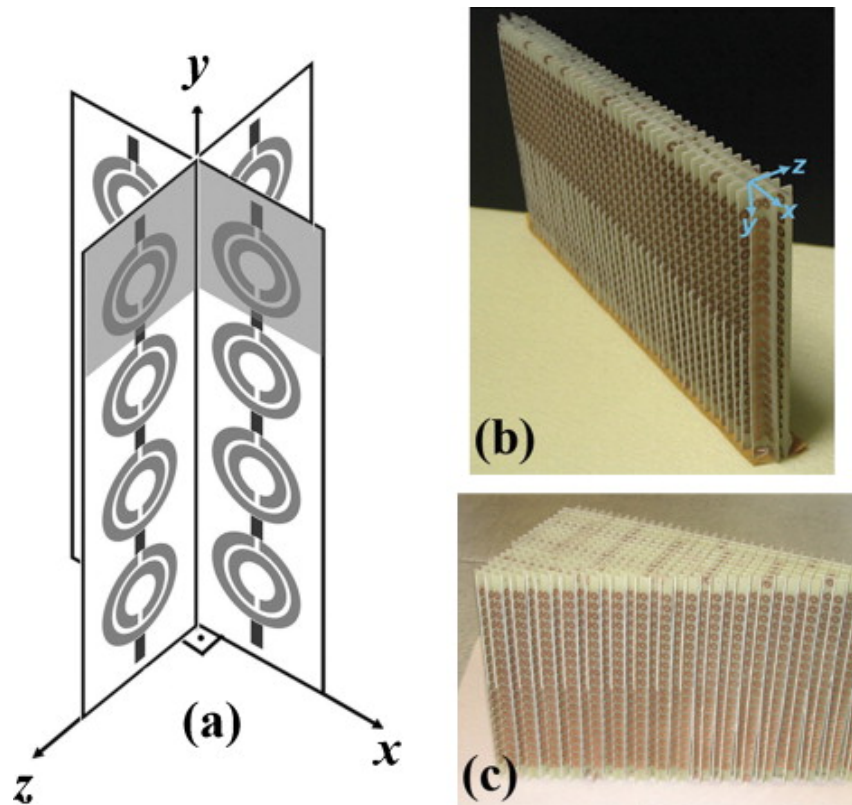


Figure 5.5: The structure of a left hand metamaterial is shown above. (a) A schematic drawing of a two dimensional split-ring resonator on the front, and wires on the back of the printed circuit board. (b) A three layer 2D slab shaped left-hand metamaterial. (c) A prism-shaped left-hand metamaterial. Image courtesy of Ozbay and Aydin (2008).

materials) was fabricated (Smith, Padilla, Vier, Nemat-Nasser, & Schultz, 2000). NIMs had brought the concept of refractive index to a new paradigm, along with thousands of potential applications to manipulate light with revolutionary impacts on the present-days' optical technology.

For instance, a slab made of negative refractive index material can be used to focus all Fourier components of a 2D image. This is contrasted to conventional lens where the sharpness of image is limited by the diffraction limit, which is related to the wavelength of light (Pendry, 2000). Metamaterial antennas are shown to have greatly increased radiated power compared to conventional antennas (Enoch, Tayeb, Sabouroux, Guérin, & Vincent, 2002). Furthermore, metamaterials with effective ϵ and effective μ near to zero had become subject of investigation of nonlinear optics. Such materials may be found naturally at infrared and optical region, or artificially synthesized as metamaterials at a desired frequency. With that, it is possible to "squeeze" electromagnetic waves to tunnel through a narrow channel, which is filled with ϵ -near-zero materials (Silveirinha

& Engheta, 2006).

Given that the Casimir force between plates depends on the material constants, metamaterials are proven to be interesting materials for research in Casimir force. In depth research was done by several researchers. For instance, the possibility of quantum levitating an ultrathin conductor have been investigated by having a NIM lens sandwiched between two perfectly conducting plates (Zhang et al., 2005). Furthermore, Yang et al. (2010) has studied the variation of Casimir force between metamaterial plates. As previously emphasised, the Lifshitz formula requires the material constants of both plates on all frequencies as input. Hence, we will model the dispersive constants of a metamaterial by using the Drude-Lorentz single resonant model, as given below.

$$\{\varepsilon, \mu\} = 1 + \frac{\omega_{P_v}^2}{\omega_{T_v}^2 - \omega^2 - i\gamma_v\omega} \quad (5.8)$$

In Eq. (5.8), $v = e, m$ refers to ε and μ respectively, while ω_{P_v} , ω_{T_v} , γ_v are the plasma frequency, the resonance frequency, and the damping frequency respectively.

5.3.2 Casimir force on Metamaterials

In this part, the Casimir force between a metamaterial and a perfectly conducting plate is considered (Yang et al., 2010). The metamaterial is modelled using Eq. (5.8) with parameter $\omega_{P_e} = \omega_0$, $\omega_{T_e} = 0.05\omega_0$, $\omega_{P_m} = 5.5\omega_0$, $\omega_{T_m} = 2.5\omega_0$, and $\gamma_{e(m)} = 10^{-2}\omega_{T_{e(m)}}$. The real part of metamaterial's dielectric function and permeability is plotted in Fig. (5.6 a). In the figure, we notice that the material is mainly electric in lower frequency. In mid-frequency band, the material is magnetic. Hence in this case we expect a stable equilibrium in the Casimir force. As usual, the Casimir force between these plate are plotted in Fig. (5.6 b), for varied distance. As expected, with the right combination, it is indeed possible for metamaterials to exhibit stable equilibrium.

It is possible to change the position of equilibrium, and it's stability by changing the values of resonant frequency and plasma frequency, for both electric and magnetic part (Yang et al., 2010). For instance, a change in plasma frequency of the dielectric function (while keeping the resonant frequency constant) will result in a higher dominance in the overall electric property of the material. The change in this feature is plotted in Fig. (5.7 a). As we can notice, a slight change in the dielectric function's plasma

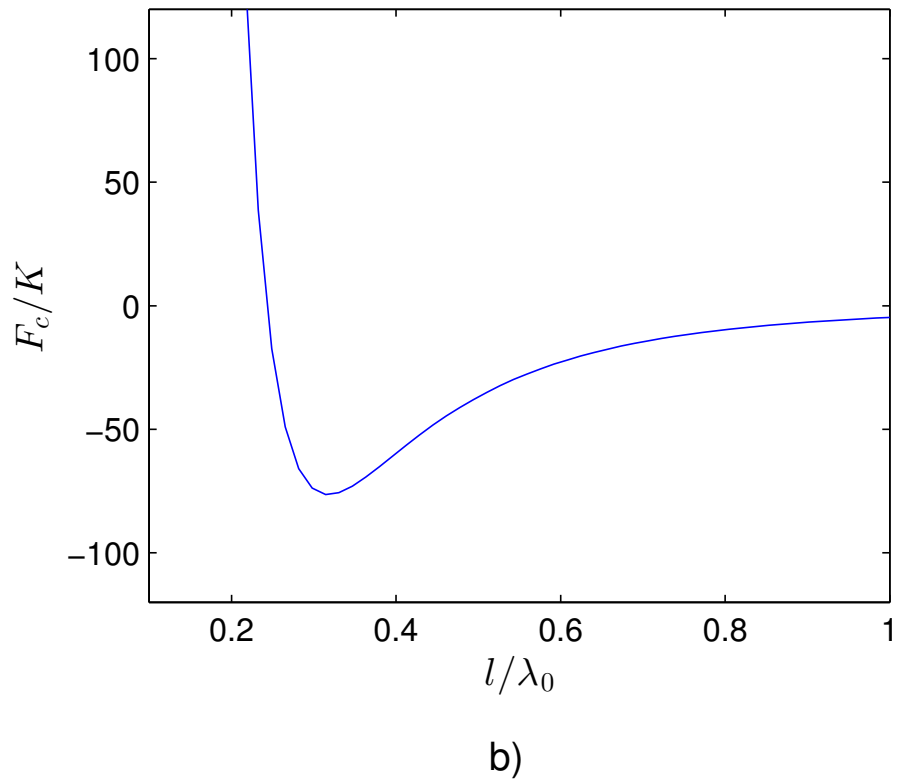
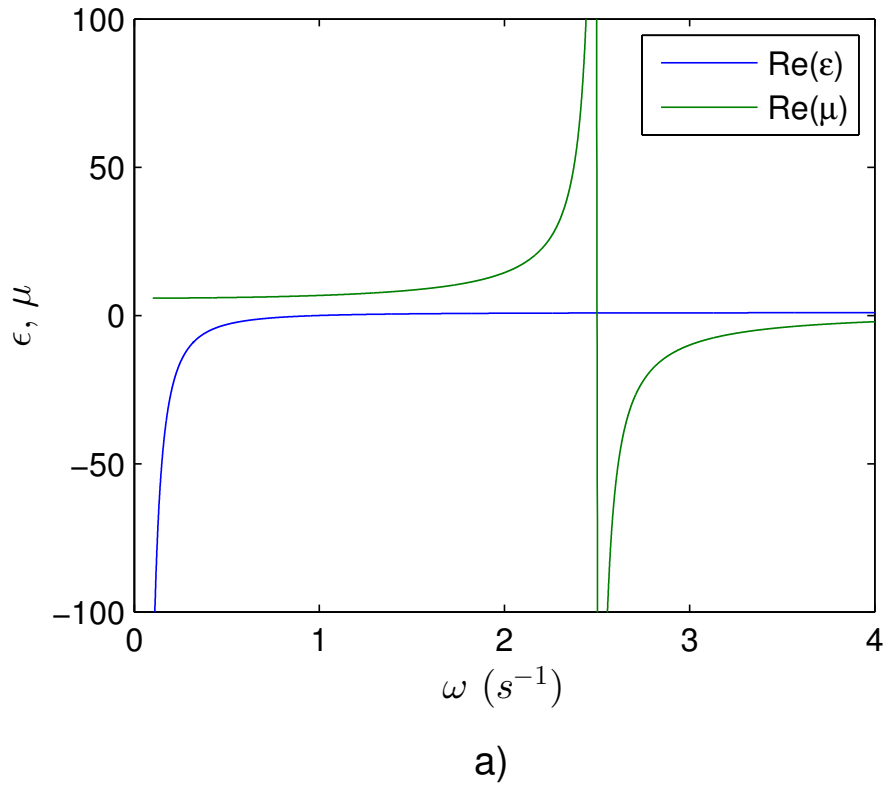


Figure 5.6: (a) The dielectric function and magnetic permeability of metamaterial modelled with Eq. (5.8) as a function of frequency. (b) Variation of Casimir force for a system of two parallel plates consists of a metamaterial plate and a perfectly conducting plate against distances.

frequency shifted the overall graph towards the attractive region. On the other hand, a change in the magnetic permeability's plasma frequency shifts the overall graph towards the magnetic region, as depicted in Fig. (5.7 b).

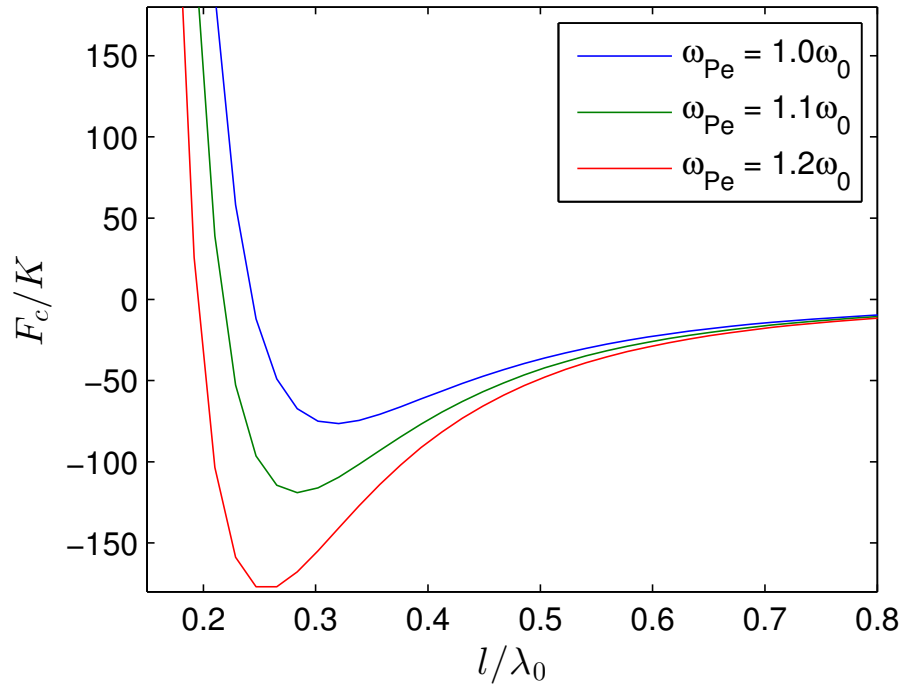
Another rather interesting feature is shown if the resonant frequency was shifted (while keeping the plasma frequency intact). As the resonant frequency ω_{T_e} increases, the location of stable equilibrium is shifted slightly towards the repulsive region, as in Fig. (5.8 a). Also, the gradient of F_c around $F_c = 0$ decreases. This corresponds to an equilibrium which is less stable, as a slight change in inter-plate distance Δl will be counteracted by a weaker restoring force. Qualitatively, an increase in the electric resonant frequency implies that both plates must be closer together to feel the attraction force. Hence, we see an overall decrease in the attraction force between both plates. On the other hand, a change in the magnetic resonant frequency ω_{T_m} will give the opposite result, as depicted in Fig. (5.8 b). As ω_{T_m} increases, the overall graph is shifted towards the attractive side, while the gradient of F_c around $F_c = 0$ increases.

5.4 Optimizing the Casimir Force

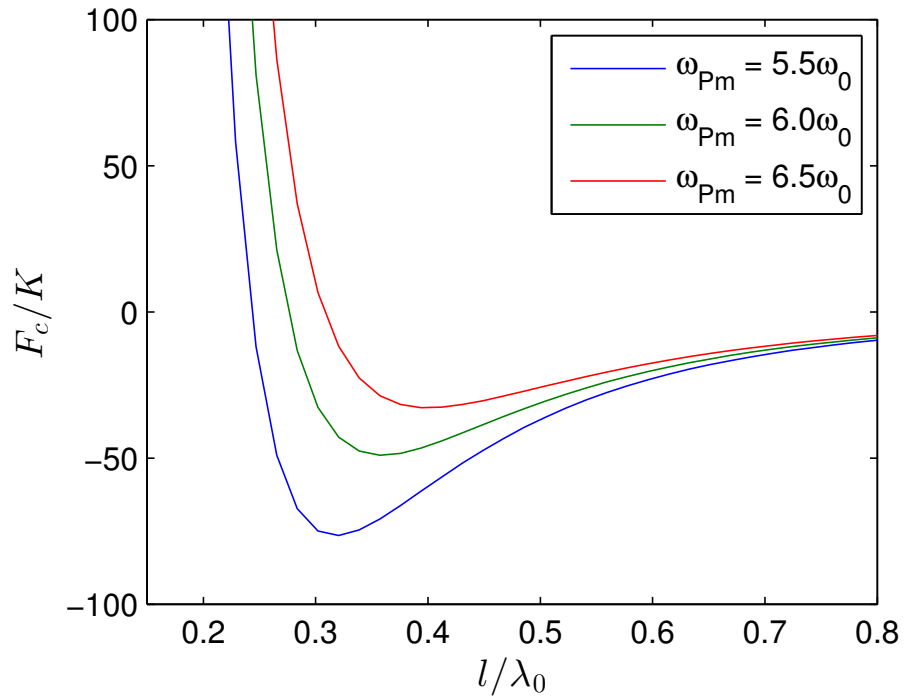
In the previous section, we have examined the equilibrium points of Casimir force, which exist largely due to the capability of some materials to exhibit different magnetic and electrical properties at different frequency range. Till date, metamaterial is one of the materials that possess such unique characteristic, which makes it an interesting material for experimental Casimir research. To further expand the idea of "material dependent Casimir force", we set forward to find any local extrema of the Casimir force. A local maximum in Casimir force may be useful for researcher to perform experimental verification of existing data, as the larger value of Casimir force reduces the requirement of highly sensitive devices. In this section, we will first attempt to understand the nature of Casimir force over a range of ϵ and μ . Then, the metamaterial model will be considered.

5.4.1 Changes of Casimir force for different ϵ & μ

As a start, an attempt was made to maximize the Casimir force between a perfectly conducting plate ($r_{TE} = -1$, $r_{TM} = 1$), and a plate with real dielectric constant ϵ and magnetic permeability μ over all frequencies. While this case had been discussed briefly

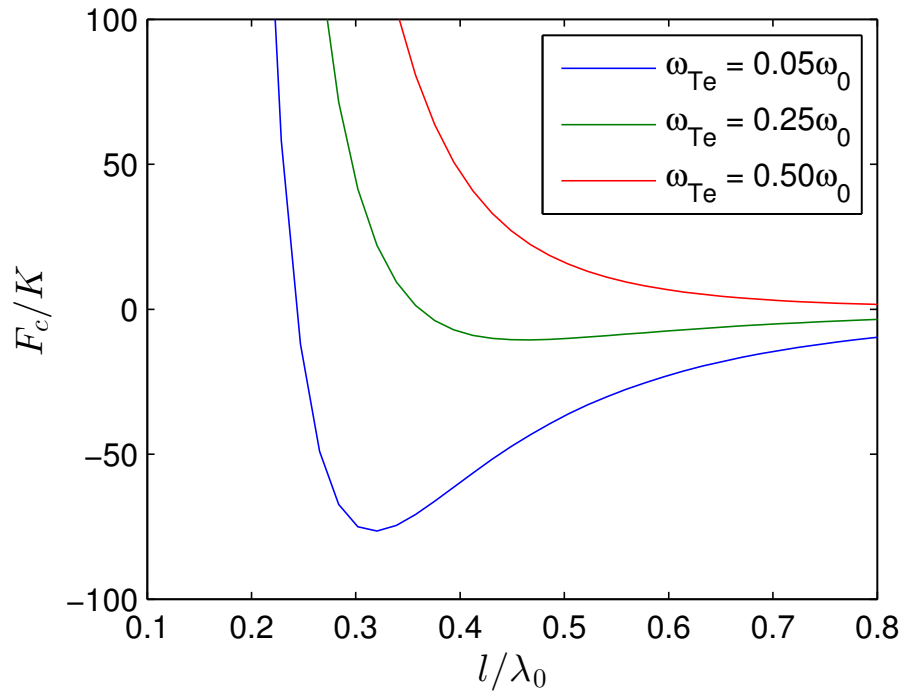


a)

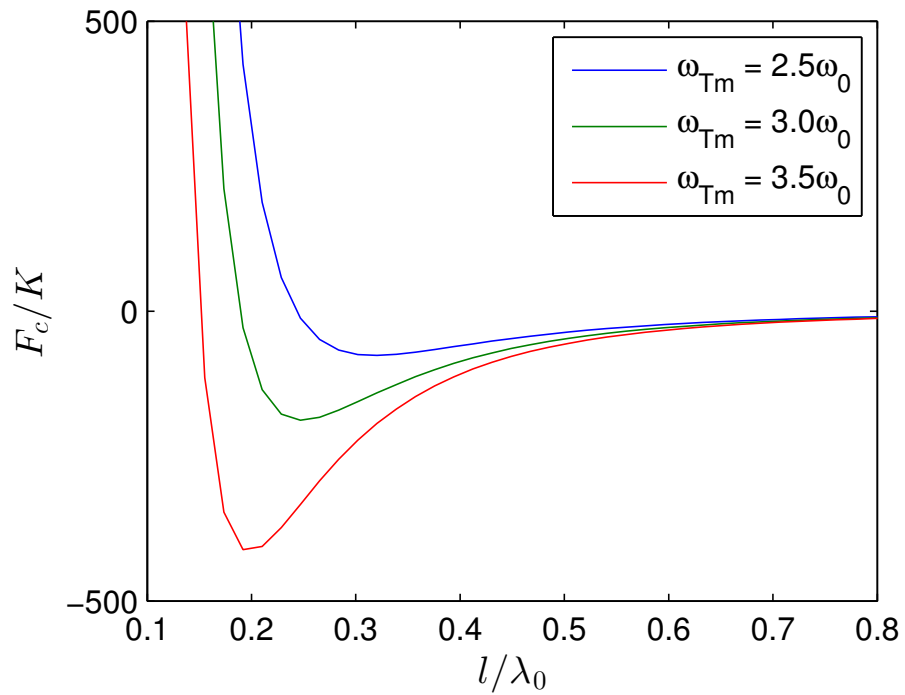


b)

Figure 5.7: Variation of Casimir force for a system of two parallel plates consists of a metamaterial plate and a perfectly conducting plate against distances. (a) Changes in dielectric function's plasma frequency ω_{Pe} and (b) changes in magnetic permeability's plasma frequency ω_{Pm} , in units of ω_0 . Blue line indicates the original configuration that was considered.



a)



b)

Figure 5.8: Variation of Casimir force for a system of two parallel plates consists of a metamaterial plate and a perfectly conducting plate against distances. (a) Changes in resonant frequency ω_{Te} and (b) ω_{Tm} , in units of ω_0 . Blue line indicates the original configuration that was considered.

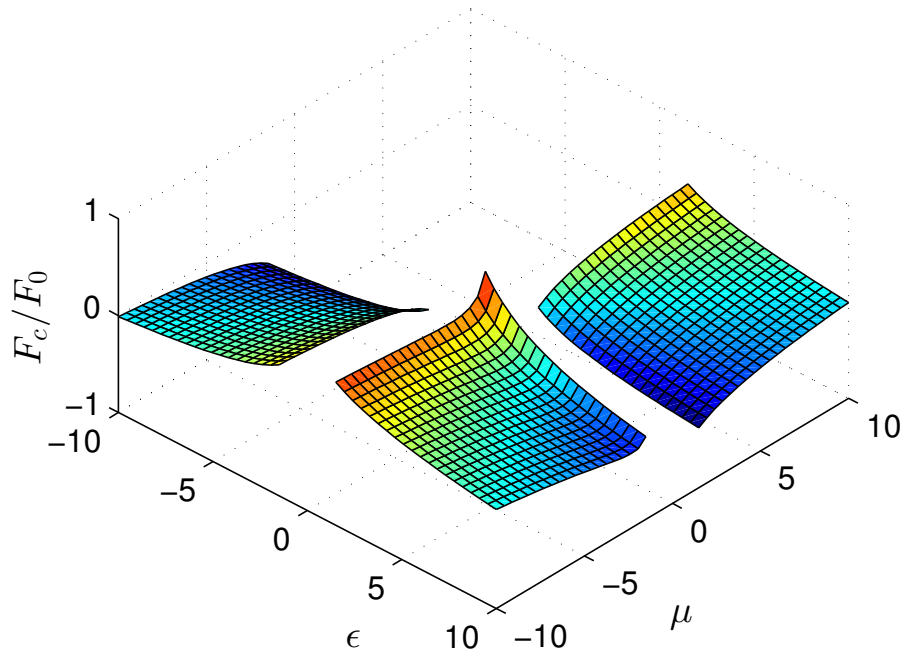


Figure 5.9: Variation in normalized Casimir force as ϵ and μ changes.

in Section 5.1, the idea was expanded over the negative regions of dielectric function and magnetic permeability here, to account for potential advancements in metamaterials which makes it possible. The variation of Casimir force for this case is plotted in Fig. (5.9). The figure is again, normalized to the attraction force between two perfectly conducting plate, F_0 . From the plot, we see that there are no values for certain regions. This is expected as the assumption of ϵ and μ being constant and real over all frequencies does not obeys the Kramer-Kronig's relationship. The breakdown of causality is apparent in above figure, when μ is positive and ϵ is negative, which Lifshitz's formula fails. However, the general result of the figure may still be useful in understanding the property of Casimir force for different materials.

An obvious result was found here: the Casimir force varies between two ideal cases, that is between:

- Two perfectly conducting plate (or two perfectly magnetic plate), F_0
- One perfectly conducting plate and one perfectly magnetic plate, $-\frac{7}{8}F_0$

This result is not surprising. Qualitatively, we notice that the reflectivity coefficient in Eq. (3.45) for each frequency, ω will always vary in the set $[-1, 1]$. Hence, the maximum force for either direction is attained by having the reflectivity for *all* frequencies

to be $r_N(\omega) = \pm 1$. The force is attractive if both plates have similar material properties, and repulsive if the material properties are completely different. Also, it is noticed that the Casimir force between two plate approaches maximum attraction force when $\varepsilon \rightarrow \infty$, for any finite magnetic permeability $\pm\mu$. Of course, a higher value of μ will require a higher value of ε as compensation to achieve maximum attraction force. Another interesting case that offers strong attraction force between plates is at $\mu \rightarrow 0^-$, and $\varepsilon \rightarrow -\infty$. The Casimir force between plates become strongly repulsive as $\mu \rightarrow \pm\infty$, for any finite value of ε . However, the figure shown a rather plain result, as there are no local extrema. For completeness sake, we will continue our investigation on more realistic cases in an attempt to find a local extrema.

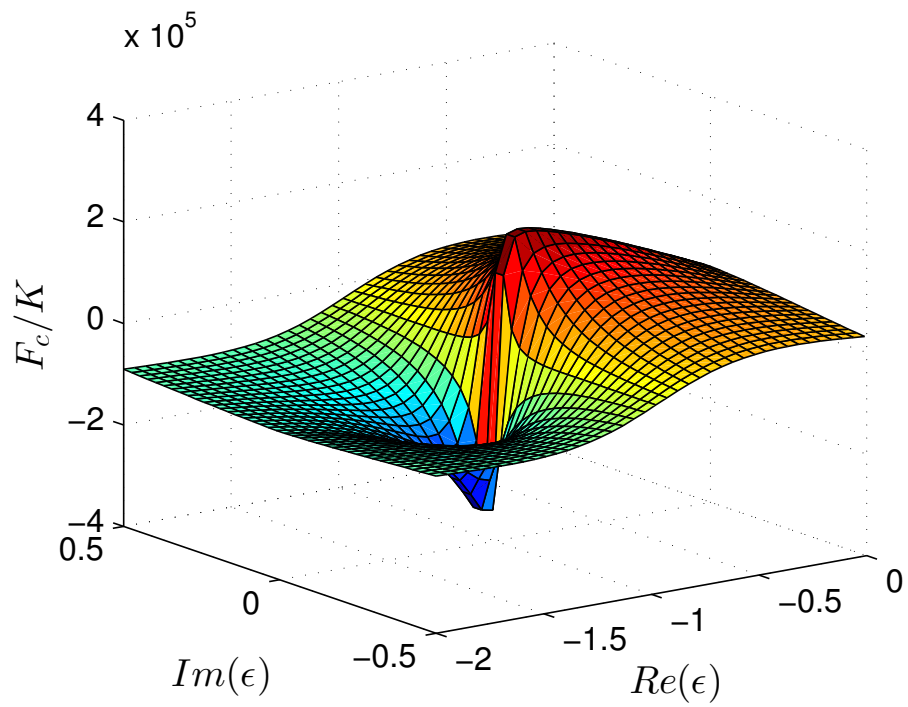
To include complex valued ε and μ into the scheme, Fig. (5.10 a) was plotted with $\mu = 1$, while varying ε in the complex plane. A rather interesting result is found. It is noticed that a maximum Casimir repulsion is observed at $\text{Re}(\varepsilon) \rightarrow -1^+$, and $\text{Im}(\varepsilon) \rightarrow 0$. This result is not plotted in the previous figure (Fig. (5.9)) because without a complex dielectric function, the value of Casimir force will diverges. Furthermore, it is noticed that a maximum Casimir attraction is obtained at $\text{Re}(\varepsilon) \rightarrow -1^-$, and $\text{Im}(\varepsilon) \rightarrow 0$.

Similarly, Fig. (5.10 b) was plotted with $\varepsilon = 1$, while varying μ in the complex plane. As expected, the figure is basically a mirror of Fig. (5.10 a) on the xy -plane. We see a maximum Casimir attraction at $\text{Re}(\mu) \rightarrow -1^+$, and $\text{Im}(\mu) \rightarrow 0$, while a maximum Casimir repulsion is observed at $\text{Re}(\mu) \rightarrow -1^-$, and $\text{Im}(\mu) \rightarrow 0$.

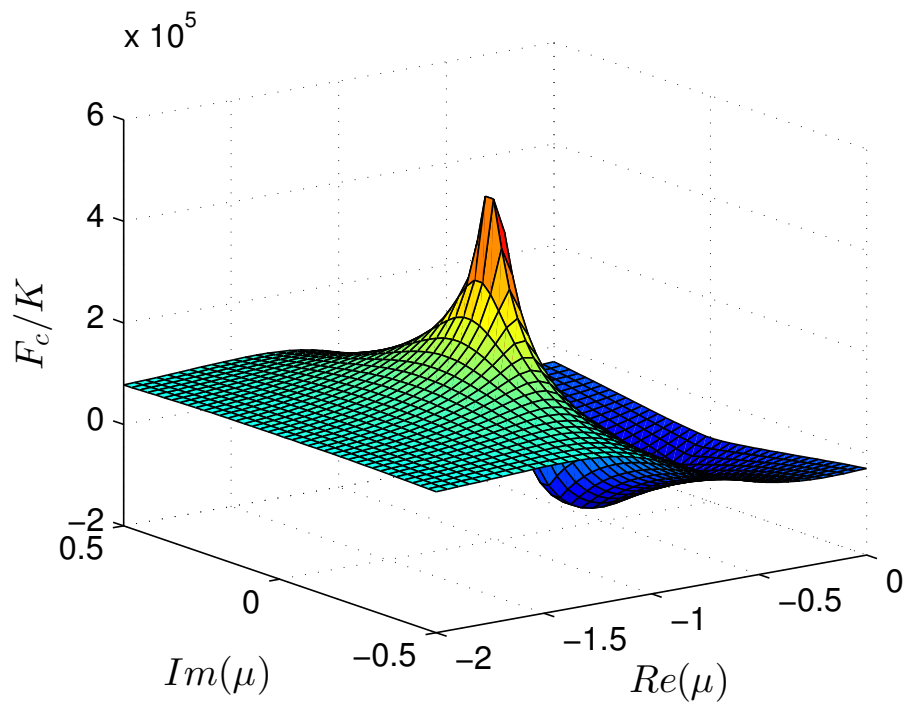
This result is rather interesting. With an addition of complex material constant, the Casimir force was shown to exhibit a maximum and minimum point near $\text{Re}(\varepsilon) \rightarrow -1$ (or $\text{Re}(\mu) \rightarrow -1$), with $\text{Im}(\varepsilon) \rightarrow 0$ (or $\text{Im}(\mu) \rightarrow 0$). However, all materials that we have encountered so far does not exhibit near-zero material constant for a wide band. For example, ε -near-zero metamaterial shown the possibility of exhibiting near-zero value for ε only for a narrow band. Furthermore, the absorption in this narrow band is particularly high (Feng & Halterman, 2012). With this, we turn our attention to more realistic models.

5.4.2 Optimizing the Metamaterial Model

Given the recent improvement in metamaterial fabrication, it is possible to alter both the dielectric constant and magnetic permeability of a material. As the Casimir force is



a)



b)

Figure 5.10: Changes in Casimir force between a perfectly conducting metal and a plate made of material: (a) ϵ complex, $\mu = 1$. (b) $\epsilon = 1$, μ complex.

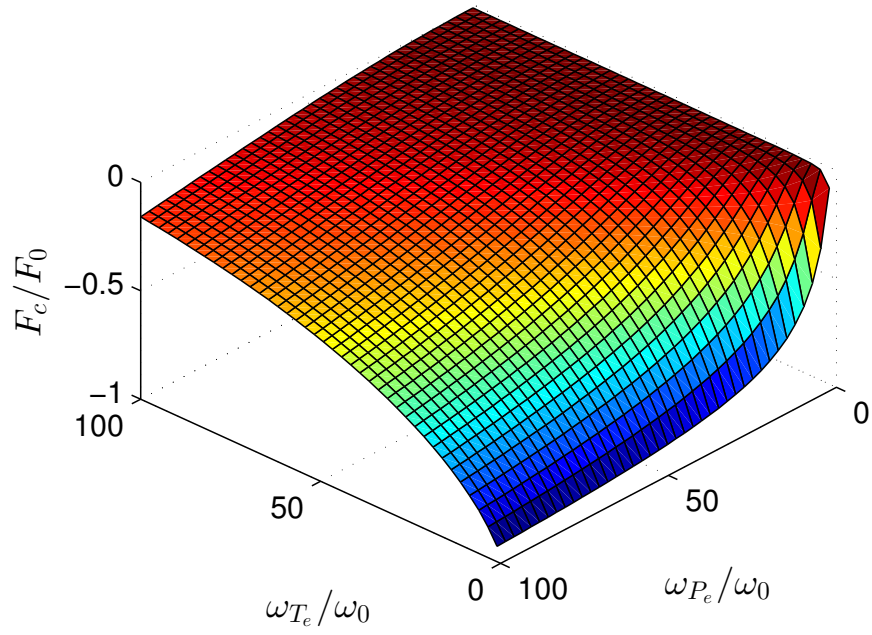
highly dependent on material constants, we will attempt to compute the Casimir force between a perfectly conducting plate, and a plate with ε given by Eq. (5.8), while $\mu = 1$. There are three variables in the Drude-Lorentz model, Eq. (5.8), i.e. the plasma frequency ω_{P_e} , the resonant frequency ω_{T_e} , and the damping frequency γ_e . In this case, we will vary ω_{P_e} and ω_{T_e} , for $\gamma_e = 0.01\omega_{T_e}$. The plot is given in Fig (5.11 a). From the figure, we notice a maximum attraction force is attained by having $\omega_{P_e} \rightarrow \infty$ and $\omega_{T_e} \rightarrow 0$. Furthermore, it is noted that when the order of ω_{T_e} is close to that of ω_0 , a small increase in ω_{P_e} produces a quick increase in the Casimir attraction between plates, which quickly saturates after $\omega_{P_e} \approx 40\omega_0$. Also, we noticed that there are no local extrema in this case.

Another similar case was then considered, where the Casimir force between a perfectly conducting plate, and a plate with $\varepsilon = 1$, μ given by Eq. (5.8) is computed. The variation of Casimir force is plotted in Fig. (5.11). In this case, we can see a similar result, where a maximum repulsive force may be obtained by having $\omega_{T_m} \rightarrow 0$ and $\omega_{P_m} \rightarrow \infty$. Similarly, when the order of ω_{T_m} is close to that of ω_0 , a small increase in ω_{P_m} is suffice to produce a quick increase in the Casimir repulsion between plates. However, there are no local extrema in this case too. A combination of both ε and μ specified by Eq. (5.8) exhibits similar characteristic.

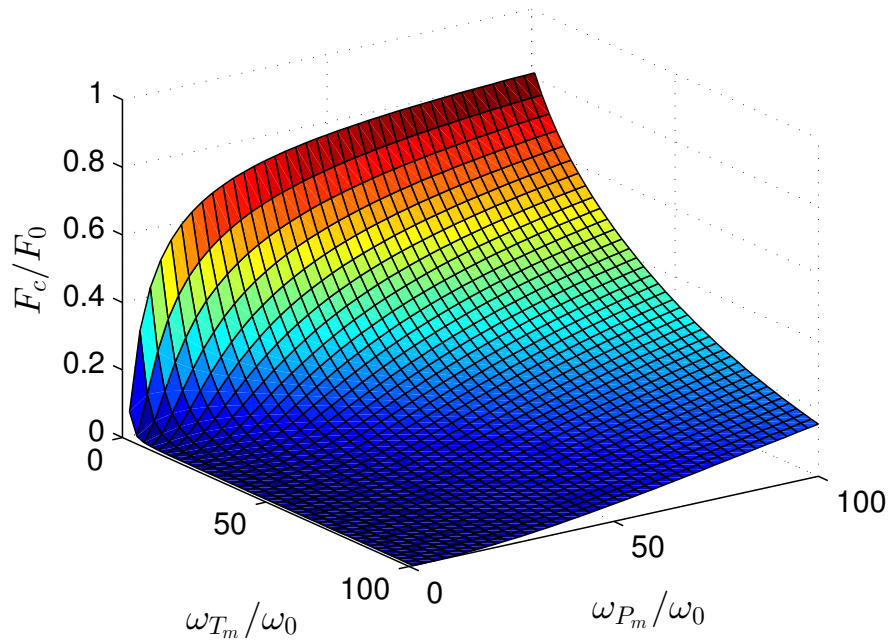
5.5 Discussions

In this chapter, we have examined the change in Casimir force for different materials. Materials with magnetic properties at certain frequency range, such as metamaterials are found to exhibit both attractive and repulsive Casimir force, at different distances. Furthermore, the idea of Casimir force was extended towards the concept of stable equilibrium and unstable equilibrium. This notion is rather new in the field of Casimir effect, until the introduction by Yang et al. (2010). We then see that a nicely tuned metamaterial, with appropriate material constant will exhibit either stable or unstable equilibrium. With the idea of stable equilibrium, the problem of stiction in NEMS may be solved.

To build a parallel plate system consisting of a perfectly conducting plate and a metamaterial plate which is in stable equilibrium, at $l = 100nm$ apart, would require metamaterials with a resonant frequency in the visible spectrum. In this particular example, we see that $\omega_0 \approx 5 \times 10^{15} s^{-1}$, which roughly corresponds to the violet light in the



a)



b)

Figure 5.11: Change in normalized Casimir force for a parallel plate configuration consists of a perfectly conducting plate and (a) a metamaterial with $\mu = 1$, ϵ given by Eq. (5.8); (b) a metamaterial with $\epsilon = 1$, μ given by Eq. (5.8).

electromagnetic spectrum. With the metamaterial parameters we have considered in Section 5.3.2, the electric resonant frequency required will be at $\omega_{T_e} \approx 2.5 \times 10^{14} s^{-1}$, while the magnetic resonant frequency required is $\omega_{T_m} \approx 1.25 \times 10^{16} s^{-1}$. A $\pm 5\%$ change in the inter-plate distances will result in a mean change of Casimir pressure of $\Delta F_c \approx 0.16 N/m^2$. This is relatively small compared to the atmospheric pressure, and may require very precise detecting devices. However as previously highlighted, a NEMS system may still be affected by such a small change in force due to its size. With recent advancement in metamaterial fabrication, successful attempts in fabricating metamaterial with resonant frequency at visible light region were recorded. For instance, Shalaev et al. (2005) had shown that a double-periodic array of pairs of parallel gold nanorods exhibits negative refractive index near the visible light's range. Several nano-fishnet structures were also shown to exhibit negative refractive index near the optical region (Zhang et al., 2006, 2005). Then, Dolling, Wegener, Soukoulis, and Linden (2007) had successfully miniaturize a silver-based negative-index metamaterial design and demonstrated that the material exhibits negative refractive index at $\lambda = 780nm$. Burgos, de Waele, Polman, and Atwater (2010) then shown that it is possible to have a negative-index material with effective refractive index of -2 in the blue spectral region. These findings are crucial towards experimental realization of Casimir control via material properties.

Next, we have seen that the Casimir force of real materials varies between two extreme values, with no local extrema found. It is rather interesting to note that the Casimir force is a rather smooth varying function. Nevertheless, these findings may be useful for future studies on Casimir force, and design of nanoelectromechanical systems, where we have stated the conditions for obtaining the maximum and minimum Casimir force.

Lastly, it had been suggested that our model, which uses two parallel, infinitely large plates is a large simplification compared to the shapes of devices in the real world systems, such as those found in NEMS. We do acknowledge that in real world applications, nano-sized materials are usually varied in shape, such as nanogears and nanotubes. However, the core idea of manipulating Casimir force by changing the material constant, especially those with huge magnetic permeability, still holds for different geometries. With that in mind, we leave this topic as it is and turn into another interesting problem.

CHAPTER 6

INTENSITY DEPENDENT CASIMIR FORCE

In the previous chapter, the problem of stiction in NEMS was raised. With that, we have explored the possibility of controlling the Casimir force by using different materials, in an attempt to search for repulsive Casimir force and stable equilibrium. Metamaterials, with the right parameter was shown to be able to exhibit stable equilibrium. However, a real-time change in the Casimir force was not possible in those cases, thus limiting the capability to control the Casimir force in NEMS. In this chapter, we will present the idea of optical control on Casimir force. By considering optical induced change in material constants, we are able to indirectly control the Casimir force between two parallel plates. It is noteworthy that the idea in this chapter had been recently published (Ooi & Khoo, 2012).

In the first section, we will introduce the AC Kerr effect. A mathematical treatment of the Kerr effect, and an outline of deriving a model for the Kerr effect via both classical and quantum mechanics was presented. Next, an overview on the intensity dependence of Casimir force was presented. The chalcogenide glass as a highly nonlinear material was then introduced, along with models for its refractive indices. Lastly, we present the Casimir force between a metamaterial plate placed parallel to a chalcogenide glass plate, which ultimately shows the possibility of optical control on Casimir force.

6.1 AC Kerr Effect

The interaction between a rapidly oscillating electric field of a linearly polarized light wave and an optically isotropic medium causes the isotropic medium to temporarily become anisotropic. The material will then temporarily behave optically as it was a uniaxial crystal with the electric field of the light pulse defines the optical axis. This phenomenon was first theoretically proposed by Buckingham (1956), and was later called the optical Kerr effect (OKE, also known as AC Kerr effect). The optical Kerr effect is somewhat contrasted to the traditional Kerr electro-optic effect (also known as DC Kerr effect), first

observed by Kerr (1877), which uses a DC electric field to induce birefringence in the material.

Experimental observation of the OKE was reported in 1964, by Maker et al., where a nanosecond ruby laser was used to measure the intensity-dependent rotation of molecule in liquids, and the nonlinear susceptibility was inferred. Furthermore, a nonlinear change in index of refractive index associated with the OKE was measured later by Duguay and Hansen (1969); Shimizu and Stoicheff (1969).

Generally, there are few physical mechanisms that were theorized to explain the optically induced birefringence. When a Kerr material, which was composed of polarizable molecule was exposed to an external intense laser pulse (the pump field), a dipole moment is induced along the "axis of maximum polarizability" of each molecule. The induced dipole moment interacts with the \vec{E} component of laser pulse, which then causes the molecules to realign itself with the polarization of the pump pulse. Furthermore, if permitted, the molecules may spatially redistribute themselves to minimize the free energy of the system. Since the polarizability of the molecules will affect the index of refraction, the pump field is then said to induce a birefringence, which may be noticed by a "probe" field. This mechanism accounts for the Kerr effects of most polar liquids, such as CS_2 (Shimizu & Stoicheff, 1969) and nitrobenzene (Duguay & Hansen, 1969).

On the other hand, the applied pump field can also change the density of the material, and/or the electronic charge distribution of a material. This leads to a change in the susceptibility and the index of refraction of a material (Sauter, 1996). Furthermore, an amplification on the third order susceptibility, $\chi^{(3)}$ of a material may occur if the changes of frequency lies close to some Raman transition of the material, which is the basis of Raman-Induced Kerr effect (Heiman, Hellwarth, Levenson, & Martin, 1976).

We proceed to present some mathematical insight related to the Kerr effect. In a nonlinear, isotropic dielectric medium, the Maxwell's second order equation takes form as below.

$$\nabla^2 \vec{E} - \frac{1}{c^2} \frac{\partial^2 \vec{E}}{\partial t^2} = \mu_0 \frac{\partial^2 \vec{P}}{\partial t^2} \quad (6.1)$$

Generally, the polarizability, \vec{P} may be expanded in a Taylor series in terms of electric

field strength, \vec{E} (Boyd, 2002).

$$\vec{P} = \epsilon_0 \chi^{(1)} \vec{E} + \epsilon_0 \chi^{(2)} \vec{E}^2 + \epsilon_0 \chi^{(3)} \vec{E}^3 + \dots \quad (6.2)$$

In above equation, $\chi^{(1)}$ is known as the linear susceptibilities. It is a second-rank tensor. The variables $\chi^{(2)}$ and $\chi^{(3)}$ is known as the second, and third-order nonlinear optical susceptibilities. They are tensor of rank three, and four, respectively. It is convenient to separate the polarizability in Eq. (6.2) as a sum of linear $\epsilon_0 \epsilon \chi$, and nonlinear parts, \vec{P}_{NL} .

$$\vec{P} = \epsilon_0 \chi \vec{E} + \vec{P}_{NL} \quad (6.3)$$

With these in place, the second order Maxwell equation, Eq. (6.1) will then take below form.

$$\nabla^2 \vec{E} - \frac{n^2}{c^2} \frac{\partial^2 \vec{E}}{\partial t^2} = \frac{1}{\epsilon_0 c^2} \frac{\partial^2 \vec{P}_{NL}}{\partial t^2} \quad (6.4)$$

It is interesting to note that the nonlinear terms gathered in the right hand side of Eq. (6.4). The nonlinear term is normally regarded as the source term in the partial differential equation. This is the basic equation that underlies the theory of nonlinear optics.

An in-depth analysis (Boyd, 2002) reveals that the physical processes that occur as a result of the second-order polarization, $\vec{P}^{(2)}$ tend to be distinct from the third-order polarization, $\vec{P}^{(3)}$. Several physical processes that are related to the second-order polarization include second-harmonic generation (SHG), difference-frequency generation (DFG), and optical rectification (OR). However, second-order nonlinear optical interactions can only occur on non-centrosymmetric crystals, that is, crystals that are not inversion symmetric. Since most crystals, liquids and amorphous solids are centrosymmetric, the second-order term vanishes.

The third-order nonlinear optical interactions, on the other hand occur on all crystals. Physical processes associated in this case include the third-harmonic generation and the intensity-dependent refractive index. The latter is also known as the Kerr effect.

Mathematically, we may define the intensity-dependent refractive index as below.

$$n = n_0 + n_2 I \quad (6.5)$$

In above equation, n_0 is the linear refractive index of the material, while n_2 is known as the Kerr coefficient (or the second order nonlinear refractive index). In this case, it is

noted that the effective refractive index depends on the product of n_2 and I , the intensity of impinging light. The relationship between the Kerr coefficient and $\chi^{(3)}$ is found to be as below (Boyd, 2002).

$$n_2 = \frac{3}{4n_0^2\epsilon_0 c} \chi^{(3)} \quad (6.6)$$

With this in mind, we take our focus towards the third-order nonlinear susceptibility, $\chi^{(3)}$, of different materials. There are multiple factors that contribute to the third-order nonlinearity, such as the nonresonant electronic nonlinearities, nonlinearities due to molecular orientation, thermal nonlinear optical effects and semiconductor nonlinearities.

The nonlinear response of bound electrons towards an applied optical field will result in the nonresonant electronic nonlinearities. While this nonlinearity is not large compared to contribution from other processes, e.g. $n_2 \sim 5 \times 10^{-21} m^2/W$), but it is important as it present in all dielectric material (Boyd, 2002). In the rest of this section, we present two novel models that were used to calculate the nonlinear susceptibility contributed by this factor.

6.1.1 Classical Anharmonic Oscillator Model

The third-order nonlinear susceptibility contributed by nonresonant bound electrons may be modelled using a classical, anharmonic oscillator model. In this model, the potential well that binds the electrons to the nucleus of an atom deviates from parabolic potential. The potential well is approximated by:

$$U(r) = \frac{1}{2}m\omega_0^2|r|^2 - \frac{1}{4}mb|r|^4 \quad (6.7)$$

where b is a phenomenological nonlinear constant. Its value is of the same order as ω_0^2/d^2 , where d is a typical atomic dimension. By solving an electron in such potential well, the third-order susceptibility may be taken as below.

$$\chi_{ijkl}^{(3)}(\omega = \omega + \omega - \omega) = \frac{Nbe^4 [\delta_{ij}\delta_{kl} + \delta_{ik}\delta_{jl} + \delta_{il}\delta_{jk}]}{3\epsilon_0 m^3 D(\omega)^3 D(-\omega)} \quad (6.8)$$

where $D(\omega) = \omega_0^2 - \omega^2 - 2i\omega\gamma$.

By taking the resonant terms into account, we may let $i = j = k = l$, and we set

$b = \omega_0^2/d^2$ to arrive:

$$\begin{aligned}
\chi^{(3)}(\omega = \omega + \omega - \omega) &= \frac{Nbe^4}{\epsilon_0 m^3 D(\omega)^3 D(-\omega)} \\
&= \frac{Nbe^4}{\epsilon_0 m^3 [\omega_0^2 - \omega^2 - 2i\omega\gamma]^3 [\omega_0^2 - \omega^2 + 2i\omega\gamma]} \\
&= \frac{N\omega_0^2 e^4}{\epsilon_0 m^3 d^2 [\omega_0^2 - \omega^2 - 2i\omega\gamma]^3 [\omega_0^2 - \omega^2 + 2i\omega\gamma]} \quad (6.9)
\end{aligned}$$

For the case of far-off-resonant excitation (ie $\omega \ll \omega_0$), we may replace $D(\omega)$ with ω_0^2 to obtain:

$$\chi^{(3)} \simeq \frac{Ne^4}{\epsilon_0 m^3 \omega_0^6 d^2} \quad (6.10)$$

6.1.2 Quantum Theory Model

In this section, we present an outline for the derivation of the nonlinear optical susceptibility, based on the quantum mechanical perturbation theory of the atomic wavefunction. The expression that was derived using this formalism can make accurate predictions of the nonresonant response of atomic and molecular systems (Boyd, 2002). The derivation begin by having an atomic wavefunction, $\psi(\vec{r}, t)$, which is the solution to time dependent Schrodinger equation below.

$$i\hbar \frac{\partial \psi}{\partial t} = (H_0 + V(t)) \psi \quad (6.11)$$

Here, the Hamiltonian is the sum of a free atom Hamiltonian H_0 and an interaction Hamiltonian, $V(t) = -\vec{\mu} \cdot \vec{E}(t)$, that describes the interaction of an atom with an external electromagnetic field. Here, $\vec{\mu} = -e\vec{r}$ is the electric dipole moment. It is interesting to note that in this derivation, we have only considered the interaction of electromagnetic field with the electric dipole moment of an atom. This is justified since the nonlinear susceptibility, contributed by the Optical Kerr effect is mainly the change of refractive index in response to applied electric field (Boyd, 2002).

For the case with no external field, the Hamiltonian in Eq. (6.11) is basically the Hamiltonian of an free atom, and the Schrodinger equation may be solved to obtain the eigenfunctions. These eigenstates are known as the stationary states. The time evolution of these states are given by a simple exponential factor, as in Eq. (6.12).

$$\psi(\vec{r}, t) = u_n(\vec{r}) e^{-i\omega t} \quad (6.12)$$

It is noted that $u_n(\vec{r})$ satisfies the time-independent Schrodinger equation, $H_0 u_n(\vec{r}) = E_n u_n(\vec{r})$, where $E_n = \hbar\omega$. For general cases where an atom is exposed to electromagnetic field, Eq. (6.11) cannot be solved exactly. In this case, the Schrodinger equation is solved with perturbation theory. In this scheme, the Hamiltonian in the Schrodinger equation is replaced by:

$$H = H_0 + \lambda V(t) \quad (6.13)$$

where λ is a continuously varying parameter ranging from 0 to 1 that characterizes the strength of interaction. By expanding the wavefunction $\psi(\vec{r}, t)$ in power series, we then obtain, for $N = 1, 2, 3, \dots$,

$$\begin{aligned} i\hbar \frac{\partial \psi^{(0)}}{\partial t} &= H_0 \psi^{(0)} \\ i\hbar \frac{\partial \psi^{(N)}}{\partial t} &= H_0 \psi^{(N)} + V \psi^{(N-1)} \end{aligned} \quad (6.14)$$

The solutions to Eq. (6.14) may be represented as:

$$\begin{aligned} \psi(\vec{r}, t) &= u_g(\vec{r}) e^{-iE_g t/\hbar} \\ \psi^{(N)}(\vec{r}, t) &= \sum_l a_l^{(N)}(t) u_l(\vec{r}) e^{-i\omega_l t} \end{aligned} \quad (6.15)$$

where the atom was assumed to be in the ground state g initially. The N th-order contribution to wavefunction $\psi^{(N)}(\vec{r}, t)$ was also represented as a sum. Meanwhile, $a_l^{(N)}(t)$ is the probability amplitude that the atom is in energy eigenstate of l at time t , corrected to the N th order perturbation.

By substituting Eq. (6.15) into Eq. (6.14), the recursive function for $a_l^{(N)}(t)$ was found to be (Boyd, 2002):

$$a_m^{(N)}(t) = (i\hbar)^{-1} \sum_l \int_{-\infty}^t dt' V_{ml}(t') a_l^{(N-1)}(t') e^{i\omega_{ml}t'} \quad (6.16)$$

To use the recursive function, we set $a_l^{(0)} = \delta_{lg}$, corresponding to an atom known to be in g state in zero order. With this information, we may compute the third-order susceptibility. The dipole moment per atom, correct to third order perturbation theory, is given by:

$$\langle \vec{p}^{(3)} \rangle = \langle \psi^{(0)} | \vec{\mu} | \psi^{(3)} \rangle + \langle \psi^{(1)} | \vec{\mu} | \psi^{(2)} \rangle + \langle \psi^{(2)} | \vec{\mu} | \psi^{(1)} \rangle + \langle \psi^{(3)} | \vec{\mu} | \psi^{(0)} \rangle \quad (6.17)$$

Also we recall the definition of third-order susceptibility (Boyd, 2002),

$$\vec{P}_k(\omega_p + \omega_q + \omega_r) = \epsilon_0 \sum_{hij} \sum_{(pqr)} \chi_{kjih}^{(3)}(\omega_\sigma, \omega_r, \omega_q, \omega_p) E_j(\omega_r) E_i(\omega_q) E_h(\omega_p) \quad (6.18)$$

By applying the definition of third-order susceptibility on Eq. (6.17), the nonlinear susceptibility is computed to be:

$$\chi_{kjih}^{(3)}(\omega_\sigma, \omega_r, \omega_q, \omega_p) = \frac{N}{\epsilon_0 \hbar^3} P_F \left[\sum'_{lmn} \frac{\mu_{gn}^k \mu_{nm}^j \mu_{ml}^i \mu_{lg}^h}{(\omega_{ng} - \omega_\sigma)(\omega_{mg} - \omega_q - \omega_p)(\omega_{lg} - \omega_p)} - \sum_{ln} \frac{\mu_{gn}^k \mu_{ng}^j \mu_{gl}^i \mu_{lg}^h}{(\omega_{ng} - \omega_\sigma)(\omega_{lg} + \omega_p)(\omega_{lg} - \omega_p)} \right] \quad (6.19)$$

where P_F is the full permutation function, defined in Eq. (6.20). Also $\vec{\mu}_{ml} = \int u_m^* \vec{\mu} u_l d^3 r$ appearing in Eq. (6.19) are the electric dipole transition moments. The prime symbol that are added on the first summation indicates the terms corresponding to $m = g$ should be omitted from the summation over m .

$$\begin{aligned} (-\omega_\sigma, \omega_q, \omega_p) &\rightarrow (-\omega_\sigma, \omega_p, \omega_q), (\omega_q, -\omega_\sigma, \omega_p), (\omega_q, \omega_p, -\omega_\sigma), \\ &(\omega_p, -\omega_\sigma, \omega_q), (\omega_p, \omega_q, -\omega_\sigma) \end{aligned} \quad (6.20)$$

Eq.(6.19) was then applied to the case of nonlinear refractive index, $\chi_{kjih}^{(3)}(\omega, \omega, \omega, -\omega) = \chi_{kjih}^{(3)}(\omega = \omega + \omega - \omega)$. However, rather than taking all 48 terms in the expanded Eq. (6.19) into account, only the near resonant terms were considered, which is expected to make the largest contributions to $\chi^{(3)}$. The resonant contribution is then given by (Boyd, 2002):

$$\begin{aligned} \chi_{kjih}^{(3)}(\omega, \omega, \omega, -\omega) &= \frac{N}{6\epsilon_0 \hbar^3} \\ &\times \left(\sum'_{lmn} \frac{\mu_{gn}^k \mu_{nm}^h \mu_{ml}^i \mu_{lg}^j + \mu_{gn}^k \mu_{nm}^h \mu_{ml}^j \mu_{lg}^i + \mu_{gn}^h \mu_{nm}^k \mu_{ml}^i \mu_{lg}^j + \mu_{gn}^h \mu_{nm}^k \mu_{ml}^j \mu_{lg}^i}{(\omega_{ng} - \omega)(\omega_{mg} - 2\omega)(\omega_{lg} - \omega)} \right. \\ &\left. - \sum_{ln} \frac{\mu_{gn}^k \mu_{ng}^j \mu_{gl}^h \mu_{lg}^i + \mu_{gn}^k \mu_{ng}^i \mu_{gl}^h \mu_{lg}^j + \mu_{gn}^h \mu_{ng}^i \mu_{gl}^k \mu_{lg}^j + \mu_{gn}^h \mu_{ng}^j \mu_{gl}^k \mu_{lg}^i}{(\omega_{ng} - \omega)(\omega_{lg} - \omega)(\omega_{lg} - \omega)} \right) \end{aligned} \quad (6.21)$$

As a side note, the indices p, q, r are the discrete sum over all \vec{E} field's frequency. The indices l, m, n are the sum of each energy eigenstate (from the recursive relation). Lastly, h, i, j, k are the Cartesian indices.

6.2 Intensity Dependence - An Overview

With the knowledge of Kerr effect, we may now introduce the optical control on the Casimir force. To achieve that, a laser beam of intensity $I(\omega)$ is introduced to induce AC Kerr effect on the plates. It is useful to formally re-state the formula for the Kerr effect, Eq. (6.5) again, with frequency dependence included. With AC Kerr effect taken into

account, the effective index of refraction is given by

$$n_N(\omega) = \sqrt{\epsilon_N(\omega)\mu_N(\omega)} + n_{2,N}(\omega)I(\omega) \quad (6.22)$$

where $n_{2,N}$ is the Kerr coefficient for each plate. Also, the intensity $I(\omega) = If(\omega)$, which indicates that the spectral shape $f(\omega)$ or transient character of the laser pulse. The laser pulse, in this case, may also determine the effective index of refraction. Also, it is noteworthy to know that $n_0(\omega) = \sqrt{\epsilon(\omega)\mu(\omega)}$, while $N = A, B$ in this case is the indices for both plates.

From the formula for refractivity, Eq. (3.45), we notice that the magnitude of the refractive index may determine the sign of the reflectivity by competing with the first term in the numerator. This in turns affects the Casimir force, as we have discussed in the previous chapter. In order to understand the intensity dependence of Casimir force in this scheme, an idealized magnetic plate impinged by intense laser field, with $\epsilon_A = 10$, $\mu_A = 1$, and n_2 finite, is placed in parallel to a perfectly conducting plate ($r_{TE}^B = -1$, $r_{TM}^B = 1$, $n_2 = 0$). The variation of Casimir force F_c between these plates at a function of intensity of the impinging laser, for inter-plate distance of $a = 0.1\lambda_0$ is plotted in Fig. (6.1 a). Here, a similar normalization factor as introduced in Chapter 5 is employed. It is notice that plate A is electric. With that, the Casimir force is expected to be attractive. From figure, it is noticed that the Casimir force initially increases with increasing laser intensity, to reach an optimum Casimir attraction at about $n_2I \approx 2$. This slight increase in the magnitude of Casimir force is caused by the transverse electric (TE) reflectivity, which decreases quicker compared to the transverse magnetic (TM) reflectivity. At higher intensities, the Casimir force between plates becomes less attractive. However, the change in Casimir force is not very significant in this case, and no transition between Casimir attraction and Casimir repulsion occurs.

A similar figure is plotted in Fig. (6.1 b), with plate A being substituted with a plate of material constant $\epsilon_A = 1$, $\mu = 10$, and n_2 finite. This plate, on the other hand, is noted to be magnetic. Hence, we will generally expect a repulsive Casimir force between this plate and a perfectly conducting plate. In this case, a maximum Casimir repulsion is noticed at $n_2I \approx 2$. With this, we may generally state that for $\epsilon > \mu$ ($\epsilon < \mu$), r_{TE} (r_{TM}) decreases quicker compared to r_{TM} (r_{TE}), giving a small increase in magnitude on the

original attractive (repulsive) Casimir force at very low intensities. At higher intensities, the Casimir force between plates becomes less repulsive.

In this quick overview, we see that the Casimir force between two plates can be changed by considering the Kerr effect. However, in both idealized case, we see that the change in the Casimir force is very small, and more importantly, no change in sign of the Casimir force was observed. Nevertheless, this intriguing idea may be expanded by considering more realistic materials.

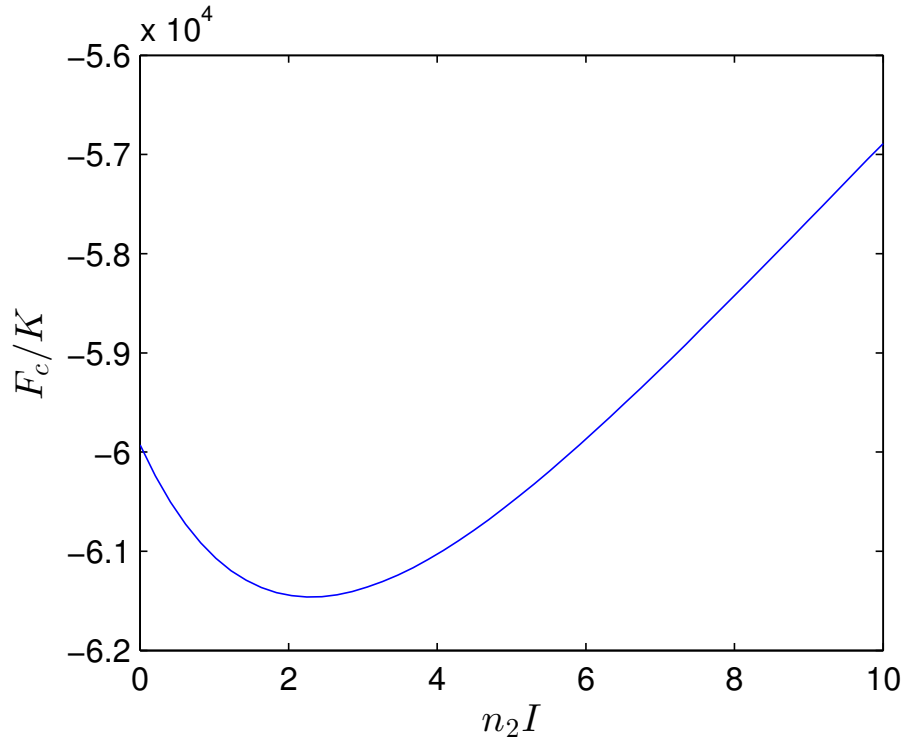
6.3 Optical control on Piecewise Model

We recall from the previous chapter that a piecewise model may be used to represent a material that behaves differently at different frequencies. In this section, a quick demonstration was done to show that with the right parameters, the Casimir force between a perfectly conducting plate and a material modelled by the piecewise model can exhibit large change in the Casimir force upon intensity impinging.

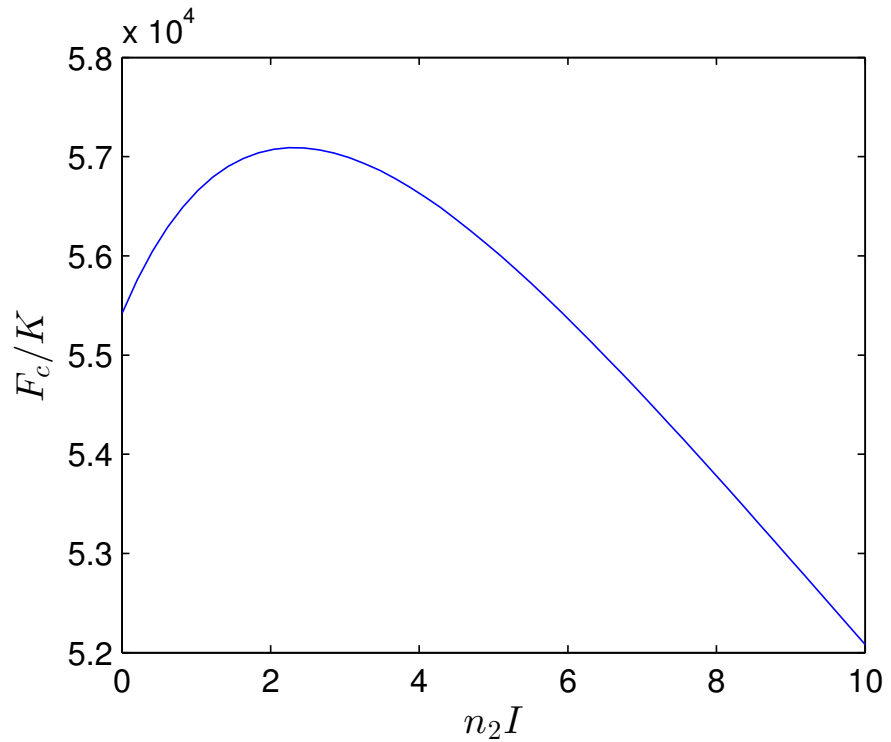
In this section, a plate made of material constant as described by Eq. (6.23), with n_2 finite is considered. The change in Casimir force between this plate and a perfectly conducting plate, for different intensities and distances is plotted in Fig. (6.2 a). A corresponding two-dimension plot was included in Fig. (6.2 b). Generally, it is noted that the Casimir force is very sensitive to changes in intensity at short distances. Furthermore, for inter-plate distance of $a \approx 0.2\lambda_0$, an impinging laser intensity of $n_2 I \approx 40$ is sufficient to change the Casimir force from attractive to repulsive.

$$\varepsilon = \begin{cases} 10, & \omega < 0.8\omega_0, \\ 1, & \omega \geq 0.8\omega_0, \end{cases} \quad \mu = \begin{cases} 0.5, & \omega < 0.8\omega_0, \\ 100, & \omega \geq 0.8\omega_0, \end{cases} \quad (6.23)$$

This is rather new, as we did not see a change in sign in the previous model. It turns out that materials that exhibits big change in material property can effectively have its Casimir force switched between attractive and repulsive by an impinging laser. With this, we recalled that metamaterials resembles these properties, where it may be electric at certain frequency, and magnetic in others. However, we noticed that current metamaterials does not yet exhibit strong nonlinear properties. As the optical control of Casimir force requires a material with strong nonlinear properties, we turned our focus to one of such material: the chalcogenide glasses.

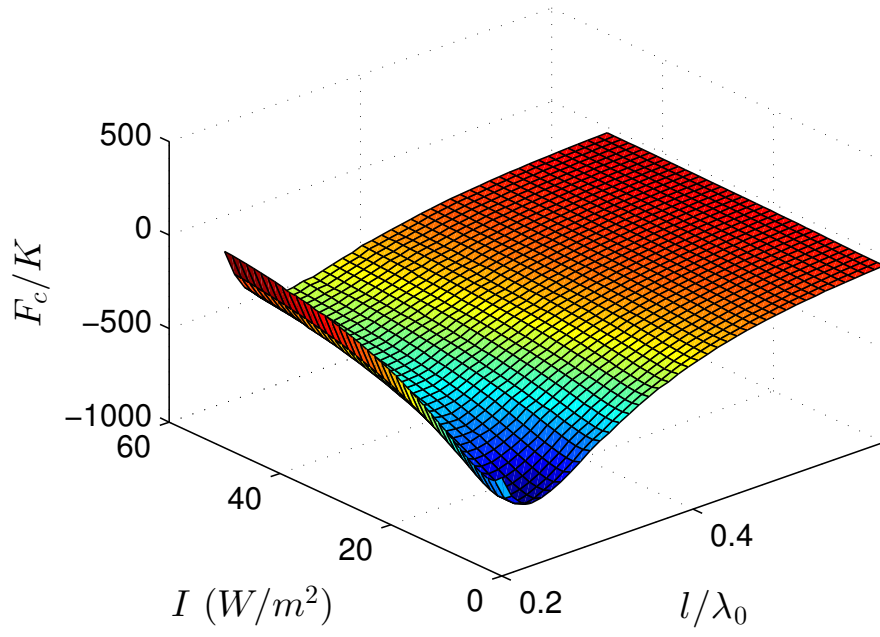


a)

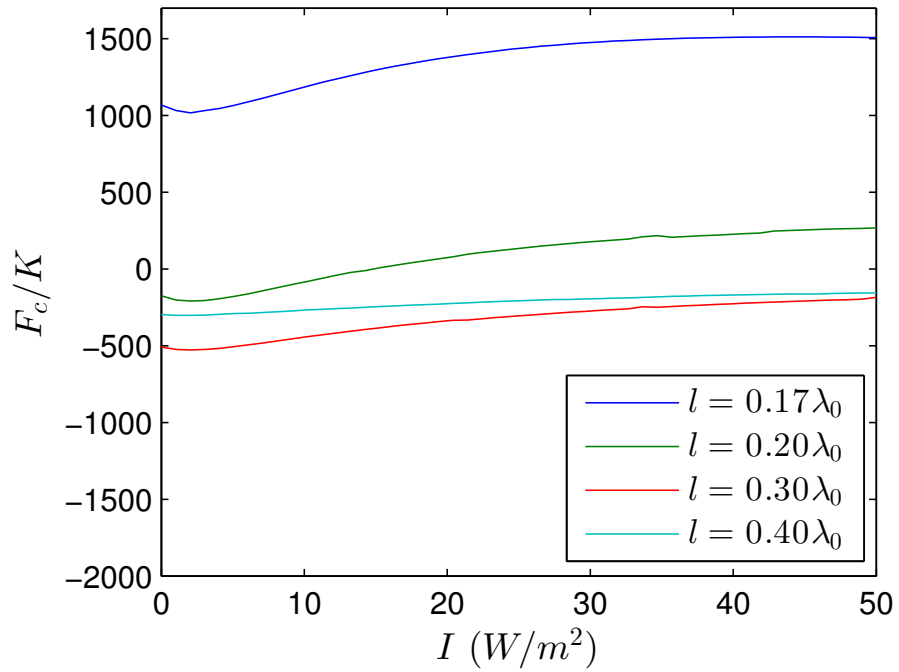


b)

Figure 6.1: Casimir force between a perfectly conducting plate and a plate with (a) $\epsilon = 10$, $\mu = 1$ and b) $\epsilon = 1$, $\mu = 10$, as a function of intensity of impinging laser $n_2 I$. Inter-plate separation is taken as $l = 0.1\lambda_0$. A stationary point (maxima or minima) was observed at $n_2 I \approx 2$. This is an effect whereby for $\epsilon > \mu$ ($\epsilon < \mu$), r_{TE} (r_{TM}) decreases quicker compared to r_{TM} (r_{TE}), giving a small increase in magnitude on the original attractive (repulsive) Casimir force at very low intensities.



a)



b)

Figure 6.2: Casimir force, F_c between a perfectly conducting plate and a piecewise-dispersive material with material constants given by Eq. (6.23), as a function of inter-plate separation and laser intensity. (a) 3D plot and (b) curves for several interesting inter-plate distances.

6.4 Chalcogenide Glass

A chalcogenide glass (ChG) is a class of glass in which a major constituent is one, or more chalcogen elements, which are covalently bonded to network formers such as *As*, *Ge*, *Sb*, and so on. Chalcogen elements are elements from group-16 (in this case, excluding Oxygen). As an amorphous semiconductor, chalcogenide glasses are widely used in solar cells, sensors and photonics. Chalcogenide glasses are comprised of covalently bonded heavy elements, which gives them unique properties in nonlinear and infrared optics (Eggleton, Luther-Davies, & Richardson, 2011). The ChGs are transparent until the mid-infrared region. Interesting effects are found upon doping ChGs with rare-earth elements (Tveryanovich & Tverjanovich, 2004). Furthermore, ChGs are known with their photosensitivity, that is, the chemical bonds will change when exposed to light with a frequency near the band-edge (Shimakawa, Kolobov, & Elliott, 1995). This property was used as phase-change memories in rewritable-CDs (CD-RW) (Ovshinsky, 1968).

In addition to above mentioned properties, ChGs have unexceptionally high density compared to oxide glasses. Combining with strong polarizability, ChGs have relatively high refractive index of $n_0 \approx 2 - 3$ (Eggleton et al., 2011). According to the empirical Miller's rule, high linear refractive index will leads to high nonlinear refractive index n_2 (Wang, 1970). Measurements (Kosa et al., 1993; Smektala, Quemard, Couderc, & Barthélémy, 2000) have confirmed that ChGs' nonlinear refractive index is up to a thousand times higher than silica. This remarkable nonlinear property makes ChGs an interesting material that we shall consider in our research. Given that our methodology is mainly theoretical, the rest of this section will focus on modelling the material constants of ChGs.

Two particularly important material constants that is needed in the computation of Casimir force is the linear and nonlinear refractive index. While most experimental values for refractive indices are quoted at certain frequency (see for example: Lide (2012)), it is not well suited for calculating the Casimir force since the Casimir force is computed by integrating over all frequencies, as in Eq. (3.44). As Casimir effect is a wide band problem, it is important to ensure that the model for refractive indices, $n_0(\omega)$ and $n_2(\omega)$ obey the Kramer-Kronig relation. The Kramer-Kronig relation for an arbitrary function

$\rho(\omega) = \rho_1(\omega) + i\rho_2(\omega)$ is given in Eq. (6.24).

$$\begin{aligned}\rho_1(\omega) &= \frac{1}{\pi} P \int_{-\infty}^{\infty} \frac{\rho_2(\omega')}{\omega' - \omega} d\omega' \\ \rho_2(\omega) &= -\frac{1}{\pi} P \int_{-\infty}^{\infty} \frac{\rho_1(\omega')}{\omega' - \omega} d\omega'\end{aligned}\quad (6.24)$$

where P denotes the Cauchy principal value of the integration. The Kramer-Kronig relation ensures that the function is analytic in the upper half-plane. These relations are used to calculate the real part (or imaginary part) of a response functions in physical system, because causality implies the analyticity condition (Toll, 1956). In our case, it is noteworthy to realize that both $n_0(\omega)$ and $n_2(\omega)$ must obey the Kramer-Kronig relation. With this, it is worthy to dive into potential models for material constants of chalcogenide glasses.

6.4.1 Wemple Model for n_0

In 1971, Wemple and DiDomenico Jr attempted to model the frequency-dependent dielectric constant n_0 using a single-oscillator description. It was shown that the single-oscillator description is a "natural" approximation to the dielectric response function for more than 100 widely different solids and liquids (Wemple & DiDomenico Jr, 1971). Later, the linear refractive index $n_0(\omega)$ of some chalcogenide glasses were modelled using the Wemple equation, and it was shown to fit quite well (Yayama et al., 1998). In order to show the elegance of this simple yet surprisingly useful model, the original derivation is briefly outlined.

It is well known that the absorption part of dielectric function may be computed by using the perturbation theory, in the framework of one-electron band theory. However, it is noted that this procedure will require an integration over the whole Brillouin zone, on all frequencies. This may obscure any important physical quantities (Wemple & DiDomenico Jr, 1971). In an attempt to address the problem, Wemple and DiDomenico Jr then attempt to approximate the dielectric function "in ways that display explicitly certain physically meaningful parameters". In this scheme, a single-oscillatory system is considered. First, we introduce the notation $\varepsilon = \varepsilon_1 + i\varepsilon_2$. By using the time-dependent perturbation theory, the real part of dielectric function may be written as:

$$\varepsilon_1(\omega) = 1 + \frac{e^2}{\pi^2 m_e} \sum_{i,j} \int_{BZ} d^3k \frac{f_{ij}^\alpha(\vec{k})}{\omega_{ij}^2(\vec{k}) - \omega^2} \quad (6.25)$$

where e is the electronic charge, and m_e is the electron mass. The volume integral extends over the entire Brillouin zone, while the discrete sum extends to all bands i and j , omitting $i = j$. Meanwhile, f_{ij}^α is the interband oscillator strength for polarization direction α , and ω_{ij} is the interband oscillator frequency. There are several approximations to Eq. (6.25). These approximations contain parameters that are able to be measured experimentally and hence useful. Here, we will consider the frequency dependence of dielectric constant as derived by Wemple and DiDomenico Jr (1971). For a single group of valence and conduction band, Eq. (6.25) can be written as

$$\varepsilon_1(\omega) = 1 + \frac{4\pi e^2}{m\Omega} \sum_{\vec{k}} \frac{f_{cv}^\alpha(\vec{k})}{\omega_{cv}^2(\vec{k}) - \omega^2} \quad (6.26)$$

where Ω is the volume of the crystal, and c and v denote conduction and valence bands. Next, the important interband transitions in the Brillouin zone are approximated by individual oscillators, and each valence electron is assumed to contribute to one of such oscillator. With this, Eq. (6.26) can be approximated by (Wemple & DiDomenico Jr, 1971)

$$\varepsilon_1(\omega) = 1 + \omega_p^2 \sum_n \frac{f_n}{(\omega_n^2 - \omega^2)} \quad (6.27)$$

where f_n is the electric-dipole oscillator strength associated with transition frequency ω_n , and ω_p is the plasma frequency of the valence electrons. A further mathematical treatment by isolating the strong oscillator from Eq. (6.27) then allow the single-oscillator dielectric function to be approximated by (Wemple & DiDomenico Jr, 1971)

$$\varepsilon_1(\omega) - 1 = \frac{F}{E_s^2 - (\hbar\omega)^2} \quad (6.28)$$

Eq. (6.28) contains two parameters E_s and F , which are related straightforwardly to f_n and ω_n in Eq. (6.27). Here, E_s is known as the Sellmeier gap. Also, Wemple and DiDomenico Jr (1971) further introduce the electronic oscillator energy, $E_d = F/E_s$. In terms E_d , the linear refractive index then can be written as:

$$n_0^2(\omega) - 1 = \frac{E_d E_s}{E_s^2 - (\hbar\omega)^2} \quad (6.29)$$

Eq. (6.29) is known as the Wemple equation, and it is well known as a two-parameter approximation for the dielectric function of more than 100 solids and liquids. To take absorption into account, Eq. (6.29) is then compared to the classical Drude model, i.e.

Eq. (5.8). Both equations are almost identical, except for the absorption term, $i\hbar^2\omega\gamma$.

With this we arrive at:

$$n_0^2(\omega) - 1 = \frac{E_d E_s}{E_s^2 - (\hbar\omega)^2 - i\hbar^2\omega\gamma} \quad (6.30)$$

where E_s is the Sellmeier gap and E_d is the electronic oscillator energy. Also, γ in Eq. (6.30) is the damping factor, which have the dimension of s^{-1} . It is later shown that the Wemple equation offer quite a good fit for some chalcogenide glasses, with error of less than $\pm 2.0 \times 10^{-3}$ from near infrared region to ultraviolet region (Yayama et al., 1998). The electronic oscillator energy, $E_d \approx 26eV$ for many chalcogenides (Slusher et al., 2004).

6.4.2 Two-Band Model for n_2

To model the Kerr coefficient for chalcogenide glasses, we first recall from Sec. (6.1), where several theoretical frameworks for computing n_2 had been developed. However, these models are developed by computing the nonlinearity caused by bound electrons only, which may not be complete. Furthermore, these models may require microscopic parameters that are not readily measurable. In pursuit of a better model, Sheik-Bahae et al. (1991) published an *ab initio* calculation, using a two-band model to calculate the scaling and spectrum of nondegenerate nonlinear absorption. The nonlinear refractive index was also derived by using the Kramer-Kronig relation. The model has taken several processes into account, which is: two-photon absorption, raman transition, linear stark effect, and quadratic stark effect. This model fits well for many materials (Sheik-Bahae et al., 1991). It was later incorporated into the bond-orbital theory by Lines (1990), which allows a semi-empirical representation of the Kerr constant as a function of readily available measures, such as formal valency, bond length, ionic radii and so on. Lines later compared the nonlinear refractive index calculated by the bond-orbital theory against pretransitional-metal halides and chalcogenides, obtaining an RMS accuracy of 9%. The model was later adopted by other researchers (Laniel, Hô, Vallée, & Villeneuve, 2005; Lenz et al., 2000; Slusher et al., 2004) to model the nonlinear refractive index of chalcogenides. In this model, the nonlinear refractive index is given by:

$$n_2(\omega) = 1.7 \times 10^{-18} (n_0^2 + 2)^3 (n_0^2 - 1) \left(\frac{d}{n_0 E_s} \right)^2 G \left(\frac{\hbar(\omega + i\gamma)}{E_g} \right) \quad (6.31)$$

Contribution	$G(x)$
Two-Photon Absorption	$\frac{1}{(2x)^6} \left[-\frac{3}{8}x^2(1-x)^{-1/2} + 3x(1-x)^{1/2} - 2(1-x)^{3/2} + 2\Theta(1-2x)(1-2x)^{3/2} \right]$
Raman	$\frac{1}{(2x)^6} \left[-\frac{3}{8}x^2(1+x)^{-1/2} - 3x(1+x)^{1/2} - 2(1+x)^{3/2} + 2(1+2x)^{3/2} \right]$
Linear Stark	$\frac{1}{(2x)^6} \left[2 - (1-x)^{3/2} - (1+x)^{3/2} \right]$
Quadratic Stark	$\frac{1}{2^{10}x^5} \left[(1-x)^{-1/2} - (1+x)^{-1/2} - \frac{x}{2}(1-x)^{-3/2} - \frac{x}{2}(1+x)^{-3/2} \right]$
Divergent Term	$\frac{1}{(2x)^6} \left[-2 - \frac{35x^2}{8} + \frac{x}{8}(3x-1)(1-x)^{-1/2} - 3x(1-x)^{1/2} + (1-x)^{3/2} + \frac{x}{8}(3x+1)(1+x)^{-1/2} + 3x(1+x)^{1/2} + (1+x)^{3/2} \right]$

Table 6.1: The dispersion of the nonlinear refraction, $G(x)$. $\Theta(x)$ is the Heaviside step function. (Sheik-Bahae et al., 1991)

where d (in units of nanometers) is the mean anion–cation bond length of the bonds that are primarily responsible for the nonlinear response, and E_g is the optical gap of the material. It is noteworthy to know that Sellmeier gap, E_s , is related to the optical gap by $E_s \sim 2.5E_g$ (Slusher et al., 2004). As usual, γ is the damping factor. Dispersion of the Kerr coefficient is given in the function $G(\hbar(\omega + i\gamma)/E_g)$, and it may be estimated with the two-band model (Sheik-Bahae et al., 1991). The functions $G(x)$ are given in Table (6.1).

At this point, it is interesting to point out that Eq. (6.31) is obtained semi-empirically, but it is generally similar to the Kerr coefficient as defined by (Sheik-Bahae, Said, Wei, Hagan, & Van Stryland, 1990) for semiconductors, i.e.:

$$n_2 = K \frac{\hbar c \sqrt{E_p}}{n_0^2 E_g^4} G_2 \left(\frac{\hbar \omega}{E_g} \right) \quad (6.32)$$

where E_p is nearly material-independent. It possesses a value of $E_p \approx 21eV$ for most direct gap semiconductor (Sheik-Bahae et al., 1991). Meanwhile, K is another material

independent constant, given by (Sheik-Bahae et al., 1991)

$$K = \frac{2^9 \pi}{5} \frac{e^4}{\sqrt{m_e c^2}} \quad (6.33)$$

where m_e is the free electron mass.

Furthermore, it is instructive to have a brief understanding of the origin of the two-band model, which provides the dispersion function of the Kerr coefficient, G in Eq. (6.31). Based on the Kramers-Kronig relation, Eq. (6.24), the refractive index $n(\omega)$ and the absorption coefficient $\alpha(\omega)$ of a linear material can be related explicitly as below.

$$n(\omega) - 1 = \frac{2}{\pi} \int_0^\infty \frac{\alpha(\omega')}{\omega'^2 - \omega^2} d\omega' \quad (6.34)$$

Here, we notice that the lower integration limit have been changed to 0, compared to Eq. (6.24), due to the fact that $n(\omega)$ and $\alpha(\omega)$ are both even function (Hutchings, Sheik-Bahae, Hagan, & Van Stryland, 1992). In order to extend the Kramers-Kronig relation to include nonlinear refractive index, a small perturbation δ is added into the system. Since the Kramers-Kronig relation imply that a change in the refractive index $\Delta n(\omega)$ is associated with the change in the absorption $\Delta \alpha(\omega')$, and vice versa, we can mathematically write:

$$[n(\omega) + \Delta n(\omega; \delta)] - 1 = \frac{2}{\pi} \int_0^\infty \frac{\alpha(\omega') + \Delta \alpha(\omega'; \delta)}{\omega'^2 - \omega^2} d\omega' \quad (6.35)$$

A quick subtraction between Eq. (6.34) and Eq. (6.35) then allows us to write:

$$\Delta n(\omega; \delta) = \frac{2}{\pi} \int_0^\infty \frac{\Delta \alpha(\omega'; \delta)}{\omega'^2 - \omega^2} d\omega' \quad (6.36)$$

Eq. (6.36) is basically the Kramers-Kronig relations in nonlinear optics. Here, the parameter δ basically denotes the "cause" of the change in absorption. It can be both optical, or non-optical external perturbation (Sheik-Bahae et al., 1991). The nonlinear Kramers-Kronig equation allows the change in the refractive index being computed for a perturbation δ . In example, the change in refractive index of a system due to a thermal shift of the band edge had been calculated (Wherrett, Hutchings, & Russell, 1986). Furthermore, the change in refractive index of a semiconductors and wide-gap optical solids due to two-photon absorption, raman transition, linear stark effect, and quadratic stark effect had been computed by Sheik-Bahae et al. (1991). These results are essentially

the functions G in Eq. (6.31), which are summarized in Table (6.1) (Sheik-Bahae et al., 1991).

In order to compute n_2 using Eq. (6.36), we first have to obtain the nondegenerate absorption, $\Delta\alpha(\omega, \Omega)$, which quantify the absorption of light at frequency ω when another light field of Ω is applied to the material. This step is important even if the phenomenon is self-refractive, e.g. two-photon absorption as Ω is considered to be the perturbation in Eq. (6.36). Then, Eq. (6.36) is evaluated to obtain the dispersion functions $G(x)$. An outline of this calculation is done for two-photon absorption, and it is attached in Appendix A.

6.5 Metamaterial & Chalcogenide Glass

In Section 6.3, the possibility of switching Casimir force between attractive and repulsive is shown. However, the material we have considered so far is idealized. Moreover, the material that resemblances a piecewise material constant, i.e. metamaterials were not designed to have high nonlinearity. In this section, the idea of optical control over Casimir force was expanded to real materials by considering both metamaterials and chalcogenide glass. The arrangement for this case consists of two plates placed in parallel in vacuum, where one of the plate is a metamaterial as modelled by the Drude-Lorentz model, while the other plate is a chalcogenide glass. Two different models will be presented to model the material constants for the chalcogenide glass.

6.5.1 Constant $n_0(\omega)$ and $n_2(\omega)$ model

To simplify the problem, the material constants for the chalcogenide glass are taken to be constant over the whole range of frequencies. While this simplification violates the Kramer-Kronig relation, it allows us to probe into various characteristics of this arrangement. In this case, the metamaterial plate is modelled with Eq. (5.8), with parameters $\omega_{P_e} = 0.5\omega_0$, $\omega_{T_e} = 10^{-3}\omega_0$, $\omega_{P_m} = 3\omega_0$, $\omega_{T_m} = 2\omega_0$, $\gamma_{e(m)} = 10^{-2}\omega_{T_{e(m)}}$. Furthermore, it is assumed that the metamaterial exhibits negligible nonlinearity, $n_2 = 0 \text{ m}^2/W$. Meanwhile, the chalcogenide glass is chosen to be As_2Se_3 , with its material constant given by

(Lenz et al., 2000):

$$\begin{aligned} n_0(\omega) &= 2.78 \\ n_2(\omega) &= 1.3 \times 10^{-17} m^2/W \end{aligned} \tag{6.37}$$

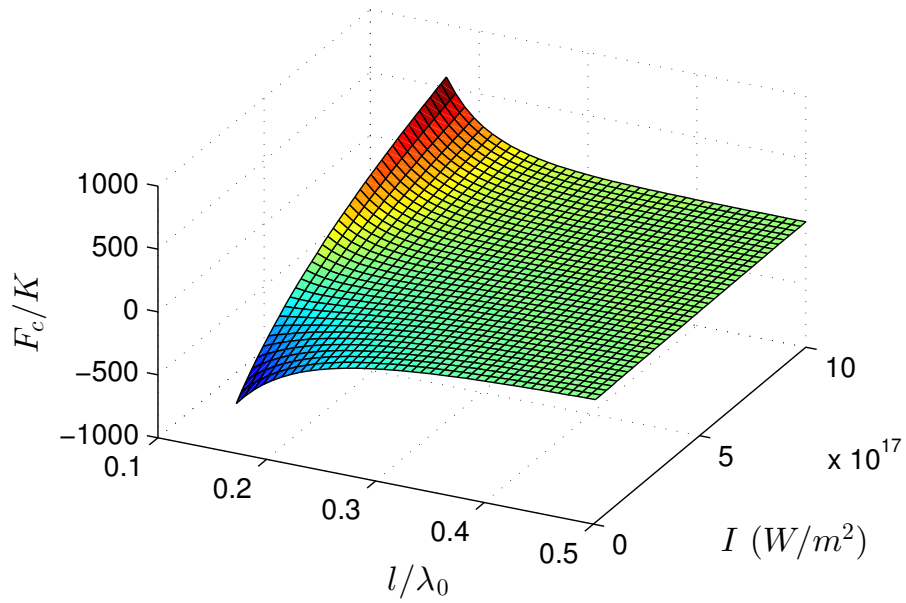
With all these information, the Casimir force of mentioned setup is plotted in Fig. (6.3), for different distances and laser intensity. In this plot, for inter-plate distance $a = 0.20\lambda_0$, we notice that the Casimir force can be switched from attractive to repulsive by using a laser intensity of $I \approx 5 \times 10^{17} W/m^2$. This unique feature allows optical control on the Casimir force between two parallel plate.

As a quick comparison, it is noted that the nonlinear refractive index for fused silica, $n_2 = 2.6 \times 10^{-20} m^2/W$ (Lenz et al., 2000). With that, the intensity of light required to achieve change in Casimir force's sign is ~ 500 times larger than the one plotted in Fig. (6.3). This quickly justifies the reason of using chalcogenide glass.

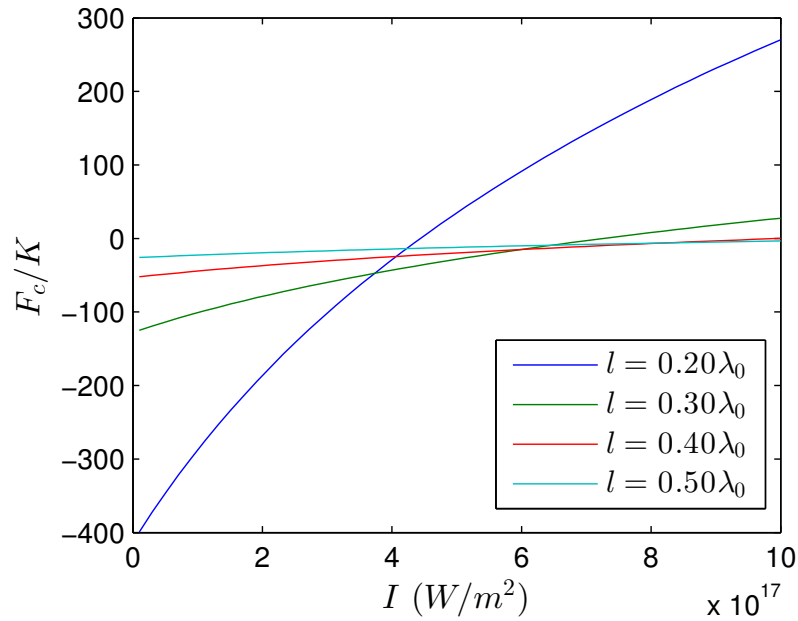
6.5.2 Complex Linear and Nonlinear Coefficients

With the previous section showing the feasibility of our model, we move forward to fully develop the model by considering realistic models for chalcogenide glass. In this section, we will model the Casimir force between a metamaterial, again modelled by Eq. (5.8), and a chalcogenide glass, As_2Se_3 .

The linear refractive index of As_2Se_3 is modelled with the Wemple model, Eq. (6.30). For As_2Se_3 , the Sellmeier gap, $E_s = 4.1 eV$, while the electronic oscillator energy, $E_d \approx 26 eV$ for many chalcogenides (Slusher et al., 2004). The linear refractive index for As_2Se_3 is plotted in Fig. (6.4 a). On the other hand, the nonlinear refractive index of As_2Se_3 is modelled with the two-band model by Sheik-Bahae et al. (1991). The nonlinear refractive index is given in Eq. (6.31), with the mean anion-cation bond length, $d = 0.243 nm$, while the optical gap $E_g \approx 0.4 E_s$ (Slusher et al., 2004). This gives $E_g = 1.64 eV$ for As_2Se_3 . It is noteworthy to recall that this model taken a few processes into account, which includes Two-Photon Absorption, Raman transition, Linear Stark effect, and Quadratic Stark effect. These contributions are contained in the function G in Eq. (6.31), which is given in Table 6.1. The dispersion and absorption of n_2 is plotted in Fig. (6.4 b).

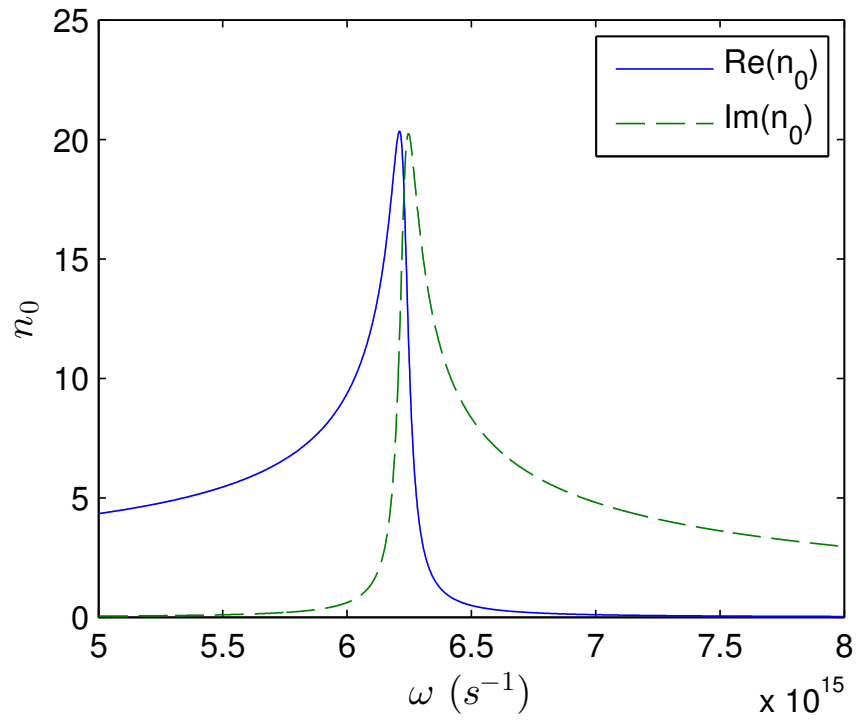


a)

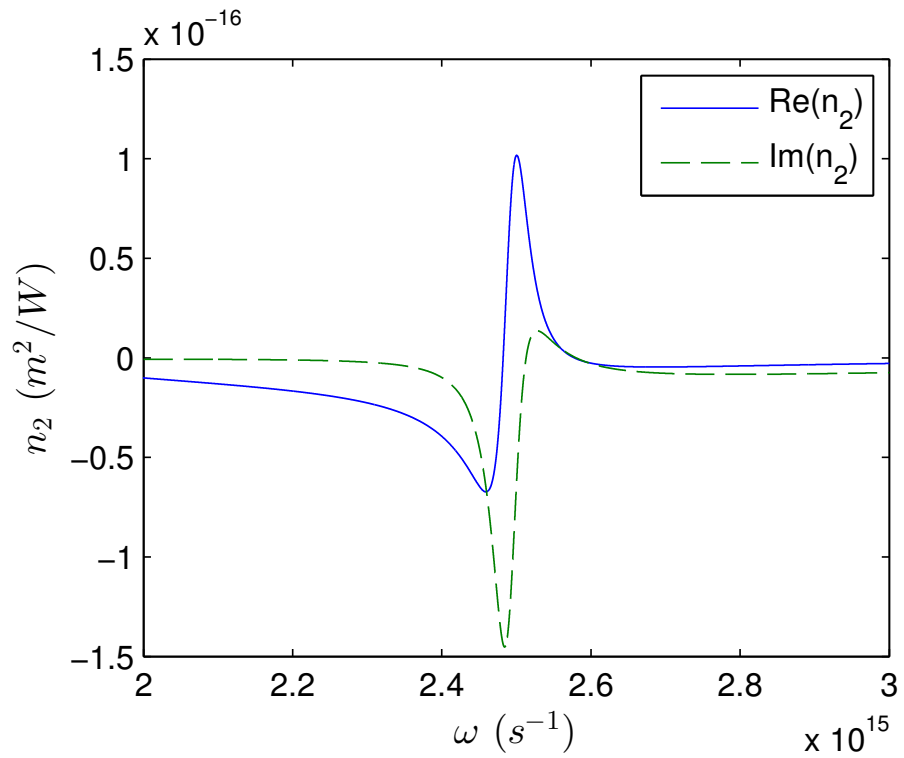


b)

Figure 6.3: The Casimir force between a metamaterial and a chalcogenide glass, As_2Se_3 is plotted as a function of inter-plate distances and impinging laser intensity. The refractive indices for As_2Se_3 is assumed constant over the whole range of frequencies. (a) 3D plot and (b) curve for several specific inter-plate spacing.



a)



b)

Figure 6.4: (a) n_0 of As_2Se_3 as modelled using the Wemple equation. (b) n_2 of As_2Se_3 as modeled by Eq. (6.31)

With all these in place, the Casimir force between these two plates are plotted in Fig. (6.5). Here we notice a similar trend as compared to the previous model in Fig. (6.3). The position, however, for the transition from Casimir attraction to Casimir repulsion have increased to $I \approx 1.5 \times 10^{18} \text{ W/m}^2$, for inter-plate spacing of $a = 0.20\lambda_0$. This value is almost three times compared to the previous model, which is rather unexpected. With this we see that a constant refractive index model may give a general picture, but the computational values are rather unreliable. The resonant effect must be taken into account for the computation of Casimir force for an overall picture.

To further understand the range of frequencies responsible for the change in sign for the Casimir force, we have plotted the derivative of Casimir force with respect to the frequencies in Fig. (6.6), for (a) $a = 0.20\lambda_0$ and (b) $a = \lambda_0$. Generally, as the intensity increases, the derivative of Casimir force increases towards positive values (repulsive). In particular, for inter-plate distance of $a = 0.2\lambda_0$, the derivative of Casimir force around the frequency range of $2 \times 10^{14} - 2 \times 10^{15} \text{ s}^{-1}$ increases towards positive value. This range corresponds to infrared-ultraviolet region of the electromagnetic spectrum. The increase in Casimir repulsion in these region eventually leads to an overall Casimir repulsion, as seen in Fig. (6.5). For the case of $a = \lambda_0$, the Casimir force changes in a lower range of frequencies ($10^{14} - 10^{15} \text{ s}^{-1}$), as the intensity increases. With this, we notice that an increase in the inter-plate distance will increase the contribution of lower frequencies towards the change of Casimir force.

6.6 Discussions

In this section, we have first introduced the AC Kerr effect. Intensity dependence is then introduced in the Casimir force. Two simple, non-dispersive materials with Kerr effect are introduced to illustrate the intensity dependence of Casimir force. However, these models do not exhibit large variations of Casimir force as the intensity increases. Then, the piecewise model was recalled to show that it is possible to change both the magnitude and sign of the Casimir force by optical means. Chalcogenide glasses are then introduced as a possible material to introduce nonlinearity into a system, which consists of a nonlinear material and a metamaterial.

Chalcogenide glasses had naturally fit into the discussion of intensity dependence

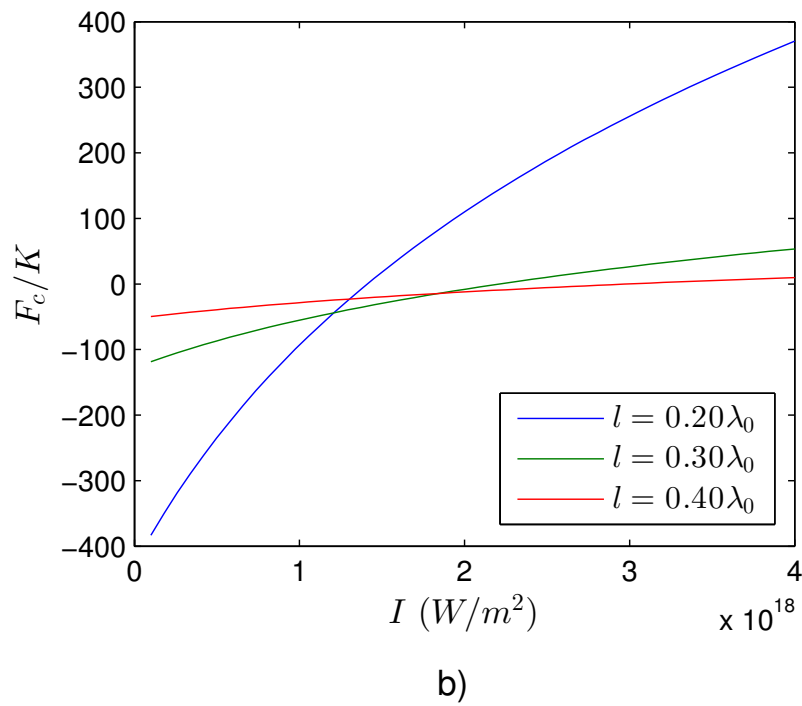
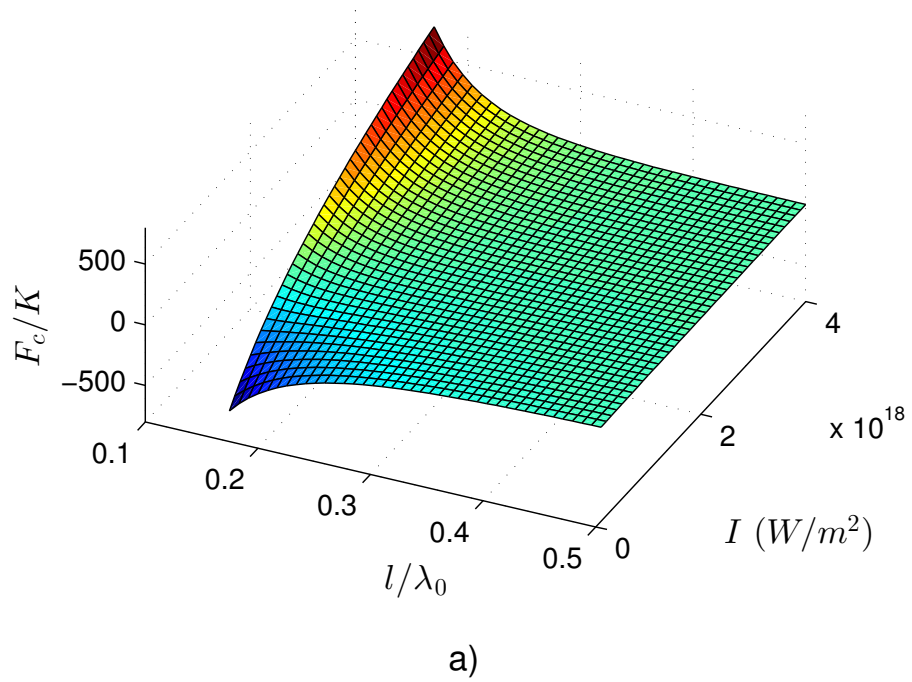
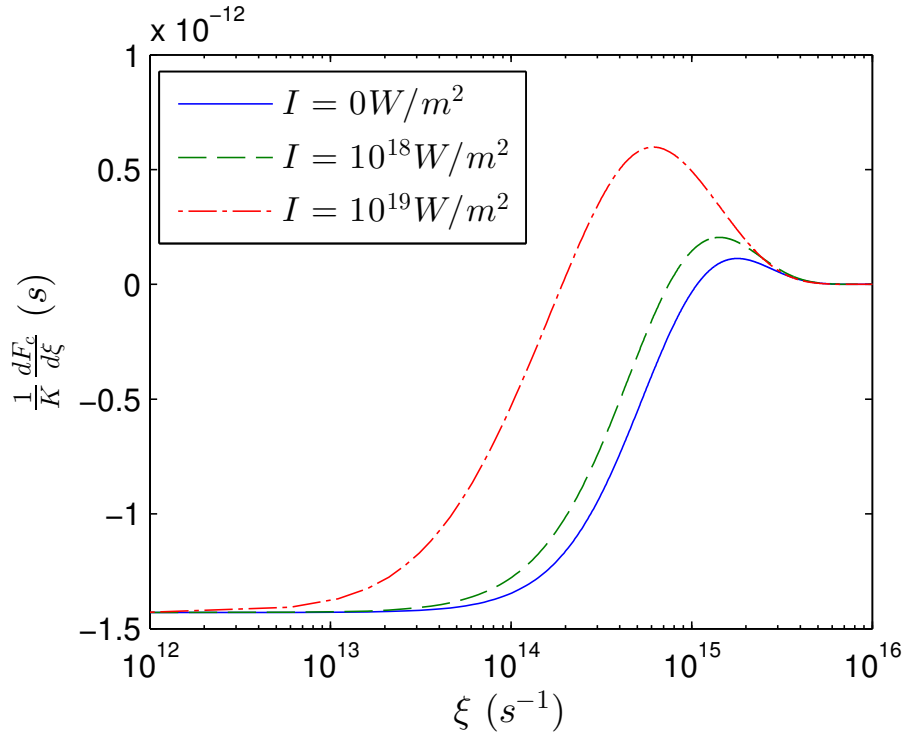
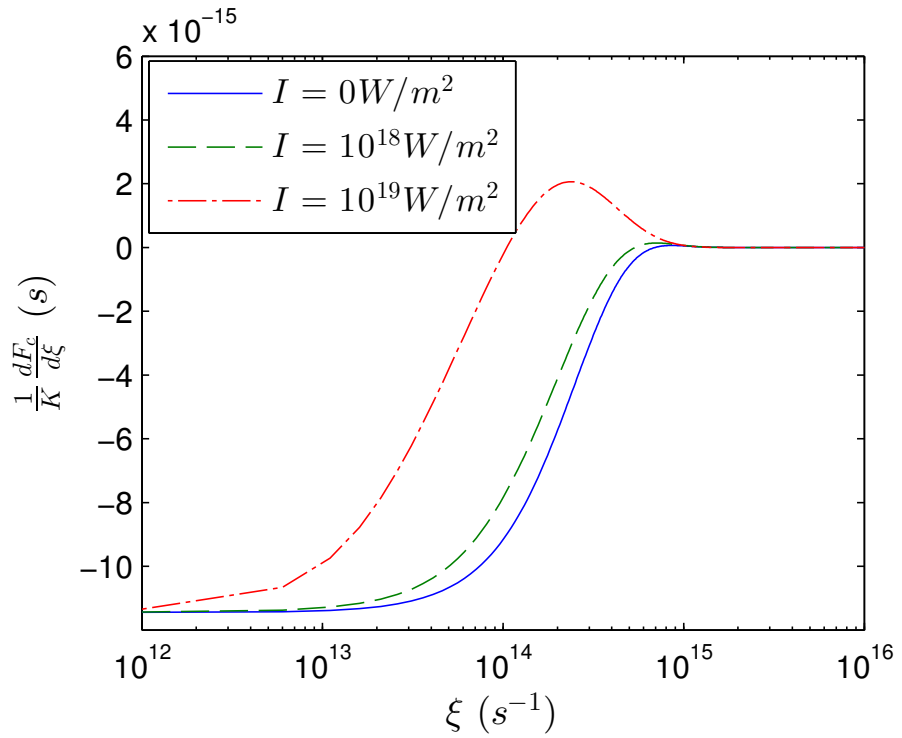


Figure 6.5: The variation of Casimir force between a metamaterial, and a chalcogenide glass, As_2Se_3 for different inter-plate distances and impinging laser intensity. (a) 3D plot and (b) curve for several specific inter-plate spacing.



a)



b)

Figure 6.6: The derivative of Casimir force, $dF_c/d\xi$ at different frequencies ξ . The inter-plate distance is (a) $l = 0.2\lambda_0$ and (b) $l = \lambda_0$. It is noted that the derivative of Casimir force increase with frequency for sufficiently large laser intensity.

of Casimir force, mainly due to the fact that it exhibits high nonlinear refractive indices (Wang, 1970). However, the choice of using As_2Se_3 as a representation of chalcogenide glass in our simulation was done mainly because there are readily available model for its refractive indices (Lenz et al., 2000).

Throughout this chapter, we have noticed that the laser intensity required for a change in sign for the Casimir force is in the order of $I \approx 10^{18}W/m^2$. This value is achievable with normal diode lasers, which is far less than the current ultrahigh laser intensity $I \approx 10^{26}W/m^2$ (Bahk et al., 2004). This enables practical control over the Casimir force via optical means.

The direction of impinging laser may be another concern here. As the laser intensity required is very high, a high radiation pressure of $P = \frac{I}{c} = 3 \times 10^9 Nm^{-2}$ is resulted. This is significantly larger than the Casimir force we are considering here, which then will dominates the net force between plates. However, since the control of nonlinear properties take place in the inner surface of the plates, we may direct the laser parallel to the plates, and it is guided along the inner surface of the plate. With this, both the radiation pressure and heating effect may be negligible. Furthermore, the heating effect of a laser is very significant only if the laser spectrum coincides with the resonant frequency of the materials. Heating effect due to this process may be avoided by using a laser with its spectrum lying outside of the resonant frequencies of the materials.

Lastly, the ability to alter the force due to quantum vacuum by using lasers provides various new possibilities. Potential application of this finding includes manipulating nanoresonators and integrating optical devices into NEMS.

CHAPTER 7

CONCLUSION

Throughout this research, we have seen various aspect of the Casimir force. It was first learned that the Casimir force is the manifestation of zero-point energy due to second quantization of the electromagnetic field. Later, several different interpretations of Casimir force were discussed. In particular, the Casimir force may be regarded as the macroscopic manifestation of the van der Waals forces. Furthermore, the force may be thought as a vacuum radiation pressure exerted on both plates. Schwinger et al. (1978) take the idea of Casimir force to a whole new level by showing that the Casimir force is a direct manifestation of the source field. The Casimir force is computed from a small change in the energy of the induced dipole in a medium, due to the source field produced by the dipole itself. In general, we have fulfilled the first objective of this research, i.e. to explore the origin of Casimir force, and its physical significance.

In the second half of this research, we have learned the dependence of Casimir force on materials. The main focus had been put on the possibilities of obtaining a stable equilibrium, or a change between attractive and repulsive Casimir force. Later, we notice that artificially made metamaterials exhibits interesting Casimir effect. This may be largely accounted to the fact that metamaterials can be electric and magnetic at different frequency region. Furthermore, we have also shown the possibility of controlling Casimir force via optical means. The use of a high intensity laser may alter material's property and subsequently alter the Casimir force. In general, this section had successfully fulfill the second objective of this research, which is to explore the possibilities of controlling the Casimir force.

Given that NEMS advances at a fast pace now, it is expected that the Casimir force will be a great impediment towards further development. Hence, it is important, both theoretically and experimentally, to understand the Casimir force. With this in mind, the idea of optical control on Casimir force should be expanded beyond our proof of concept in the paper by Ooi and Khoo (2012). For instance, a better model should be developed to

include the possibilities of heating and radiation pressure. Also, all arrangements that we have considered so far was solely based on parallel plate system. This is a big simplification compared to real world materials, which may be different in shape. A better model may be developed to take different shapes and arrangements into account. It is ultimately hoped that this idea would transform from a theoretical framework into an experimental verified theory.

Appendices

APPENDIX A

TWO-BAND MODEL: DERIVATION OF $G(X)$

In order to have a brief idea of how the nonlinear Kramers-Kronig relation may allow the computation of n_2 , we briefly outline the derivation of $G(x)$ in Eq. (6.31) using the two-photon absorption model. To compute n_2 using Eq. (6.36), we first have to know the nondegenerate absorption, $\Delta\alpha(\omega, \Omega)$, which quantify the absorption of light at frequency of ω when another light field of Ω is applied to the material. To obtain the nondegenerate absorption for two-photon absorption, the dipole approximation for the radiation interaction of Hamiltonian is used (Sheik-Bahae et al., 1991):

$$H_{int} = -\frac{e}{m_e} \vec{A} \cdot \vec{p} \quad (\text{A.1})$$

where \vec{p} is the electron's momentum operator and \vec{A} is the magnetic vector potential. Also, e is the electronic charge and m_e is the free electron mass. A two-beam interaction with both beams linearly polarized in the same direction is then considered:

$$\vec{A} = \hat{a} [A_1 \cos(\omega_1 t) + A_2 \cos(\omega_2 t + \phi)] \quad (\text{A.2})$$

where \hat{a} is a unit vector having the same direction as the optical polarization, and A_i are constants. It is highlighted (Keldysh, 1965) that this dressed state may be approximated by using a Volkov-type wavefunction (Volkov, 1935):

$$\psi_i(\vec{k}, \vec{r}, t) = u_i(\vec{k}, \vec{r}) \exp \left[i\vec{k} \cdot \vec{r} - \frac{i}{\hbar} \int_0^t E_i(\tau) d\tau \right] \quad (\text{A.3})$$

where $i = c, v$ refers to the conduction and valence band, respectively. $u_i(\vec{k}, \vec{r})$ are the usual Bloch wavefunctions which have the same periodicity as the lattice, T , i.e.:

$$u_i(\vec{k}, \vec{r}) = u_i(\vec{k}, \vec{r} + T) \quad (\text{A.4})$$

Also, E_i is the energies for electrons and holes in each band.

Now we recall that the effect of the optical field is to alter the energy of holes in the final state, and electrons in the initial states (Sheik-Bahae et al., 1991). Since only first

and second order a.c. Stark shifting of bands will give rise to $\chi^{(3)}$, we write:

$$\begin{aligned} E_c(\tau) &= E_{c0} + \Delta E_{cc}(\tau) + \Delta E_{cv} \\ E_v(\tau) &= E_{v0} + \Delta E_{vv}(\tau) + \Delta E_{vc} \end{aligned} \quad (\text{A.5})$$

where E_{c0} and E_{v0} are the energy of electrons in the conduction band and valence band, respectively, without subjected to external perturbation. It is predicted by using effective mass approximation to be (Kittel & McEuen, 1996):

$$\begin{aligned} E_{c0} &= E_g + \frac{\hbar^2 k^2}{2m_c} \\ E_{v0} &= \frac{\hbar^2 k^2}{2m_v} \end{aligned} \quad (\text{A.6})$$

Here, the hole's mass m_v is taken to be negative, while m_c denotes the effective electron mass in the conduction band. Also it is well understood that the wavevector, $k^2 = |\vec{k}|^2$. Meanwhile, the first order a.c. Stark shift is given by (Sheik-Bahae et al., 1991)

$$\Delta E_{ii}(\tau) = \frac{e\hbar\vec{k} \cdot \vec{A}(\tau)}{m_i} \quad (\text{A.7})$$

and the second order a.c. Stark shift, ΔE_{cv} and ΔE_{vc} are omitted from our derivation, as we are considering two-photon absorption only.

The transition rates are then calculated by using an S -matrix formalism (Wu & Ohmura, 1962):

$$S = -\frac{i}{\hbar} \int_{-\infty}^{\infty} dt \int d^3r \psi_c^*(\vec{k}, \vec{r}, t) H_{int} \psi_v(\vec{k}', \vec{r}, t) \quad (\text{A.8})$$

Now by inserting all information, we have:

$$\begin{aligned} S &= -\frac{i}{\hbar} \int_{-\infty}^{\infty} dt \int d^3r \psi_c^*(\vec{k}, \vec{r}, t) H_{int} \psi_v(\vec{k}', \vec{r}, t) \\ &= -\frac{i}{\hbar} \int_{-\infty}^{\infty} dt \int d^3r u_c^*(\vec{k}, \vec{r}) \exp\left[-i\vec{k} \cdot \vec{r} + \frac{i}{\hbar} \int_0^t E_c(\tau) d\tau\right] \left[-\frac{e}{m_e} \vec{A} \cdot \vec{p}\right] \\ &\quad \cdot u_v(\vec{k}', \vec{r}) \exp\left[i\vec{k}' \cdot \vec{r} - \frac{i}{\hbar} \int_0^t E_v(\tau) d\tau\right] \\ &= \frac{i}{\hbar} \frac{e}{m_e} \int_{-\infty}^{\infty} dt \int d^3r u_c^*(\vec{k}, \vec{r}) \exp\left[-i\vec{k} \cdot \vec{r} + \frac{i}{\hbar} \int_0^t E_c(\tau) d\tau - \frac{i}{\hbar} \int_0^t E_v(\tau) d\tau\right] \\ &\quad \cdot [\vec{A} \cdot \vec{p}] u_v(\vec{k}', \vec{r}) \exp\left[i\vec{k}' \cdot \vec{r}\right] \end{aligned} \quad (\text{A.9})$$

By recalling the momentum operator to be $-i\hbar\nabla$, and by introducing the interband momentum matrix, i.e.

$$\vec{p}_{vc} = -i\hbar \int d^3r u_c^*(\vec{k}, \vec{r}) \nabla u_v(\vec{k}, \vec{r}) \quad (\text{A.10})$$

we have, for $\vec{k}' = \vec{k}$,

$$\begin{aligned}
S &= \frac{e}{m_e} \delta_{kk'} \int_{-\infty}^{\infty} dt \exp \left[\frac{i}{\hbar} \int_0^t E_c(\tau) - E_v(\tau) d\tau \right] \left[\vec{A} \cdot \int d^3 r u_c^*(\vec{k}, \vec{r}) \nabla u_v(\vec{k}, \vec{r}) \right] \\
&= \frac{e}{m_e} \delta_{kk'} \int_{-\infty}^{\infty} dt \exp \left[\frac{i}{\hbar} \int_0^t E_c(\tau) - E_v(\tau) d\tau \right] \left[\frac{i}{\hbar} \vec{A} \cdot \vec{p}_{vc} \right] \\
&= \frac{e}{m_e} \delta_{kk'} \int_{-\infty}^{\infty} dt C \left[\frac{i}{\hbar} \vec{A} \cdot \vec{p}_{vc} \right]
\end{aligned} \tag{A.11}$$

Here, $\delta_{kk'}$ is the Kronecker delta function, and $C = \exp \left[\frac{i}{\hbar} \int_0^t E_c(\tau) - E_v(\tau) d\tau \right]$. Now by considering the exponential part, we have:

$$\begin{aligned}
C &= \exp \left(\frac{i}{\hbar} \int_0^t E_c(\tau) - E_v(\tau) d\tau \right) \\
&= \exp \left(\frac{i}{\hbar} \int_0^t (E_{c0} + \Delta E_{cc}(\tau)) - (E_{v0} + \Delta E_{vv}(\tau)) d\tau \right) \\
&= \exp \left(\frac{i}{\hbar} \int_0^t \left(E_g + \frac{\hbar^2 k^2}{2m_c} + \frac{e\hbar}{m_c} \vec{k} \cdot \vec{A}(\tau) \right) - \left(\frac{\hbar^2 k^2}{2m_v} + \frac{e\hbar}{m_v} \vec{k} \cdot \vec{A}(\tau) \right) d\tau \right) \\
&= \exp \left(\frac{it}{\hbar} \left(E_g + \frac{\hbar^2 k^2}{2m_c} - \frac{\hbar^2 k^2}{2m_v} \right) + \frac{i}{\hbar} \left(\frac{e\hbar}{m_c} - \frac{e\hbar}{m_v} \right) \int_0^t \vec{k} \cdot \vec{A}(\tau) d\tau \right)
\end{aligned} \tag{A.12}$$

It is important at this point to introduce the reduced mass,

$$\frac{1}{m_{vc}} = \frac{1}{m_c} - \frac{1}{m_v} \tag{A.13}$$

to simply Eq. (A.12) into:

$$\begin{aligned}
C &= \exp \left(\frac{it}{\hbar} \left(E_g + \frac{\hbar^2 k^2}{2m_c} - \frac{\hbar^2 k^2}{2m_v} \right) + \frac{i}{\hbar} \left(\frac{e\hbar}{m_c} - \frac{e\hbar}{m_v} \right) \int_0^t \vec{k} \cdot \vec{A}(\tau) d\tau \right) \\
&= \exp \left(\frac{itE_g}{\hbar} + \frac{it\hbar k^2}{2m_{vc}} + \left(\frac{ie}{m_{vc}} \right) \int_0^t \vec{k} \cdot \vec{A}(\tau) d\tau \right)
\end{aligned} \tag{A.14}$$

By evaluating the time integration on the exponential part, and by omitting the non-oscillatory part, we have:

$$\begin{aligned}
C &= \exp \left(\frac{itE_g}{\hbar} + \frac{it\hbar k^2}{2m_{vc}} + \left(\frac{ie}{m_{vc}} \right) \int_0^t \vec{k} \cdot \vec{A}(\tau) d\tau \right) \\
&= \exp \left(\frac{it}{\hbar} E_{vc} + \left(\frac{ie}{m_{vc}} \right) \left(\frac{A_1 \sin(\omega_1 t)}{\omega_1} + A_2 \frac{\sin(\omega_2 t + \phi) - \sin(\phi)}{\omega_2} \right) \vec{k} \cdot \hat{a} \right) \\
&= \exp (i\omega_{vc} t + i\eta_1 \sin(\omega_1 t) + i\eta_2 \sin(\omega_2 t + \phi))
\end{aligned} \tag{A.15}$$

In the above equation, we have defined ω_{vc} :

$$\hbar \omega_{vc} = E_g + \frac{\hbar^2 k^2}{2m_{vc}} \tag{A.16}$$

and

$$\eta_i = \frac{eA_i \vec{k} \cdot \hat{a}}{m_{vc} \omega_i} \quad (\text{A.17})$$

With the integral evaluated, the scattering matrix may now be written as:

$$\begin{aligned} S &= \frac{ei}{\hbar m_e} \delta_{kk'} \int_{-\infty}^{\infty} dt \exp \left[\frac{i}{\hbar} \int_0^t E_c(\tau) - E_v(\tau) d\tau \right] [\vec{A} \cdot \vec{p}_{vc}] \\ &= \frac{ei}{\hbar m_e} [\hat{a} \cdot \vec{p}_{vc}] \delta_{kk'} \int_{-\infty}^{\infty} dt \exp [i\omega_{vc}t + i\eta_1 \sin(\omega_1 t) + i\eta_2 \sin(\omega_2 t + \phi)] \\ &\quad \cdot [A_1 \cos(\omega_1 t) + A_2 \cos(\omega_2 t + \phi)] \\ &= \frac{i}{\hbar} \frac{e[\hat{a} \cdot \vec{p}_{vc}]}{m_e} \delta_{kk'} \int_{-\infty}^{\infty} dt \exp(i\omega_{vc}t) [A_1 \cos(\omega_1 t) + A_2 \cos(\omega_2 t + \phi)] \\ &\quad \cdot \exp[\sin(i\eta_1 \sin(\omega_1 t) + i\eta_2 \sin(\omega_2 t + \phi))] \\ &= \frac{i}{\hbar} \frac{e[\hat{a} \cdot \vec{p}_{vc}]}{m_e} \delta_{kk'} D \end{aligned} \quad (\text{A.18})$$

We then set forward to solve the time integral in the S -matrix, D . To achieve that, we recall the identity:

$$\exp(i\eta \sin(\omega t)) = \sum_{n=-\infty}^{\infty} J_n(\eta) e^{in\omega t} \quad (\text{A.19})$$

where $J_n(\eta)$ is the Bessel function of the first kind of order of n . The time integral part of Eq. (A.18), D is then given by

$$\begin{aligned} D &= \int_{-\infty}^{\infty} dt \exp(i\omega_{vc}t) [A_1 \cos(\omega_1 t) + A_2 \cos(\omega_2 t + \phi)] \\ &\quad \cdot \sum_{m,n=-\infty}^{\infty} J_m(\eta_1) e^{im\omega_1 t} J_n(\eta_2) e^{in\omega_2 t} \\ &= \sum_{m,n=-\infty}^{\infty} J_m(\eta_1) J_n(\eta_2) \int_{-\infty}^{\infty} dt \exp(it(\omega_{vc} + m\omega_1 + n\omega_2)) \\ &\quad \cdot [A_1 \cos(\omega_1 t) + A_2 \cos(\omega_2 t + \phi)] \end{aligned} \quad (\text{A.20})$$

With the integral evaluated, the S -matrix is now (Sheik-Bahae et al., 1991):

$$\begin{aligned} S &= \frac{i\pi}{\hbar} \frac{e\hat{a} \cdot \vec{p}_{vc}}{m_e} \sum_{m,n=-\infty}^{\infty} J_m(\eta_1) J_n(\eta_2) \{ A_1 [\delta((m+1)\omega_1 + n\omega_2 + \omega_{vc}) \\ &\quad + \delta((m-1)\omega_1 + n\omega_2 + \omega_{vc})] + A_2 [\delta(m\omega_1 + (n+1)\omega_2 + \omega_{vc}) \\ &\quad + \delta(m\omega_1 + (n-1)\omega_2 + \omega_{vc})] \} \end{aligned} \quad (\text{A.21})$$

The delta functions terms in Eq. (A.21) indicates various combinations of multiphoton absorption processes. We now consider the nondegenerate two-photon absorption case, i.e. when one photon from each (ω_1, ω_2) is absorbed. The term that corresponds to

nondegenerate two-photon absorption is given by $\delta(\omega_{vc} - \omega_1 - \omega_2)$ (Sheik-Bahae et al., 1991). These terms may be generated from Eq. (A.21) by having either $A_2 = 0, m = 0, n = -1$, or $A_2 = 0, m = 0, n = -1$. The sum of these two terms is then given by:

$$S = \frac{i\pi}{\hbar} \frac{e\hat{a} \cdot \vec{p}_{vc}}{m_e c} [J_0(\eta_1)J_{-1}(\eta_2)A_1 + J_{-1}(\eta_1)J_0(\eta_2)A_2] \delta(\omega_{vc} - \omega_1 - \omega_2) \quad (\text{A.22})$$

By approximating the Bessel functions to the first order, i.e. $J_n(x) \approx x^n/2^n n!$, and by noting $J_{-n}(x) = (-1)^n J_n(x)$, we then simplify Eq. (A.22) to get:

$$\begin{aligned} S &= \frac{i\pi}{\hbar} \frac{e\hat{a} \cdot \vec{p}_{vc}}{m_e c} [J_{-1}(\eta_2)A_1 + J_{-1}(\eta_1)A_2] \delta(\omega_{vc} - \omega_1 - \omega_2) \\ &= -\frac{i\pi}{\hbar} \frac{e\hat{a} \cdot \vec{p}_{vc}}{m_e c} \left[\frac{\eta_2}{2}A_1 + \frac{\eta_1}{2}A_2 \right] \delta(\omega_{vc} - \omega_1 - \omega_2) \\ &= -\frac{i\pi}{\hbar} \frac{e\hat{a} \cdot \vec{p}_{vc}}{m_e c} (\vec{k} \cdot \hat{a}) \frac{eA_2A_1}{2m_{vc}} \left[\frac{1}{\omega_1} + \frac{1}{\omega_2} \right] \delta(\omega_{vc} - \omega_1 - \omega_2) \end{aligned} \quad (\text{A.23})$$

Now, by using Fermi's golden rule (Wu & Ohmura, 1962), the change in transition rate may be obtained by performing the integral over the entire k -space. It is given by:

$$\begin{aligned} \Delta W &= \sum_{spin} \int \frac{d^3k}{(2\pi)^3} \left(\frac{\pi e^2 A_2 A_1}{2m_e m_{vc} c^2} \right)^2 |\hat{a} \cdot \vec{p}_{vc}|^2 |\vec{k} \cdot \hat{a}|^2 \left(\frac{1}{\omega_1} + \frac{1}{\omega_2} \right)^2 \\ &\quad \cdot \frac{1}{2\pi\hbar} \delta \left(E_g + \frac{\hbar^2 k^2}{2m_{vc}} - \hbar\omega_1 - \hbar\omega_2 \right) \end{aligned} \quad (\text{A.24})$$

A two-band model is then used for further simplification (Sheik-Bahae et al., 1991). In this model, the transition rates is calculated by considering a conduction band and a valence band of opposite curvature ($m_v = -m_c$), with doubly degenerate spin. Furthermore, it is noteworthy that the angular dependence in the k -space for both $|\vec{k} \cdot \hat{a}|^2$ and $|\hat{a} \cdot \vec{p}_{vc}|^2$ terms will results in a factor of 1/5 when the angular integral is performed. By assuming that \vec{p}_{vc} is parallel to \vec{k} , and by using the fact that $A_j^2 = 8\pi c I_j / n_j \omega_j^2$, we then have:

$$\begin{aligned} \Delta W &= \sum_{spin} \int \frac{d^3k}{(2\pi)^3} \left[\frac{\pi e^2 A_{01} A_{02}}{2m_e m_{vc} c^2} \right]^2 |\hat{a} \cdot \vec{p}_{vc}|^2 |\vec{k} \cdot \hat{a}|^2 \left(\frac{1}{\omega_1} + \frac{1}{\omega_2} \right)^2 \\ &\quad \cdot \frac{1}{2\pi\hbar} \delta \left(E_g + \frac{\hbar^2 k^2}{2m_{vc}} - \hbar\omega_1 - \hbar\omega_2 \right) \\ &= \frac{2}{5(2\pi)^3} \frac{8\pi I_1}{n_1 \omega_1^2} \frac{8\pi I_2}{n_2 \omega_2^2} \left[\frac{\pi e^2 |\vec{p}_{vc}|}{2m_e m_{vc} c} \right]^2 \left(\frac{1}{\omega_1} + \frac{1}{\omega_2} \right)^2 \\ &\quad \cdot \frac{1}{2\pi\hbar} \int \delta \left(E_g + \frac{\hbar^2 k^2}{2m_{vc}} - \hbar\omega_1 - \hbar\omega_2 \right) k^2 d^3k \\ &= \frac{2}{5(2\pi)^3} \frac{8\pi I_1}{n_1 \omega_1^2} \frac{8\pi I_2}{n_2 \omega_2^2} \left[\frac{\pi e^2 |\vec{p}_{vc}|}{2m_e m_{vc} c} \right]^2 \left(\frac{1}{\omega_1} + \frac{1}{\omega_2} \right)^2 \frac{1}{2\pi\hbar} E \end{aligned} \quad (\text{A.25})$$

It is important, at this point to solve the integral part E of Eq. (A.25). By taking $d^3k \rightarrow 4\pi k^2 dk$, E may be written as:

$$E = \int \delta \left(E_g + \frac{\hbar^2 k^2}{2m_{vc}} - \hbar\omega_1 - \hbar\omega_2 \right) 4\pi k^4 dk \quad (\text{A.26})$$

A change in variable is then done on Eq. (A.26), where $X = \frac{\hbar^2 k^2}{2m_{vc}}$ and $dX = \frac{\hbar^2 k}{m_{vc}} dk$. With all these changes, we have:

$$\begin{aligned} E &= \int \delta (E_g + X - \hbar\omega_1 - \hbar\omega_2) 4\pi \left(\frac{2Xm_{vc}}{\hbar^2} \right)^{3/2} \frac{m_{vc}}{\hbar^2} dX \\ &= 4\pi \left(\frac{2(\hbar\omega_1 + \hbar\omega_2 - E_g)m_{vc}}{\hbar^2} \right)^{3/2} \frac{m_{vc}}{\hbar^2} \\ &= 2\pi \left(\frac{2m_{vc}}{\hbar^2} \right)^{5/2} (\hbar\omega_1 + \hbar\omega_2 - E_g)^{3/2} \end{aligned} \quad (\text{A.27})$$

Now by inserting Eq. (A.27) into Eq. (A.25), the change in transition rate is then given by:

$$\begin{aligned} \Delta W &= \frac{2}{5(2\pi)^3} \frac{8\pi I_1}{n_1 \omega_1^2} \frac{8\pi I_2}{n_2 \omega_2^2} \left[\frac{\pi e^2 |\vec{p}_{vc}|}{2m_e m_{vc} c} \right]^2 \left(\frac{1}{\omega_1} + \frac{1}{\omega_2} \right)^2 \\ &\quad \cdot \frac{1}{2\pi \hbar} \left(2\pi \left(\frac{2m_{vc}}{\hbar^2} \right)^{5/2} (\hbar\omega_1 + \hbar\omega_2 - E_g)^{3/2} \right) \\ &= \frac{2^4 \pi}{5} \frac{e^4}{n_1 n_2 c^2} \frac{m_c^{1/2} |\vec{p}_{vc}|^2}{m_e^2} \frac{I_1 I_2}{(\hbar\omega_1)^2 (\hbar\omega_2)^2} \left(\frac{1}{\hbar\omega_1} + \frac{1}{\hbar\omega_2} \right)^2 \\ &\quad \cdot (\hbar\omega_1 + \hbar\omega_2 - E_g)^{3/2} \end{aligned} \quad (\text{A.28})$$

where n_i is the linear refractive index at frequency ω_i . Now we introduce a material-independent constant

$$K = \frac{2^9 \pi}{5} \frac{e^4}{\sqrt{m_e} c^2} \quad (\text{A.29})$$

which further simplifies Eq. (A.28) into

$$\begin{aligned} \Delta W &= \frac{K}{2^5 n_1 n_2} \frac{m_c^{1/2} |\vec{p}_{vc}|^2}{m_e^{3/2}} \frac{I_1 I_2}{(\hbar\omega_1)^2 (\hbar\omega_2)^2} \cdot \left(\frac{1}{\hbar\omega_1} + \frac{1}{\hbar\omega_2} \right)^2 (\hbar\omega_1 + \hbar\omega_2 - E_g)^{3/2} \\ &= \frac{K}{2^5 n_1 n_2} \frac{m_c^{1/2} |\vec{p}_{vc}|^2}{m_e^{3/2} (\hbar\omega_1) E_g^{7/2}} \frac{I_1 I_2 E_g^3}{(\hbar\omega_1) (\hbar\omega_2)^2} \cdot \left(\frac{1}{\hbar\omega_1} + \frac{1}{\hbar\omega_2} \right)^2 \left(\frac{\hbar\omega_1}{E_g} + \frac{\hbar\omega_2}{E_g} - 1 \right)^{3/2} \end{aligned} \quad (\text{A.30})$$

Now by letting the spectral function F to be:

$$F(x_1, x_2) = \frac{(x_1 + x_2 - 1)^{3/2}}{2^7 x_1 x_2^2} \left(\frac{1}{x_1} + \frac{1}{x_2} \right)^2 \quad (\text{A.31})$$

We then have:

$$\Delta W = 2K \frac{2}{n_1 n_2} \frac{m_c^{1/2} |\vec{p}_{vc}|^2}{m_e^{3/2} (\hbar \omega_1) E_g^{7/2}} I_1 I_2 F(x_1, x_2) \quad (\text{A.32})$$

By further using the approximation to obtain a universal scaling law, i.e. (Sheik-Bahae et al., 1991):

$$\frac{|\vec{p}_{vc}|^2}{m_e^2} \approx \frac{E_g}{2m_c} \quad (\text{A.33})$$

The equation for ΔW then simplifies to:

$$\begin{aligned} \Delta W &= 2K \frac{\sqrt{2}}{n_1 n_2} \frac{|\vec{p}_{vc}|}{m_e (\hbar \omega_1) E_g^3} I_1 I_2 F(x_1, x_2) \\ &= 2K \frac{\sqrt{E_p}}{n_1 n_2 E_g^3} \frac{1}{\hbar \omega_1} I_1 I_2 F(x_1, x_2) \end{aligned} \quad (\text{A.34})$$

where we have introduced $E_p = 2|\vec{p}_{vc}|^2/m_e$.

Using this expression for transition rate, a change in the absorption of ω_1 due to presence of ω_2 is calculated to have the general form:

$$\begin{aligned} \Delta \alpha(\omega_1; \omega_2) &= \frac{\hbar \omega}{I_1} \Delta W \\ &= 2K \frac{\sqrt{E_p}}{n_1 n_2 E_g^3} F\left(\frac{\hbar \omega_1}{E_g}; \frac{\hbar \omega_2}{E_g}\right) I_2 \end{aligned} \quad (\text{A.35})$$

The dispersion function is then evaluated by using the nonlinear Kramers-Kronig relation, Eq. (6.36). Here we notice that $\Delta n(\omega) = 2n_2(\omega)I$. The factor of two in arises from the interference between both beams (Sheik-Bahae, Wang, & Van Stryland, 1994). With that, we have,

$$\begin{aligned} n_2(\omega) &= \frac{2}{\pi} \int_0^\infty \frac{K}{\omega_1^2 - \omega_2^2} \frac{\sqrt{E_p}}{n_0^2 E_g^3} F\left(\frac{\hbar \omega_1}{E_g}; \frac{\hbar \omega_2}{E_g}\right) d\omega_1 \\ &= \frac{2}{\pi} \int_0^\infty \frac{K \hbar^2}{\hbar^2 \omega_1^2 - \hbar^2 \omega_2^2} \frac{\sqrt{E_p}}{n_0^2 E_g^5} F\left(\frac{\hbar \omega_1}{E_g}; \frac{\hbar \omega_2}{E_g}\right) d\omega_1 \end{aligned} \quad (\text{A.36})$$

Now by changing integration variable, for $x_i = \hbar \omega_i / E_g$, $i = 1, 2$, we arrive at:

$$\begin{aligned} n_2(\omega) &= K \frac{\hbar \sqrt{E_p}}{n_0^2 E_g^4} \left(\frac{2}{\pi} \int_0^\infty \frac{F(x_1; x_2)}{x_1^2 - x_2^2} dx_1 \right) \\ &= K \frac{\hbar \sqrt{E_p}}{n_0^2 E_g^4} G\left(\frac{\hbar \omega}{E_g}\right) \end{aligned} \quad (\text{A.37})$$

where G is given by this integral:

$$G(x_2) = \frac{2}{\pi} \int_0^\infty \frac{F_2(x_1, x_2) dx_1}{x_1^2 - x_2^2} \quad (\text{A.38})$$

We then set forward to evaluate the expression. By using Mathematica 9.0, we obtain similar result as (Sheik-Bahae et al., 1991), i.e.

$$G(x) = \frac{1}{(2x)^6} \left[-\frac{3}{8}x^2(1-x)^{-1/2} + 3x(1-x)^{1/2} - 2(1-x)^{3/2} + 2\Theta(1-2x)(1-2x)^{3/2} \right] \quad (\text{A.39})$$

which is same as the one in Table (6.1). Here $\Theta(x)$ is the Heaviside step function.

In this section, we have briefly run through the derivation of the dispersion for the two-band model. Specifically, we have considered the contribution of two-photon absorption towards the dispersion of semiconductors and wide-gap optical solids. To achieve this goal, we have computed the S -matrix for dipole approximation for the radiation interaction. The change in transition rate is then extracted. That allows us to compute the nondegenerate two-photon absorption's absorption coefficient, which later feed into the Kramers-Kronig relation to obtain the final form of dispersion. In the derivation, it is interesting to note that the nondegenerate two-photon absorption is used instead of the degenerate one. This is important even if we only require the self-refraction result, as the separation of two frequencies allow one of them to act as perturbation in the nonlinear Kramers-Kronig relation Eq. (6.36). Also, while the derivation provided an expression for n_2 in Eq. (A.37), we did not use the expression in Sec. (6.5). Instead, a semi-empirical expression as adopted by Lenz et al. (2000) is used, as it models chalcogenide glass to a better precision.

APPENDIX B

NUMERICAL METHODS & PROGRAM VERIFICATION

In this section, a short introduction is done on the numerical methods applied to achieve results in Chapter 5 and Chapter 6. Also, we will briefly discuss the application of parallel computing module in our program, which significantly decreases the computing time. Lastly, some verification had been made on the program to ensure its usability.

B.1 Numerical Methods

The computation of Casimir force with Lifshitz formula includes a few computational challenges. In this section, we will present several numerical methods taken to solve the Lifshitz formula.

B.1.1 Adaptive Simpson's Method

As noted, the Lifshitz formula requires the solution to a double integral over k -space and frequency space. With this, numerical integration methods were considered. While conventional constant-grid-trapezoidal rule may return some acceptable results, we have noticed that the result quickly diverges as we attempt to compute the Casimir force over a larger frequency/wavenumber. Upon further inspection, it is noticed that a very fine grid is required in this case, which is computationally inefficient and memory demanding.

As an alternative, we have used the adaptive Simpson's method. In this method, an estimate was done to the error from calculating a definite integral, using the Simpson's rule. The Simpson's rule is basically a 3-point Newton-Cotes quadrature, and it is given in Eq. (B.1) where f is any arbitrary function. If the error estimated exceeds a specified tolerance, the interval of integration is subdivided and the Simpson's method is applied to each subinterval. This process was done recursively until all error estimates are below a specified tolerance.

$$\int_a^b f(x) dx \approx \frac{b-a}{6} \left[f(a) + 4f\left(\frac{a+b}{2}\right) + f(b) \right] \quad (\text{B.1})$$

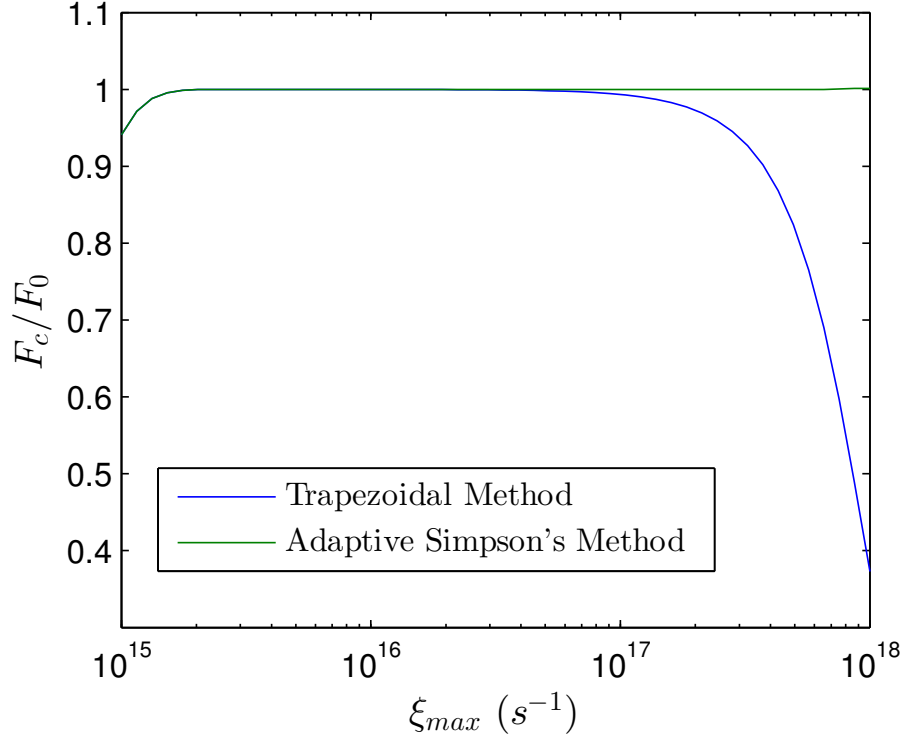


Figure B.1: An illustration of the change in normalized Casimir force for two different integration methods, as the grid size increases

As a comparison, the results from both methods are compared in Fig. (B.1), for increasing integration limit. In essence, the figure gives the Casimir force between two perfectly conducting plate, for different maximum integration limit, ξ_{max} . The Casimir force is normalized to the theoretical value obtained by calculating directly from Eq. (1.2). The trapezoidal method was run with 2500 evenly spaced grid. It is noted that after converging, the trapezoidal method fails when the grid size expands for less than two orders. As the range of integration may vary quite a little for different materials and models, we noticed that the adaptive Simpson's method is much more robust. With adaptive numerical algorithms, the integration limits was extended at least two orders higher than the conventional trapezoidal method. This provides us with greater precision and increased computation efficiency.

B.1.2 Adaptive integral limit

As we change the material constants, inter-plate distances and models, it is noticed that the shape of the integrand in the Lifshitz formula, $\partial^2 F_c / \partial \xi \partial k$, changes quite significantly. For example, the integrand of Casimir force between two perfectly conducting

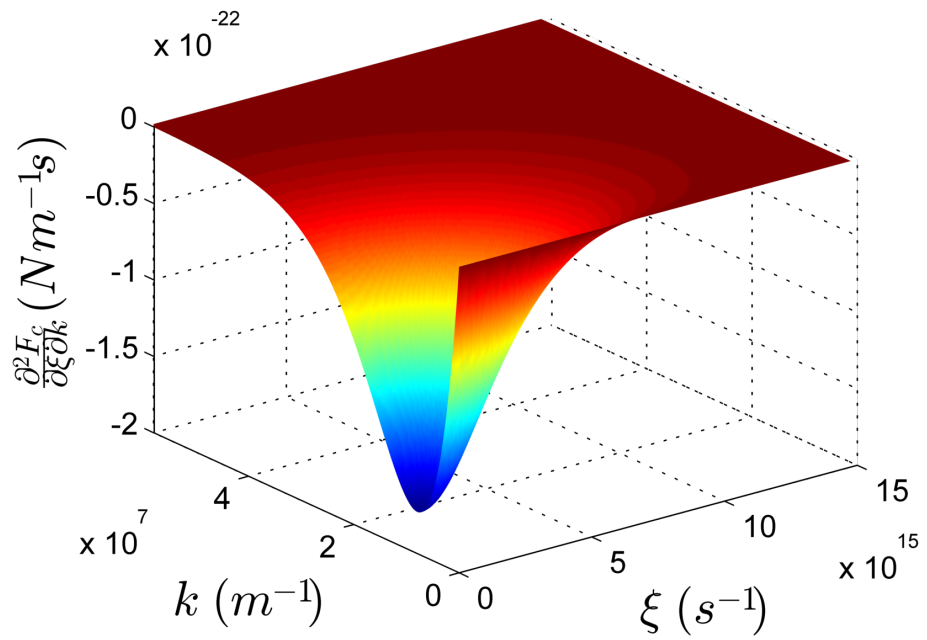
plate, at inter-plate distance of $l = 10^{-7}m$ is plotted in Fig. (B.2a). By changing one of the plate to a magnetic plate with $\mu = 10$, and with decreased distance of $l = 10^{-8}m$, the range of integration changed with a factor of 10, as seen in Fig. (B.2b). Since we may need to compute the Casimir Force for a large range of materials with different distances, it is useful to have an adaptive integral limit.

With that in mind, we have written a linear search script, which searches for the best maximum limit for integration. The search was done by finding the furthest point such that the absolute value of $\partial^2 F_c / \partial \xi \partial k$ is larger than 0.2% of the maximum value of $\partial^2 F_c / \partial \xi \partial k$.

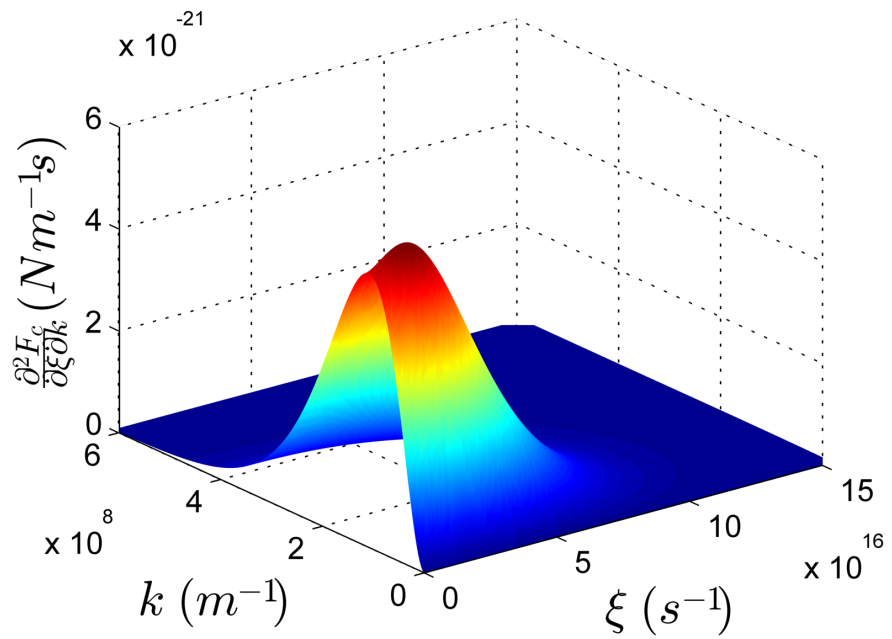
B.2 Parallel Computing

In the previous section, we have adapted several computational intensive solutions, especially a linear search for the integral limit. While these structures provide a more robust program, which can run on a far wider range of problem, we do have a trade-off in terms of computational time. In example, a quick profiling shows that the average time required for computing each point in Fig. (6.2) is about 14.5248 seconds in an Intel Core-i7 desktop, with 8GB of random access memory. While this amount of runtime may not be very large, the computational time increases significantly when we generates figures with high resolution. Hence, we have taken the advantage of present multicore processor, and Matlab's internal parallel processing module to accelerate the computation process. In particular, we have used the *parfor* module in Matlab to run four workers (slave) simultaneously. With this in place, the average time for each computation of Casimir force takes a mere 5.3097 seconds, which is about 63.4% decrease in computation time.

There are few challenges, however, in the usage of parallel processing module. In particular, as each Matlab process is isolated, it is important to ensure that each thread can be ran without much data being copied from the master to each slave. A significant overhead might causes slowdown and degradation in computing performance instead. Furthermore, most internal modules in Matlab had been programmed to utilize multiple cores whenever possible. This reduces the gain in computing speed by using *parfor* module.



a)



b)

Figure B.2: An illustration of the integral of Lifshitz formula, against the wavevector k and frequency ξ , for (a) two perfect conductor separated at distance $l = 10^{-7}m$, and (b) a perfect conducting plate and a magnetic plate with $\mu = 10$, at distance $l = 10^{-8}m$.

Arrangement	Theoretical F_c (Nm^{-2})	Computed F_c (Nm^{-2})	% differences
Maximum Attraction	-1.2997×10^5	-1.3001×10^5	-0.03%
Maximum Repulsion	1.1376×10^5	1.1373×10^5	0.03%

Table B.1: Comparison of the theoretical value of Casimir force and the computed value of Casimir force for (a) a system of two perfectly conducting plate, and (b) a system consists of a perfectly conducting plate and a perfectly magnetic plate.

B.3 Program Verification

It is important to verify and debug any program before it is used to run meaningful results. In this section, we will present several verifications we have made to ensure the program is bug-free.

B.3.1 Theoretical Limits

A straight forward verification process is to simply compare the result obtained by computation with theoretical limits. We will proceed to compare our program's output with two famous theoretical limits for Casimir force, i.e. the maximum attraction force between two perfectly conducting plates ($r_{TE} = -1$, $r_{TM} = 1$), and the maximum repulsive force between two plates when one of them is perfectly conducting plate, and the other being perfectly magnetic ($r_{TE} = 1$, $r_{TM} = -1$). For example, by taking $l = 10^{-8}m$, the comparison between theoretical result, as computed by the Lifshitz formula is compared with the values computed numerically by our program in Table (B.1).

From Table (B.1), the error percentage of our program is merely 0.03%, which is acceptable. A further reduction in the error may be achieved by increasing the precision of the adaptive Simpson's method. However, we notice the current error tolerance, $\epsilon_{tol} = 10^{-6}$ is suffice. Further increase in the tolerance might cost more runtime, which is undesirable.

B.3.2 Convergent Test

Another classical verification for numerical programs is the convergence test. In this test, the convergence of our computational value is tested by increasing the grid size of the trapezoidal method. This action will then force the integration kernel to be evaluated

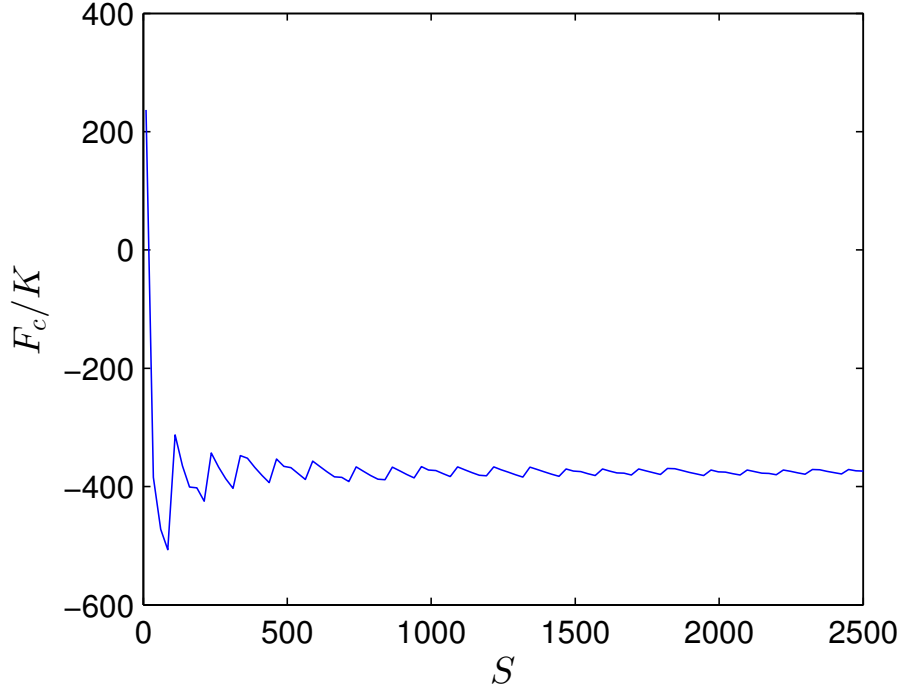


Figure B.3: An illustration of the change in the computed Casimir force against the number of grid points, S .

at smaller intervals. This test is essential, as an unstable code will fail to converge since the integration kernel is not smooth in a fine regime. The convergence in this case proves that the program is stable and capable to reproduce a result in arbitrary precision, within the computational limit.

In this test, we have evaluated the Casimir force between a perfectly conducting plate, with a material with piecewise material constant as in Eq. (B.2), at a distance of $l = 0.2\lambda_0$. The computed value of Casimir force between these plates are plotted against the number of grid points, S in Fig. (B.3).

$$\varepsilon = \begin{cases} 10, & \omega < 0.8\omega_0, \\ 1, & \omega \geq 0.8\omega_0, \end{cases} \quad \mu = \begin{cases} 0.5, & \omega < 0.8\omega_0, \\ 100, & \omega \geq 0.8\omega_0, \end{cases} \quad (\text{B.2})$$

The figure shows a rather interesting feature. When S is small, we can see that the computed value of Casimir force oscillates at a rather large range. For example, around $S \approx 100$, we can see an oscillation of $\Delta F_c/K \approx \pm 100$. If we consider $\lambda_0 = 10^{-8}m$, the oscillation is roughly $\Delta F_c \approx 10^6 Nm^{-2}$. However, at progressively higher number of grid points, we can see that the value slowly converges to a final value. This feature is important, as it shows that the integration function that we have programmed is numerically stable.

At this point, one might recall that we have already concluded in Section B.1.1 that the adaptive Simpson's method is much more powerful than the trapezoidal method. The use of trapezoidal method in this section thus requires a justification. In essence, the adaptive Simpson's method worked by recursively cutting down the range of integration until the absolute error is smaller than a certain value. Thus, the grid size in this case is not constant over the whole range of integration. This feature may complicate the comparison. The trapezoidal method, on the other hand, employs a constant grid size over the whole range, as determined by the number of grid points, S . By varying the number of grid points we can easily see that the integration kernel is stable, thus proving the robustness of our program.

APPENDIX C

SOURCE CODE

In this section, we will list the Matlab source code used to compute results from Chapter 5 and Chapter 6. In each section, a function within the core program will be presented and explained. For simplicity, we will only present the core code required for the computation of Section 6.5.2.

C.1 Core Function

This section contains the core functions required to compute the Casimir force by using Lifshitz formula. It is divided into several parts, including the main function that integrates the overall integration kernel, the adaptive grid search function, the integration kernel and several function that serves as calculation of material constants.

C.1.1 Main Function

The main function serves as the core function in this project. It performs the double integration in the Lifshitz formula using both trapezoidal method and the adaptive Simpson's method. The adaptive Simpson's method is computed repeatedly until its value converges for different limits. It then returns the Casimir force, as calculated in Lifshitz formula for a specific setup and a specific inter-plate distance.

```
function result = CasimirForce(PositionX,IT)
% Initializing Global Constants
CONST.h_bar=1.054571596*(10^(-34));
CONST.c=299792458;
CONST.epsilon_0=8.854187817*(10^(-12));
CONST.mu_0=1.256637061*(10^(-6));
CONST.lambda0=1e-6;
CONST.IT=IT;
CONST.e=1.602176565e-19;

%Computational variables (calibrated with parallel conducting plate)
t=0;
gridsize=100;
gridsizefine=2000;
a=PositionX*CONST.lambda0;
XiMin=1e-9;
```

```

XiMax=1e25;
Kmin=0.00001;
Kmax=1e25;
GridSearchPrecision=0.002;
ConvergeTestPrecision=0.01;

%LogSearch: Adaptive grid size
temp_research=1;
temp_searchdone=0;
while temp_research==1
    temp_research=0;
    temp_searchdone=temp_searchdone+1;
    if temp_searchdone > 5000
        display ('Warning: Search Failed. Using 10x old range. Inaccuracy might
            occur');
        XiMax=XiMax*10;
        Kmax=Kmax*10;
        break;
    end
    temp_searchrange=lograngefinder(XiMin,XiMax,Kmin,Kmax,GridSearchPrecision,
        gridsize,a,t,CONST);
    if temp_searchrange(1) < gridsize*0.95
        XiMax=temp_searchrange(2);
        temp_research=1;
    end
    if temp_searchrange(3) < gridsize*0.95
        Kmax=temp_searchrange(4);
        temp_research=1;
    end
    if temp_searchrange(1) >= gridsize
        XiMax=temp_searchrange(2)+temp_searchrange(5);
        temp_research=1;
    end
    if temp_searchrange(3) >= gridsize
        Kmax=temp_searchrange(4)+temp_searchrange(6);
        temp_research=1;
    end
end

%LinSearch: Adaptive grid size
temp_research=1;
temp_searchdone=0;
while temp_research==1
    temp_research=0;
    temp_searchdone=temp_searchdone+1;
    if temp_searchdone > 5000
        display ('Warning: Search Failed. Using 10x old range. Inaccuracy might
            occur');
        XiMax=XiMax*10;
        Kmax=Kmax*10;
        break;
    end
    temp_searchrange=linrangefinder(XiMin,XiMax,Kmin,Kmax,GridSearchPrecision,

```

```

        gridsize,a,t,CONST);
    if temp_searchrange(1) < gridsize*0.95
        XiMax=temp_searchrange(2);
        temp_research=1;
    end
    if temp_searchrange(3) < gridsize*0.95
        Kmax=temp_searchrange(4);
        temp_research=1;
    end
    if temp_searchrange(1) >= gridsize
        XiMax=temp_searchrange(2)+(XiMax-XiMin)/gridsize*2;
        temp_research=1;
    end
    if temp_searchrange(3) >= gridsize
        Kmax=temp_searchrange(4)+(XiMax-XiMin)/gridsize*2;
        temp_research=1;
    end
end

end

%Adaptive Simpson Method, including convergence test.
Convergence=0;
temp_XiMax=XiMax;
temp_Kmax=Kmax;
temp_convergecount=0;
temp_CurrentValue=0;
while Convergence==0
    temp_PreviousValue=temp_CurrentValue;
    myquad = @(fun,a,b,tol,trace,varargin)quad(@(x)fun(x,varargin{:})),
        a,b,'AbsTol',tol);
    temp_CurrentValue=dblquad(@(xi,k) integration_kernel(xi,k,a,0,CONST),
        0,temp_XiMax,0,temp_Kmax,1e-6,myquad);
    if (abs(abs(temp_CurrentValue)-abs(temp_PreviousValue))/
        abs(temp_PreviousValue)) < ConvergeTestPrecision &&
        temp_convergecount ~= 0
        Convergence=1;
    else
        temp_XiMax=temp_XiMax*1.2;
        temp_Kmax=temp_Kmax*1.2;
    end
    temp_convergecount=temp_convergecount+1;
    if temp_convergecount > 50
        display ('Error: Convergence not found! Integration value might be
            erroneous!!');
        break;
    end
end
result(1) = temp_CurrentValue;

%Trapezoidal method
xi_vec=linspace(XiMin,XiMax,gridsizefine);
k_vec=linspace(Kmin,Kmax,gridsizefine);
[XI,K]=meshgrid(xi_vec,k_vec);

```

```

z=integration_kernel(XI,K,a,t,CONST);
result(2)=trapz(k_vec,trapz(xi_vec,z,2));

%Plotting graph of integration kernel
surf(XI,K,real(z));
shading interp; %interp, faceted, flat
xlabel('$ \xi $', 'Interpreter', 'LaTeX')
ylabel('$ k $', 'Interpreter', 'LaTeX')
zlabel('$\frac{\partial^2 F_c}{\partial \xi \partial k} $', 'Interpreter', 'LaTeX')

%User Interface: Showing end of script
fprintf('For t=%e, x= %e, CasimirF = %e\n',t,PositionX,result(1));
end

```

C.1.2 Adaptive Grid Search Function

The adaptive grid search function is explained in Section B.1.2. Basically, both functions in this section will take in the range of ξ and k , and return the cut-off point, where the function's value at that point is no longer negligible.

```

%Adaptive Grid Search: This function will find suitable range for
integration.(LOG)
function result =
    lograngefinder(XiMin,XiMax,Kmin,Kmax,var_maxvariance,gridsize,a,t,CONST)
xi_vec=logspace(log10(XiMin),log10(XiMax),gridsize);
k_vec=logspace(log10(Kmin),log10(Kmax),gridsize);
[XI,K]=meshgrid(xi_vec,k_vec);
z=integration_kernel(XI,K,a,t,CONST);
zabs=abs(z);
z_xi_scaled=max(zabs,[],1)./max(max(zabs));
z_k_scaled=max(zabs,[],2)./max(max(zabs));

result(1:4)=0;
for tempvar_i=1:gridsize
    if abs(z_xi_scaled(gridsize+1-tempvar_i)) > var_maxvariance &&
        result(2)==0
        result(1)=gridsize+2-tempvar_i;
        if result(1)==gridsize+1
            result(2)=xi_vec(gridsize+1-tempvar_i);
        else
            result(2)=xi_vec(gridsize+2-tempvar_i);
        end
    end
end

if abs(z_k_scaled(gridsize+1-tempvar_i)) > var_maxvariance &&
    result(4)==0
    result(3)=gridsize+2-tempvar_i;
    if result(3) == gridsize+1
        result(4)=k_vec(gridsize+1-tempvar_i);
    end
end

```

```

        else
            result(4)=k_vec(gridsize+2-tempvar_i);
        end
    end
end

if result(2)~=0 && result(4)~=0
    break;
end
end
result(5)=xi_vec(gridsize)-xi_vec(gridsize-2);
result(6)=k_vec(gridsize)-k_vec(gridsize-2);
end

%Adaptive Grid Search: This function will find suitable range for
integration.(LIN)
function result =
    linrangefinder(XiMin,XiMax,Kmin,Kmax,var_maxvariance,gridsize,a,t,CONST)
xi_vec=linspace(XiMin,XiMax,gridsize);
k_vec=linspace(Kmin,Kmax,gridsize);
[XI,K]=meshgrid(xi_vec,k_vec);
z=integration_kernel(XI,K,a,t,CONST);
zabs=abs(z);
z_xi_scaled=max(zabs,[],1)./max(max(zabs));
z_k_scaled=max(zabs,[],2)./max(max(zabs));

result(1:4)=0;
for tempvar_i=1:gridsize
    if abs(z_xi_scaled(gridsize+1-tempvar_i)) > var_maxvariance &&
        result(2)==0
        result(1)=gridsize+2-tempvar_i;
        if result(1)==gridsize+1
            result(2)=xi_vec(gridsize+1-tempvar_i);
        else
            result(2)=xi_vec(gridsize+2-tempvar_i);
        end
    end
end

if abs(z_k_scaled(gridsize+1-tempvar_i)) > var_maxvariance &&
    result(4)==0
    result(3)=gridsize+2-tempvar_i;
    if result(3) == gridsize+1
        result(4)=k_vec(gridsize+1-tempvar_i);
    else
        result(4)=k_vec(gridsize+2-tempvar_i);
    end
end
end

if result(2)~=0 && result(4)~=0
    break;
end
end
end
end

```

C.1.3 Integration Kernel

In this section, we present the integration kernel for Lifshitz formula. This kernel will call the reflectivity calculation functions, and returns the value of integration kernel.

```
%Integration Kernel - gives value for  $d^2F/(dx_i dk)$ 
function result = integration_kernel(xi,k,a,t,CONST)

r_TE_A = r_TE_A_calc(xi,k,t,CONST);
r_TE_B = r_TE_B_calc(xi,k,t,CONST);
r_TM_A = r_TM_A_calc(xi,k,t,CONST);
r_TM_B = r_TM_B_calc(xi,k,t,CONST);

temp_sqrt = sqrt(((xi.^2)./(CONST.c^2)) + k.^2);

temp1 = r_TE_A.*r_TE_B.*exp(-2.*a.*temp_sqrt);
temp2 = r_TM_A.*r_TM_B.*exp(-2.*a.*temp_sqrt);
result = (CONST.lambda0^4 * 16 /CONST.c) .* k .* temp_sqrt .* (
    (temp1./(1-temp1)) + (temp2./(1-temp2)));

end
```

C.1.4 Reflectivity Calculation

As the Lifshitz formula depends on both plate's reflectivity, we have dedicated two functions for each plate for the calculation of reflectivity (one for each transverse mode). These functions will make appropriate calls to obtain the material constants, and returns the reflectivity for each case.

```
% reflectivity (TE) for plate A
function result = r_TE_A_calc(xi,k,t,CONST)

mu_A = mu_A_calc(xi,k,CONST);
eta_A = eta_A_calc(xi,k,CONST,t);
yy_temp1 = mu_A.*sqrt(xi.^2./((CONST.c)^2) + k.^2);
yy_temp2 = (eta_A).*sqrt(xi.^2./((CONST.c)^2) + k.^2./(eta_A).^2);
result=(yy_temp1-yy_temp2)./(yy_temp1+yy_temp2);

end

% reflectivity (TE) for plate B
function result = r_TE_B_calc(xi,k,t,CONST)

mu_B = mu_B_calc(xi,k,CONST);
eta_B = eta_B_calc(xi,k,CONST,t);
yy_temp1 = mu_B.*sqrt(xi.^2./((CONST.c)^2) + k.^2);
yy_temp2 = (eta_B).*sqrt(xi.^2./((CONST.c)^2) + k.^2./(eta_B).^2);
result=(yy_temp1-yy_temp2)./(yy_temp1+yy_temp2);
```

```

end

% reflectivity (TM) for plate A
function result = r_TM_A_calc(xi,k,t,CONST)

epsilon_A = epsilon_A_calc(xi,k,CONST);
eta_A = eta_A_calc(xi,k,CONST,t);
yy_temp1 = epsilon_A.*sqrt(xi.^2./((CONST.c)^2) + k.^2);
yy_temp2 = (eta_A).*sqrt(xi.^2./((CONST.c)^2) + k.^2./(eta_A).^2);
result=(yy_temp1-yy_temp2)./(yy_temp1+yy_temp2);

end

% reflectivity (TM) for plate B
function result = r_TM_B_calc(xi,k,t,CONST)

epsilon_B = epsilon_B_calc(xi,k,CONST);
eta_B = eta_B_calc(xi,k,CONST,t);
yy_temp1 = epsilon_B.*sqrt(xi.^2./((CONST.c)^2) + k.^2);
yy_temp2 = (eta_B).*sqrt(xi.^2./((CONST.c)^2) + k.^2./(eta_B).^2);
result=(yy_temp1-yy_temp2)./(yy_temp1+yy_temp2);

end

```

C.1.5 Index of Refraction Calculation

The index of refraction is part of the material constants' calculation. In these functions, the effective refractive indexes of both plates are calculated, with Optical Kerr effect taken into account. Furthermore, it is important to note that the square root in linear refractive index calculation, $n_0 = \sqrt{\epsilon\mu}$ is calculated by considering the complex plane instead. This method of calculation will preserve the sign of n_0 , especially when both ϵ and μ is negative.

```

%Index of refraction for plate A
function eta_A = eta_A_calc(xi,k,CONST,t)
mu_A = mu_A_calc(xi,k,CONST);
epsilon_A = epsilon_A_calc(xi,k,CONST);
eta_A_2 = eta_A_2_calc(xi,k,CONST);
I = I_calc(t,CONST);

[mu_A_angle, mu_A_radius] = cart2pol( real(mu_A), imag(mu_A) );
[epsilon_A_angle, epsilon_A_radius] = cart2pol( real(epsilon_A),
    imag(epsilon_A) );
eta_A = sqrt(mu_A_radius.*epsilon_A_radius) .*
    exp(1i./2.*(epsilon_A_angle+mu_A_angle))+eta_A_2.*I;
end

```

```

%Index of refraction for plate B
function eta_B = eta_B_calc(xi,k,CONST,t)
mu_B = mu_B_calc(xi,k,CONST);
epsilon_B = epsilon_B_calc(xi,k,CONST);
eta_B_2 = eta_B_2_calc(xi,k,CONST);
I = I_calc(t,CONST);

[mu_B_angle, mu_B_radius] = cart2pol( real(mu_B), imag(mu_B) );
[epsilon_B_angle, epsilon_B_radius] = cart2pol( real(epsilon_B),
    imag(epsilon_B) );
eta_B = sqrt(mu_B_radius.*epsilon_B_radius) .*
    exp(1i./2.*(epsilon_B_angle+mu_B_angle))+eta_B_2.*I;
end

```

C.1.6 Other Constant Calculation

In this section, the functions that compute material constants for both plates are presented. In essence, the dielectric function ϵ , magnetic permeability μ , and the Kerr constant n_2 is returned. Since the material constants for each plate that we have considered is nontrivial, these function will then acts as wrapper functions. They will pass the relevant variables to another function (which we will detail in the next section) for further computation.

```

%Intensity of light
function I = I_calc(t,CONST)
I = CONST.IT;
end

%Kerr coefficient for plate A
function eta_A_2 = eta_A_2_calc(xi,k,CONST)
eta_A_2 = 0;
end

%Dielectric constant for plate A
function epsilon_A = epsilon_A_calc(xi,k,CONST)
epsilon_A = DrudeLorentz(1i.*xi,2*pi*CONST.c/CONST.lambda0,1);
end

%Permeability for plate A
function mu_A = mu_A_calc(xi,k,CONST)
mu_A = DrudeLorentz(1i.*xi,2*pi*CONST.c/CONST.lambda0,2);
end

%Kerr coefficient for plate B
function eta_B_2 = eta_B_2_calc(xi,k,CONST)
eta_B_2 = As2Se3(1i.*xi,3,CONST);
end

```

```

%Dielectric constant for plate B
function epsilon_B = epsilon_B_calc(xi,k,CONST)
epsilon_B = As2Se3(1i.*xi,1,CONST);
end

%Permeability for plate B
function mu_B = mu_B_calc(xi,k,CONST)
mu_B = As2Se3(1i.*xi,2,CONST);
end

```

C.2 Drude-Lorentz Function

In this section, the material constants for a Drude-Lorentz type metamaterial is computed and returned.

```

function result =DrudeLorentz(omega,omega_0,vbr_type)

%Initial variable defining
omega_P_e=0.5.*omega_0; %changing this gives a sharper asymptote
omega_T_e=1e-3.*omega_0; %changing this redefine the position
gamma_e=1e-2.*omega_T_e;

omega_P_m=3.*omega_0;
omega_T_m=2.*omega_0;
gamma_m=1e-2.*omega_T_m;

%returning appropriate variable
if vbr_type == 1
    result=1+omega_P_e.^2./(omega_T_e.^2 - omega.^2 -
        1i.*gamma_e.*omega);
elseif vbr_type == 2
    result=1+omega_P_m.^2./(omega_T_m.^2 - omega.^2 -
        1i.*gamma_m.*omega);
end
end

```

C.3 As_2Se_3 Material Constant Calculation

The material constant for a Chalcogenide Glass, As_2Se_3 is computed and returned.

```

function result =As2Se3(omega,vbr_type,CONST)

%omega_0 is a stupid dummy variable.

% initializing As2S3 glass
mu=1+(-3.36e-10); %susceptibility by Z. CIMPL et al phys. stat. sol. 41, 535
(1970)

```

```

%refraction index
%variables
var_E_d=26 .* CONST.e; %normally, Slusher et al
var_E_s=4.1 .* CONST.e; %As2Se3 value, Slusher et al
var_gamma = 0.01 .* var_E_s ./ CONST.h_bar;

%computing refractive index
refraction_index_squared = (var_E_d .* var_E_s ./ (var_E_s.^2 -
    (CONST.h_bar .* omega).^2 - (1i .* CONST.h_bar.^2 .* omega .*
    var_gamma) )) + 1; %Slusher et al (Wemple equation)
refraction_index=sqrt(refraction_index_squared);

%returning appropriate variable
if vbr_type == 1 %epsilon
    result=refraction_index.^2./mu;
elseif vbr_type == 2 %mu
    result=mu;
elseif vbr_type == 3 %n2
    result=frequencyOKE( refraction_index, omega, CONST );
elseif vbr_type==5 %debug refractive index
    result=refraction_index;
end
end

function [ var_eta2 ] = frequencyOKE( var_eta0, omega, CONST )
%Frequency dependent n2: accepts n0 and omega as input, returns n2

%Declaring Variables
var_d=0.243; %As2Se3 Slusher et al
var_E_s=4.1 .* CONST.e; %As2Se3 Slusher et al
var_E_g=var_E_s ./ 2.5; %the usual approximation of var_E_s ~ 2.5 var_E_g
(Lenz)
var_omega_bandgap=var_E_g./CONST.h_bar;
var_gamma=0.01.*var_omega_bandgap;
var_eta0=real(var_eta0);

var_eta0_const=2.7; %Slusher et al

%computing the eta2
var_eta2=1.7e-18 .* (var_eta0_const.^2 + 2).^3 .* (var_eta0_const.^2 - 1) .*
    (var_d ./ var_eta0_const ./ (var_E_s ./ CONST.e)) .* (var_d ./
    var_eta0_const ./ (var_E_s ./ CONST.e)) .*
    funcGall(omega,var_omega_bandgap,var_gamma);
end

function result=funcGall( x_omega,omega_bandgap,gamma)
x_cutoff=0.05.*omega_bandgap;
y=funcG(x_omega,omega_bandgap,gamma,1)
    +funcG(x_omega,omega_bandgap,gamma,2)
    +funcG(x_omega,omega_bandgap,gamma,3)
    +funcG(x_omega,omega_bandgap,gamma,4)
    -funcG(x_omega,omega_bandgap,gamma,5);
y_cutoff=funcG(x_cutoff,omega_bandgap,gamma,1)
    +funcG(x_cutoff,omega_bandgap,gamma,2)

```

```

+funcG(x_cutoff,omega_bandgap,gamma,3)
+funcG(x_cutoff,omega_bandgap,gamma,4)
-funcG(x_cutoff,omega_bandgap,gamma,5);
y_normalized=y./real(y_cutoff);
test1 = (x_omega < x_cutoff).*1;
test2 = (x_omega >= x_cutoff).*y_normalized;
result = test1 + test2;
end

function result = funcG( x_omega,omega_bandgap,gamma,type)
    x=(x_omega + 1i.*gamma)./omega_bandgap;
    if (type==1) %two photon absorption
        result = (1./(2.*x).^6) .* (-3./8.*x.^2.*(1-x).^(-1/2) +
            3.*x.*(1-x).(1/2) - 2.*(1-x).(3/2) +
            2.*heavisidefunc(1-2.*x).(1-2.*x).(3/2));
    elseif (type==2) %Raman
        result = (1./(2.*x).^6) .* (-3./8.*x.^2.*(1+x).^(-1/2) -
            3.*x.*(1+x).(1/2) - 2.*(1+x).(3/2) + 2.*(1+2.*x).(3/2));
    elseif (type==3) %Linear Stark
        result = (1./(2.*x).^6) .* (2 - (1-x).(3/2) - (1+x).(3/2));
    elseif (type==4) %Quadratic Stark
        result=(1./ 2.^10 ./ x.^5) .* ((1-x).^(-1/2) - (1+x).^(-1/2) -
            (x./2.*(1-x).^(-3/2)) - (x./2.*(1+x).^(-3/2)) );
    elseif (type==5) %Divergent term
        result=(1./(2.*x).^6) .* (-2 - (35.*x.^2./8) +
            (x./8.*(3.*x-1).(1-x).^(-1/2)) - (3.*x.*(1-x).(1/2)) +
            ((1-x).(3/2)) + (x./8.*(3.*x+1).(1+x).^(-1/2)) +
            (3.*x.*(1+x).(1/2)) + ((1+x).(3/2)) );
    elseif (type==99) %for debugging
        result = (1./(2.*x).^6) .* (-3./8.*x.^2.*(1-x).^(-1/2) +
            3.*x.*(1-x).(1/2) - 2.*(1-x).(3/2) +
            2.*heavisidefunc(1-2.*x).(1-2.*x).(3/2));
    else
        error('Error on funcG: No idea which type is used');
    end
end
end

function Y = heavisidefunc (X)
    Y = zeros(size(X));
    Y(X > 0) = 1;
    Y(X == 0) = .5;
end

```

C.4 Plotting Function

Lastly, we also presents the plotting function for Fig. (6.5 a). This function will run the main function at different inter-plate spacing and intensity, and return the matrices of values as well as a graph. This is a great example for the usage of *parfor* module to speed up the computation. As we can see, each thread in this case does not require much

overhead, and hence this will speed up the overall computation.

```
precisionX=40;
precisionI=40;
Xrun=linspace(0.17,0.5,precisionX);
Irun=linspace(0.1e18,4e18,precisionI);
Frun=zeros(precisionI,precisionX);

for runx=1:precisionX
    temp_X=Xrun(runx);
    parfor runi=1:precisionI
        dummy=CasimirForceITDL(0,0.8,temp_X,Irun(runi));
        Frun(runi,runx)=dummy(3);
    end
end

[Xbig,Ibig]=meshgrid(Xrun,Irun);
surf(Xbig,Ibig,real(Frun));
shading interp;
```

REFERENCES

- Abramowitz, M., & Stegun, I. (1965). *Handbook of mathematical functions: with formulas, graphs, and mathematical tables*. New York, NY: Dover publications.
- Ahlfors, L. (1979). *Complex analysis: an introduction to the theory of analytic functions of one complex variable*. New York, NY: McGraw-Hill.
- Arfken, G., Weber, H., & Harris, F. (2005). *Mathematical methods for physicists*. Salt Lake City, UT: Academic Press.
- Bahk, S., Rousseau, P., Planchon, T., Chvykov, V., Kalintchenko, G., Maksimchuk, A., . . . Yanovsky, V. (2004). Generation and characterization of the highest laser intensities (10^{22} W/cm²). *Optics letters*, 29(24), 2837–2839.
- Barash, Y., & Ginzburg, V. (1975). Electromagnetic fluctuations in a substance and molecular (van der Waals) interbody forces. *Soviet Physics Uspekhi*, 18, 305.
- Bordag, M., Klimchitskaya, G., Mohideen, U., & Mostepanenko, V. (2009). *Advances in the Casimir effect*. Oxford: Oxford University Press.
- Bordag, M., Petrov, G., & Robashik, D. (1984). Calculation of the Casimir effect for a scalar field with the simplest non-stationary boundary conditions. *Soviet Journal of Nuclear Physics*, 39(5), 828–831.
- Boyd, R. (2002). *Nonlinear optics*. Salt Lake City, UT: Academic press.
- Boyer, T. (1968). Quantum electromagnetic zero-point energy of a conducting spherical shell and the Casimir model for a charged particle. *Physical Review*, 174(5), 1764–1776.
- Brown, L., & Maclay, G. (1969). Vacuum stress between conducting plates: an image solution. *Physical Review*, 184(5), 1272–1279.
- Buckingham, A. (1956). Birefringence resulting from the application of an intense beam of light to an isotropic medium. *Proceedings of the Physical Society. Section B*, 69(3), 344–349.
- Burgos, S. P., de Waele, R., Polman, A., & Atwater, H. A. (2010). A single-layer wide-angle negative-index metamaterial at visible frequencies. *Nature Materials*, 9(5), 407–412.
- Capasso, F., Munday, J., Iannuzzi, D., & Chan, H. (2007). Casimir forces and quantum electrodynamical torques: Physics and nanomechanics. *IEEE Journal of Selected Topics in Quantum Electronics*, 13(2), 400–414.
- Casimir, H. (1948). On the attraction between two perfectly conducting plates. *Proc. K. Ned. Akad. Wet.*, 51, 793–795.
- Casimir, H., & Polder, D. (1948). The influence of retardation on the London-van der Waals forces. *Physical Review*, 73, 360–372.
- Chan, H., Aksyuk, V., Kleiman, R., Bishop, D., & Capasso, F. (2001). Nonlinear micromechanical Casimir oscillator. *Physical Review Letters*, 87(21), 211801.
- Collin, R. (1991). *Field theory of guided waves* (Vol. 2). New York, NY: Wiley-IEEE Press.
- Davydov, A. (1969). *Quantum mechanics*. Oxford: Pergamon Press.
- De Los Santos, H. (2003). Nanoelectromechanical quantum circuits and systems. *Proceedings of the IEEE*, 91(11), 1907–1921.
- Dolling, G., Wegener, M., Soukoulis, C. M., & Linden, S. (2007). Negative-index metamaterial at 780 nm

- wavelength. *Optics Letters*, 32, 53–55.
- Duguay, M., & Hansen, J. (1969). An ultrafast light gate. *Applied Physics Letters*, 15(6), 192–194.
- Ederth, T. (2000). Template-stripped gold surfaces with 0.4-nm rms roughness suitable for force measurements: Application to the Casimir force in the 20–100-nm range. *Physical Review A*, 62(6), 062104.
- Eggleton, B., Luther-Davies, B., & Richardson, K. (2011). Chalcogenide photonics. *Nature Photonics*, 5(3), 141–148.
- Elizalde, E., & Romeo, A. (1991). Essentials of the Casimir effect and its computation. *American Journal of Physics*, 59(8), 711–719.
- Enoch, S., Tayeb, G., Sabouroux, P., Guérin, N., & Vincent, P. (2002). A metamaterial for directive emission. *Physical Review Letters*, 89(21), 213902.
- Erdélyi, A., Magnus, W., Oberhettinger, F., Tricomi, F., & Bateman, H. (1953). *Higher transcendental functions*. New York, NY: McGraw-Hill.
- Feng, S., & Halterman, K. (2012). Coherent perfect absorption in epsilon-near-zero metamaterials. *Physical Review B*, 86(16), 165103.
- Genet, C., Lambrecht, A., & Reynaud, S. (2003). Casimir force and the quantum theory of lossy optical cavities. *Physical Review A*, 67(4), 043811.
- Griffiths, D. (2005). *Introduction to quantum mechanics*. Upper Saddle River, NJ: Pearson Prentice Hall.
- Harris, B., Chen, F., & Mohideen, U. (2000). Precision measurement of the Casimir force using gold surfaces. *Physical Review A*, 62(5), 052109.
- Heiman, D., Hellwarth, R. W., Levenson, M. D., & Martin, G. (1976). Raman-induced Kerr effect. *Physical Review Letters*, 36, 189–192.
- Hutchings, D., Sheik-Bahae, M., Hagan, D., & Van Stryland, E. (1992). Kramers-Krönig relations in nonlinear optics. *Optical and Quantum Electronics*, 24(1), 1–30.
- Jackson, J. (1998). *Classical Electrodynamics*. Hoboken, NJ: Wiley.
- Keldysh, L. (1965). Ionization in the field of a strong electromagnetic wave. *Sov. Phys. JETP*, 20(5), 1307–1314.
- Kenneth, O., & Klich, I. (2006). Opposites attract: A theorem about the Casimir force. *Physical Review Letters*, 97(16), 160401.
- Kenneth, O., Klich, I., Mann, A., & Revzen, M. (2002). Repulsive Casimir forces. *Physical Review Letters*, 89(3), 33001.
- Kerr, J. (1877). XLIII. On rotation of the plane of polarization by reflection from the pole of a magnet. *The London, Edinburgh, and Dublin Philosophical Magazine and Journal of Science*, 3(19), 321–343.
- Kittel, C., & McEuen, P. (1996). *Introduction to solid state physics* (Vol. 7). Wiley New York.
- Klimchitskaya, G., Mohideen, U., & Mostepanenko, V. (2000). Casimir and van der Waals forces between two plates or a sphere (lens) above a plate made of real metals. *Physical Review A*, 61(6), 062107.
- Kosa, T., Rangel-Rojo, R., Hajto, E., Ewen, P., Owen, A., Kar, A., & Wherrett, B. (1993). Nonlinear optical properties of silver-doped as_2s_3 . *Journal of Non-Crystalline Solids*, 164, 1219–1222.
- Lamoreaux, S. (1997). Demonstration of the Casimir force in the 0.6 to 6 μm range. *Physical Review Letters*, 78(1), 5–8.

- Laniel, J., Hô, N., Vallée, R., & Villeneuve, A. (2005). Nonlinear-refractive-index measurement in as_2s_3 channel waveguides by asymmetric self-phase modulation. *Journal of the Optical Society of America B*, 22(2), 437–445.
- Lenz, G., Zimmermann, J., Katsufuji, T., Lines, M., Hwang, H., Spälter, S., . . . Aggarwal, I. (2000). Large Kerr effect in bulk Se-based chalcogenide glasses. *Optics Letters*, 25(4), 254–256.
- Levin, M., McCauley, A., Rodriguez, A., Reid, M., & Johnson, S. (2010). Casimir repulsion between metallic objects in vacuum. *Physical Review Letters*, 105(9), 90403.
- Lide, D. (2012). *CRC handbook of Chemistry and Physics*. Boca Raton, FL: CRC press.
- Lifshitz, E. (1956). The theory of molecular attractive forces between solids. *Sov. Phys. JETP*, 2(1), 73–83.
- Lines, M. (1990). Bond-orbital theory of linear and nonlinear electronic response in ionic crystals. II. Nonlinear response. *Physical Review B*, 41(6), 3383–3390.
- London, F. (1930). Theory and systematics of molecular forces. *Zeitschrift für Physik*, 63, 245.
- Maker, P., Terhune, R., & Savage, C. (1964). Intensity-dependent changes in the refractive index of liquids. *Physical Review Letters*, 12(18), 507–509.
- Mehra, J. (1967). Temperature correction to the Casimir effect. *Physica*, 37(1), 145–152.
- Milonni, P., & Eberlein, C. (1994). *The quantum vacuum: an introduction to quantum electrodynamics* (Vol. 1). New York, NY: Academic press.
- Milonni, P., & Shih, M. (1992). Casimir forces. *Contemporary Physics*, 33(5), 313–322.
- Milonni, P. W., Cook, R. J., & Goggin, M. E. (1988). Radiation pressure from the vacuum: Physical interpretation of the Casimir force. *Physical Review A*, 38, 1621–1623.
- Mulliken, R. (1924). The band spectrum of boron monoxide. *Nature*, 114(2862), 349–350.
- Munday, J., Capasso, F., & Parsegian, V. (2009). Measured long-range repulsive Casimir–Lifshitz forces. *Nature*, 457(7226), 170–173.
- Ooi, C. H. R., & Khoo, Y. Y. (2012). Controlling the repulsive Casimir force with the optical kerr effect. *Physical Review A*, 86, 062509.
- Ovshinsky, S. R. (1968). Reversible electrical switching phenomena in disordered structures. *Physical Review Letters*, 21, 1450–1453.
- Ozby, E., & Aydin, K. (2008). Negative refraction and imaging beyond the diffraction limit by a two-dimensional left-handed metamaterial. *Photonics and Nanostructures-Fundamentals and Applications*, 6(1), 108–115.
- Pendry, J. (2000). Negative refraction makes a perfect lens. *Physical Review Letters*, 85(18), 3966–3969.
- Pendry, J., Holden, A., Robbins, D., & Stewart, W. (1999). Magnetism from conductors and enhanced nonlinear phenomena. *IEEE Transactions on Microwave Theory and Techniques*, 47(11), 2075–2084.
- Reid, M., Rodriguez, A., White, J., & Johnson, S. (2009). Efficient computation of Casimir interactions between arbitrary 3D objects. *Physical Review Letters*, 103(4), 40401.
- Roy, A., Lin, C., & Mohideen, U. (1999). Improved precision measurement of the Casimir force. *Physical Review D*, 60(11), 111101.
- Ruggiero, J., & Zimmerman, A. (1977). Application of analytic regularization to the Casimir forces. *Revista Brasileira de Física*, 7(3), 663–687.

- Sabisky, E., & Anderson, C. (1973). Verification of the Lifshitz theory of the van der Waals potential using liquid-helium films. *Physical Review A*, 7(2), 790–806.
- Sauter, E. (1996). *Nonlinear optics* (Vol. 44). Hoboken, NJ: Wiley-Interscience.
- Schwinger, J. (1967). Sources and electrodynamics. *Physical Review*, 158(5), 1391–1407.
- Schwinger, J. (1968). Sources and magnetic charge. *Physical Review*, 173(5), 1536–1544.
- Schwinger, J. (1970). Theory of sources. *Contemporary Physics: Trieste Symposium*, 2, 59–83.
- Schwinger, J. (1975). Casimir effect in source theory. *Letters in Mathematical Physics*, 1(1), 43–47.
- Schwinger, J., DeRaad, L., & Milton, K. (1978). Casimir effect in dielectrics. *Annals of Physics*, 115(1), 1–23.
- Serry, F., Walliser, D., & Maclay, G. (1998). The role of the Casimir effect in the static deflection and stiction of membrane strips in microelectromechanical systems (MEMS). *Journal of Applied Physics*, 84, 2501–2506.
- Shalaev, V. M., Cai, W., Chettiar, U. K., Yuan, H.-K., Sarychev, A. K., Drachev, V. P., & Kildishev, A. V. (2005). Negative index of refraction in optical metamaterials. *Optics Letters*, 30(24), 3356–3358.
- Sheik-Bahae, M., Hutchings, D., Hagan, D., & Van Stryland, E. (1991). Dispersion of bound electron nonlinear refraction in solids. *IEEE Journal of Quantum Electronics*, 27(6), 1296–1309.
- Sheik-Bahae, M., Said, A. A., Wei, T.-H., Hagan, D. J., & Van Stryland, E. W. (1990). Sensitive measurement of optical nonlinearities using a single beam. *IEEE Journal of Quantum Electronics*, 26(4), 760–769.
- Sheik-Bahae, M., Wang, J., & Van Stryland, E. (1994). Nondegenerate optical kerr effect in semiconductors. *IEEE Journal of Quantum Electronics*, 30(2), 249–255.
- Shimakawa, K., Kolobov, A., & Elliott, S. (1995). Photoinduced effects and metastability in amorphous semiconductors and insulators. *Advances in Physics*, 44(6), 475–588.
- Shimizu, F., & Stoicheff, B. (1969). Study of the duration and birefringence of self-trapped filaments in CS_2 . *IEEE Journal of Quantum Electronics*, 5(11), 544–546.
- Silveirinha, M., & Engheta, N. (2006). Tunneling of electromagnetic energy through subwavelength channels and bends using ϵ -near-zero materials. *Physical Review Letters*, 97, 157403.
- Slusher, R., Lenz, G., Hodelin, J., Sanghera, J., Shaw, L., & Aggarwal, I. (2004). Large raman gain and nonlinear phase shifts in high-purity As_2Se_3 chalcogenide fibers. *Journal of the Optical Society of America B*, 21(6), 1146–1155.
- Smektala, F., Quemard, C., Couderc, V., & Barthélémy, A. (2000). Non-linear optical properties of chalcogenide glasses measured by Z-scan. *Journal of Non-Crystalline Solids*, 274(1), 232–237.
- Smith, D. R., Padilla, W. J., Vier, D. C., Nemat-Nasser, S. C., & Schultz, S. (2000). Composite medium with simultaneously negative permeability and permittivity. *Physical Review Letters*, 84, 4184–4187.
- Sparnaay, M. (1958). Measurements of attractive forces between flat plates. *Physica*, 24(6), 751–764.
- Toll, J. S. (1956). Causality and the dispersion relation: Logical foundations. *Physical Review*, 104, 1760–1770.
- Tveryanovich, Y., & Tverjanovich, A. (2004). *Rare earth doped chalcogenide glass in semiconducting chalcogenide glass III Applications of chalcogenide glasses*. Amsterdam: Elsevier.

- Van Kampen, N., Nijboer, B., & Schram, K. (1968). On the macroscopic theory of van der Waals forces. *Physics Letters A*, 26(7), 307–308.
- Volkov, D. M. (1935). Concerning a class of solutions of the Dirac equation. *Zeitschrift für Physik*, 94, 250–260.
- Wang, C. (1970). Empirical relation between the linear and the third-order nonlinear optical susceptibilities. *Physical Review B*, 2, 2045–2048.
- Wangsness, R. (1986). *Electromagnetic fields* (Vol. 1). Hoboken, NJ: Wiley.
- Wemple, S., & DiDomenico Jr, M. (1971). Behavior of the electronic dielectric constant in covalent and ionic materials. *Physical Review B*, 3(4), 1338–1351.
- Wherrett, B. S., Hutchings, D., & Russell, D. (1986). Optically bistable interference filters: optimization considerations. *Journal of the Optical Society of America B*, 3(2), 351–362.
- Wu, T.-Y., & Ohmura, T. (1962). *Quantum theory of scattering* (Vol. 2). Prentice-Hall London.
- Yang, Y., Zeng, R., Chen, H., Zhu, S., & Zubairy, M. (2010). Controlling the Casimir force via the electromagnetic properties of materials. *Physical Review A*, 81(2), 022114.
- Yayama, H., Fujino, S., Morinaga, K., Takebe, H., Hewak, D., & Payne, D. (1998). Refractive index dispersion of gallium lanthanum sulfide and oxysulfide glasses. *Journal of Non-Crystalline Solids*, 239(1), 187–191.
- Zhang, S., Fan, W., Malloy, K. J., Brueck, S. R., Panoiu, N. C., & Osgood, R. M. (2006). Demonstration of metal-dielectric negative-index metamaterials with improved performance at optical frequencies. *JOSA B*, 23(3), 434–438.
- Zhang, S., Fan, W., Panoiu, N. C., Malloy, K. J., Osgood, R. M., & Brueck, S. R. J. (2005). Experimental demonstration of near-infrared negative-index metamaterials. *Physical Review Letters*, 95, 137404.